
Masters Theses

Student Theses and Dissertations

Spring 2017

A study of the potential applications of AM241, and determining the feasibility of using Gamma spectroscopy for future physical validation

Eric A. Feissle

Follow this and additional works at: https://scholarsmine.mst.edu/masters_theses



Part of the [Elementary Particles and Fields and String Theory Commons](#), [Nuclear Commons](#), and the [Nuclear Engineering Commons](#)

Department:

Recommended Citation

Feissle, Eric A., "A study of the potential applications of AM241, and determining the feasibility of using Gamma spectroscopy for future physical validation" (2017). *Masters Theses*. 8074.
https://scholarsmine.mst.edu/masters_theses/8074

This thesis is brought to you by Scholars' Mine, a service of the Missouri S&T Library and Learning Resources. This work is protected by U. S. Copyright Law. Unauthorized use including reproduction for redistribution requires the permission of the copyright holder. For more information, please contact scholarsmine@mst.edu.

**A STUDY OF THE POTENTIAL APPLICATIONS OF AM241, AND
DETERMINING THE FEASIBILITY OF USING GAMMA SPECTROSCOPY
FOR FUTURE PHYSICAL VALIDATION**

BY

ERIC ANTHONY FEISSLE

A THESIS

**Presented to the Faculty of the Graduate School of the
MISSOURI UNIVERSITY OF SCIENCE AND TECHNOLOGY**

In Partial Fulfillment of the Requirements for the Degree

MASTER OF SCIENCE IN NUCLEAR ENGINEERING

2017

Approved by:

Shoaib Usman, Advisor

Xin Liu

Ayodeji B. Alajo

ABSTRACT

Am241 is typically produced via Pu241 decay in a uranium fueled reactor. Presence of Am241 can be used as the age estimation tool for spent fuel, which is a focus of this thesis along with the interest of the measurement and the ratio of production rates of Am241's activation products; Americium-242 and its first excited state of Americium-242m. MCNP models of the core and BEGe 3825 detector were built. These models were compared with established and physical measurements of gamma/x-ray standards that were available at the reactor. Thermal fluxes at 200 kW for potential foils centered in the source holder tube were within a factor of 1.5 when compared to existing known MSTR thermal flux values. Unmodified simulated BEGe 3825 detector full energy peak efficiency values were well within a factor of 2 for both the Mixed and Europium source validation. Am241 build-up in Plutonium can be predicted to be measured to great certainty, using the BEGe 3825 that is available at the reactor by analyzing 59.50 keV using Prospect with estimated net uncertainty of 0.796% and 5.841%, for reactor grade and weapons fuel after 1 year of storage using the corrected BEGe 3825 simulation. Uncertainty values decreased as further time passed. Simulation considered full photon spectrum. Time estimate range values for modified WG plutonium differed by +1.11% and -0.895% error during the specific modified count time 19 year decay case. Study into Am242 and Am242m production revealed that the combined 102.616 keV displays a very reliable simulated Prospect net cps uncertainty around 1-2% free of Am241 photopeaks at irradiation times greater than 30 minutes for both the exempt and non-exempt quantities of Am241 used as standard sources.

ACKNOWLEDGEMENTS

I would like to thank my advisor Dr. Usman for the aid in reviewing this thesis and providing aid throughout the research and writing process. I would like to thank my committee members of Dr. Liu and Dr. Alajo for reviewing and evaluating this thesis, and the Reactor staff for allowing the usage of their equipment. I would like to thank the Office of Graduate Studies for their provision of the Chancellors Fellowship which covered the tuition costs of this Master's degree. I would like to thank my family for their support during my studies.

TABLE OF CONTENTS

	Page
ABSTRACT.....	iii
ACKNOWLEDGEMENTS.....	iv
LIST OF FIGURES	vi
LIST OF TABLES.....	ix
SECTION	
1. PURPOSE/INTRODUCTION.....	1
2. BACKGROUND	4
3. PROCEDURE.....	34
4. PHYSICAL MEASUREMENT OF STANDARDS FOR BEGE 3825	39
5. MODEL DESCRIPTIONS AND VALIDATION WITH PREVIOUS WORK/STANDARD MEASUREMENTS.....	58
6. SIMULATION RESULTS	125
7. CONCLUSIONS/LIMITATIONS.....	162
APPENDICES	
A. SIMULATION CODES AND SCHEMES	167
B. SOURCE CERTIFICATES AND CORE CONFIGURATION	232
REFERENCES	236
VITA.....	238

LIST OF FIGURES

Figure	Page
2.1. Primary reaction, buildup of Am241 and Am242	5
2.2. Burn-up scheme for U235/U238 Fuel	5
2.3. Cross sections of Am241, total, radiative capture, fission.....	6
2.4. Activation branch path ratio for Am241 undergoing radiative capture.....	7
2.5. U235 fission cross section	8
2.6. Am242m is generated from reaction chains involving Pu239, A comparison of Pu239 fission cross sections	8
2.7. Am242 fission cross section	9
2.8. Am242m fission cross section	9
2.9. Typical actinide build-up in 3000 MWth at 1 year irradiation , only initial U235/U238, using 0.0253 eV data, 26 actinides examined for an arbitrary 2% w/0 U235 at 100 metric tons of Uranium, total burn-up is ~11000 MW-d/MT	11
2.10. Am241 build-up behavior in used fuel, production via Pu241, isotopes in final amount under neutron flux in Figure 2.9 allowed to only undergo decay for 5 years with no flux, all 26 isotopes examined during decay.	12
2.11. 5 year decay with only the 6 Plutonium isotopes considered 'reprocessed', no initial Am241 present, same Pu values used behind analysis for Figure 2.10 from the net buildup in arbitrary thermal reactor (Figure 2.9), U235 not included, as it was removed for reprocessing status	13
2.12. Typical weapons grade Plutonium stockpile, decay time since initial Plutonium separation, arbitrary total mass, up to 75 years of decay	16
2.13. Reactor grade Plutonium Am241 build-up behavior to 75 years	16
2.14. Age estimate dependent upon change in Am241 activity.....	18
2.15. Ratio of 1 as arbitrary upper limit was examined in study	19
4.1. Clockwise from top left, end-cap with protective cover, end-cap without protective cover showing carbon window, Mixed isotope cylinder with active disk, Europium disk source	41
4.2. The source and detector orientation.....	41
4.3. Europium standard at 10 minutes of live time.....	45
4.4. Europium standard absolute peak efficiency plot.....	50
4.5. Mixed standard at 10 minutes of live time.....	53
4.6. Mixed standard absolute efficiency plot.....	56

5.1. XY view of the MCNP MSTR 101W approximate.....	60
5.2. XY plane of 10-2016 MCNP Model.....	61
5.3. Standard fuel assembly approximated in MCNP.....	62
5.4. Control rod assembly approximated in MCNP.....	63
5.5. Regulating rod assembly approximated in MCNP.....	63
5.6. Approximate position of current core grid with respect to modeled reactor pool.....	64
5.7. The relative location of tally cells, mimicking proposed test foil, not to scale.....	66
5.8. Schematic of BEGe 3825, as provided by Canberra.....	77
5.9. Diagram of shielding set-up.....	79
5.10. MCNP model of BEGe 3825, and shield.....	80
5.11. Europium FEPE ratio as given by photon/electron treatment option.....	86
5.12. FEPE ratio of Mixed source considering photon/electron treatment options.....	89
5.13. FEPE ratio as a function of simulated active sample position only, actual position is ~1.40 cm above, between Position 2 and Position 3.....	98
5.14. Position tests for simulated 105.3 keV photopeak from Europium inventory.....	99
5.15. Mixed FEPE ratio, as a function of simulated active sample distance only, actual position is ~1.50 cm above carbon window, between simulated Position 1 and Position 2.....	102
5.16. 59.5 keV source-window distance net cps test, error bars included but are not visible at utilized dimensions.....	103
5.17. Full energy peak efficiency (FEPE) ratios as the front inactive Ge layer is increased.....	106
5.18. Simulated Mixed dead layer test results, all other parameters held at measured/given values.....	108
5.19. The Eu FEPE ratio, as a function of simulated active radius, all non-radius parameters fixed to measured/given, 1.40 cm source-window distance.....	111
5.20. The FEPE ratio as a function of spectrum multiplier.....	114
5.21. Mixed FEPE ratio as a function of multiplier.....	117
5.22. Unmodified spectrum difference between MCNP F8 derived and measured spectrum, for Europium source, underestimation occurred below 200 keV in non-examined non-validated peaks that were not a part of the given gamma/x-ray loading, BEGe model corrected (underestimated) background consistently, but uncorrected (overestimated) all photopeaks that were attributed to given source isotopes.....	119
5.23. Corrected (underestimated) count difference for Mixed and Europium count spectrums.....	120

5.24. Corrected FEPE ratio for Europium and Mixed test case.....	124
6.1. Gives a suitable multiplier for an accepted error of Am242, based off of suitably short live measurement time for short lived Am242, ~16 hours.....	141
6.2. Gives a suitable multiplier for an accepted error of Am242m, to be used in conjunction with the above, longer half-life allows for larger live measurement time where Am242m activity can be considered constant	142

LIST OF TABLES

Table	Page
2.1. Thermal fission cross section value comparison	10
2.2. Reactor/Weapons grade Plutonium composition, by weight	14
2.3. Am241 photon energies and intensities	24
2.4. Most intense photon emissions for Am242	25
2.5. Most intense photon emissions for Am242m	26
2.6. Meaning of MCNP relative error for tally	31
4.1. Physical measurement of BEGe 3825 end-cap with and without the protective cover.	39
4.2. Physical measurement of validated photon sources.....	40
4.3. Initial parameters for Europium standard, taken from source certificate	42
4.4. Corrected parameters for Europium standard, taken from source certificate	43
4.5. Calibration equation information taken from the BEGe 3825 detector of interest in reactor bay.....	44
4.6. Automated peak analysis settings used by Prospect software to eliminate human error in determining regions of interest, these settings are used to compare measured and simulated standard spectrums, and then used to analyze Am241/Am242/Am242m activities	46
4.7. Prospect analysis of 10 min Europium standard count.....	47
4.8. Determining the physical detector absolute peak efficiency with the Europium standard.....	48
4.9. Mixed standard initial parameters, taken from source certificate	51
4.10. Corrected Mixed standard parameters, taken from source certificate	52
4.11. Mixed standard peaks of interest	54
4.12. Mixed standard absolute peak efficiencies	55
5.1. MSTR model component certainty	58
5.2. Components of the 101W and 10-2016 approximate	61
5.3. Reactor pool parameters	64
5.4. MCNP kcode parameters for 101W MSTR model flux validation only	65
5.5. Location specific 3 group neutron flux, 200 kW, 101W	67
5.6. Location specific 3 group neutron flux, 100 kW, 101W	67
5.7. MSTR model 101W, 200 kW three group flux estimates	67

5.8. MSTR model 101W, 100 kW three group flux estimates	68
5.9. Source holder position 3 group flux, near core, 200 kW, 101W	68
5.10. Source holder position 3 group flux, near core, 100 kW, 101W	68
5.11. Comparison with 3 group flux for MSTR at 200 kW in the 101W configuration.....	69
5.12. Comparison with 3 group flux for MSTR at 100 kW in the 101W configuration.....	69
5.13. Percentage of 3 group flux for MSTR at 200 kW, 101W	70
5.14. Percentage of established 3 group flux for MSTR at 100 kW, 101W	70
5.15. MCNP statistical checks for F4 validation tallies.....	71
5.16. FOM for F4 validation tallies	72
5.17. Core wide 3 groups neutron flux from MSTR approximate, 200 kW and 100 kW, 10-2016 configuration, approximate flux values expected during a 200 kW irradiation in the source holder tube	73
5.18. Source holder 3 group neutron flux from MSTR approximate, 200kW and 100 kW, 10-2016 configuration	74
5.19. BEGe 3825 model component certainty	75
5.20. BEGe 3825 detector parameters	77
5.21. Shield physical parameters	79
5.22. Color scheme for model figure	80
5.23. Parameters for the GEB setting on the F8 tally	81
5.24. Photon count multiplier (mid, min, max) used on source particle normalized F8 tally results	82
5.25. Europium Prospect automated analysis using three different photon/electron treatments	83
5.26. Mixed source Prospect automated peak analysis considering photon/electron treatment options.....	87
5.27. F8 tally statistical checks for Europium photon/electron method test.....	90
5.28. F8 tally figure of merit and computer run time (minutes) for Europium standard	91
5.29. F8 tally statistical check for Mixed photon/electron options.....	91
5.30. Figure of Merit and computer run time (minutes) for mixed standard	92
5.31. Photon interaction information and alterations used, neutron physics kept at default settings.....	93
5.32. Carbon window to source distance FEPE testing for simulated Eu sample	95
5.33. Mixed simulation FEPE, as a function of carbon window to sample distance.....	100

5.34. Simulated Europium Ge dead layer thickness tests, using local deposition and measured source to window distance	104
5.35. Simulated Mixed front inactive Ge layer tests on FEPE ratio effect.....	107
5.36. Simulated Eu FEPE analysis, as a function of active radius.....	109
5.37. Eu simulated FEPE analysis, as a function of the multiplier.....	112
5.38. Mixed FEPE analysis, as a function of multiplier	115
5.39. BEGe model MCNP parameters for BEGe 3825 model for the validation and experiment simulation runs	118
5.40. Corrected (underestimated) Europium sample simulation tests, all parameters measured/given	121
5.41. Corrected (underestimated) Mixed sample simulation tests, all parameters measured/given.....	123
6.1. Expected equal simulated sample mass of weapons/reactor grade plutonium, initially pure, it is assumed that the plutonium exists in some form such as plutonium dioxide.....	126
6.2. Weapons grade, uncorrected simulated BEGe 3825 response.....	130
6.3. Weapons grade, corrected simulated BEGe 3825 response.....	132
6.4. Weapons grade, corrected, 10 day measurement time, 19 year decay time tests	134
6.5. Reactor grade, uncorrected	135
6.6. Reactor grade corrected	137
6.7. Initial activities and irradiation time cases to allow for irradiation times to be investigated in determining the feasibility of using the BEGe 3825 to determine Am242/Am242m production rates in MSTR	143
6.8. Case 1 Am242 simulated peaks of interest, no viable Am242m peaks, 200 kW, used same Prospect peak search settings as with Mixed and Europium source validation, continuum=.2 FWHM, uncorrected F8 tally/Prospect results (unmodified model).....	145
6.9. Case 1 Prospect analysis for Am242 102 and 118 peaks, using a corrected MCNP derived tally spectrum (modified BEGe 3825 model)	147
6.10. Case 1 Am242 peaks differed in reliability when analyzed by Prospect; changing the continuum setting in increments of .2 FWHM for 11 runs showcased the well-defined Am242 peak of 102.616 keV, while the 118.247 suffered from its close proximity to said 102.616 keV peak (uncorrected case) (unmodified model).....	149
6.11. Case 1 peak analysis by Prospect, testing effect of continuum setting from .01 to 2 FWHM, for the assumed corrected spectrum tally (modified model).....	149

6.12. Comparison between the photon rates of Am242 and the pre-existing Am241 photon rates for Case 1 in the energy regions of interest	150
6.13. Comparison of Am241 and Am242 photon rates for the peaks of interest used to measure Am242 for Case 1	150
6.14. Case 2 Am242 peaks, no viable peaks of Am242m were detected, net cps and uncertainty values were obtained using Prospect peak setting 'continuum' value of .2 FWHM, similar to Mixed and Europium comparison tests. uncorrected Prospect analysis (unmodified BEGe 3825 model)	153
6.15. Case 2 corrected simulated BEGe 3825 response for Am242 102 and 118 keV peak analyses (modified BEGe 3825 model)	155
6.16. Outcome of Prospect peak analysis when the setting 'continuum estimate' is increased by .2 FWHM for 11 runs for Case 2, uncorrected (unmodified model F8 tally)	157
6.17. Outcome of Prospect peak analysis when the setting 'continuum estimate' is increased by .2 FWHM for 11 runs for Case 2, corrected (modified model F8 tally)	157
6.18. Compiles photon rate of Am242 to Am241 for Case 2 burn data in the energy regions of interest	158
6.19. Compares photon rates in energy ranges 99-105 and 113-124 for photopeaks of Am241 to generated photon rates of Am242 at the given burn times for Case 2, to show that small times Am241 contaminates the energy regions of interest for Am242	160

1. PURPOSE/INTRODUCTION

The purpose of this study is two-fold, but both goals are centered around the isotope Americium-241, its suitability to determine the age of Pu based fuel, and for the production of Am²⁴²/Am^{242m} in the MSTR from a standard sample of Am²⁴¹. The study provides a path to develop and optimize the technique through simulation of an irradiation experiment in the MSTR involving pure Am²⁴¹ to examine the production rates of its activation products of Am²⁴² and Am^{242m} in the MSTR's source holder tube directly after irradiation in a single measurement without using Am^{242m}/Am²⁴² isomeric transition and secular equilibrium to back calculate Am^{242m} activity indirectly. Subsequently, simulation of detector and gamma emissions from the irradiated Am²⁴¹'s Am²⁴² and Am^{242m} provided the estimate of the net efficiency of the proposed technique of direct detection of Am²⁴² and Am^{242m} photopeaks with the BEGe 3825. Goal one is to examine how Am-241 is produced in a typical thermal reactor fuel where U²³⁵ enrichment is an average 2% (arbitrarily chosen for general investigation of behavior) by weight, as well as to examine the potential application of Am²⁴¹ in dating the pre-MOX fuel's Pu²⁴¹ component of reactor/weapons grade plutonium for a series of mock decay times, using established reactor/weapons grade plutonium isotopic fractions. These results will allow for the determination of the time-span at which the Plutonium was formed into PuO₂ before the inclusion into MOX fuel via measuring the buildup in Am²⁴¹ (Travers, 1999). The other goal is to determine the feasibility of developing and optimizing Gamma Spectroscopy to measure Am-241 after irradiating at 200 kW, for 1 minute, 30 minute, and 8 hour in the MSTR to determine the production rates of Am²⁴² and Am^{242m}. Two standard sources were examined for this purpose; a NRC exempt quantity of pure Am²⁴¹ and a non-exempt pure sample. The connection between both goals lie in the validation of the BEGe detector model, which uses a Am²⁴¹ validation source, with a given activity, and the simulated behavior of Am²⁴¹ in the foils used by the computer models. While the Am^{242m}/Am²⁴² detection tests and production rate investigation uses a MCNP model of the MSTR, for reactor and weapon grade materials Am²⁴¹ content in a Plutonium inventory was varied to reflect typical values for an arbitrary sized simulated sample to generate the resultant isotope. A series of decay times were simulated post measurement by BEGe detector to determine the range of

decay times at which Am²⁴¹'s 59.50 keV peak becomes viable in the BEGe 3825, and thus useful in quantifying the age of the plutonium sample. Mixed Oxide Fuel is one method of removing Pu²³⁹ from the supply, as a means to limit proliferation. Gamma spectroscopy would offer the advantage of non-destructive testing on the sample, and thus allow for multiple irradiations with the same foil or sample for the long-lived Am^{242m} and Am²⁴¹, allowing for the evaluation of how the saturation activity changes in different neutron energy environments in the core, as well as help to avoid any chemical separation techniques. This isotope (Am²⁴¹) is a long-term contributor to radioactivity when compared to the shorter half-lives of the uranium fission products. Am²⁴¹ is produced via the beta- decay from Pu²⁴¹ with its half-life of 14.29 years \pm 2.2 days. Am-241 undergoes fission as well as radiative capture reactions. Its activation products of Am-242 and Am-242m have much higher thermal fission cross sections compared to the base of Am²⁴¹, and the first excited state Am-242m has a half-life of 141.0 \pm 2 years, while the ground state of Am²⁴² has a half-life of 16.02 hours \pm 1.2 minutes (Chadwick, Herman, Oblozinsky, & et al., 2011). The utility of Am-242m as a fissile material has been noted due to its relatively stable form and much higher fission cross section when compared with U²³⁵ and Pu²³⁹ (see next section). The branch yield between the ground state of Am-242 and the excited state of Am-242m is energy dependent, but at thermal energies skews toward the ground state. When a pure sample of Am-241 is burned in the MSTR, fission products, activation products and decay products are produced. Their impact is expected to cause an interference with the count in the shielded BEGe 3825 detector in the reactor bay for the Am-242m which has its most intense gamma emission at 49 keV. Am²⁴² most intense photon emissions are the result of a series of highly compacted x-rays centered in the 102 and 118 keV energy region, with a weighted centroids of 102.616, 118.247 keV. Using a MCNP model of the MSTR, a simulated sample of pure Am-241 is deposited onto an Aluminum plate, which is then irradiated, the resulting activation, fission and decay products can be tracked by the MCNPX code. Similar foil geometry will be utilized for the Plutonium/Am²⁴¹ investigation for its 59.50 keV gamma which is its most intense peak above 40 keV. For the purposes of this study, the projected activities for each simulated burn/analysis will be taken as true activities when comparing their simulated spectrums in the BEGe 3825

model to determine when the peaks from Am-242m, Am242, and Am241 become viable in their respective background spectrums. By using Canberra's Prospect's analysis software, performing automated/and fitted peak analysis on simulated spectrums from a validated model of BEGe 3825, the optimized irradiation parameters for the physical experiment and Plutonium/Am241 behavior over decay time parameters can be estimated. All photon energies and intensities are taken from the ENDF/B-VII.1 radioactive decay library.

2. BACKGROUND

Am-241 is produced in reactors via the decay of Pu-241, which is itself produced from neutron capture events with Uranium and Plutonium. For the second goal of examining Am242/Am242m production rates in the MSTR, the exempt quantity of Am241 that can be utilized without NRC regulations is .05 μCi , will be simulated via MCNP (NRC, n.d.), and compared with a non-exempt quantity of 1 μCi . Both resultant simulated isotope loadings will be used to generate simulation results of their activations and to determine the viability of using gamma spectroscopy (via the BEGe 3825 detector) to measure the resultant Am242 and Am242m activities for the purpose of determining the age and other characteristics of the spent fuel. The first excited state of Americium-242 (242m) has been examined as a fuel material due to its greater fission cross section at thermal and intermediate energies. It has been investigated for its use in outer space applications due to its potential for a very compact foil arranged core (Benetti, Cesana, Cinotti, Raselli, & Terrani, 2006). Although the simulations used by this study is only concerned with the behavior of a pre-existing amount of pure Am-241 and its activation products, the production method and general buildup of its parent, Pu241, in a typical thermal commercial reactor. The isotope Pu241 would be carried over into MOX fuel, and decay to Am241 any successful high fidelity measurement of Am241 can be used to determine the age of MOX fuel (Tsoulfanidis, *The Nuclear Fuel Cycle*, 2013). The Net burn-up scheme for Pu241 and subsequently Am241, Am242m and Am242, was examined in depth with a forward difference scheme with typical thermal reactor parameters in Figure 2.2, this scheme will also examine isotope decay-only for initially pure Plutonium isotopes. Figure 2.1 shows the primary reaction of interest for this study, the buildup of Am241 (half-life of 432.608 years) and Am242 (half-life of 16.02 hours), with their respective photon energies. These photon energies are the target to investigate the validity of using the BEGe 3825 detector in the described applications. The irradiation of Am241 to Am242 can be utilized to substitute for Am241, as its half-life is much less than Am241. Saturation activity after a suitable period of irradiation (saturation activity not goal of study, only detection with on-campus BEGe 3825) would then allow the Am241 activity to be estimated. This situation might arise if its 59.50 keV peak is overshadowed by another isotope's similar energy photopeak.

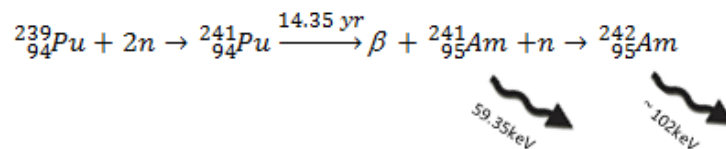


Figure 2.1. Primary reaction, buildup of Am²⁴¹ and Am²⁴²



Figure 2.2. Burn-up scheme for U²³⁵/U²³⁸ Fuel, data obtained via (Chadwick, Herman, Oblozinsky, & et al., 2011)

Am²⁴¹'s energy dependent radiative capture cross sections are of principal interest. For Am-241, its radiative, total and fission cross sections are given in Figure 2.3. Decay scheme for Figure 2.2 represents the scope of the Forward Euler burnup system, as well as for the buildup of Am²⁴¹ in weapons and reactor grade plutonium samples. Further addition was ignored as photon rates of potential additions were compared with starting and target photopeaks to ensure that they would be negligible and could be ignored. As shown in Figure 2.3, the radiative capture cross section is dominated by the thermal energy groups. As the MSTR is noted as a thermal reactor, the validation of a MCNP model will primarily examine this low energy for its neutron flux values. With the thermal groups Outsized impact in the reaction rates, the ability for the MSTR MCNP model to accurately predict neutron flux values for a given core configuration will be crucial to provide a baseline for a physical irradiation.

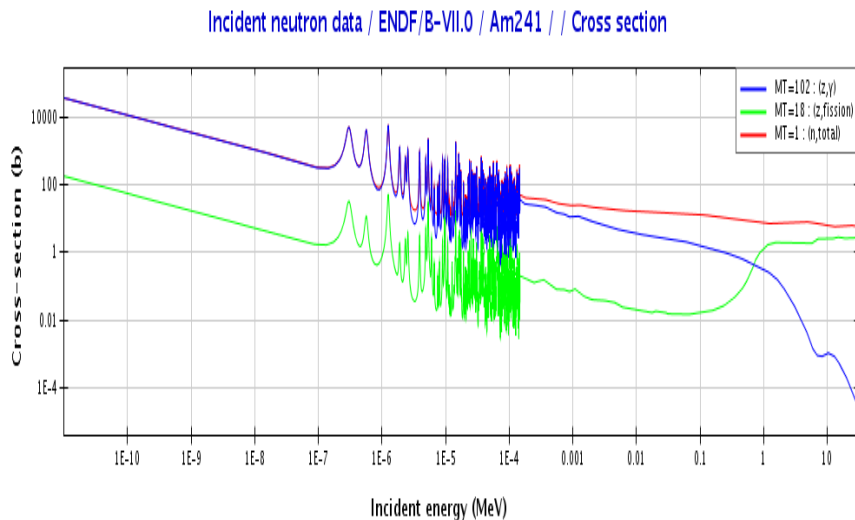


Figure 2.3. Cross sections of Am241, total, radiative capture, fission (Chadwick, Oblozinsky, Herman, & al, 2006) (OECD-NEA, 2013)

Its branch ratio when activated to Am-242 or Am-242m is given below in Figure 2.4; it is also dependent on the neutron energy. For this study its final approximation was obtained by measuring the ratio of linear reaction rates within the simulated MSTR, as well as in the future. This value will be the energy integrated production rate ratio of Am242 and then Am242m, skewed toward the thermal region for the MSTR. As one goal of this thesis is to examine the viability of measuring Am242 and Am242m, the subsequent action is to take the measurements and derive the production rates of Am242 and Am242m. This value could then be used to further provide a benchmark to validate the current MCNP model of the MSTR. As mentioned above, this value should be around 0.10, as the thermal neutron flux groups dominate in the MSTR core. Knowledge of this value for the MSTR could also allow for future experiments in which the more active and emissive Am242 could be used to predict the production rate Am242m for short irradiation times. Am242m production inside of the MSTR, while expected, would suffer due to its thermal dominance which would limit the amount of Am242m that could be produced for any given mass of Am241 and irradiation time. For this study, Am242m, like Am242 was investigated for with the BEGe 3825 available on campus.

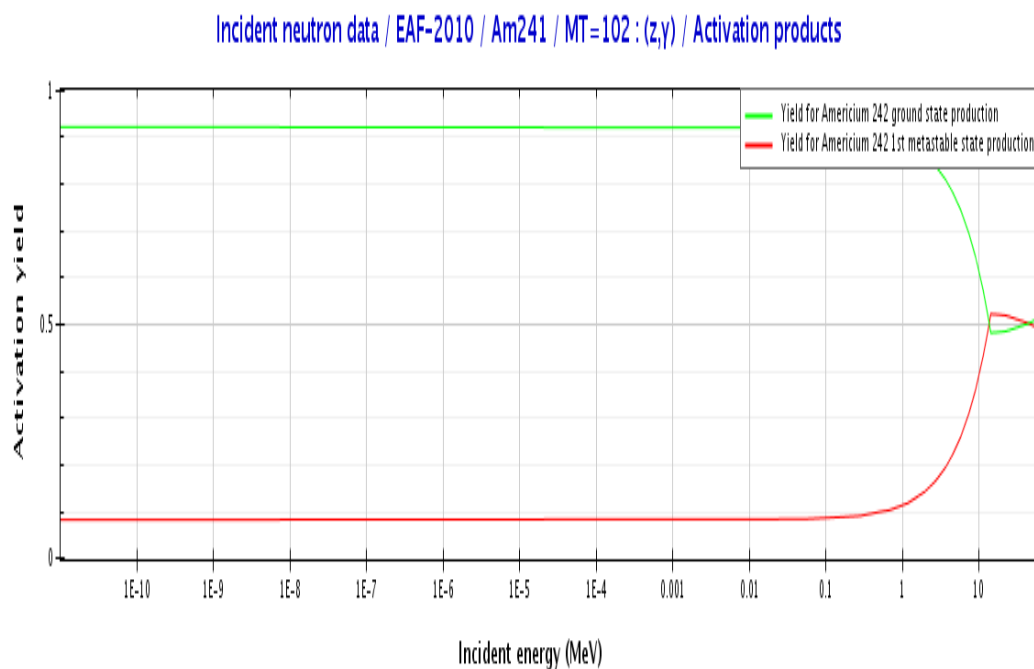


Figure 2.4. Activation branch path ratio for Am241 undergoing radiative capture (Chadwick, Oblozinsky, Herman, & al, 2006) (OECD-NEA, 2013)

Due to inconsistencies, the branch path ratio data was taken from EAF-2010 data rather than the ENDF/B-VII.0 data which matches the .70c library that was chosen in MCNP for Am241. The EAF-2010 data was chosen to show the general trend of the branch ratio, its precise value is handled via the ENDF/B-VII.0 data as well. The interest in Am-242m stems from its high fission cross section compared to common fissile isotopes U-235 and Pu-239, as seen in Figures 2.5, 2.6, 2.7 and 2.8. Am-242 fission cross section are included as well, but its half-life of $16.02 \text{ hrs} \pm 1 \text{ min}$, would limit its useful application as a stable fuel source. Although this study does not examine Am242m as a fissile fuel mass for a reactor, its production was simulated via MCNPX in order to determine if the BEGe 3825 was capable of measuring its photopeaks. If the detector that is located on campus is unable to measure the gamma/x-ray emissions of Am242m's decay, then another method would have to be undertaken, to measure its alpha particle output. This would open up new difficulties as only 0.459% of Am242m disintegrations involve alpha decay. Coupled with the expected Am241 dominant alpha decay, detector

resolution will need to be of great quality. This alpha spectrometry matter was not further explored by this thesis, only the gamma and x-ray emissions for Am242m were examined for. To further highlight the potential of Am242m, fission cross sections were given for U235, Pu239 to be compared with Am242m as well as Am242.

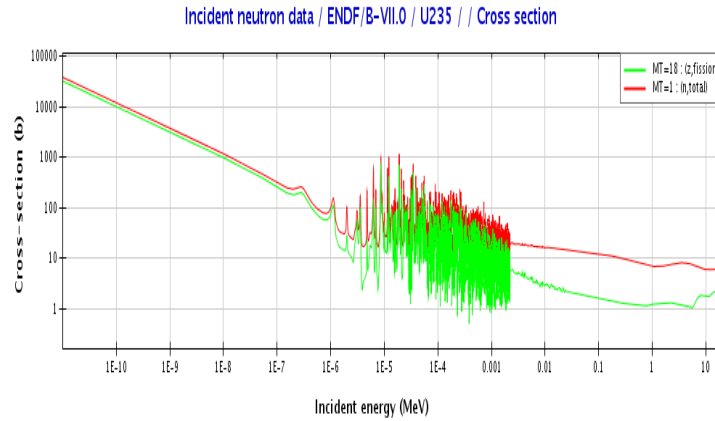


Figure 2.5. U235 fission cross section (Chadwick, Oblozinsky, Herman, & al, 2006) (OECD-NEA, 2013)

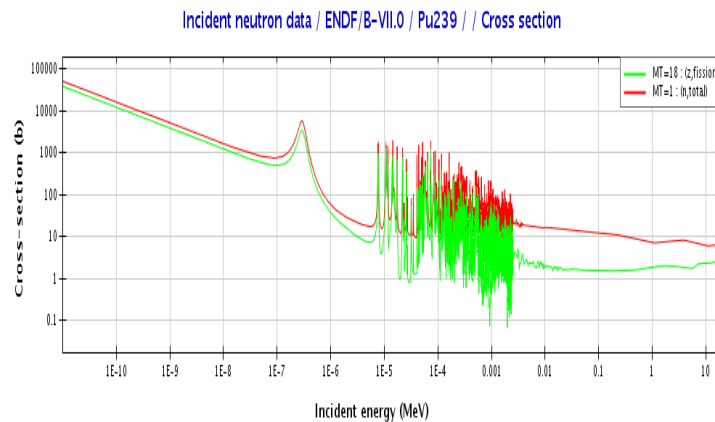


Figure 2.6. Am242m is generated from reaction chains involving Pu239, A comparison of Pu239 fission cross sections (Chadwick, Oblozinsky, Herman, & al, 2006) (OECD-NEA, 2013)

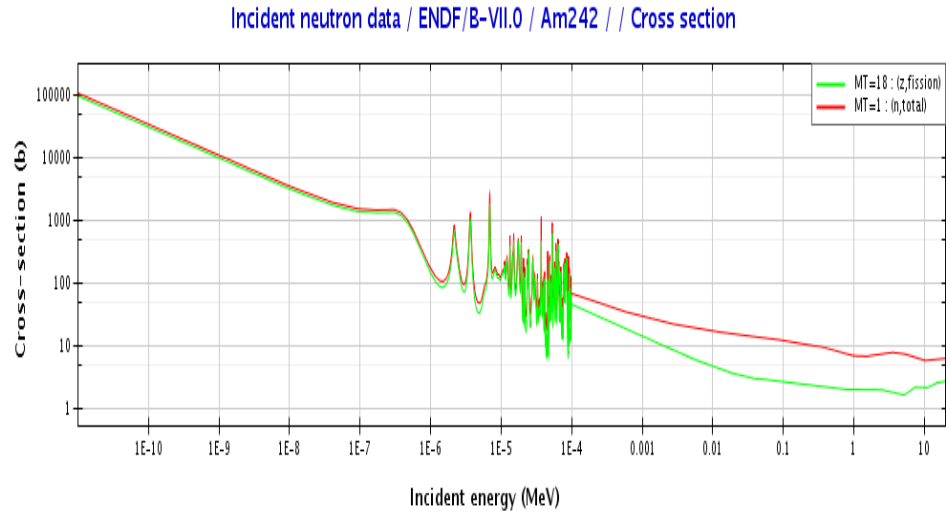


Figure 2.7. Am242 fission cross section (Chadwick, Oblozinsky, Herman, & al, 2006)
(OECD-NEA, 2013)

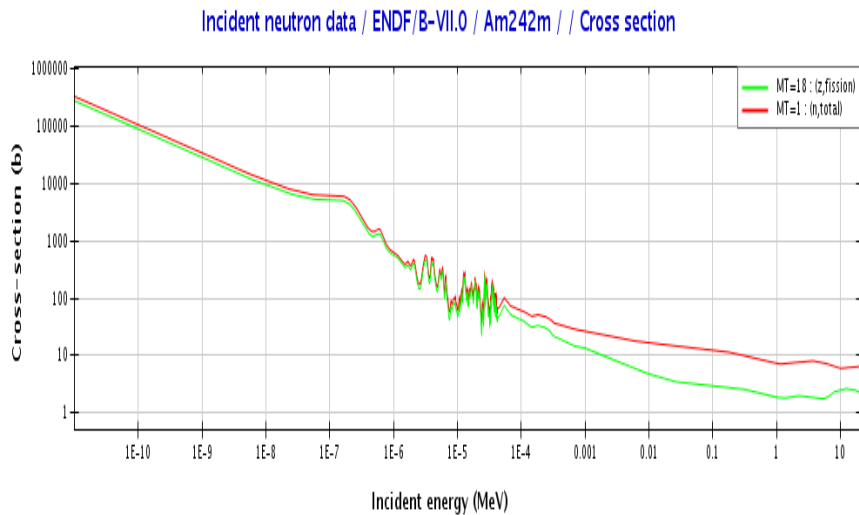


Figure 2.8. Am242m fission cross section (Chadwick, Oblozinsky, Herman, & al, 2006)
(OECD-NEA, 2013)

In the energy region of .0253 eV, Am242m fission cross section is far greater than U-235 and Pu-239. As given by Table 2.1 below, this draws the values from the plot for

clarity, uncertainties were not included in Table 2.1. Am242m use as a fissile material is of great potential, but not the primary purpose of this study.

Table 2.1. Thermal fission cross section value comparison

Isotope	Fission cross section at .0253 eV (b) (ENDF/B-VII.0)
U-235	584.9773
Pu-239	747.8344
Am-242	2094.862
Am-242m	6400.444

The production of Am241, the base isotope of interest in this study, originates from the beta- decay of Pu241, which the majority of all Pu241 decay leads to:



This reaction is simulated with MCNP for the MSTR's source holder tube location, and a 1-group approximation. The 63 group MCNP approximation of the neutron groups is expected to be more accurate than a 1-group assumption, but run at a slower pace compared to the 1-group scheme. The 1-group scheme will be used to provide a quick way to explore isotope behavior without considering the exact geometry of the MSTR or an approximated neutron flux spectrum. All analysis will be done using MCNPX.

$$\frac{dN_{Pu241}}{dt} = N_{Pu240}\sigma_{\gamma,Pu240}(E)\phi(E,r) + \lambda_{Np241}N_{Np241} - \lambda_{Pu241}N_{Pu241} - N_{Pu241}\sigma_{a,Pu241}(E)\phi(E,r) \quad (2)$$

$$\frac{dN_{Am241}}{dt} = .999976\lambda_{Pu241}N_{Pu241} - \lambda_{Am241}N_{Am241} - N_{Am241}\sigma_{a,Am241}(E)\phi(E,r) \quad (3)$$

A Forward Euler difference scheme was constructed examining the 26 isotopes shown in the chart above. A typical 3000 MWt thermal reactor with 100 tons of Uranium, with enrichment of 2% by weight of U235 was assumed for the purpose of examining Pu241 buildup over the course of 1 year (between refueling) with the same fuel considered (Duderstadt & Hamilton, 1976), and then decay for an arbitrary 5 years to examine Am241 production in typical commercial thermal reactors, as shown in Figure 2.9. All fission, radiative and absorption cross sections are at the .0253 eV values, as is branching activation yield fractions. All of the physical constants for the nuclides are taken from the specified source (Chadwick, Herman, Oblozinsky, & et al., 2011).

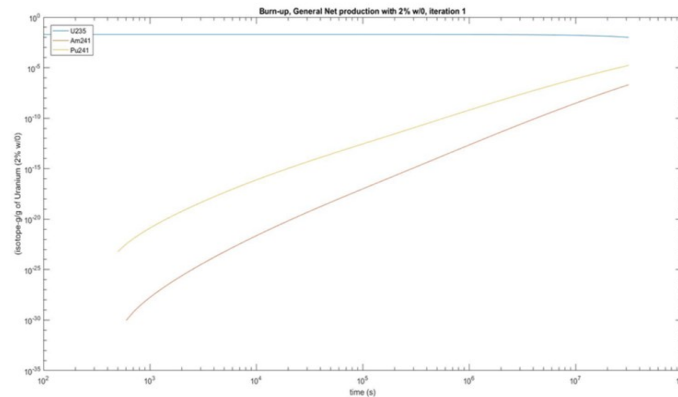


Figure 2.9. Typical actinide build-up in 3000 MWth at 1 year irradiation , only initial U235/U238, using 0.0253 eV data, 26 actinides examined for an arbitrary 2% w/o U235 at 100 metric tons of Uranium, total burn-up is ~11000 MW-d/MT

The Am241 production during entire inventory decay only was examined over 5 years, via Pu-241, as shown in Figure 2.10. 5 years being an upper range value before fuel replacement and storage or reprocessing.

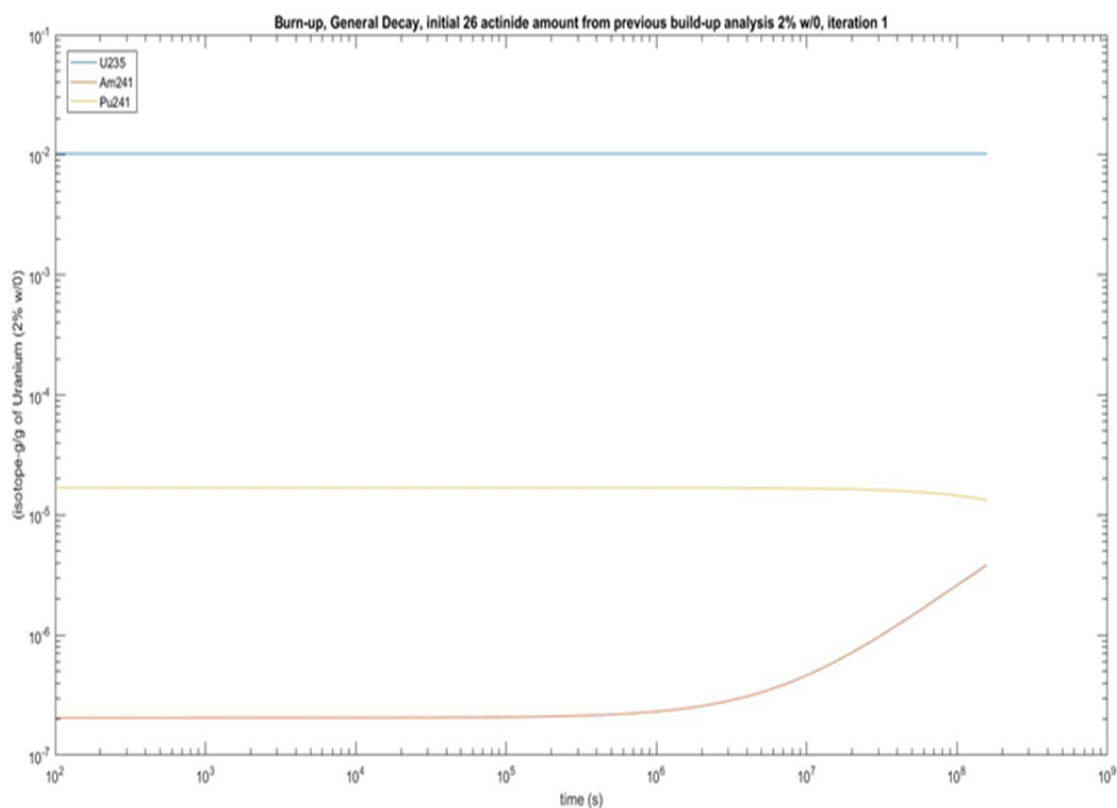


Figure 2.10. Am241 build-up behavior in used fuel, production via Pu241, isotopes in final amount under neutron flux in Figure 2.9 allowed to only undergo decay for 5 years with no flux, all 26 isotopes examined during decay

Since Am241 is produced only by Pu241 decay, for the scenario where the reactor-grade plutonium was reprocessed, the 5 year decay with only initial Plutonium isotopes was examined (all other initial non-plutonium actinides set to 0) and is shown in Figure 2.11. All non-plutonium isotopes were removed, and only the plutonium isotopes were allowed to decay for the 5 years. This was to analyze the Am241 buildup that could be expected from the plutonium generated in thermal reactor grade fuel alone, and to

ignore the Am241 that was built-up during the power production stage of the fuel, when decay rates were competing with production and radiative capture rates.

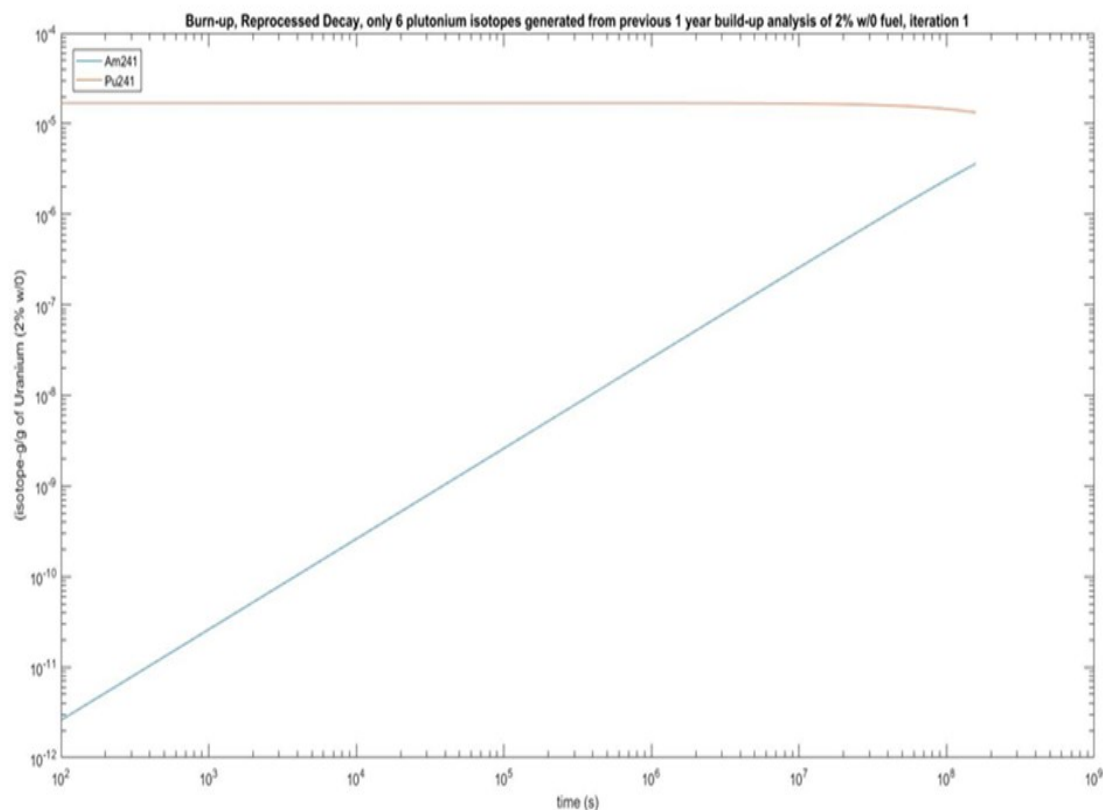


Figure 2.11. 5 year decay with only the 6 Plutonium isotopes considered 'reprocessed', no initial Am241 present, same Pu values used behind analysis for Figure 2.10 from the net buildup in arbitrary thermal reactor (Figure 2.9), U235 not included, as it was removed for reprocessing status

As seen by Figure 2.10 (Decay alone analysis for all 26 actinides), Am241 production via decay of a Pu241 alone occurs more slowly than when the Pu241 amount was increasing under irradiation in a thermal reactor. Am241 is produced only by Pu241 decay, for the scenario where the general reactor-grade plutonium was reprocessed, the 5 year decay with only initial Plutonium isotopes was examined (Figure 2.11) (all other

initial non-plutonium actinides set to 0) to show the production of Am241 from an initially zero amount, which would otherwise be obscured by the already present Am241 activity. In Figure 2.10 and Figure 2.11 the Am241/Pu241 quantities (U235 for Figure 2.10) are normalized to the feed material (Uranium (arbitrary) 2% w/o), to showcase the two different scenarios in which Am241 is produced, in used vs reprocessed fuel. The used fuel Pu241 and reprocessed Pu241 are both still dependent upon their initial U238/U235 amounts, which is why that normalization is used. As expected, the only difference between Figure 2.10 and Figure 2.11 is the magnitude and initial quantity of Am241. In both initial composition scenarios as Pu241 is no longer being produced via Uranium, production rates of Am241 will decline as Pu241 decays. In this study, a scenario will be examined where simulated samples of reprocessed Plutonium of various isotopic compositions will be allowed to decay for 1,5 and 19 years, with their photon inventories examined via a BEGe 3825 model to test for the viability of using that detector type to measure Am241's 59.50 keV peak to determine sample lifetime.

The photon analysis of simulated Plutonium samples assumed a sample of certain mass with given Plutonium isotopic fractions for reactor and weapons grade plutonium in metallic/chemical form options that would then be deposited into MOX fuel. The analysis below is not connected to the above Am241 buildup plots (Figure 2.9 to 2.11), but rather with an arbitrarily small known mass ($5.00\text{E}-07$ g) of a simulated WG/RG Plutonium stockpile (Table 2.2), to test the capability of using the BEGe 3825 to determine stockpile age when initial composition is unknown. This small amount will provide a trial case; where under relatively low changing activities of Am241 throughout time are used to determine sample age.

Table 2.2. Reactor/Weapons grade Plutonium composition, by weight (Travers, 1999)

Isotope	Weapons Grade (w/o)%	Reactor Grade (w/o)%
Pu238	0.05	1.0

Table 2.2. Reactor/Weapons grade Plutonium composition, by weight (Travers, 1999)
(cont.)

Pu239	94.3	59.0
Pu240	5.0	24.0
Pu241	0.6	11.0
Pu242	0.05	5.0

The above data will be utilized in an arbitrarily small sample of Plutonium (to represent a check for a given stockpile of Plutonium) to examine the resulting isotope inventories after a series of decay times, and then insert the full gamma/x-ray distributions through the validated BEGe 3825 model to look for Am241 59.50 keV peak as a representation of its build-up, and use the simulated Prospect derived net cps and the measured FEPE for the 59.50 keV region (using Europium disk source since foil modeled with same normal vector as disk with respect to detector carbon window) to determine the decay time for the sample, and thus the age of the stockpile. Although Am241's simulated photon detector response behavior at times greater than 20 years was not examined, the behavior of the atom quantity Am241 as a function of decay time and initial Pu241 atom count, was. For a decay time of 75 years ('Old' Plutonium stockpiles) the atom count/activity of Am241 and Pu241 using WG typical initial compositions are shown Figure 2.12, while for RG the composition time dependence is shown in Figure 2.13. As the mass of the sample will be kept similar for both the weapons and reactor grade plutonium, to simulate lack of knowledge of their compositions, the reactor grade plutonium will have more Am241 mass at a certain point in time compared to the weapons grade plutonium. This means that the reactor grade is expected to require less counting time to ensure low net peak uncertainty, when compared to the weapons grade, which have to be compensated with an increased mass of the stockpile taken as a sample,

or merely increasing the counting time, while keeping in mind the time span between measurements that plays an impact in the upper age value before divergence to infinity.

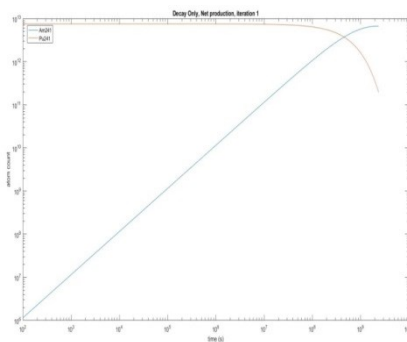


Figure 2.12. Typical weapons grade Plutonium stockpile, decay time since initial Plutonium separation, arbitrary total mass, up to 75 years of decay

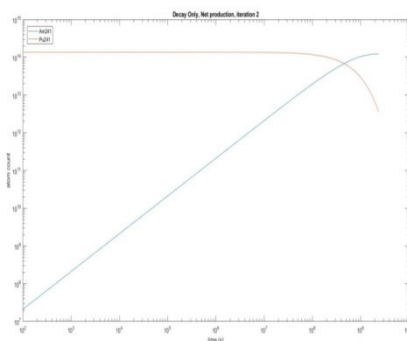


Figure 2.13. Reactor grade Plutonium Am241 build-up behavior to 75 years

Buildup in Am241 activity can be tracked with multiple measurements at known times, allowing the back extrapolation to when the Am241 activity was negligible, the moment when the Plutonium isotopes were chemically separated and purified into the reactor or weapons grade stockpile. The activities or the measured count rates (with a known time spacing) of a plutonium sample that has been allowed to decay for a certain amount of time will be utilized to back calculate for the true age of the plutonium sample,

where the Am241 content was zero. Utilizing the general decay chain equation for the activity at multiple points in time (Lamarsh & Baratta, 2001), the ratio of net count values could be derived for. Both t_1 and t_2 are included in the equation, but for this study, t_1 will be taken as 0.

$$\alpha_{B,1} = \alpha_{B,0}e^{-\lambda_B(t_1+t_x)} + \frac{\alpha_{A,0}\lambda_B}{\lambda_B - \lambda_A}(e^{-\lambda_A(t_1+t_x)} - e^{-\lambda_B(t_1+t_x)}) \quad (4)$$

And:

$$\alpha_{B,2} = \alpha_{B,0}e^{-\lambda_B(t_2+t_x)} + \frac{\alpha_{A,0}\lambda_B}{\lambda_B - \lambda_A}(e^{-\lambda_A(t_2+t_x)} - e^{-\lambda_B(t_2+t_x)}) \quad (5)$$

When taking their ratio, the unknown t_x , the age of the plutonium sample at the moment it was reprocessed from the material that it was generated from, can be solved for. t_1 for this study was always taken to be 0, as the span between 2 measurements were only considered. The net count rates for Am241 59.50 keV peak can be used approximate the activities if the uncertainty in the count rate is small.

$$R_{cps} = \frac{N_{cps,1}}{N_{cps,2}} \approx R_\alpha = \frac{\alpha_{B,1}}{\alpha_{B,2}} = \frac{e^{-\lambda_A(t_1+t_x)} - e^{-\lambda_B(t_1+t_x)}}{e^{-\lambda_A(t_2+t_x)} - e^{-\lambda_B(t_2+t_x)}} \quad (6)$$

In this study, the Newton-Raphson method was utilized in order to solve for the unknown age of the Pu sample and thus the age of the stockpile where it had originated from (Ackleh, Allen, Hearfott, & Seshaiyer).

$$f(t_x) = \frac{e^{-\lambda_A(t_1+t_x)} - e^{-\lambda_B(t_1+t_x)}}{e^{-\lambda_A(t_2+t_x)} - e^{-\lambda_B(t_2+t_x)}} - \frac{N_{cps,1}}{N_{cps,2}} = 0 \quad (7)$$

With the final iterative scheme given as:

$$t_{x,n+1} = t_{x,n} - \frac{f(t_{x,n})}{f'(t_{x,n})} \quad (8)$$

This is the Newton-Raphson root finder method. The derivative of the function is given in the relative function of the scheme in the Appendix A for this specific problem. It is expected that this manner of determining the age of the Plutonium sample is limited, in that it requires the amount of Am241 to change relative to the previous measurement. When the ratio of net count rates were taken to ~ 1 , for a set of time spans of .1, .2, .3, .4, .5, 1, 1.5 and 2 years, the maximum age that could be predicted and considered accurate when the ratio between subsequent counts is less than 1 was ~ 72 years (actual upper time at ratio=1 dependent upon time spans), before Am241 activity stopped changing (ratio=1, dependent upon time span) in the sample and stockpile (Figure 2.14 and Figure 2.15). 72 years is deemed acceptable when considering potential age of stockpiles, with the examined time spans between measurements.

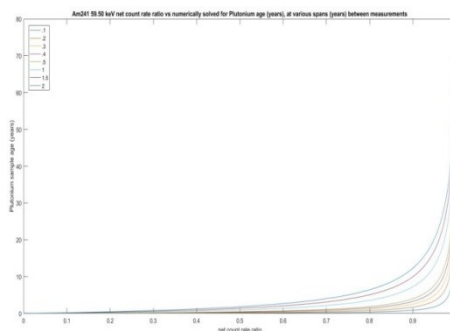


Figure 2.14. Age estimate dependent upon change in Am241 activity

Variations in age estimate for a single ratio value exist in the non-extremes of the plot as the ratio is dependent upon time span, and is unique for a given case. Figure 2.14 should only be examined for the general behavior and the time limit for existence of the age estimates as the ratio varies from $0 < \text{ratio} \leq 1$ (arbitrary range). For when the ratio is greater than 1 (at examined timespans), the method sometimes converges and other times diverge (to infinity), depending on the magnitude of the time span proportional to the ratio greater than 1. At the examined time spans, it is considered in this paper that divergence occurs when ratio is greater than 1 and stated as such in later sections, but this

is not necessarily true. The greater the time span, the greater beyond 1 the ratio can be taken, at small time spans, the upper possible age estimate decreases, as one would expect. A ratio value is dependent upon the time span and its respective data points, they are not independent values, and would have to be matched together, Figure 2.14 only offers 8 time span cases. Figure 2.15 is zoomed in on the $\sim < 1$ net count ratio values. It is noted that for Figure 2.14 and 2.15 that the selected ratio value only went from 0 to 1, but at the higher examined time spans, such as 1.5 and 2 years, the Newton-Raphson method was able to exceed 1 by a small amount, before diverging using the specific test ratio step sizes as shown in Appendix A. This study ignores a scenario where the Am241 will be declining in a sample from a stockpile. Divergence observations are limited to specific testing parameters as shown in Appendix A, due to sensitivity of the method to ratios.

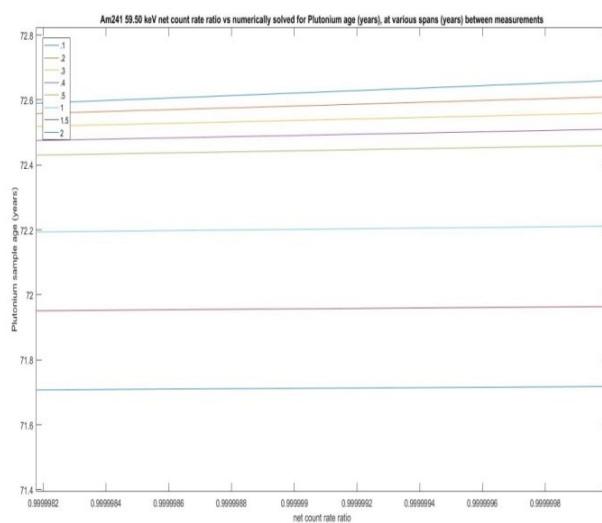


Figure 2.15. Ratio of 1 as arbitrary upper limit was examined in study

For the analysis involving a test case of plutonium, it is expected that simulated uncertainty in the net count rate will require a measurement span greater than 6 months, if the simulated counting times are kept at 1 hour. Uncertainty is expected to decrease if the counting time was increased, and is shown in the analysis to be true as a special case,

where some weapons grade plutonium time estimates exhibit an unacceptable age estimate range.

For the analysis that prepares for a future irradiation of a pure dedicated foil of Am241 to validate MCNP derived production rates of Am242 and Am242m, the behavior of a simulated sample of Am-241 in the steady state MSTR under the influence of its constant in time neutron flux is expected to be modeled by (Duderstadt & Hamilton, 1976):

$$\frac{dN_{Am241}}{dt} = -\lambda_{Am241}N_{Am241} - N_{Am241}\sigma_{a,Am241}(E)\phi(E, r) \quad (9)$$

No production terms were included, since the irradiation target is assumed to be free of all other actinides, except trace amounts of Np-237. For the net production of Am-242 and Am-242m the following buildup equation is derived, and utilized for the Forward Euler 1-group burn-up scheme. MCNPX will deploy a similar burn-up scheme. This 1-group simple burnup will use the thermal group cross sections and half-life data from the same compiled source. The goal will be use the faster run-time of the 1-group code to make predictions and preparations.

$$\begin{aligned} \frac{dN_{Am242}}{dt} = & \alpha_{Am242}(E)N_{Am241}\sigma_{\gamma,Am241}(E)\phi(E, r) \\ & - \lambda_{Am242}N_{Am242} - N_{Am242}\sigma_{a,Am242}(E)\phi(E, r) \end{aligned} \quad (10)$$

$$\begin{aligned} \frac{dN_{Am242m}}{dt} = & \alpha_{Am242m}(E)N_{Am241}\sigma_{\gamma,Am241}(E)\phi(E, r) \\ & - \lambda_{Am242m}N_{Am242m} \\ & - N_{Am242m}\sigma_{a,Am242m}(E)\phi(E, r) \end{aligned} \quad (11)$$

If a one-group effective flux and absorption/radiative capture cross sections were utilized, the above ODE's have the well-established general activated isotope (i+1) solution as a function of time (Tsoulfanidis & Landsberger, 2011):

$$N_{i+1}(t) = \frac{1}{\lambda_{i+1}} \frac{\sigma_i N_i(t) \phi}{1 + \frac{(\sigma_{i+1} - \sigma_i) \phi}{\lambda_{i+1}}} (e^{(-\sigma_i \phi t)} - e^{-(\lambda_{i+1} + \sigma_{i+1} \phi)t}) \quad (13)$$

For the short irradiation times relative to activated half-life and absorption cross section, the exponential terms are approximated as:

$$e^{(-\sigma_i \phi t)} \approx 1 - \sigma_i \phi t \quad (14)$$

And then the next simplification is given by the following:

$$e^{-(\lambda_{i+1} + \sigma_{i+1} \phi)t} \approx 1 - (\lambda_{i+1} + \sigma_{i+1} \phi)t \quad (15)$$

Production term (radiation capture) for the activated isotope being noted as:

$$P = \sigma_i N_i(0) \phi \quad (16)$$

This then allows for the Production rates alone to be determined for a given final Am242, Am242m activity and irradiation time. Since MCNP values are used in this study when determining Am242, Am242m reaction rates, there is no time delay or need to consider measurement procedures. The energy and space integrated Net reaction rates derived from experimental output data simplify to:

$$P = \frac{N_{i+1}(t)}{t_{irr}} \quad (17)$$

Since over a short irradiation time (relative to Am242's half-life) the production terms dominate and the activity build-up is linear in nature, the net energy and space integrated reaction rates will simplify to their respective production rates in a manner equal to the above approximations for the double integrals shown below. The following equations will not be solved, but will be simplified and simulated output data will be used to provide for the approximations. The following simplifications are only valid over short irradiation times, when the production from radiative capture of Am241 is dominant and all other destruction rates are negligible. Due to this time constraint, conditions to reach saturation activity will not be simulated with MCNPX, rather the goal will be the shortest irradiation time that yields viable photopeaks of Am242 and/or Am242m.

$$P_{Am242} = \iint \alpha_{Am242}(E) N_{Am241}(t) \sigma_{\gamma, Am241}(E) \phi(E, r) dE dr \quad (18)$$

$$P_{Am242m} = \iint \alpha_{Am242m}(E) N_{Am241}(t) \sigma_{\gamma, Am241}(E) \phi(E, r) dE dr \quad (19)$$

Since the position being used in the core simulation is constant, the flux is not assumed to change spatially. The irradiation time of 8 hours is also expected to result in a time constant Am241 atom count, and constant power/flux is assumed and planned for. The Ratio of interest would then be (short irradiation times):

$$R = \frac{P_{Am242m}}{P_{Am242}} \quad (20)$$

To extract this data from the Gamma spectrum information of the net peak area, either simulated or physically measured, the output values would be applied in a ratio:

$$R \approx \frac{K_{Am242m}}{K_{Am242}} \quad (21)$$

Where, with very short irradiation times, losses due to half-life and absorption are ignored, for MCNP and instantaneous detector measurement of photo-peaks:

$$K_{Am242m} = \frac{A_{Am242m}}{\lambda_{Am242m}} \left(\frac{1}{t_{irr}} \right) = \frac{NC_{Am242m}}{f_i \varepsilon_{a,i} \lambda_{Am242m}} \left(\frac{1}{t_{irr}} \right) \quad (22)$$

$$K_{Am242} = \frac{A_{Am242}}{\lambda_{Am242}} \left(\frac{1}{t_{irr}} \right) = \frac{NC_{Am242}}{f_i \varepsilon_{a,i} \lambda_{Am242}} \left(\frac{1}{t_{irr}} \right) \quad (23)$$

If accurate knowledge of the absolute efficiencies is not known, then the similarity of the peaks of interest in their energies can allow for an approximation with their ratio. As all Am241 irradiations will be simulated, the Net peak efficiencies as predicted by the detector simulation can be evaluated from their initial ‘true’ amount (MCNP uncertainty in the Am241 radiative capture rates will still be taken into account). These reaction rates will be handled by MCNPX with a burn card, actinides and fission products will be tracked, for long term decay analysis, the burn card will be augmented with a wide range of available isotopes by setting the minimum atomic fraction cutoff to (1E-45) in order to force the program to track the fission products. In the event of accidental Uranium/Plutonium contamination, production of Am242 and Am242m does not occur via the decay of Pu242, unlike the production of Am241 which arises from the beta decay of Pu241. The primary concern of this study was at which activity and irradiation time and power would best produce a gamma spectrum that could be observed for the Am242 and Am242m specific gamma peaks in the face of the expected peaks from other actinides and fission products, while ensuring that the irradiation time and power remained realistic with the capabilities of the MSTR. The decay tables of Am242 and Am242m are provided by the source (LNHB, n.d.).

The primary photon emissions for each Am242 and Am242m that is of interest depends upon their relative intensity and how they compare with the longer lived base Am241, as such Am241 photon lines are prevalent around Am242 and Am242m photon energies. The major gamma/x-rays from Am241, Am242 and Am242m are given in Tables 2.3, 2.4, and 2.5. Since the resolution of the specific detector in the reactor bay is

relatively low, it is expected that photopeaks within 7-8 keV (FWHM calibration equation) of each other will be added together. This is primarily expected for Am242's compact x-ray radiation in the 99-105 and 114-122 energy region. A summed expected photopeak for Am242 in those energy regions will be given to compare the Prospect derived output values.

Table 2.3. Am241 photon energies and intensities (LNHB, n.d.)

Energy (keV)	Intensity %	Type
59.5409	35.92	γ
16.96	18.58	$X_{L\beta}$
13.852	13.02	$X_{L\alpha}$
21.16	4.83	$X_{L\gamma}$
26.3446	2.31	γ
11.89	0.844	$X_{L\iota}$
15.876	0.384	$X_{L\eta}$
33.1963	0.1215	γ
43.42	0.0669	γ
98.97	0.0203	γ
102.98	0.0195	γ
55.56	0.0181	γ
32.183	0.0174	γ
42.704	0.0055	γ
57.85	0.0052	γ
125.3	0.0041	γ
69.76	0.0029	γ
101.059	0.00181	$X_{K\alpha 1}$

Table 2.3. Am241 photon energies and intensities (LNHB, n.d.), (cont.)

97.069	0.001134	$X_{K\alpha 1}$
123.05	0.001	γ
208.005	0.000786	γ
114.1497	0.000658	$X_{K'\beta 1}$
75.9	0.0006	γ

Table 2.4. Most intense photon emissions for Am242 (LNHB, n.d.)

Energy (keV)	Intensity (%)	Type
18.08	18	X_L
17.1385	10.8	X_L
103.734	5.6	$X_{K\alpha 1}$
99.525	3.55	$X_{K\alpha 2}$
117.13	2.06	$X_{K'\beta 1}$
121.0173	0.72	$X_{K'\beta 2}$
42.13	0.04	γ
44.54	0.014	γ

Table 2.5. Most intense photon emissions for Am242m (LNHB, n.d.)

Energy (keV)	Intensity (%)	Type
17.6065	25	X_L
16.681	0.37	X_L
49.371	0.134	γ
101.069	0.03	$X_{K\alpha 1}$
86.674	0.0229	γ
97.069	0.019	$X_{K\alpha 2}$

Based upon the above tables, and the energy windows given by photon emissions of the base Am241, which largely shadows the x-ray/gamma lines of the activation products the indicator peaks for measuring the activities of Am242 and Am242m are found. The X-rays around 100 and 118 keV will be looked as indicators of viability for Am242 in the BEGe 3825 simulation from the isotope inventory after the simulated burn at various times with a power of 200 kW that would result in a thermal neutron flux of $2E+12$ n/cm²-sec at the location of irradiation. The gamma lines of 49 and 86 keV (free of Am241 interference) keV will be the indicators for the viability of producing a measurable amount of Am242m under the imposed power and irradiation time conditions. All photons of energy less than 40 keV are inherently suspect as the BEGe simulation does not show good agreement below that energy value.

The detector used is Canberra's BEGe 3825, with the major physical parameters for the crystal and window to crystal spacing, information on the structural materials and their geometries were taken from Canberra. Also from their diagrams information concerning the thickness of the Germanium dead layer was extracted. This inactive Ge layer cuts down on lower energy photons, and varying its thickness caused the Am-241

59.5 keV peak to shrink in amplitude while having no effect on the 1173.2 keV peak from Co-60. This was utilized to sort errors seen in the MCNP model, improper source geometry, placement effected the entire spectrum, while the Ge dead layer only effected the low energy peaks, <40 keV. Error propagation was a serious concern, and uncertainty (MCNP, Validated Activity) information regarding the simulated counts was lost when input into Prospect when trying to validate the model. The error propagation method used when multiplying and dividing uncertainties values were (Nardo) the following. This equation was converted into its simpler form, as all values used by the study are expected to be uncorrelated.

$$\sigma_f = \sqrt{\left(\frac{\partial f}{\partial E_1} \sigma_1\right)^2 + \left(\frac{\partial f}{\partial E_2} \sigma_2\right)^2 + 2 \frac{\partial f}{\partial E_1} \frac{\partial f}{\partial E_2} \text{cov}(E_1, E_2)} \quad (24)$$

For the uncorrelated values in this experiment, which will be assumed completely uncorrelated, to be the physical measurement data from the BEGe 3825 from the photon standards with the physical data of the source, (activity), as well as simulation output, in order to produce absolute full energy peak efficiency and by taking the ratio between the measured and simulated full energy peak efficiency. This procedure follows a similar simulated vs experimental full energy peak ratio determination with a similar confidence level of k=2 (Diago, 2005). The following equation is used:

$$\frac{\sigma_f}{f} = \sqrt{\left(\frac{\sigma_1}{E_1}\right)^2 + \left(\frac{\sigma_2}{E_2}\right)^2} \quad (25)$$

For the correlated values used, (Nardo), (included as some verification work could considered correlated), the non-simplified error propagation equations were utilized to provide when taking the ratios of reaction rates obtained from single MCNP runs with the same underlying F4 or F2 tally results. These tallies were modified by differing cross sections, (radiative capture/fission) to derive production/destruction rates. F2 results were

omitted in this study as they were primarily used to check for differences with F4 results. For any correlated values when taking ratios, the following were used:

$$\text{cov}(E_1, E_2) = \sigma_1^2 \quad (26)$$

$$f = \frac{E_1}{E_2} \quad (27)$$

$$\frac{\sigma_f}{f} = \sqrt{\left(\frac{\sigma_1}{E_1}\right)^2 + \left(\frac{\sigma_2}{E_2}\right)^2 - \frac{2\sigma_1^2}{E_1E_2}} \quad (28)$$

The expanded uncertainty provided for the verified Gamma/x-ray sources was used to evaluate the physical validation data and provide the minimum and maximum multipliers used to scale the MCNP F8 photon tallies. The expanded nature of the uncertainty was explicitly stated for the mixed standard; it was not stated explicitly and is assumed for the Europium standard. The expanded uncertainty is (NIST, n.d.):

$$U = ku_c \quad (29)$$

The coverage factor of k was explicitly given for the mixed standard as being equal to 2. It is assumed that this is similar for the europium standard. Expanded uncertainty will only be used when using the physical data in conjunction with the simulation data, results derived principally from models will not use a coverage factor/confidence interval for its uncertainty. Activity corrections for the major given isotopes were handled via:

$$A(t) = A_0e^{-\lambda t} \quad (30)$$

The peak analysis performed by Prospect, which was automated for both the validated, tests simulation, and case simulations to eliminate any user error, used the following equations/algorithms to determine the centroid of fitted peaks using the step continuum, all peaks treated as singlets (Canberra, 2012). For the Prospect centroid determination (Canberra, 2012), the following relations are utilized.

$$Centroid = \frac{\sum_i i \cdot ss_i}{\sum_i ss_i} \quad (31)$$

The value i is the channel number, while:

$$ss_i = \frac{dd_i}{sd_i} \quad (32)$$

$$dd_i = \sum_{j=-k}^{j=k} c_j y_{i+j} \quad (33)$$

Standard deviation, y is counts per channel, is given as the following:

$$sd_i = \sqrt{\sum_{j=-k}^{j=k} c_j^2 y_{i+j}} \quad (34)$$

$$c_j = \frac{100(j^2 - cw^2)}{cw^2} \cdot e^{-\frac{j^2}{2cw^2}} \quad (35)$$

The above equation defines the coefficients that k depends upon, the value cw is:

$$cw = \frac{FWHM}{2.355} \quad (36)$$

Prospect fit a curve to the peak counts and determined the net area, uncertainty, FWHM via its own algorithms. Due to the omission of parameter information in software reference material, only the centroid algorithm is given explicitly above, while the net area, uncertainty, and FWHM were observed but not given here (Canberra, 2012).

The automated peak analysis of the F8 tally data by Prospect was used to ensure consistency in choosing the regions of interest for potential photopeaks and eliminate human error in managing the data. MCNP was used to provide the data, while the precision of the values were taken as the uncertainty in some cases, such as in the reaction rates of Am241, when taking the F8 tally, the counts in each energy bin were accepted as integers into the Prospect software, in that case the goal was to minimize the MCNP error altogether so that it could be ignored while the pseudo-statistical errors from the simulated peak analysis could be compared with the actual measurement data for validation purposes. Three tally types were used throughout this study, the F2 type surface fluence tally, the F4 type cell fluence tally, and the F8 type pulse height tally. For the F2 type tally (which was used to verify and test procedures, but not used for analysis:

$$\bar{\phi}_s = \frac{1}{A} \int dE \int dt \int dA \int d\Omega \Psi(\vec{r}, \hat{\Omega}, E, t) \quad (37)$$

Final units in this tally are *particles/cm²*. For the F4 tally, this was used for both individual cells as well as larger FMESH for full core analysis:

$$\bar{\phi}_v = \frac{1}{V} \int dE \int dt \int dV \int d\Omega \Psi(\vec{r}, \hat{\Omega}, E, t) \quad (38)$$

Units for this tally type are also *particles/cm²*. For the F8 tally type, the physical quantity examined is the energy pulses deposited in an energy bin for a particle history. The reaction density tally results were converted to reaction rate densities by the use of the conversion multiplier at Powers of 100 kW and 200 kW for a U-235 fueled core (for model comparison with previous work):

$$M = (3.467E10)vP \quad (39)$$

A multiplier was used for the F8 tallies as well, the product of the intended live counting time with the total source strength of the sample (all isotopes photon rates) to acquire the total number of source particles emitted to provide a scaling factor. The parameter ν was determined from previous runs of the simulation to be 2.439 for the study MSTR approximate. This Multiplier was applied directly to the tally multiplier cards, along with the appropriate reaction rate information (atomic density taken from the chosen activity of Am241 to the surface area or cell volume), to determine the radiative capture and fission rate density for each of the F2 and F4 tally types, an SD card was used to produce only reaction rates by accounting for the power scaling, area.

For the F8, F2 and F4 tallies undertaken throughout this study, the relative error obtained can be interpreted by Table 2.6. All tallies undertaken for validation and analysis kept their MCNP errors below 5%, through the choices made in number of source particles, and number of cycles (for the F4 and F2 tallies made during criticality runs. Relative error was balanced against the run-time of the particular simulation, and error allowances were made (still less than 5%) in order to increase the amount of runs that could be accomplished in a reasonable time. For the F8 tally, the regions around major photopeaks were watched for their error and made to ensure that the MCNP relative error was less than 5% in the major energy regions that could expected once the Gaussian energy broadening card had been employed to mimic the Gaussian response once discrete photon lines interacted with the detector mass.

Table 2.6. Meaning of MCNP relative error for tally (X-5 Monte Carlo Team, 2003)

Range of R	Quality of the Tally
.5 to 1	“Garbage”
.2 to .5	“Factor of a few”
.1 to .2	“Questionable”

Table 2.6. Meaning of MCNP relative error for tally (X-5 Monte Carlo Team, 2003), (cont.)

<.10	“Generally reliable except for point detector”
<.05	“Generally reliable for point detector”

As such, the error for each of the tally bins had a target of less than .05. The uncertainty provided by MCNPX in the rates will be used to analyze the Am241 to Am242/Am242m simulation. The full energy peak absolute efficiency which was utilized to compare the simulated spectrums with the validated photon emissions from the standards is given as (El-Khatib, Mona, Mohamed, Sherif, & Ekram, 2013):

$$FEPE = \frac{N(E)}{tAP(E)} \prod C_i \quad (40)$$

Since the detector system accounts for dead time, and activity corrections were made, the FEPE can be considered for each photopeak. Decay constants and decay times were considered to be well known, since their uncertainties were mostly much smaller than their values. Uncertainties in activities for the standards were taken into account, by creating a minimum and maximum count spectrum when uploading the values into Canberra’s Prospect peak analysis software. The ratio of the measured vs the simulated was taken to highlight the discrepancy from unity between the standard measurements and the model results, as observed in other validation works of simulated BEGe detectors (Diago, 2005). Deviation from 1 is expected to be caused by primarily general model/system discrepancies, while deviation from FEPE ratio average is attributed to uncertainties in the count rates for the respective individual photopeaks, simulated and measured. Some model discrepancies such as source-window distance might introduce higher than expected count rates and thus a higher Prospect derived uncertainty which would affect the FEPE ratio spread around its average, but it is not expected that any base

improvement derived from the decrease in the FEPE ratio value spread could cover for less than desirable physical measurements (FEPE values) when accounting for live counting times that may or may not be suitable for the test cases that were examined to validate the BEGe 3825 MCNP model. For this study it is assumed that such effects as the geometry discrepancies in the model on the FEPE ratios, is expected to cause deviation from the physical results; any improvement in the spread in the average FEPE ratio that would be introduced by, for example, simulating the sources at a closer distance to the crystal and decreasing simulated count uncertainty would not change the accuracy of the model, in a meaningful magnitude or way when compared to physical results. Discrepancies that could affect photopeaks dependent upon their energies, such as the Ge dead layer thickness, was examined in the validation phase of the BEGe 3825 detector model. Deviations in the Ge dead layer thickness will impact ~40 keV photopeaks more so than the higher energy photopeaks. Due to this observation, the behavior and spread of the >40 keV photopeaks is of primary importance, even if impact on photopeaks of energy greater than 40 keV is still expected, although ever decreasing.

$$R_{FEPE} = \frac{FEPE_{Standard}}{FEPE_{MCNP}} \quad (41)$$

3. PROCEDURE

This study was undertaken to determine the feasibility of two applications of Am²⁴¹ and the use of the MSTR and the BEGe 3825. One was to determine the minimum irradiation time for a given (0.05 μ Ci and 1.0 μ Ci) amount of Am²⁴¹ that would be required to generate a viable amount of Am^{242m} and Am²⁴² with the single burn at the maximum MSTR power of 200 kW. The other was to observe and simulate the Am²⁴¹ build-up in typical Weapons/Reactor grade plutonium, both of these applications could be potentially measured by a shielded BEGe 3825 in the reactor bay. In order to accomplish this, the following logical tasks were performed.

1. MSTR Model Development: A model of the MSTR was built in MCNP5, blueprints for the fuel assemblies and control rod assemblies were utilized, the regulating rod assembly and core pool were built upon its description in the reactor procedures handbook. Material (non-fuel) compositions were taken from its descriptions provided either upon its blueprints or handbook. Fuel compositions and non-core structural materials were taken from past work with another MCNP model of the MSTR (Richardson, Castano, King, Alajo, & Usman, 2012). The layout of the validation core adopted the 101W core configuration undertaken by Kulage in order to validate the models 3 group neutron flux with Kulage's work but was expanded to the current configuration, Model was run at approximately critical values, with control rods near the positions described by Richardson in his verification of his model of the core.

2. Am²⁴¹ Inventory Estimates: A Forward Euler, constant flux method was generated to solve the coupled differential equations that came about when considering the build-up scheme for the production of Am²⁴¹ in a typical thermal reactor with initial uranium fuel only (26 actinides examined). This program was also used (zero neutron flux) to provide a general overview of the buildup and decay behavior of typical weight fractions of Plutonium isotopes in a reactor and the weapons grade material for decay times in the region of 1, 5, and 19 years. 12 actinides were covered by this decay scheme, all primary decay products of described plutonium isotopes, and some secondary. Investigation into further additions of short-lived secondary decay products (Th²³¹, Pa²³³) yielded negligible photon rates compared to Am²⁴¹ and Pu²⁴¹ in a given sample of typical compositions at any time. The composition was assumed to be pure plutonium

that had been separated from the used fuel where it was generated, either in a commercial reactor or a special Plutonium-239 generator at low burnup. The purpose of this task was to examine the decay times for typical Plutonium at which Am241 buildup would allow for Gamma Spectroscopy to become a viable option. To determine when the Plutonium was separated from the used fuel, the stock is assumed to be homogenous and uniform when it is separated from its used fuel, before being added to the MOX. As this is a matter of ensuring that Plutonium proliferation is hampered, its behavior once mixed with Uranium in a MOX fuel is ignored by this study. An arbitrarily small mass of Plutonium with established isotope weight fractions (Travers, 1999), was chosen for simulation studies what would be comparable to $\sim 1\mu\text{Ci}$ activity which was the source strength of simulated Am241. Plutonium activity limit of $1\mu\text{Ci}$ was necessary to ensure that deadtime and other artifact of radiation measurements would not interfere with the models assumption and the physical measurement. It is assumed that any large quantity of Plutonium would be uniform in its composition, and that a smaller sample could be removed and put into the BEGe 3825, deposited onto an Aluminum foil and allow for the decay time to be determined if the mass of the quantity and sample are known.

3. BEGe 3825 Detector Model Development: A model of the shielded BEGe 3825 in the reactor bay was constructed in MCNP5. The shield geometry and material was taken from Canberra's diagram and material descriptions for its shielding unit. The physical parameters for the active Germanium and distance from the detector window were taken directly from the detector data sheet. Parameters such as the structural materials surrounding the crystal, and the Ge dead layer in the crystal were taken from Canberra's technical diagrams. Validation efforts would use two isotope gamma standards available at the reactor; their current activities at the time of validation; correcting for decay. The approximate distance from the sample center (disk, cylinder) to the detector window was taken as ~ 1.4 cm for the physical Europium disk source and ~ 1.5 cm the mixed cylindrical source. There is uncertainty in the estimate due to the unknown internal source geometry and geometrical imperfections in the mixed sample surface that prevented the cylinder from lying flush on its container surface. Both sources consisted of an active deposition on a disk, which was subsequently sealed. Both sources were modeled to be centered directly on the end cap protective cover, inside of

their sealed case. Exact physical source geometry and position definition was deemed unnecessary for detector model verification, since the simulated samples would be tested at a series of source-window distances, at which point the general behavior of the model would be observed, and any deviation from the FEPE ratio unity noted. The variation for the ratio of the measured to MCNP derived absolute FEPE (Full Energy Peak Efficiency) as a function of sample distance from the detector, as well as the Europium surface source radius was analyzed. Since the technical specifications for the detector's Ge crystal and major structural components were obtained, it was assumed that all bulk discrepancy between simulated and physical FEPE measurements at specific distance and source radius values came from the source distance and source geometry uncertainties. While any spread in FEPE ratio values from its average are attributed to uncertainties in the net count rates and/or uncertainties in the photon rate itself. It is assumed in this study than any effect upon the spread of the FEPE ratio values from its average caused by simulating decreasing source-window (lowering uncertainty in the FEPE value) is negligible compared to the effect of the source-window distance on the deviation from unity. At each position/radius value the standard peak FEPE ratios were derived. For the effect of the uncertainty of the multiplier, the measured distances and radius and simplest photon treatment were utilized. The mixed source contained more information for its geometry, and thus its possible radial variation was not explored. The sources were modeled as approximated surface and volume geometry, based upon their descriptions given in their calibration certificates accordingly. Physical detector and model spectrums were compared via Prospect with the exact same analysis settings, as well as their resulting absolute peak efficiencies for the standard gamma peaks given by the source certificates at varying source to window distances, source active radii (for the Europium standard), and the range of multipliers to account for the sample activity uncertainty that is lost when transferring F8 tally results in Prospect and its subsequent net cps uncertainties.

4. Detector Simulation for Am241: The weapons/reactor grade plutonium simulated samples with Am241 buildup after 1, 5, and 19 years of decay were used to simulate the BEGe 3825 model response. The full gamma/x-ray spectrum for each actinide between and around U235/U238 to Am241 was included in the model (12

actinides). Prospect automated peak analysis was used at similar validation settings was used to generate net peak area of Am241 dominant 59.50 keV peak and determine overall reliability between the different sample compositions and decay times. Time spans of .5, 1, 1.5 and 2 years between simulated 1 hour measurements of Am241 59.50 keV count rate were taken for each decay time case. The Newton-Raphson method used this ratio and time spans to solve for the unknown sample age (when Am241 content was nonexistent). The amount of relative uncertainty in simulated net cps as predicted by Prospect was utilized to judge the viability measuring the Am241 59.50 keV peak in a plutonium sample of typical weapons and reactor grade composition and decay inventory with the actual BEGe 3825 located on campus.

5. Simulation of Am241 Irradiation: Using the model of the MSTR expected physical samples with varying activities were put into the source holder tube region of the model, and the burn card of MCNPX was ran for a series of times at 200 kW, this being near the maximum power for a single irradiation offered by the MSTR. Activities ranged from the .05 μCi that is exempt from campus regulations to 1 μCi . Burn times were split up in 3 independent sections of 1,30, 480 minutes, each followed by a time segment of two hours of decay, in order to capture the decay behavior of the Am242 and Am242m, as well as the other fission products and actinides that were produced in the burn-up calculation. Two hours of decay were to simulate an expected cool down period. Saturation Activity of Am242m or Am242 is not expected to be reached in a feasible time frame at MSTR for a single session irradiation.

6. Detector Simulation for Am241 Irradiation Product: Finally, the fission and activation products of Am241 were simulated for its gamma spectrum using the BEGe3825 detector. For each initial Am241 activity (case), the inventories of the fission products and actinides, up to as low as 1E-60 atom fraction were included to generate a gamma/x-ray spectrum. Their discrete gamma/x-ray line energies and intensities were taken from the MCNP results, and a source and probability distribution for the new material was written into the surface source for the irradiated foil situated approximately 1.0 cm above the detector window. A fixed geometry of the foil on a casing which was placed on the protective cover of the detector was simulated. For this geometry irradiation times and activities can be analyzed for their effect upon photopeak net cps

values as obtained by the Prospect software. Simulated Gamma spectra were analyzed by the automated peak analysis software Prospect, allowing for their simulated net count rates to be determined for each peak. At each irradiation time, simulated peaks associated with Am242m and Am242 were examined and evaluated for their viability for a specified simulated live count time. This process continued for each point in time for the selected initial Am241 activity. The entire process was repeated for the other initial Am241 activity. For each case, after the full irradiation time, the simulated full peak absolute efficiencies (FEPE) were calculated using the full photon energy/probability distribution of the MCNP tier 3 fission products and actinide inventory after the given burn and cooling times.

4. PHYSICAL MEASUREMENT OF STANDARDS FOR BEGE 3825

Efficiency of BEGe 3825 was measured in the lab to estimate the feasibility of the measurement techniques being developed for burnup analysis using activation product of Am241. For this purpose, physical measurements of standard gamma sources with the BEGe 3825 were obtained using a mixed isotopes source and a Europium source. These standards sources are available in the lab/reactor with their respective calibration certificates (Appendix B). Both were measured sitting directly on the protective window of the detector. The detector dimensions were measured from the top of the cryostat cylinder (origin) and source system measurements as shown in Figures 4.1 and 4.2. The geometric description of the setup is given in Tables 4.1 and 4.2 below.

Table 4.1. Physical measurement of BEGe 3825 end-cap with and without the protective cover

Parameter	Approximate Value (cm)
Height of detector end-cap with protective cover	11.5
Height of detector end-cap without protective cover	11.1
Distance from carbon window to surface where sample system was located (Cover gap)	0.4

A standard ruler was used to obtain the physical measurements. Extreme care was taken inside of the detector when protective cover was removed, and physical touching of the end-cap was minimized to avoid damage to the crystal and vacuum barrier. Reattachment of the protective cover was done to avoid putting pressure on the end-cap edges and thus possibly rupturing the vacuum seal, or deforming and damaging the

germanium crystal itself. Due to these precautions, the physical measurements should be noted as approximate values, and that the precision could still be improved.

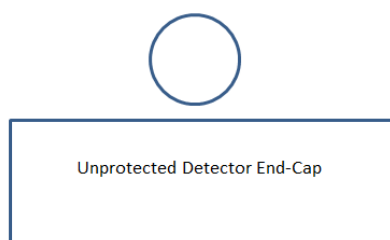
Table 4.2. Physical measurement of validated photon sources

Parameter	Mixed (active disk inside cylinder)	Europium (active disk inside disk)
Active Radius (cm)	0.25	NA
Sample Total Radius (cm)	1.125	2.54
Sample Disk thickness (cm)	X	0.30
Sample Cylinder Length (cm)	5.50	X
Relevant Sample Casing thickness (cm), Cylinder does not sit perfectly on surface	<0.20	0.80
Distance from carbon window to protective end-cap cover (cm)	0.40	0.40
Internal Distance from nearest active source surface to outside of sample surface (cm)	0.875	0.15 (value assumed because of sealed source)
Total Distance from carbon window to active source disk (nearest surface) (cm)	1.475	1.35



Figure 4.1. Clockwise from top left, end-cap with protective cover, end-cap without protective cover showing carbon window, mixed isotope cylinder with active disk, Europium disk source

Mixed Source Cylinder with embedded active disk



Europium Source disk with embedded active disk

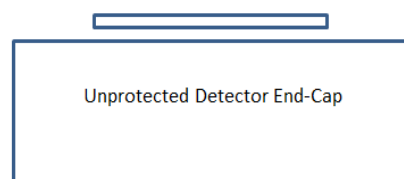


Figure 4.2. The source and detector orientation

The mixed and europium test sources were a different geometry, which was accounted for in the MCNP model. The activities and photon/s as well as calibration dates were given, allowing for decay correction for current activities and photon emission

rates. For the multiple europium source, the given major peaks, activities and rates, photon rates were given with an average uncertainty of 5% for the stated activity, which was assumed to be an expanded uncertainty with $k=2$ to mirror the Eu standard. This 5% activity uncertainty was then given as the expanded uncertainty for each of 3 activities and their respective photon rates for the Europium standard. All uncertainties for the photon absolute intensity fractions and other physical standard data gathered from evaluated libraries were ignored in this study due to their relative insignificance to the activity uncertainties. Table 4.3 gives the europium source calibration information at time of validation.

Table 4.3. Initial parameters for Europium standard, taken from source certificate

Parameters at Calibration Date: 6-27-2002			
Isotope (half-life, yrs.)	Energy (keV)	Photon/s for each photopeak	Initial Activity (Bq)
Eu-152 (13.6)	40.1 (SmKa)	4910	8470
	121.8 (doublet)	2410	
	244.7	635	
	344.3	2250	
	1408.0	1760	
Eu-154 (8.59)	123.1	3560	8820
	591.7	406	
	723.3	1740	
	873.2	1070	
	1004.8	1550	
	1274.5	3040	
	1596.5	163	

Table 4.3. Initial parameters for Europium standard, taken from source certificate, (cont.)

Eu-155 (4.76)	60.0	122	11100
	86.5	3440	
	105.3	2400	

For the updated values given in Table 4.4, uncertainties in the intensities for the major photon emissions are ignored, time uncertainty of 24 hours is considered much smaller than the time that has passed when determining the time intervals between standard calibration and measurement dates.

Table 4.4. Corrected parameters for Europium standard, taken from source certificate

Decay Parameters at Measurement Date: 8-17-2016 "current"			
Isotope (half-life, yrs.)	Energy (keV)	Photon/s for each photopeak	Current (Bq)
Eu-152 (13.6)	40.1 (SmKa)	1580.	4105.
	121.8 (doublet)	1177	
	244.7	312	
	344.3	1090	
	1408.0	865	
Eu-154 (8.59)	123.1	1140	2821
	591.7	140	
	723.3	566	
	873.2	341	

Table 4.4. Corrected parameters for Europium standard, taken from source certificate, (cont.)

	1004.8	508	
	1274.5	983	
	1596.5	51	
Eu-155 (4.76)	60.0	17	1411
	86.5	433	
	105.3	298	

The detector calibration equations that were utilized by the Prospect software in analyzing photopeaks, the energy and FWHM equations were utilized in setting up the energy bins of the F8 tally, as well as the Gaussian Energy Broadening modification that was applied. These equations were taken directly from the BEGe 3825 detector of interest and are given in Table 4.5.

Table 4.5. Calibration equation information taken from the BEGe 3825 detector of interest in reactor bay

Energy	$E = 8.178 + .184Ch$
FWHM	$FWHM = 7.508 + 8.657(10^{-4})\sqrt{E}$
Low Tail	$Low Tail = 2.553 + 3.992(10^{-3})E$

The Europium sample was counted for 10 minutes centered on the detector window, the full range spectrum was acquired as well as magnified views for each of the viable validated peaks, and some peaks were not present, as the measurement time was

short to allow for relatively isolated major peaks only to improve validity of comparison with the MCNP simulation. Full Eu source spectrum on linear scale is shown in Figure 4.3. The 10 minute live count time, while chosen to allow limited interference in the spectrum, caused a relatively high uncertainty for the europium validated photopeak count rates that would be used to validate the BEGe 3825 MCNP model with a europium x-ray and gamma loading. This uncertainty is expected to increase the spread around the FEPE value.

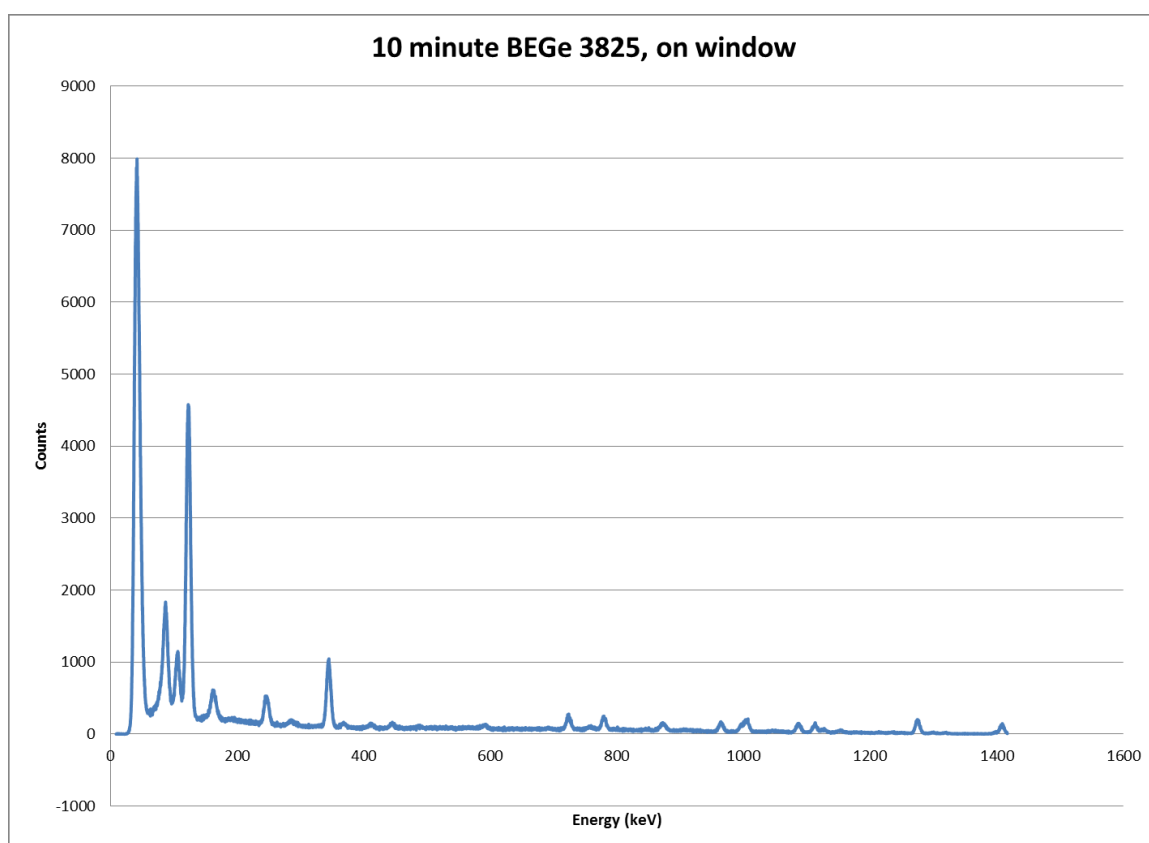


Figure 4.3. Europium standard at 10 minutes of live time

Using the automated peak finder software provided by Canberra, Prospect, the peaks were found with the sensitivity parameters shown in Table 4.6. The continuum was

the main cause of discrepancy in net peak areas if the peak was poorly defined. It was determined from testing with the Am242 peaks of 102 and 118 keV that too high of continuum estimate (greater than 2 FWHM) resulted in an erroneous curve that did not apply to the count compilation in the extreme. Peak analysis settings only affected the Prospect software peak analysis, while the calibration information was taken from the previous calibration of the BEGe 3825 detector. The Prospect analysis setting for continuum estimate was chosen to be the relatively low value, 0.2 FWHM. At greater than a 2 FWHM for the initial continuum estimate, analysis resulted in poor resolution and peaks that were not distinct. It is assumed that in the comparison of physical and simulated standard spectrums, the use of the exact same settings eliminate their impact on the model error, when used to model Am241/Am242/Am242m activities, it is assumed that any potential future physical measurements would utilize the exact same peak analysis settings that are not unique to the BEGe 3825 detector.

Table 4.6. Automated peak analysis settings used by Prospect software to eliminate human error in determining regions of interest, these settings are used to compare measured and simulated standard spectrums, and then used to analyze Am241/Am242/Am242m activities

Analysis Continuum Type:	Step
Continuum (FWHM):	0.2
Peak Search Sensitivity:	5.0

The peak analyses for all found validated peaks are as follows in Table 4.7 (dead time already factored in). These values will be used to compare with the MCNP simulation of europium source of the same activity and composition. Their Full Energy Peak Efficiencies (FEPE) will be compared, and a ratio will be taken. The behavior and trends of the model will be found and accounted for so that future simulation can be made

more precise. An upper and lower window will be utilized to account for discrepancies in the general model and allow for its general output for the plutonium age estimation analysis and the analysis of Am241 to Am242/Am242m irradiation.

Table 4.7. Prospect analysis of 10 min Europium standard count

Centroid (keV)	Net Area	Net cps	FWHM (keV)	Gaussian Ratio
86.258	70704.068 ± 1042	117.84 ± 1.74	8.2	1.228
105.297	23713.502 ± 915.7	39.522 ± 1.53	6.581	.957
122.512	205373.371±1338	342.28895±2.23	8.421	.995
245.682	20660.4 ± 576.163	34.434 ± .96	9.392	1.001
343.967	43602.618 ± 573.82	72.67103 ± .96	8.177	.981
591.334	1458.436 ± 467.3	2.431 ± .78	6.784	2.057
722.731	8199.989 ± 379.72	13.667 ± .63	8.139	1.296
871.08	5072.852 ± 388.38	8.455 ± .65	10.969	1.085
1003.031	11003.852 ± 520.47	18.340 ± .87	9.948	1.243
1273.435	8910.685 ± 252.80	14.851 ± .42	8.671	1.071
1407.314	5006.862 ± 943.41	8.345 ± 1.57	7.757	1.157
1595.257	366.295 ± 256.60	.6105 ± .43	8.288	9.386

As can be seen from some of the validation peaks, the relatively short count time of 10 minutes caused a large error to develop in some of the less well defined peaks. These count rates determined from the physical measurements in the BEGe 3825 were then compared to their given activities and photon rates for each isotope to determine full peak efficiency and % error with the given centroid. The measured 122.512 keV peak was not included as it appears to be the sum of the 121.8 and 123.1 keV peaks and did not offer a clear chance to determine absolute efficiencies at this stage. Analysis of the above data provided by Prospect yielded Full Energy Peak Efficiency and other information as provided by Table 4.8. Thesis standard values, primarily their FEPE value, will provide the baseline for comparison and validation of the MCNP model for the BEGe 3825 detector system. This data will be compared and contrasted with a mixed source with different geometry to further validate the source/detector modeling procedure and give a general behavior of the model's response.

Table 4.8. Determining the physical detector absolute peak efficiency with the Europium standard

Given Peak Energies (keV)	Measured Peak Centroids (keV)	Centroid Error %	Given photon/Expanded uncertainty, (k=2)	Measured Net cps	Uncertainty (Prospect)	Relative uncertainty (Prospect) %	Peak Absolute Efficiency %	Expanded relative uncertainty % (k=2)
86.5000	86.2580	0.2798	433.1833	117.8400	1.7400	1.4766	27.2033	5.8070
105.3000	105.2970	0.0028	298.0301	39.5220	1.5300	3.8713	13.2611	9.2167

Table 4.8. determining the physical detector absolute peak efficiency with the Europium standard, (cont.)

244.70 00	245.68 20	0.4013	312.28 60	34.434 0	0.9600	2.7879	11.026 4	7.4894
344.30 00	343.96 70	0.0967	1090.3 265	72.671 0	0.9600	1.3210	6.6651	5.6551
591.70 00	591.33 40	0.0619	139.64 97	2.4310	0.7800	32.085 6	1.7408	64.365 6
723.30 00	722.73 10	0.0787	566.06 78	13.667 0	0.6300	4.6096	2.4144	10.487 9
873.20 00	871.08 00	0.2428	340.82 01	8.4550	0.6500	7.6878	2.4808	16.168 1
1004.8 000	1003.0 310	0.1761	508.08 52	18.340 0	0.8700	4.7437	3.6096	10.724 4
1274.5 000	1273.4 350	0.0836	982.75 66	14.851 0	0.4200	2.8281	1.5112	7.5493
1408.0 000	1407.3 140	0.0487	864.98 72	8.3450	1.5700	18.813 7	0.9648	37.958 1
1596.5 000	1595.2 570	0.0779	50.710 2	0.6105	0.4300	70.434 1	1.2039	140.95 68

A plot of the full peak absolute efficiency as a function of energy for the multi-europium source on the protective cover window is shown in Figure 4.4. Uncertainty in FEPE value is a consequence of the relatively short live counting time used. It is expected to have an impact in the comparison with the simulated spectrums, and the association of

the FEPE ratio average with each FEPE ratio value for the europium case, as well as for the mixed case when its uncertainty is factored in with its FEPE behavior. The 591.70 and 1596.5 keV peaks suffered from an unusually high uncertainty percentage relative to the rest of the spectrum. Overall the physical detector was able to match the centroids of the photopeaks with the given and expected values. This reaffirms that detector energy calibration carried over from a previous date of measurement when it was observed to have been carried out. From the examined photopeaks, 9 specific energies were chosen to compare with the MCNP model (MCNP model still considered all gamma/x-ray radiation from the europium source). This was done in order to simplify the process, and remove photopeaks that were already covered by a similar energy value in a general region. Close in value photopeaks were omitted from the analysis, but not the simulated loading to provide for this simplicity. The 1596.5 keV photopeak was eliminated for validation due to its ~70% net count rate uncertainty. The 591.70 keV photopeak was kept in order to compare with how the MCNP model handled a high error peak.

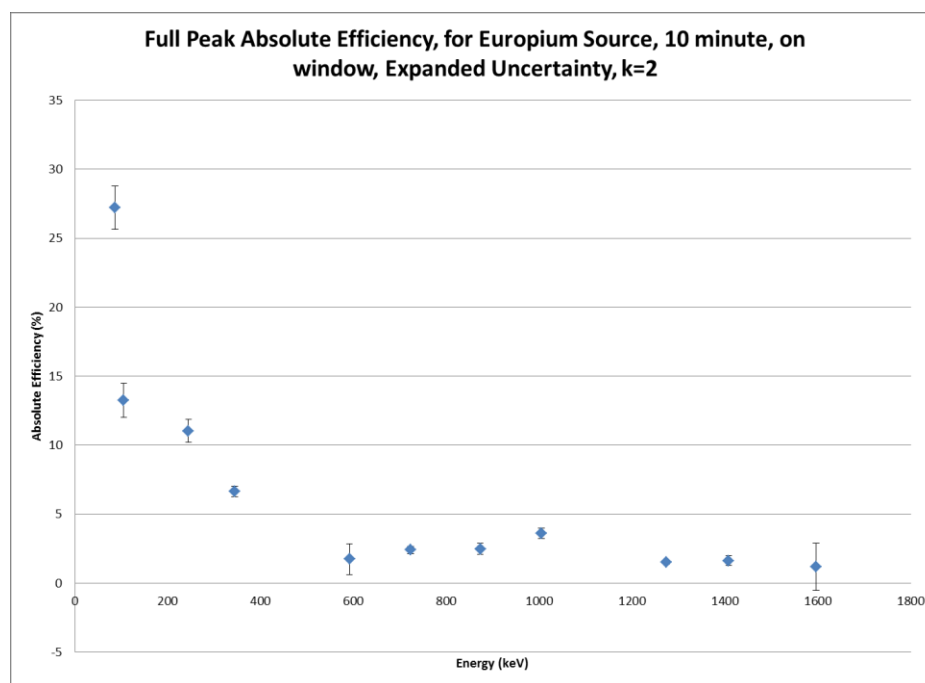


Figure 4.4. Europium standard absolute peak efficiency plot

Another mixed isotope gamma standard source was acquired and analyzed with the BEGe 3825, with an assortment of isotopes as listed in Table 4.9. This source is also provided by the reactor staff.

Table 4.9. Mixed standard initial parameters, taken from source certificate

Parameters at Evaluation Date: 10-1-2012					
Isotope	Half-life (s)	Energy of interest	Initial photons/s for each peak	Initial Activity (Bq)	Expanded Relative Uncertainty (%)
Am241	1.3651E+10	59.5000	2014.0000	5610.0279	3.5000
Cd109	3.9969E+07	88.0000	2846.0000	76918.9189	4.7000
Co57	2.3484E+07	122.1000	1517.0000	1772.1963	4.1000
Ce139	1.1889E+07	165.9000	2148.0000	2708.6280	3.9000
Hg203	4.0271E+06	279.2000	4591.0000	5628.9848	3.8000
Sn113	9.9446E+06	391.7000	2948.0000	4572.3482	3.9000
Cs137	9.4867E+08	661.7000	1937.0000	2154.6162	4.0000
Y-88	9.2102E+06	898.0000	7140.0000	7621.4826	3.9000
Co-60	1.6632E+08	1173.2000	3636.0000	3641.4622	4.0000
Ba-137m	1.5312E+02	661.7000	1937.0000	2154.6162	4.0000
Ag-109m	3.9600E+01	88.0000	2846.0000	76918.9189	4.7000
In-113m	5.9685E+03	391.7000	2948.0000	4572.3482	3.9000

It is noted that due to the relatively short half of Ba-137m, Ag-109m and In-113m with their parent nuclide Cs-137, Cd109, and Sn113, respectively, it is assumed that secular equilibrium has been reached for the isotope at the time of evaluation, and that the

activities of these isotopes are equal to their parents at the time of the detector calibration. It is also assumed that their uncertainties between mother and daughter nuclide are equal or close. Activities of short-lived daughters assume the values of their parents; it is not intended to show an addition to the total activity sum. Corrected to time of measurement values are given in Table 4.10. Correction uses standard decay equation, uncertainty in exact time is ignored. Due to the shorter half-lives of some of the isotopes, the available photopeaks provided by the mixed source is less when compared with the europium test source. Despite this, due to the greater activity of the isotopes that are still present at the date of measurement, the source strength for the mixed source is greater than the europium source. This will allow less uncertainty in the photopeak count rate to occur when the count rate is derived from Prospect, leading to better results when using the 10 minute live count time, as the magnitude of the photopeaks present in the mixed spectrum will be greater when compared to the europium spectrum photopeaks. This will allow observation to how count rate uncertainty affects the FEPE ratio spread.

Table 4.10. Corrected Mixed standard parameters, taken from source certificate
Parameters at Measurement Date: 8-17-2016 “current”

Isotope	Half-life (s)	Energy of interest	Current photons/s for each photopeak	Current Activity (Bq)	Expanded Relative Uncertainty (%), k=2
Am241	13651000000.0	59.500	2001.527	5575.286	3.500
Cd109	39969000.000	88.000	341.031	9217.061	4.700
Co57	23484000.000	122.100	40.993	47.889	4.100
Ce139	11889000.000	165.900	1.715	2.162	3.900
Hg203	4027100.000	279.200	0.000	0.000	3.800
Sn113	9944600.000	391.700	0.584	0.905	3.900
Cs137	948670000.000	661.700	1771.366	1970.374	4.000
Y-88	9210200.000	898.000	0.716	0.764	3.900
Co-60	166320000.000	1173.200	2183.690	2186.970	4.000
Ba-137m	153.120	661.700	1771.366	1970.374	4.000
Ag-109m	39.600	88.000	341.031	9217.061	4.700
In-113m	5968.500	391.700	0.584	0.905	3.900

This isotope was also used for BEGe 3825 calibration. The geometry for the measurement was discussed previously. A 10 minute spectrum was collected as shown in Figure 4.5. As seen in Figure 4.5, the mixed spectrum shows less overall photopeaks than the europium spectrum, but the magnitude of those photopeaks are generally greater (examined photopeaks of Europium). As compared to the europium spectrum, the mixed relative error percentages for the 5 examined photopeaks were generally lower than the europium photopeaks. The 122.1 keV peak from the mixed source showed anomalous uncertainty when compared to the other photopeaks in the spectrum. This irregularity will be examined for in the MCNP model to see if a similar uncertainty is predicted when the model responds to the full gamma/x-ray loading for the mixed source (all isotopes considered). FEPE ratio spread will be examined for the mixed and europium cases, and how they compare with each other.

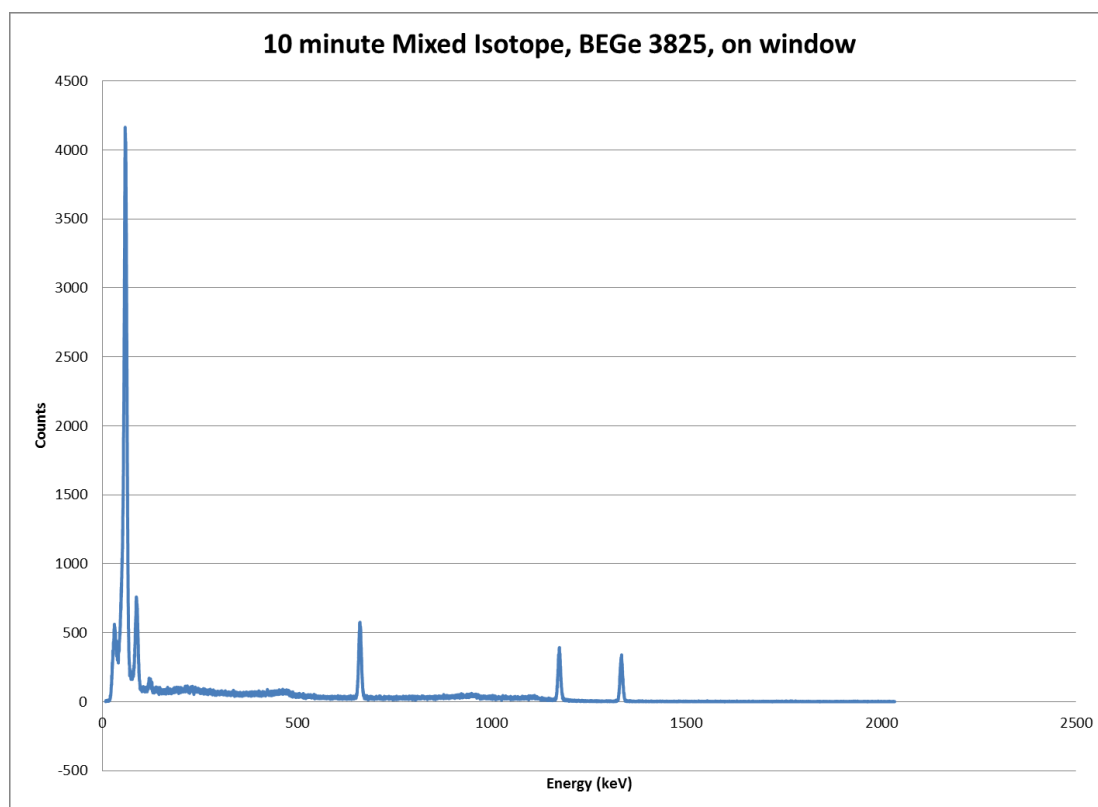


Figure 4.5. Mixed standard at 10 minutes of live time

Peak analyses for the validated peaks were completed under similar scanning parameters for Europium source using Canberra's Prospect software in Table 4.11 and 4.12.

Table 4.11. Mixed standard peaks of interest

Centroid (keV)	Net Area	Net cps	FWHM (keV)	Gaussian Ratio
59.5	196175.343 ± 1310.28	326.959 ± 2.18	8.208	1.224
88	27148.658 ± 597.67	45.248 ± 1.00	8.451	1.117
122.1	2704.375 ± 509.818	4.507 $\pm .85$	8.308	4.06
661.7	24146.625 ± 509.031	40.244 $\pm .85$	7.928	1.058
1173.2	15981.555 ± 274.61	26.636 $\pm .46$	8.003	1.082

Due to the relatively small measurement time, many of the less active isotopes were not included in the analysis at the specified searching resolution. However generally, the mixed net count rate for each photopeak was much greater than their europium counterpart, which lowers the uncertainty in the peak area and thus count rate. As shown in the physical measurements, the choice of the 10 minute live count time affected the europium test case more so than the mixed test case. This will provide ample data to compare the effect of count rate uncertainty upon the FEPE ratio and the average of the FEPE ratio as well as its spread around that average value. Two geometry test cases will allow for the determination of how a single correction factor affects the FEPE ratio for each test case, and to test its validity for each different geometry case, europium disk, and mixed cylinder.

Table 4.12. Mixed standard absolute peak efficiencies

Given Peak Energies (keV)	Measured Peak Centroids (keV)	% Error	Given photo n/s	Expanded Uncertainty (k=2) %	Measured Net cps	uncertainty	uncertainty %	Peak Absolute Efficiency %	Expanded Relative Uncertainty (k=2) %
59.500	59.445	0.092	2001.528	3.500	326.959	2.180	0.667	16.335	3.745
88.000	87.996	0.005	341.031	4.700	45.248	1.000	2.210	13.268	6.452
122.100	121.913	0.153	40.993	4.100	4.507	0.850	18.860	10.995	37.941
661.700	661.206	0.075	1771.366	4.000	40.244	0.850	2.112	2.272	5.818
1173.200	1172.543	0.056	2183.690	4.000	26.636	0.460	1.727	1.220	5.285

A plot of the full peak absolute efficiencies is given below in Figure 4.6. Although it is not apparent in Figure 4.6, the mixed photopeak uncertainty percentage is lower than the europium test case. This is a sign that the inherent higher count rate for the mixed compensates for the 10 minute live count time which causes the europium test case uncertainty to trend higher relative to the mixed. This issue, for future validation attempts could improve by increasing the live counting time for the physical measurement of the sample. Overall at the present, this uncertainty discrepancy will be used to observe the effects of uncertainty on the FEPE ratio spread and its respective average for the europium and mixed test case.

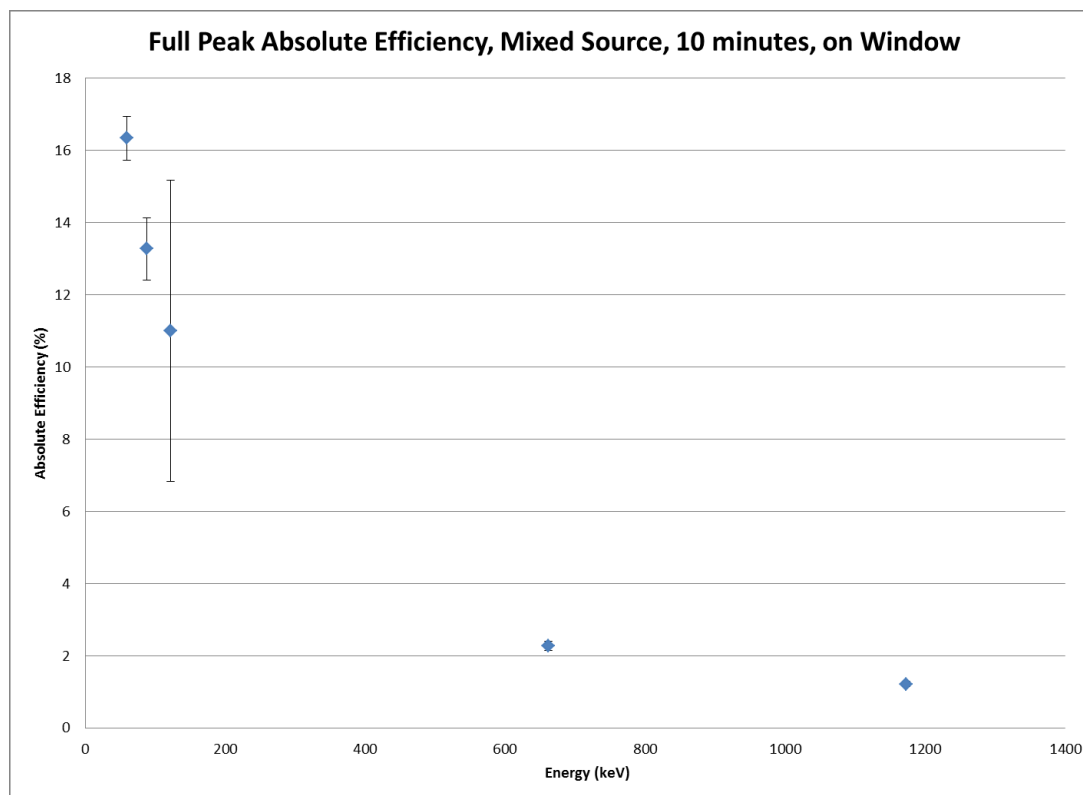


Figure 4.6. Mixed standard absolute efficiency plot

As can be seen in Figure 4.6, one of the errors is substantially larger perhaps due to small measurement time, and of the two gamma standards. Differences in the absolute efficiencies for the given validated peaks differ for similar energies between the mixed and europium test cases. This is expected since the geometry, and its arrangement of the test sources is different; the mixed source was a disk of known dimension inside a polymer cylinder while the Europium source was a disk of unknown dimension inside of a disk of unknown material. These source geometries are accounted for when modeling is done for the detector model validation, but the non-active casing materials are ignored for self-shielding from the sources. This conservative approach would result in higher initial activity for the Am241, giving a higher sensitivity to isotope detection. Since the goal of this model is to examine the viability of using the specified BEGe 3825, its simulation providing a positive bias toward detecting target photopeaks will allow the elimination of buildup conditions that are not useful. Irradiation time, decay time, and initial activity

cases of the examined sources that do not yield viable photopeaks in a model that would be prone to overestimate their magnitudes should be discarded. Depending upon the model's response, the behavior can be accounted for if the model shows a trend of overestimation/underestimation for a majority or all photopeaks examined.

5. MODEL DESCRIPTIONS AND VALIDATION WITH PREVIOUS WORK/STANDARD MEASUREMENTS

Two models were created for this study, both used MCNP V5 and as much as possible utilizing blue-prints, diagrams, and product information to create the geometry and material cards. The MSTR MCNP model was constructed due to its capability to track the behavior and production of isotopes in a given system. For a given initial activity of Am241, MCNP model approximates the MSTR and creates a radioactive inventory (mainly Am242 and Am242m in addition to other minor isotopes) that the BEGe 3825 model can simulate. The BEGe 3825 MCNP model will be utilized to mimic the physical detector response to a given photon loading, and determine if the use of that detector is viable. Gaps or uncertainties were bridged by the taking of relevant information from pre-existing works that used their own MCNP models of equal (MSTR) or similar (BEGe 3825) systems (Richardson, Castano, King, Alajo, & Usman, 2012). In the following description of the models, any information and/or parameters that were not taken from the original sources (MSTR/BEGe 3825) will be cited to the original document. Also before each model section, a table will be given that will qualitatively describe the low and high uncertainty that each aspect of the model holds, any component omissions, and any known errors that have not been fixed at time of writing. These tables are only to provide a general statement of the reliability for a given model's output, and how their comparison with established/measured work could possibly be affected.

For the MSTR general model, which was arranged into two distinct configurations for this study, the following is said regarding its sub-components in Table 5.1. Table 5.1 is to show any simplifications or issues that could be improved upon.

Table 5.1. MSTR model component certainty

High Certainty/Consistent With Previous Works	Low Certainty	Omitted	Known Errors/Inconsistencies with Established Models

Table 5.1. MSTR model component certainty, (cont.)

Dimensions of Fuel Plate, curvature, thickness, and Fuel plate water gap, Similar for Cladding, material and geometry	Regulating Rod Geometry	Non-Core Structural Components	Assembly local x-axis orientation
Number of fuel plates per Fuel/Control/Regulating assembly, and their side walls geometry and material	Core Grid Plate Geometry	Temperature Effects	Fresh Fuel composition (no burn-up considered)
Ideal Mass of U235 per Fuel plate	Bare and Cadmium Rabbit Tube Geometry	Hot Cell	
Control Rod, Material and Geometry	Source Holder Tube Geometry	Thermal Beam Port	
Configuration of 101W Core	Core's Position in Pool		
Configuration of MSTR as of 10/2016			
Regulating Rod Material			
Relative Location of Irradiation 101W Comparison, and Current Configuration with respect to other Core Components			
Core Grid Plate Material			
Pool			

The model of the MSTR was assembled into two different configurations, the 101W configuration was chosen for validation purposes since that was the one for Kulage's work in assembling a 3 group neutron flux for the MSTR, and 10-2016 configuration which is the current set-up. A full XY view of the MSTR in 101W configuration, Z midplane is shown in Figure 5.1. Table 5.2 gives the quantity of assemblies for both configuration types.

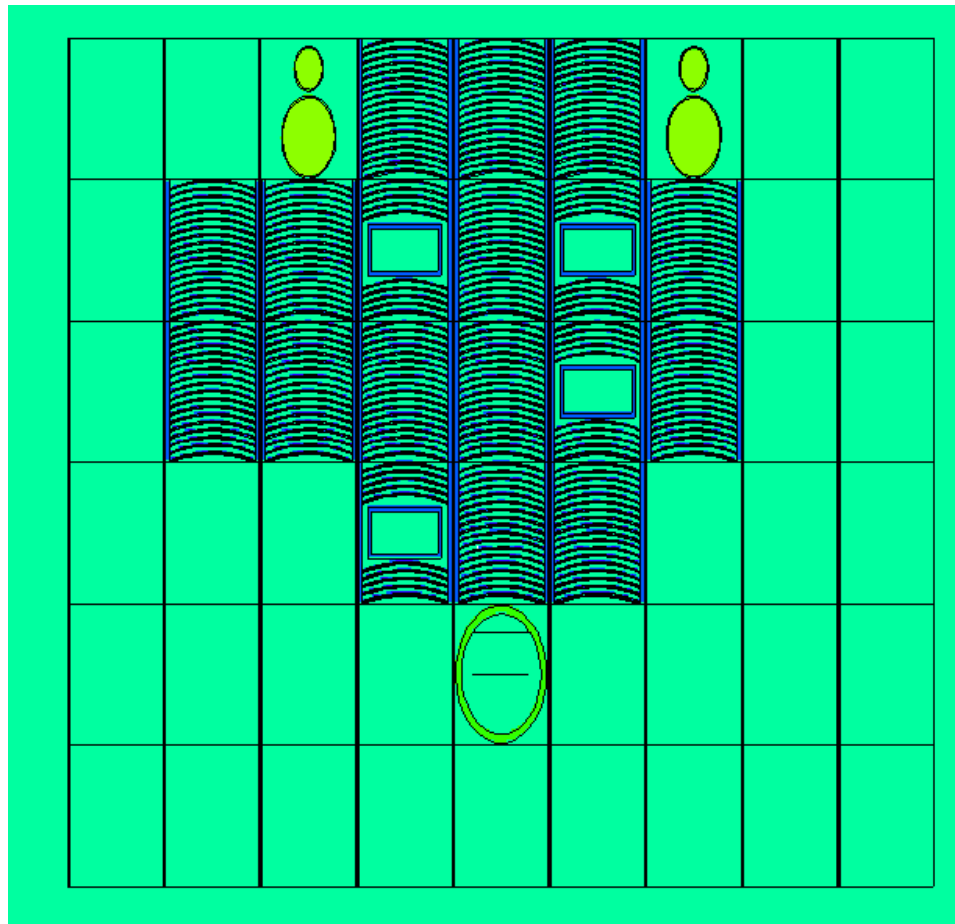


Figure 5.1. XY view of the MCNP MSTR 101W approximate

Table 5.2. Components of the 101W and 10-2016 approximate

Core Components	Quantity,101W	Quantity, 10-2016
Full Fuel assembly	14	15
Control Rod assembly	3	3
Regulating Rod assembly	1	1
Rabbit tube	1	1
Cd lined Rabbit tube	1	1
Source holder tube	1	1

Figure 5.2 shows the current core configuration (10-2016) with the simulated sample water foil in source holder tube exaggerated to locate.

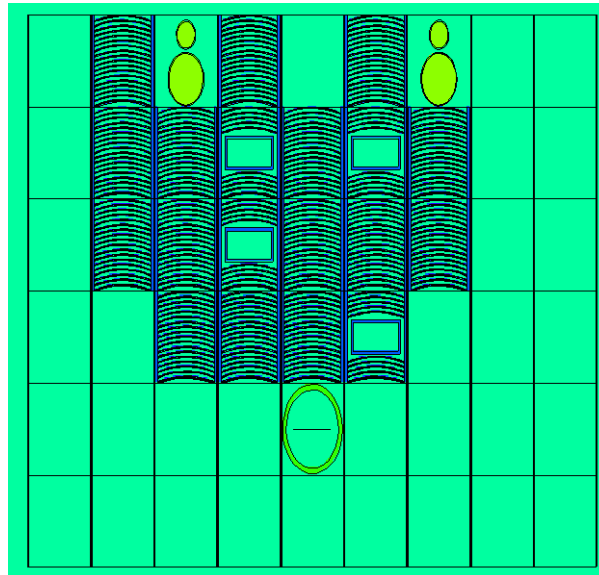


Figure 5.2. XY plane of 10-2016 MCNP model

View is at the midplane, core set up to be critical, the control/regulating rods were moved to the upper z plane values of the core to mirror that of previous work with MSTR.

Differences between configurations can be seen as the Control/Reg rods were switched around when transition to the current system and an additional fuel element is added to the core. In Figures 5.3, 5.4 and 5.5 a separate fuel assembly, a control assembly and the regulating assemblies are shown respectively. For both configurations the same fuel and control/regulating rods are used.

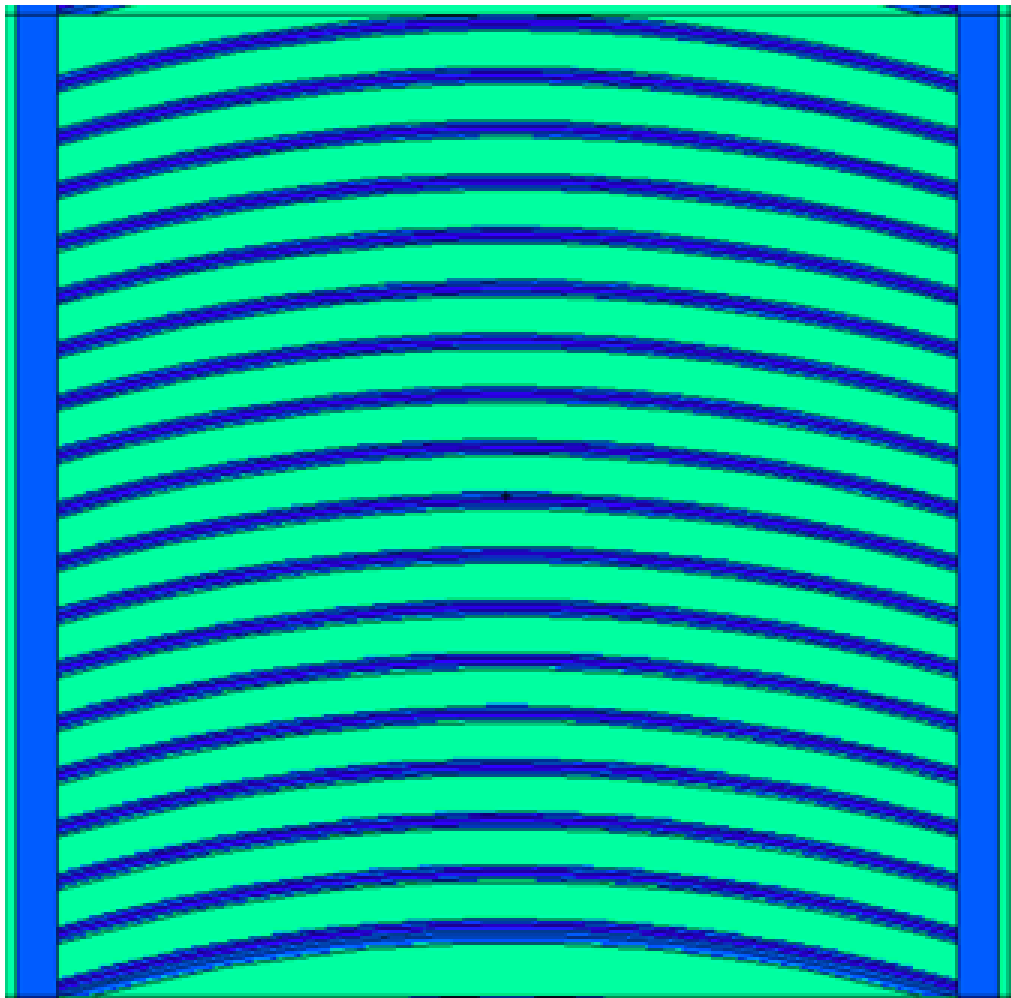


Figure 5.3. Standard fuel assembly approximated in MCNP

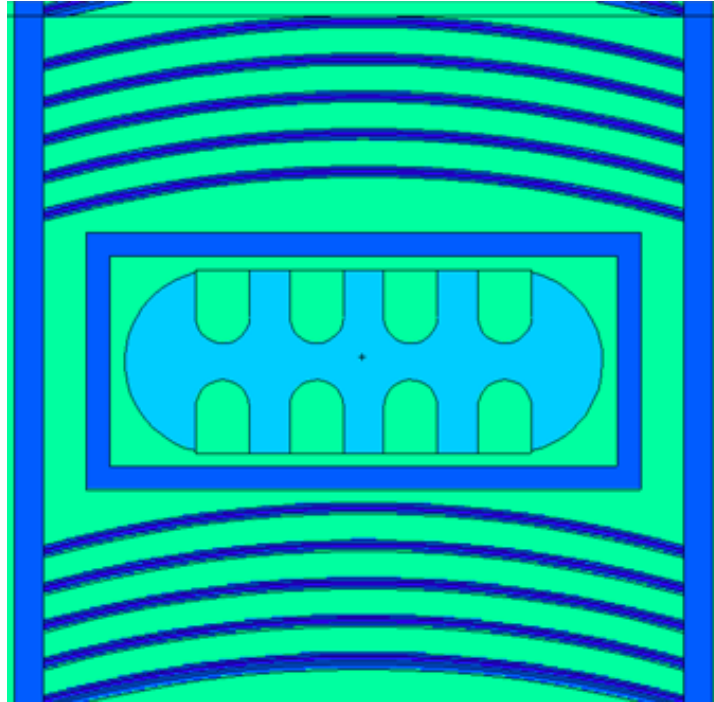


Figure 5.4. Control rod assembly approximated in MCNP

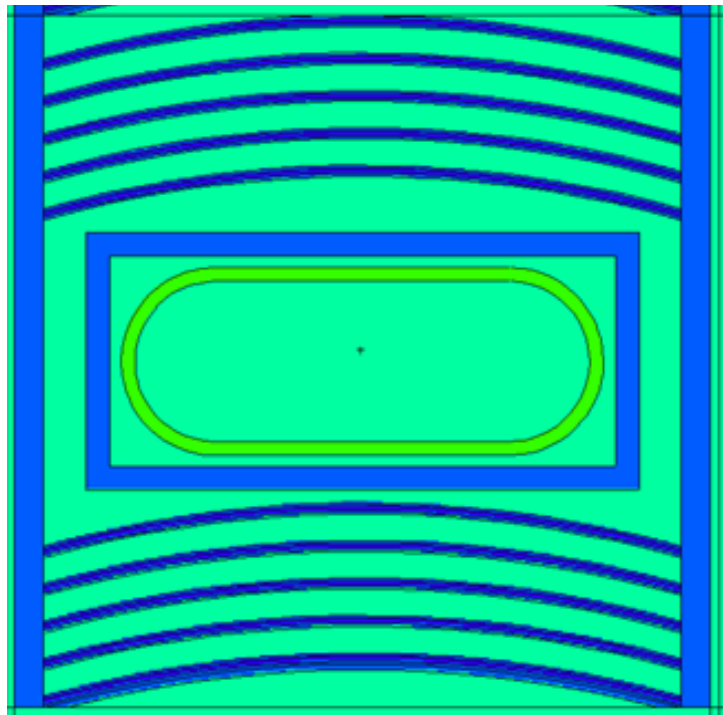


Figure 5.5. Regulating rod assembly approximated in MCNP

Figure 5.6 shows the Core configuration in relation with reactor pool while Table 5.3 provides the specific dimensions of the pool.

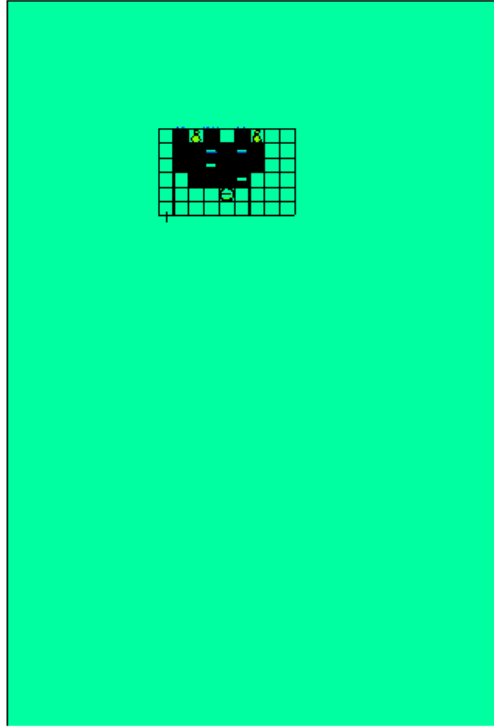


Figure 5.6. Approximate position of current core grid with respect to modeled reactor pool

Table 5.3. Reactor pool parameters

Boundary description	Value (cm)
Pool depth (z axis)	850
Pool width (x axis)	274
Pool length (y axis)	579

The core was fueled at approximately 20% U-235 (atom), and each fuel plate contains approximately 12.5261 g of U-235, active z length of fuel was 63 cm, and the grid plate and other external materials were taken from Richardson (Richardson, Castano, King, Alajo, & Usman, 2012). Fuel plate composition was taken from King's original model, verified by Richardson's. Grid plate and lower cylinders was approximated, upper core structural materials were omitted. The complete geometry and material cards that were used for this study can be found in the appendix A.

There are specific uncertainties in the exact placement of the tally for the purpose of validating the flux groups of this model; as a result the comparison suffers to a degree. The location that is tallied is at the midplane of the fuel (12 inches) from the core grid plate, to mirror the irradiation placement in the previous work (Kulage, Castano, Usman, & Mueller, 2013). The model that this study used produced a core-wide neutron flux, as well as more location specific estimates using regions that would take up a 5x5x.0005 cm Am241 foil. Table 5.4 displays the MCNP kcode parameters used for the simulation while Tables 5.5, 5.6, 5.7, 5.8, 5.9, and 5.10 shows the MCNP output converted to flux for 101W configuration at two power levels. For the validation of the neutron flux the number of source particles was 20000, for the MCNPX to decrease runtime, the number of source particles and active cycles were lowered

Table 5.4. MCNP kcode parameters for 101W MSTR model flux validation only

MCNP parameters for Validation	
NPS per cycle	20000
Initial K guess	1
Inactive cycles	50
Active cycles	300

To compare the models flux output with Kulage's work, a $5 \times 5 \times .0005$ region within the source holder tube at the center of the tube, a region at the limit of the source holder region and a region that was flush with the nearest fuel assembly was assigned a F4 neutron tally (Figure 5.7), split up into similar energy groups with different end power multipliers for conversion to flux.

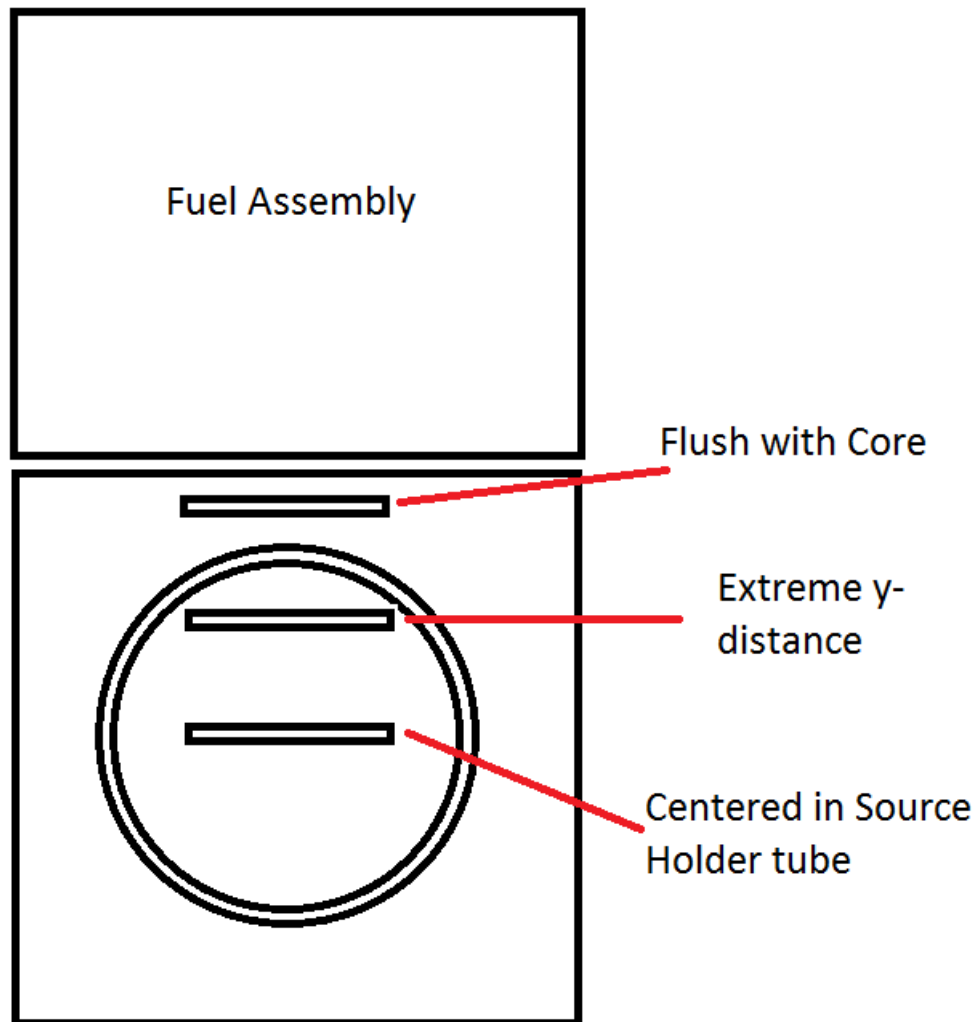


Figure 5.7. The relative location of tally cells, mimicking proposed test foil, not to scale

Table 5.5. Location specific 3 group neutron flux, 200 kW, 101W

Source holder position, centered, 12" above core plate Study Flux Groups, critical 101W, 200kW			
Energy	Flux ($\frac{neu}{cm^2s}$)	Uncertainty (%) (MCNP)	Fraction of Total %
0-.625 eV	2.07652E+12	2.44	6.22E+01
.625eV -100 keV	6.62519E+11	3.78	1.98E+01
>100 keV	6.0022E+11	2.63	1.80E+01
Total	3.33926E+12	1.82	1.00E+02

Table 5.6. Location specific 3 group neutron flux, 100 kW, 101W

Source holder position, centered, 12" above core plate Study Flux Groups, critical 101W, 100kW			
Energy	Flux ($\frac{neu}{cm^2s}$)	Uncertainty (%) (MCNP)	Fraction of Total %
0-.625 eV	1.03826E+12	2.44	62.18498456
.625eV -100 keV	3.3126E+11	3.78	19.84027743
>100 keV	3.0011E+11	2.63	17.97463676
Total	1.66963E+12	1.82	100

Due to the uncertainty in determining comparable measuring coordinates/elements, the spatial dependence upon the flux groups were examined, the same geometry element was near the interior edge of the source holder cell, and then another element flush with the nearest fuel element:

Table 5.7. MSTR model 101W, 200 kW three group flux estimates

Source holder position, Extreme end, 12" above core plate Study Flux Groups, critical 101W, 200kW			
Energy	Flux ($\frac{neu}{cm^2s}$)	Uncertainty (%) (MCNP)	Fraction of Total %
0-.625 eV	2.17743E+12	2.06	49.63870187
.625eV -100 keV	1.10903E+12	2.63	25.28258331
>100 keV	1.10008E+12	2.47	25.07852213
Total	4.38655E+12	1.44	100

Table 5.8. MSTR model 101W, 100 kW three group flux estimates

Source holder position, Extreme end, 12" above core plate Study Flux Groups, critical 101W, 100kW			
Energy	Flux ($\frac{neu}{cm^2s}$)	Uncertainty (%) (MCNP)	Fraction of Total %
0-.625 eV	1.08871E+12	2.06	49.63870187
.625eV -100 keV	5.54517E+11	2.63	25.28258331
>100 keV	5.50041E+11	2.47	25.07852213
Total	2.19328E+12	1.44	100

Table 5.9. Source holder position 3 group flux, near core, 200 kW, 101W

Source holder position, flush with core, 12" above core plate, Study Flux Groups, critical 101W, 200kW			
Energy	Flux ($\frac{neu}{cm^2s}$)	Uncertainty (%) (MCNP)	Fraction of Total %
0-.625 eV	1.94691E+12	2.03	3.53E+01
.625eV -100 keV	1.66445E+12	2.3	3.02E+01
>100 keV	1.89722E+12	1.93	3.44E+01
Total	5.50857E+12	1.26	1.00E+02

Table 5.10. Source holder position 3 group flux, near core, 100 kW, 101W

Source holder position, flush with core, 12" above core plate, Study Flux Groups, critical 101W, 100kW			
Energy	Flux ($\frac{neu}{cm^2s}$)	Uncertainty (%) (MCNP)	Fraction of Total %
0-.625 eV	9.73454E+11	2.03	35.34323759
.625eV -100 keV	8.32223E+11	2.3	30.21555732
>100 keV	9.48612E+11	1.93	34.44129715
Total	2.75429E+12	1.26	100

This placement closer to the fuel element (Flushed) produce better agreement between the intermediate and fast group of this model and the established values by Kulage, while the thermal flux was not as affected. These position dependent neutron flux groups could be compared with the validated 3 group flux from Kulage (Kulage, Castano, Usman, & Mueller, 2013), as shown in Tables 5.11, 5.12, 5.13, and 5.14.

Table 5.11. Comparison with 3 group flux for MSTR at 200 kW in the 101W configuration (Kulage, Castano, Usman, & Mueller, 2013)

% Difference between Kulage's and Modeled 3 Group fluxes at 200 kW			
Energy	Extreme y plane of Source Holder tube	Centered in Source holder Cell	Flush with Fuel assembly
0-.625 eV	29.8030045	34.425455	40.6429227
.625eV -100 keV	50.5866217	94.9432681	11.0969693
>100 keV	82.6604891	126.131733	33.1092211
Total	53.0044238	77.3374148	31.2656636

Table 5.12. Comparison with 3 group flux for MSTR at 100 kW in the 101W configuration (Kulage, Castano, Usman, & Mueller, 2013)

% Difference between Kulage's and Modeled 3 Group fluxes at 100 kW			
Energy	Extreme y plane of Source Holder tube	Centered in Source holder Cell	Flush with Fuel assembly
0-.625 eV	154.423867	152.472291	149.706066
.625eV -100 keV	29.1845939	76.7703972	11.1942653
>100 keV	63.3473344	111.73945	11.091007
Total	10.7259349	16.50544	33.2023602

Fractional percentages of Kulage's 3 group flux were then obtained, as shown in Table 5.13. Better agreement is found at the 200 kW thermal energy groups than compared with the fast and intermediate values.

Table 5.13. Percentage of 3 group flux for MSTR at 200 kW, 101W (Kulage, Castano, Usman, & Mueller, 2013)

Model's 3 group flux fractional percent of Kulage's 3 Group fluxes at 200 kW			
Energy	Extreme y plane of Source Holder tube	Centered in Source holder Cell	Flush with Fuel assembly
0-.625 eV	74.06212806	70.62993438	66.22138539
.625eV-100 keV	59.62544102	35.61930151	89.4863774
>100 keV	41.51252667	22.64982502	71.59338358
Total	58.10000235	44.22864666	72.96125753

Table 5.14. Percentage of Established 3 group flux for MSTR at 100 kW, 101W (Kulage, Castano, Usman, & Mueller, 2013)

Model's 3 group flux fractional percent of Kulage's 3 Group fluxes at 100 kW			
Energy	Extreme y plane of Source Holder tube	Centered in Source holder Cell	Flush with Fuel assembly
0-.625 eV	777.6523446	741.614311	695.3245466
.625eV-100 keV	74.53180128	44.52412688	111.8579718
>100 keV	51.89065834	28.31228127	89.49172948
Total	111.3337608	84.75286352	139.8115468

As seen in Tables 5.11 through 5.14, MCNP model of the MSTR shows varying levels of agreement with the established 3 group flux. Of the three element locations, the best (Total group) results were obtained when the fluence was tallied near the boundary of the nearest fuel assembly (flush), Power dependent, at 200 kW, with best case being a total group percent difference of ~31%, and the total expected flux being ~73% of the established values from Kulage at that power, at 100 kW, the best total group percent difference was found at the extreme limit at the source holder interior wall, being a percent difference of ~11% and with the total group flux being ~111% of Kulage's established 100 kW flux value. Overall thermal flux estimations suffered consistently at all three tested locations when at 100 kW, with the cause being unknown, but this issue will be ignored since the power value of 200 kW will be utilized in the upcoming Burn-up analysis. Some primary differences between the F4 tally of this study and Kulage's experiment would have been the exact location of the element, as can be seen throughout the comparison tables above, the intermediate and fast group fluxes varied greatly as the y dimensions of the test element was changed. An exact location (besides the z position above the core plate) inside the source holder tube was not given, and thus the reason why multiple test element locations were utilized. Statistical checks were made for the two cell tallies by MCNP, and figure of merits for the validation tests are provided. Uncertainty in the above flux values were not taken into account, as the goal was to show that at 200 kW, neutron flux values in the source holder tube match the general magnitude as predicted by Kulage. This power of 200 kW is the value that will be used for the 2nd goal of examining irradiation of Am241 to Am242/Am242m. Table 5.15 gives the results of statistical checks made of a specific bin for the F4 validation tallies.

Table 5.15. MCNP statistical checks for F4 validation tallies

	Centered F4 Tally	Extreme y-limit F4 Tally	Flush F4 Tally
MCNP Statistical Check	Outcome	Outcome	Outcome
Mean behavior	Yes	Yes	Yes
Relative Error<.1	Yes	Yes	Yes

Table 5.15. MCNP statistical checks for F4 validation tallies, (cont.)

Relative Error decrease	Yes	Yes	Yes
Relative Error decrease rate 1/sqrt(nps)	Yes	Yes	Yes
Variance of the variance value	Yes	Yes	Yes
Variance of the variance decrease	Yes	Yes	Yes
Variance of the variance decrease rate 1/nps	Yes	Yes	Yes
Figure of Merit Value constant	Yes	Yes	Yes
Figure of Merit behavior random	Yes	Yes	Yes
Pdf slope>3	Yes	Yes	Yes

All F4 tallies passed their statistical check for the specific bin, to lower runtime, the Burn-up analysis for the simulated Am241 irradiation to Am242/Am242m will use less particles and less cycles, as will be highlighted below. Table 5.16 gives the figure of merit for each of the validation F4 tallies.

Table 5.16. FOM for F4 validation tallies

Simulation (ctm=202.76)	FOM for tally
Centered F4 Tally	3.723E+01
Extreme y-limit F4 Tally	2.852E+01
Flush F4 Tally	1.783E+01

As can be seen above, the MSTR model generates an approximate of the established 3 neutron group flux, being heavily affected by the position within the source

holder cell within an order of magnitude at full power. It is expected that a test element on the extreme y-plane away from the core to be less in magnitude and more skewed to the thermal energies. On a whole the model underestimates the flux in each energy group, which is expected to cause the model to underestimate the amount of actinides and fission products produced in a given time-step, which will then cause the burn times required to produce enough Am-242m for each initial Am241 activity case to be measurable, to be over-estimated. Core-Wide and Source holder Neutron fluxes were then updated for the 10-2016 core configuration, with the relevant 3 group fluxes, comparisons with Kulage's work are not performed. By establishing that the model has produced fluxes that are comparable with established groups at 200 kW, it is assumed that the MSTR, in the current configuration, its energy dependent neutron flux is approximated by the present model, and shares the same underestimation trend of the actual neutron fluxes, at primary importance being the thermal flux. The centered source holder tube flux values are of great importance and the current configuration flux values are given in Table 5.18, as the irradiation simulations will occur in that location for the Am241 to Am242/Am242m tests. The Core wide flux groups for the current configuration by Table 5.17 is given only to showcase the position dependence that is assumed for both configurations of the MSTR, and which was accounted for with the 101W validation by mirroring the fluence tally location of Kulage's experiment.

Table 5.17. Core wide 3 groups neutron flux from MSTR approximate, 200 kW and 100 kW, 10-2016 configuration, approximate flux values expected during a 200 kW irradiation in the source holder tube

Core-Wide Study Flux Groups, critical 10-2016, 200 kW			
Energy	Flux ($\frac{neu}{cm^2s}$)	Uncertainty (%) (MCNP)	Fraction of Total %
0-.625 eV	1.19226E+12	0.0683929	41.02554258
.625eV -100 keV	7.57965E+11	0.0426691	26.08153151
>100 keV	9.5592E+11	0.0555794	32.89315859
Total	2.90614E+12	0.0371384	100

Table 5.17. Core wide 3 groups neutron flux from MSTR approximate, 200 kW and 100 kW, 10-2016 configuration, approximate flux values expected during a 200 kW irradiation in the source holder tube, (cont.)

Core-Wide Study Flux Groups, critical 10-2016, 100 kW			
Energy	Flux ($\frac{neu}{cm^2s}$)	Uncertainty (%) (MCNP)	Fraction of Total %
0-.625 eV	5.96129E+11	0.0683929	41.02554258
.625eV -100 keV	3.78983E+11	0.0426691	26.08153151
>100 keV	4.7796E+11	0.0555794	32.89315859
Total	1.45307E+12	0.0371384	100

Table 5.18. Source holder 3 group neutron flux from MSTR approximate, 200kW and 100 kW, 10-2016 configuration

Source holder position, Centered, Study Flux Groups, critical 10-2016, 200kW			
Energy	Flux ($\frac{neu}{cm^2s}$)	Uncertainty (%) (MCNP)	Fraction of Total %
0-.625 eV	1.98682E+12	3.16	61.28687418
.625eV -100 keV	6.87811E+11	5.12	21.21668483
>100 keV	5.67206E+11	3.75	17.49644099
Total	3.24184E+12	2.44	100
Source holder position, Centered, Study Flux Groups, critical 10-2016, 100kW			
Energy	Flux ($\frac{neu}{cm^2s}$)	Uncertainty (%) (MCNP)	Fraction of Total %
0-.625 eV	9.93411E+11	3.16	61.28687418
.625eV -100 keV	3.43905E+11	5.12	21.21668483
>100 keV	2.83603E+11	3.75	17.49644099
Total	1.62092E+12	2.44	100

The F4 and FMESH core wide flux estimates given by MCNP for the MSTR in the most current configuration of fuel/control/regulating elements passed (only F4 determined) their statistical tally check, with a FOM of 23.81 and a ctm of 87.70 minutes. For the purpose of the Am241/Am242/Am242m buildup analysis, the nps and cycle values were lowered from the 101W validation phase to an nps=10000, and 250 cycles with 50 inactive for the MSTR current approximate flux estimates, which is a primary cause in the lower run times. The exact same initial fission source point distribution was utilized of for the burn-up simulations.

The second model that this study used was one that would simulate BEGe 3825 response to the activity of the irradiated sample inventory. The inventory final activity, at various times of irradiation were taken as true values (once MCNP precision was increased) from which a photon distribution could be constructed using all gamma/x-ray decay lines from every fission product, activation product and actinide. This model was based off of the BEGe 3825 that is housed inside the reactor bay inside a lead shielded container. For the BEGe 3825 general model, the following is said regarding its sub-components via Table 5.19.

Table 5.19. BEGe 3825 model component certainty

High Certainty/Consistent With Previous Works	Low Certainty	Omitted	Known Errors/Inconsistencies with Established Works
Ge Crystal Geometry and Material	Europium Sample Active Dimensions	Non-Crystal End-Cap Internal components (Copper Crystal Holder)	X
End-Cap Geometry and Material	Interior non-crystal component dimensions and material	Inner and Outer Grooves on Ge Crystal	X
Sample-Source Dimensions	X	Sample material	X

Table 5.19. BEGe 3825 model component certainty, (cont.)

Mixed Sample Dimensions	X	Detector Window's Protective Cover	X
Shield Material, Geometry	X	X	X
Ge Dead layer (top, radial)	X	X	
FWHM behavior	X	X	
Channel Energy	X	X	

The BEGe 3825 model is separate from the MSTR model, isotope activity values from the MSTR model are fed into spreadsheets to determine photon energy and probability distributions and then those are inputted into the BEGe 3825 model's photon source definition card for a uniformly sampled disk of some radius. Use of the multiplier (the total amount of source photons emitted by a source) will be used to scale the F8 normalized tally results in its 16384 energy bins. The live counting time is factored into the multiplier. Multiplier will not change channel relative counts. Multiplier does not consider change over time, analysis of potential live times will have to be done in order to limit photon rate error and ensure realism, however, for non-target photopeaks, is expected to cause any possible interference from short-lived isotopes (relative to Am241, Am242) to be overestimated which can be useful. Figure 5.8 gives a Canberra provided schematic of the BEGe 3825 with internal geometries outline. The model was simplified and the intricacies of the internal detector were omitted or generalized. Unlike the MSTR model, diagrams of the model geometry in MCNP were unable to be used to verify principal structures and assembly. As such particular importance was put on describing the position of the source geometry, as well as factors as dead layer thickness, europium active radius (unknown), and the effect of the uncertainty in the multiplier used to scale the F8 tallies on the FEPE ratio between the measured FEPE and the MCNP/Prospect derived FEPE ratio value. These parameters were tested for both the mixed and europium case where valid and the simulated results were compared with the physical measurements resulting in the FEPE ratio.

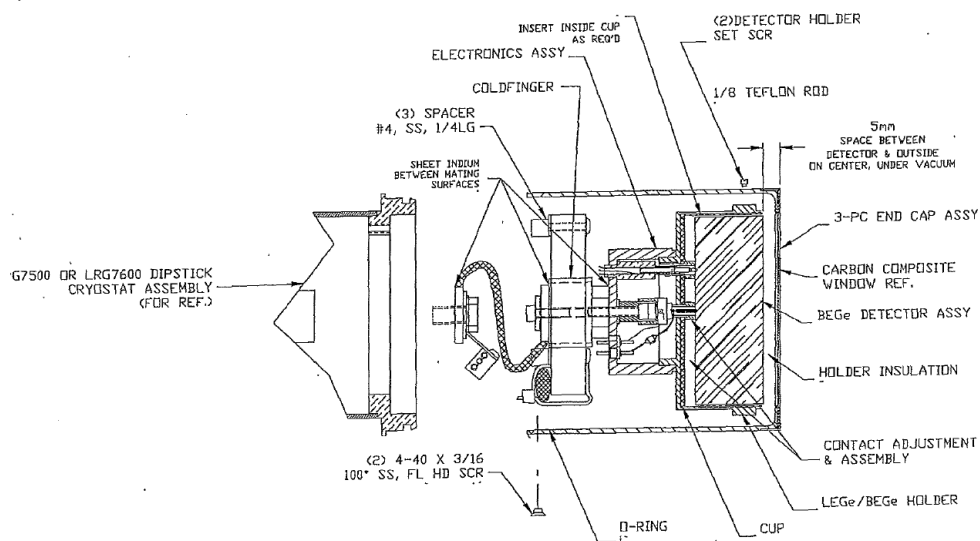
Detector S/N 08088371

Figure 5.8. Schematic of BEGe 3825, as provided by Canberra

The following parameters (Table 5.20) were directly obtained from the Canberra technical diagram of the BEGe 3825 detector:

Table 5.20. BEGe 3825 detector parameters (Canberra)

Parameter	Value (mm)
Diameter (crystal)	70.0
Thickness (crystal)	25.0
Groove ID (omitted)	14.5
Groove OD (omitted)	22.0
Front Dead Layer	.3E-03
Side Dead Layer	.5
Back Dead Layer	.5
Front Corner Radius (omitted)	1.0

Table 5.20. BEGe 3825 detector parameters (Canberra),
(cont.)

Carbon Composite Window thickness	.6
Cryostat End Cap material (Aluminum) thickness	1.5
Crystal Holder Material (Copper) thickness	NA
Distance from top of crystal to top of window	5

From this information, a model in MCNP was constructed; simplifications were made to the geometry of and around the Germanium crystal. The structures behind the crystal holder (away from the window) were ignored. The Ge dead layers were not modified for this study, which is a common need for simulated Germanium detectors. As such the simulation should not be used for energy peaks below 40 keV as it greatly overestimates in this region compared with the measured standards (Figure 5.22 and 5.23, <40 keV region). The model also incorporated the lead shielding that the detector was housed in, from Canberra, as shown in Figure 5.9. The shielding had liners of copper and tin to prevent lead x-rays from incident electrons from interfering with the detector. Shield components and geometry is given by Table 5.21. By using this assumption, the run-time could be further decreased for the full photon/electron test. Inner and outer groove diameters, assumed for the germanium crystal were omitted. This was done as the effects of the grooves were assumed to be minimal. The side and back germanium dead layers were included as well on the germanium crystal cylinder. Other geometrical considerations, such as the corner radius were omitted due to fear of misinterpretation when modeling the surfaces and cells in MCNP. The copper holder and other interior parameters, assumed to cup the Ge crystal cylinder at some side thickness and diameter, and the window material, were both taken from (Fantinova & Fojtik, 2014). The complete geometry description for the BEGe 3825 model can be found in Appendix A.

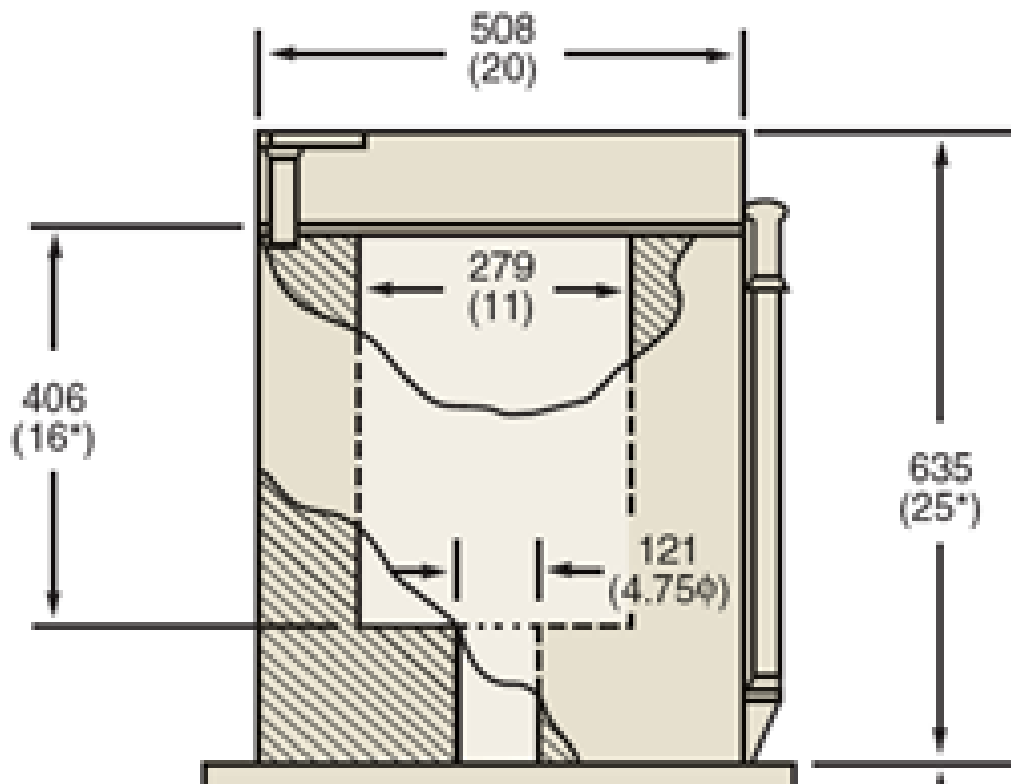


Figure 5.9. Diagram of shielding set-up (Canberra Industries, 2013)

Table 5.21. Shield physical parameters

Material Specification		
Component	Material	Typical Thickness
Outer Jacket	Low carbon steel	9.5 mm
Bulk Shield	Lead	10 cm
Graded Lining	Tin	1 mm
	Copper	1.6 mm

The MCNP model simplified some of the geometry not-related to the Germanium crystal, but kept all component dimensions where applicable. Figure 5.10 shows complete MCNP model of BEGe 3825. Major visible components are described by Table 5.22.

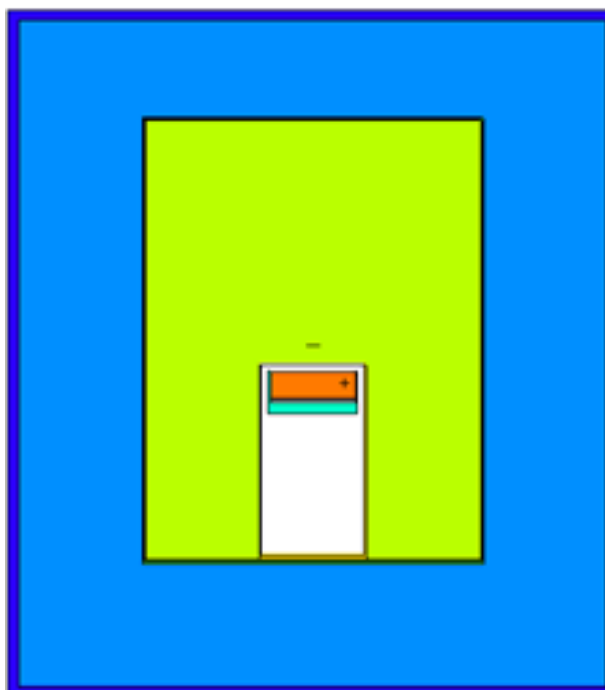


Figure 5.10. MCNP model of BEGe 3825, and shield

Table 5.22. Color scheme for model figure

Visible Color	Material (Except air/vacuum, room temperature solids)
Green	Air (sea-level)
Blue	Lead
Purple	SS 304
Light Blue	Copper

Table 5.22. Color scheme for model figure, (cont.)

White	Vacuum
Orange	Ge material

In order to match the widening of the physical peaks due to signal noise, the Gaussian Energy Broadening (GEB) feature on the F8 tally was employed, the specific parameters were taken from the FWHM calibration data that Prospect gave for the BEGe 3825 detector of interest. The GEB parameters for the BEGe 3825 detector were taken directly from the coefficients of the FWHM calibration equation for the detector and are given in Table 5.23.

Table 5.23. Parameters for the GEB setting on the F8 tally

a (MeV)	b (MeV ^{1/2})	C (unit-less)
.007508	2.73758E-05	0

Attempts to fit a line to the energy vs experimental FWHM data resulted in an equation of very poor fit due to the insufficient number of data points and the many outliers that existed within the sample. As such the GEB parameters (table 41) were taken directly from the FWHM calibration equation that was generated in the specific BEGe 3825 detector during its FWHM calibration. The sources were modeled as an infinitely thin disk. The MCNP F8 tally was separated into 16384 energy bins to mimic the channel number of the Prospect derived output spectrum. The model of the BEGe 3825 was compared to the acquired physical results with the Mixed and the Europium Gamma standards. The absolute peak efficiencies were acquired from the simulated spectrum and the true data, and then compared with the real peak efficiencies. In both the Mixed and

Europium standard's dead time was accounted for by ensuring the live time duration was 10 minutes. For the simulation this involved multiplying the MCNP normalized tally count by the total photon rate from the actual source and the use of a live time of 600 seconds to account for the dead time that the detector experienced. The expanded uncertainty ($k=2$) in the activity of the gamma standards, and thus the total photon count released in the 10 minutes of live counting was not transferred over into the Prospect software. Instead, a low and high estimation of the total photon count was taken to compare with the physical gamma standard measurements. Actual FEPE ratio values are expected to vary within the observed value ranges for a given isotope due to this uncertainty in multiplier. The Europium standard was assumed that each activity had an expanded relative uncertainty of 5%. The derived multipliers and their min/max for each validation simulation were taken using the expanded uncertainty of the photon emission rates for each standard, and are given in Table 5.24.

Table 5.24. Photon count multiplier (mid, min, max) used on source particle normalized F8 tally results

Simulation	Total photon/s (all gamma and x-rays)	Total live time (min)	Total photon Count, $k=2$ (multiplier)
Europium	16101.3 ± 805.065	10	$9.661E6 \pm 4.83E5$
Mixed	20961.49 ± 895.158	10	$1.258E7 \pm 5.37E5$

For both Europium and the mixed standard, tests were run using MCNP's three different approaches to modeling photon interactions for the F8 tally, and their comparisons with each other. These approaches are 1st, where photon interactions can generate electrons and these electrons are then tracked in a given history, 2nd, photon interactions use the thick target bremsstrahlung model, where electrons are generated, but

immediately absorbed, but the resulting x-rays are tracked, 3rd, all of the photoelectric incidents result in immediate electron absorption, and no bremsstrahlung x-rays are generated. These three types of models were used to determine the possible benefits from using the computationally expensive full treatment option in the Ge mass alone. This coupled photon/electron model was simplified to allow for feasible times, by setting all electron importance's outside of the Germanium mass (detector, dead layers) to zero, only the electrons inside of the Germanium were tracked, their escape from the germanium mass would be considered absolute, and the electron is no longer tracked. Incident photon energies would be reduced once the entire history of the photon and its products had its deposited energy in the Ge measured and tallied by the F8 pulse height tally into the appropriate energy bin (channel). The Prospect derived peak parameters, using the automated peak finder function, as well as the full energy peak efficiency value (FEPE) for the Europium standard using the three different approaches discussed above are given in Table 5.25. A visual accounting for the FEPE of the examined photopeak is given in Figure 5.11. For all BEGe 3825 error analysis, it is assumed that the results from the model and physical experiments are random and independent of each other and that counting statistics apply in their derived peak net area results, for both model and experimental data. The described multipliers will be used to scale the F8 tallies for both europium and mixed test cases by the total number of photons emitted during the live count time. The uncertainty in the multiplier is tested for by examining its minimum and maximum value when considering its composite nature.

Table 5.25. Europium Prospect automated analysis using three different photon/electron treatments

Photon/electron treatment	Given Centroid (keV)	MCN P Centroid (keV)	% Error	MCN P Net Count rate	Uncertainty % Prospect)	FEPE (%)	Uncertainty % k=2	Measured FEPE to MCN P FEPE Ratio	Ratio Uncertainty % (k=2)
Full	86.5000	86.4610	0.0451	96.4114	1.2331	22.2565	5.5751	1.2223	8.0500

Table 5.25. Europium Prospect automated analysis using three different photon/electron treatments, (cont.)

	105.3 000	105.1 290	0.162 4	50.52 09	2.292 3	16.95 16	6.783 7	0.782 3	11.44 40
	244.7 000	245.6 230	0.377 2	58.90 37	1.584 1	18.86 21	5.919 3	0.584 6	9.546 1
	344.3 000	344.0 990	0.058 4	81.72 52	1.093 8	7.495 5	5.457 6	0.889 2	7.859 1
	591.7 000	591.3 080	0.066 2	5.066 3	12.03 25	3.627 8	24.57 90	0.479 8	68.89 89
	723.3 000	722.7 290	0.078 9	18.60 62	3.288 1	3.286 9	8.261 1	0.734 5	13.35 07
	1004. 8000	1003. 6020	0.119 2	18.27 83	4.327 6	3.597 5	9.995 7	1.003 4	14.66 03
	1274. 5000	1273. 4590	0.081 7	18.56 33	2.067 4	1.888 9	6.488 2	0.800 0	9.954 4
	1408. 0000	1406. 9680	0.073 3	14.69 45	1.986 5	1.698 8	6.386 3	0.567 9	38.49 16
	Given Centr oid (keV)	MCN P Centr oid (keV)	% Error	MCN P Net Count rate	Uncer tainty % Prop spect)	FEPE (%)	Uncer tainty % k=2	Measu red FEPE to MCN P FEPE Ratio	Ratio Uncer tainty % (k=2)
TTB appro ximat ion	86.50 00	86.47 10	0.033 5	96.84 84	1.208 6	22.35 74	5.553 6	1.216 7	8.035 2
	105.3 000	105.1 140	0.176 6	50.47 30	2.321 5	16.93 55	6.823 3	0.783 0	11.46 75
	244.7 000	245.8 710	0.478 5	54.87 77	11.44 69	17.57 29	23.43 34	0.627 5	24.60 11
	344.3 000	344.1 070	0.056 1	81.88 52	1.090 9	7.510 2	5.455 3	0.887 5	7.857 5
	591.7 000	591.3 240	0.063 5	4.727 9	13.75 97	3.385 6	27.97 00	0.514 2	70.18 01
	723.3 000	722.7 020	0.082 7	18.90 34	3.131 5	3.339 4	8.014 0	0.723 0	13.19 92
	1004. 8000	1003. 6690	0.112 6	18.43 03	4.416 2	3.627 4	10.14 94	0.995 1	14.76 56
	1274. 5000	1273. 4760	0.080 3	18.72 89	2.038 9	1.905 8	6.452 1	0.792 9	9.930 8
	1408. 0000	1406. 9630	0.073 7	14.89 83	1.948 0	1.722 4	6.338 7	0.560 1	38.48 37

Table 5.25. Europium Prospect automated analysis using three different photon/electron treatments, (cont.)

	Given Centr oid (keV)	MCN P Centr oid (keV)	% Error	MCN P Net Count rate	Uncer tainty % Prospect)	FEPE (%)	Uncer tainty % k=2	Measu red FEPE to MCN P FEPE Ratio	Ratio Uncer tainty % (k=2)
Local deposi tion	86.50 00	86.46 00	0.046 2	96.28 29	1.197 7	22.22 68	5.544 2	1.223 9	8.028 6
	105.3 000	105.1 200	0.170 9	50.50 65	2.334 0	16.94 68	6.840 4	0.782 5	11.47 77
	244.7 000	245.6 120	0.372 7	58.95 83	1.577 5	18.87 96	5.912 2	0.584 0	9.541 7
	344.3 000	344.1 080	0.055 8	78.39 96	3.697 3	7.190 5	8.926 3	0.926 9	10.56 69
	591.7 000	591.3 270	0.063 0	4.773 3	14.03 86	3.418 1	28.51 89	0.509 3	70.40 07
	723.3 000	722.6 990	0.083 1	18.82 82	3.158 1	3.326 1	8.055 7	0.725 9	13.22 46
	1004. 8000	1003. 5630	0.123 1	18.85 98	4.228 9	3.711 9	9.825 2	0.972 4	14.54 47
	1274. 5000	1273. 4620	0.081 4	19.37 33	1.999 5	1.971 3	6.402 5	0.766 6	9.898 7
	1408. 0000	1406. 9570	0.074 1	15.58 28	1.875 2	1.801 5	6.250 2	0.535 5	38.46 92

Minimal impacts from photon/electron treatment options are seen, and the MCNP model is able to predict the relatively large uncertainty percentage for the 591.7 keV photopeak that was observed during the physical measurement of the europium standard source. The 1408 keV peak that displayed a relatively higher uncertainty during measurement was not simulated with a large uncertainty, suggesting that the model's overestimation of photopeaks introduces negative uncertainty and biases the model toward the successful detection of photopeaks given that it overestimates the photopeak net area and thus its count rate for a given counting time.

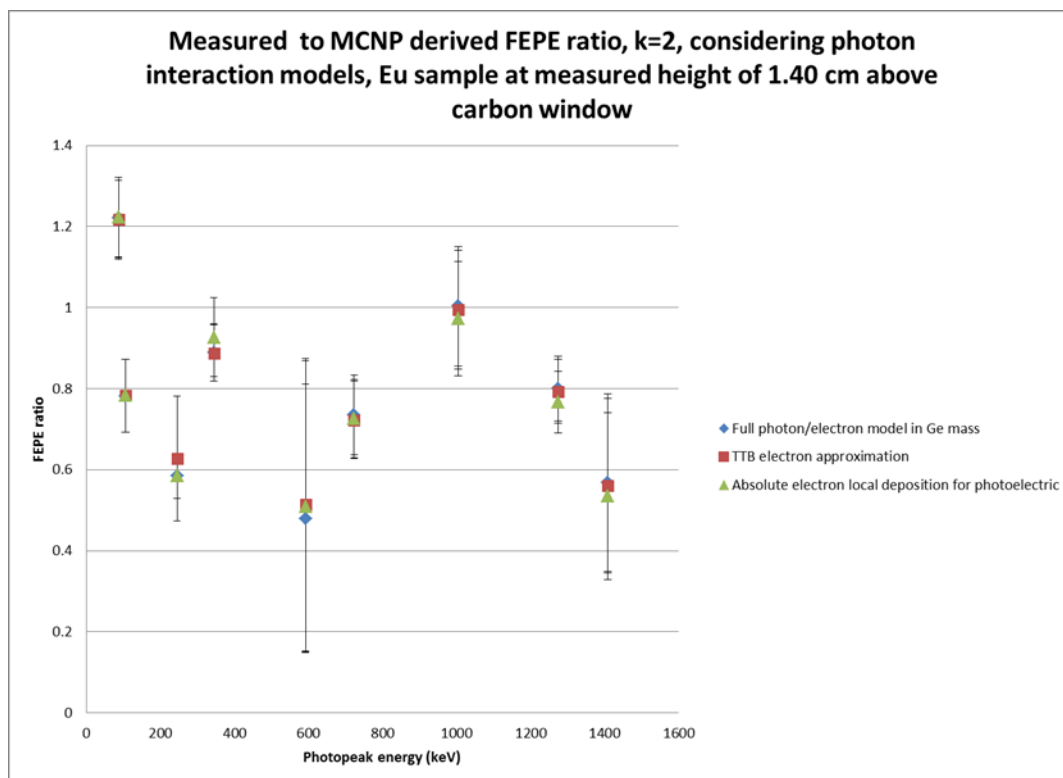


Figure 5.11. Europium FEPE ratio as given by photon/electron treatment option

The 591.7 keV peak displayed the largest error margins consistently for all 3 MCNP methods for photon interaction. All photon/electron treatment options yielded similar FEPE ratio values when compared with the measured data for the Europium source, as such, the approach with the lowest run time was chosen for the Am241/Am242/Am242m simulated sample loadings, Absolute electron local deposition for photons undergoing a photoelectric interaction with materials. The Full photon/electron model was limited to only the Ge detector mass as the lead shielding which surrounded the physical detector, and included in the model contained layers of tin and copper to shield against the bremsstrahlung x-rays from any generated electrons interacting with lead. Since these interaction x-rays could be ignored, the run-time could be greatly shortened by limiting electron transport inside the germanium mass for examination of its effect upon the FEPE ratio for the mixed and europium test cases.

The same was done for the mixed source with the MCNP F8 tallies and Prospect analysis software from Canberra as shown in Table 5.26 and Figure 5.12. The same live count time of 10 minutes was utilized, which was less of a problem for this case.

Table 5.26. Mixed source Prospect automated peak analysis considering photon/electron treatment options

Photon/electron treatment	uncertainty % k=2	Given Centroid (keV)	MCNP Centroid (keV)	% Error	MCNP Net Count rate	Uncertainty % Prospect	FEP E (%)	Uncertainty % k=2	Measured FEP E to MCNP FEP E Ratio	Ratio Uncertainty % (k=2)
Full	3.5000	59.5000	59.5770	0.1294	412.3217	0.3531	20.6003	3.5705	0.7930	5.1746
	4.7000	88.0000	88.0280	0.0318	69.2582	1.1989	20.3085	5.2763	0.6533	8.3347
	4.1000	122.1000	122.0210	0.0647	6.9356	8.2828	16.9192	17.0655	0.6498	41.6025
	4.0000	661.7000	661.2260	0.0716	53.1615	1.3154	3.0012	4.7876	0.7570	7.5343
	4.0000	1173.2000	1172.4480	0.0641	38.3237	1.3615	1.7550	4.8389	0.6950	7.1655
	uncertainty % k=2	Given Centroid (keV)	MCNP Centroid (keV)	% Error	MCNP Net Count rate	Uncertainty % Prospect	FEP E (%)	Uncertainty % k=2	Measured FEP E to MCNP FEP E Ratio	Ratio Uncertainty % (k=2)
TTB	3.5000	59.5000	59.5740	0.1244	412.8666	0.3669	20.6276	3.5761	0.7919	5.1785
	4.7000	88.0000	88.0430	0.0489	69.5639	1.1912	20.3981	5.2693	0.6505	8.3302
	4.1000	122.1000	121.9580	0.1163	6.9195	8.2080	16.8798	16.9202	0.6513	41.5432

Table 5.26. Mixed source Prospect automated peak analysis considering photon/electron treatment options, (cont.)

	4.000 0	661.7 000	661.2 180	0.072 8	53.57 98	1.159 6	3.024 8	4.623 8	0.751 1	7.431 2
	4.000 0	1173. 2000	1172. 4110	0.067 3	37.48 20	1.439 5	1.716 5	4.928 3	0.710 6	7.226 2
	uncer tainty % k=2	Give n Centr oid (keV)	MCN P Centr oid (keV)	% Error	MCN P Net Coun t rate	Unce rtaint y % Prosp ect)	FEP E (%)	Unce rtaint y % k=2	Meas ured FEP E to MCN P FEP E Ratio	Ratio Unce rtaint y % (k=2)
Local depo sition	3.500 0	59.50 00	59.57 40	0.124 4	412.4 082	0.365 9	20.60 47	3.575 7	0.792 8	5.178 2
	4.700 0	88.00 00	88.05 50	0.062 5	69.50 11	1.193 9	20.37 97	5.271 8	0.651 0	8.331 8
	4.100 0	122.1 000	121.9 260	0.142 5	6.830 7	8.263 4	16.66 33	17.02 78	0.659 8	41.58 71
	4.000 0	661.7 000	661.2 240	0.071 9	53.90 17	1.144 5	3.042 9	4.608 6	0.746 6	7.421 8
	4.000 0	1173. 2000	1172. 4350	0.065 2	39.87 59	1.322 0	1.826 1	4.794 9	0.668 0	7.135 9

As can be seen, the mixed source displays less uncertainty in its count peak than the europium source (relative uncertainty). This is expected to improve the spread around the average FEPE ratio for the mixed case, which can be seen in Figure 5.12. Compared to the europium source, in which the count rates suffered a higher uncertainty percentage when compared to the mixed source, the spread from its average was worse. Based upon the behavior of the mixed and europium test sources, it is expected that the MCNP model can provide an accurate representation of the true physical system, once its discrepancies in the source-window distance, among other parameters is made negligible through more precise measurements of the sources active location. Another fix is to provide a scaling factor to account for the geometrical fault, which would affect all photopeaks uniformly and without regard to their energy.

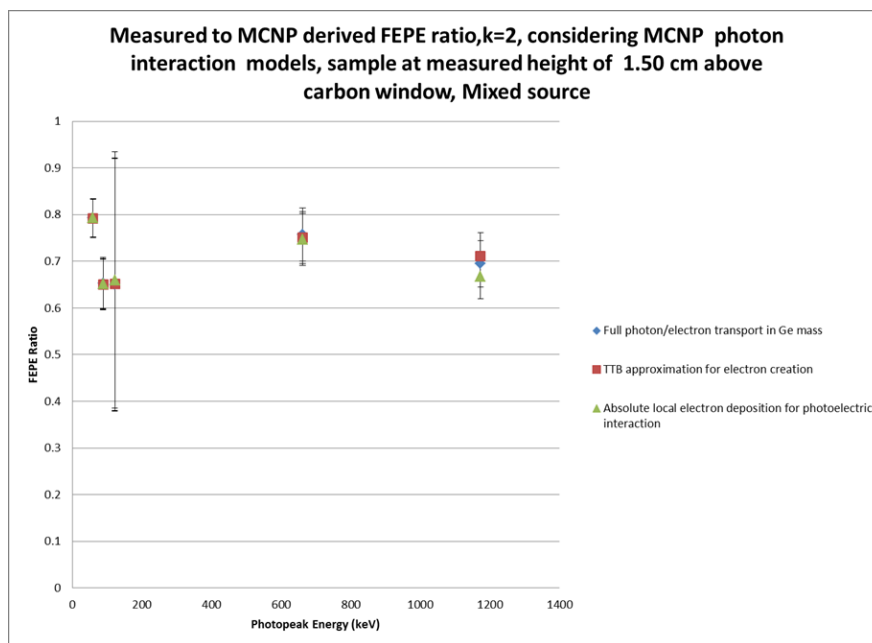


Figure 5.12. FEPE ratio of Mixed source considering photon/electron treatment options

As can be seen above for the Europium and Mixed standards, the model, when using the dimensions given by the schematic, very similar results are obtained with respect to the physically measured absolute full energy peak efficiency values for a given photon treatment, well within their own uncertainty ranges. For simplicity, groove on back end of Ge mass was omitted due to its expected negligible effect upon final Prospect derived simulated net peak areas when comparing with the local deposition approach. Since is gained from considering electron transport in the Germanium masses, with the heavy cost in computation time, the simplest and quickest approach with the highest figure of merit will be considered for validation and study analysis that uses the BEGe 3825 model.

All approaches overestimate, except at 86.50 keV, the net area of a given photopeak. While the possible reasons as to why this model does this is discussed in details later in this study. The imprecise sample to window distance, discrepancies in given typical vs actual Ge dead layer thickness for the BEGe 3825 model can be attributed as the reason for deviation from unity, uncertainty from the choice of live time

for both real and simulated photopeak net count rates and the inherent uncertainty provided by those validated sources and thus the photon probability distribution is expected to cause the deviation in the FEPE ratio values from their respective average for each case. As shown in the mixed case, where the uncertainty in both the given source activity and the average net count rate was lower compared to the Europium test case, the mixed FEPE ratio values were more collapsed rather than spread out, relative to the Europium test case. To illustrate the computation cost that results in little difference between FEPE ratio values with the physical results, the MCNP statistical checks, figure of merit (FOM) and computer run time (min) are given below (Table 5.27 through 5.30) for the Europium and Mixed samples. Slight issues were observed with the EU full photon/electron figure of merit behavior simulation, which was not observed for its counterpart, the mixed test case. This issue with the figure of merit was ignored.

Table 5.27. F8 tally statistical checks for Europium photon/electron method test

For tally F8	EU, Full photon/electron treatment	EU, TTB approximation, x- rays considered	EU, photoelectric local deposition,
MCNP Statistical Check	Outcome	Outcome	Outcome
Mean behavior	Yes	Yes	Yes
Relative Error <.1	Yes	Yes	Yes
Relative Error decrease	Yes	Yes	Yes
Relative Error decrease rate 1/sqrt(nps)	Yes	Yes	Yes
Variance of the variance value	Yes	Yes	Yes
Variance of the variance decrease	Yes	Yes	Yes
Variance of the variance decrease rate 1/nps	Yes	Yes	Yes
Figure of Merit Value constant	No (decrease)	Yes	Yes
Figure of Merit behavior random	No (decrease)	Yes	Yes

Table 5.27. F8 tally statistical checks for Europium photon/electron method test, (cont.)

Pdf slope>3	Yes	Yes	Yes
-------------	-----	-----	-----

Table 5.28. F8 tally figure of merit and computer run time (minutes) for Europium standard

nps=120E+6	EU, Full photon/electron treatment	EU, TTB approximation, x-rays considered	EU, photoelectric local deposition
Figure of Merit (computer run time, min)	1.038E+05 (376.07)	1.274E+06 (30.63)	1.64E+06 (23.81)

Table 5.29 gives the statistical checks for the mixed case; no issues were seen, as compared to the europium test case, which showed an irregularity in its figure of merit behavior over the simulation run.

Table 5.29. F8 tally statistical check for Mixed photon/electron options

For tally F8	Mixed, Full photon/electron treatment	Mixed, TTB approximation, x-rays considered	Mixed, photoelectric local deposition,
MCNP Statistical Check	Outcome	Outcome	Outcome
Mean behavior	Yes	Yes	Yes
Relative Error<.1	Yes	Yes	Yes
Relative Error decrease	Yes	Yes	Yes
Relative Error decrease rate 1/sqrt(nps)	Yes	Yes	Yes

Table 5.29. F8 tally statistical check for Mixed photon/electron options, (cont.)

Variance of the variance value	Yes	Yes	Yes
Variance of the variance decrease	Yes	Yes	Yes
Variance of the variance decrease rate 1/nps	Yes	Yes	Yes
Figure of Merit Value constant	Yes	Yes	Yes
Figure of Merit behavior random	Yes	Yes	Yes
Pdf slope>3	Yes	Yes	Yes

Table 5.30 gives the figure of merit and simulation run time in minutes for the mixed F8 tallies. Due to minimal impact, future simulations used the quickest and simplest photon and electron transport model that was offered by MCNP for the BEGe 3825 model.

Table 5.30. Figure of Merit and computer run time (minutes) for mixed standard

nps=120E+6	Mixed, Full photon/electron treatment	Mixed, TTB approximation, x-rays considered	Mixed, photoelectric local deposition
Figure of Merit (computer run time, min)	1.417E+05 (210.91)	1.271E+06 (23.50)	1.6167E+06 (18.47)

For the full photon/electron model, the tally for the Europium source had an increasing figure of merit, which went from 106453 to 110667 over the course of 111.808E+6 photon histories. This was not observed when using the mixed standard with the full photon/electron transport in the Ge mass.

For the full energy peak efficiency, the simulated net cps is considered to be uncorrelated with the given photon/s derived from the standard/simulated activity. The photon interaction parameters used by MCNP for the BEGe 3825 simulation are given in Table 5.31, based upon the above results of using the various MCNP photon/electron interaction models and the lack of benefit of using the most accurate, but computationally expensive yielding minimal impact on the FEPE ratio. Due to the lack of an impact, the simplest photon treatment option was chosen in light of the number of simulations that were desired to be run, and the limited time frame allowed for the study.

Table 5.31. Photon interaction information and alterations used, neutron physics kept at default settings

Mode	P
Physics Card	P, 100, 1, 0, 0, 0
1 st col "P"	Photons Physics Card
2 nd col "100"	Upper energy cut-off (100 MeV) for detailed physics
3 rd col "1"	Photons will not produce electrons, photoelectric assumes total capture
4 th col "0"	Coherent scattering will occur
5 th col "0"	No Photonuclear interactions
6 th col "0"	Doppler photon energy broadening will occur

Based upon the above observations for the Measured to MCNP derived FEPE values using the different photon/electron models, for the analysis of the Am241/Am242m/Am242, the BEGe 3825 MCNP model does not consider the production of secondary electrons or its bremsstrahlung x-rays. All photons that are less than 100 MeV will be treated with the ‘detailed’ MCNP photon physics. As such it is expected that all photons in this study to be allowed to undergo, photoelectric absorption can cause fluorescent emission, modified Thomson and Klein-Nishina differential cross sections, and coherent scattering (X-5 Monte Carlo Team, 2003). This was done to allow a higher number of the photons to undergo the detailed MCNP photon analysis at a more feasible run time, also since the purpose of this model is to allow for the determination of feasibility through eliminating non-viable irradiation/decay cases involving Am241, A model that possibly overestimates the net peak area (all photons are considered to deposit their respective energy in mass, thus giving a count for that energy bin in the F8 tally, some incident energy might be lost if Ge x-ray and photoelectron escape the Ge mass) is already biased towards the viability of analyzing a certain peak which then allows for non-viable conditions/parameters to be identified immediately. Also, the lead shielding material that the detector sits in has tin and copper grading designed to limit lead x-rays from any electrons that escape into the lead mass. It is also noted here; that no electrons (Beta-) from the validated source decay were considered. In the following tests, source position, Ge dead layer thickness, Eu source radius, and the F8 tally multiplier range were examined to determine their effect upon the Full peak energy efficiency (FEPE) value, and to determine if the model could be improved if these parameters were known with a greater precision.

These standard Mixed and Europium photon loadings was analyzed for multiple distances away from the detector, to determine the sensitivity to sample-window distance due to the relative imprecision in the knowledge of the actual sample position compared to their active isotope activities. For this analysis, there will be a fixed source geometry that will be used, and the medium multiplier will only be used (without uncertainty considered). This is done to ascertain the behavior of the measured to MCNP derived FEPE responses for each of the validated peaks of interest as a function of position for each standard. Uncertainty is included as well. It is noted that the model parameters of

the front germanium dead layer, detailed End-cap internals, Prospect peak search parameters, and source geometry was not changed and kept constant for each position test, only the sensitivity of the models behavior to sample distance in relation to the constant physical sample is being examined, as shown in Table 5.32 and Figure 5.13. The sources to window distance test were expected to affect each photopeak equally, and without regard to the specific energies of the photons. As this parameter is the primary value that was controllable in the physical measurement, it is the most susceptible to measurement error, especially considering that it is the sum of multiple such measurements.

For the Europium source:

Table 5.32. Carbon window to Source distance FEPE testing for simulated Eu sample

Position 1	Given Centroid (keV)	MCN P Centroid (keV)	% Error	MCN P Net Count rate	Uncertainty % Prospect	FEPE (%)	Uncertainty % k=2	Measured FEPE to MCN P FEPE Ratio	Ratio Uncertainty % (k=2)
0.5000	86.5000	86.4640	0.0416	135.148	1.0283	31.1911	5.4065	0.8721	7.9342
	105.3000	105.1120	0.1785	72.0910	1.9559	24.1892	6.3484	0.5482	11.1915
	244.7000	245.6130	0.3731	88.5401	1.2728	28.3523	5.6107	0.3889	9.3579
	344.3000	344.0990	0.0584	125.0288	0.8778	11.4671	5.2993	0.5812	7.7500
	591.7000	591.2300	0.0794	10.6645	7.7111	7.6366	16.2124	0.2280	66.3760
	723.3000	722.7040	0.0824	28.9925	2.5727	5.1217	7.1747	0.4714	12.7071
	1004.8000	1003.6070	0.1187	29.3172	3.4535	5.7701	8.5269	0.6256	13.7011
	1274.5000	1273.5100	0.0777	29.8449	1.5010	3.0369	5.8320	0.4976	9.5396

Table 5.32. Carbon window to source distance FEPE testing for simulated Eu sample, (cont.)

	1408. 0000	1406. 9870	0.071 9	23.48 58	0.996 4	2.715 2	5.382 5	0.355 3	38.33 78
Positi on 2	Given Centr oid (keV)	MCN P Centr oid (keV)	% Error	MCN P Net Count rate	Uncer tainty % Prosp ect)	FEPE (%)	Uncer tainty % k=2	Meas ured FEPE to MCN P FEPE Ratio	Ratio Uncer tainty % (k=2)
1.000 0	86.50 00	86.46 70	0.038 2	112.1 437	1.121 9	25.88 83	5.480 4	1.050 8	7.984 7
	105.3 000	105.1 150	0.175 7	59.35 43	2.142 6	19.91 55	6.585 1	0.665 9	11.32 74
	244.7 000	245.6 110	0.372 3	70.16 53	1.438 8	22.46 83	5.768 9	0.490 8	9.453 6
	344.3 000	344.1 050	0.056 6	93.82 08	1.701 4	8.604 8	6.048 1	0.774 6	8.280 1
	591.7 000	591.3 140	0.065 2	5.805 7	11.92 01	4.157 3	24.35 89	0.418 7	68.82 07
	723.3 000	722.7 010	0.082 8	22.50 05	2.916 7	3.974 9	7.683 0	0.607 4	13.00 09
	1004. 8000	1003. 5960	0.119 8	22.85 69	3.890 5	4.498 6	9.248 9	0.802 4	14.16 17
	1274. 5000	1273. 4720	0.080 7	23.40 29	1.812 8	2.381 3	6.176 1	0.634 6	9.753 8
	1408. 0000	1406. 9800	0.072 4	18.80 91	1.698 0	2.174 5	6.044 3	0.443 7	38.43 63
Positi on 3	Given Centr oid (keV)	MCN P Centr oid (keV)	% Error	MCN P Net Count rate	Uncer tainty % Prosp ect)	FEPE (%)	Uncer tainty % k=2	Meas ured FEPE to MCN P FEPE Ratio	Ratio Uncer tainty % (k=2)
2.000 0	86.50 00	86.45 60	0.050 9	77.02 23	1.323 9	17.78 05	5.657 8	1.529 9	8.107 5
	105.3 000	105.1 460	0.146 2	40.21 71	2.581 3	13.49 43	7.186 9	0.982 7	11.68 75
	244.7 000	245.6 180	0.375 2	46.13 05	1.792 4	14.77 19	6.152 3	0.746 4	9.692 4
	344.3 000	344.0 960	0.059 3	64.01 23	1.233 9	5.870 9	5.575 9	1.135 3	7.941 7

Table 5.32. Carbon window to source distance FEPE testing for simulated Eu sample,
(cont.)

	591.7 000	591.3 460	0.059 8	3.519 7	18.60 36	2.520 4	37.54 17	0.690 7	74.51 39
	723.3 000	722.7 060	0.082 1	14.41 45	4.078 1	2.546 4	9.566 7	0.948 1	14.19 57
	1004. 8000	1003. 5510	0.124 3	14.64 08	4.830 1	2.881 6	10.87 74	1.252 7	15.27 52
	1274. 5000	1273. 4700	0.080 8	14.94 28	2.299 3	1.520 5	6.793 2	0.993 9	10.15 58
	1408. 0000	1406. 9190	0.076 8	12.04 12	2.283 5	1.392 1	6.771 9	0.693 0	38.55 74
Positi on 4	Given Centr oid (keV)	MCN P Centr oid (keV)	% Error	MCN P Net Count rate	Uncer tainty % Prospect)	FEPE (%)	Uncer tainty % k=2	Meas ured FEPE to MCN P FEPE Ratio	Ratio Uncer tainty % (k=2)
2.500 0	86.50 00	86.46 00	0.046 2	64.48 51	1.440 2	14.88 63	5.770 3	1.827 4	8.186 4
	105.3 000	105.1 210	0.170 0	33.57 87	2.827 6	11.26 69	7.548 7	1.177 0	11.91 34
	244.7 000	245.6 180	0.375 2	38.07 31	1.981 1	12.19 17	6.379 5	0.904 4	9.838 1
	344.3 000	344.1 020	0.057 5	50.49 88	5.003 8	4.631 5	11.18 72	1.439 1	12.53 53
	591.7 000	591.3 530	0.058 6	2.878 7	21.57 98	2.061 4	43.44 82	0.844 5	77.65 74
	723.3 000	722.7 080	0.081 8	11.86 74	4.323 0	2.096 5	9.987 7	1.151 6	14.48 27
	1004. 8000	1003. 6340	0.116 0	11.88 91	5.534 6	2.340 0	12.14 61	1.542 6	16.20 31
	1274. 5000	1273. 4790	0.080 1	12.29 26	2.607 1	1.250 8	7.224 1	1.208 1	10.44 90
	1408. 0000	1406. 9700	0.073 2	9.866 4	2.557 7	1.140 6	7.153 1	0.845 8	38.62 62

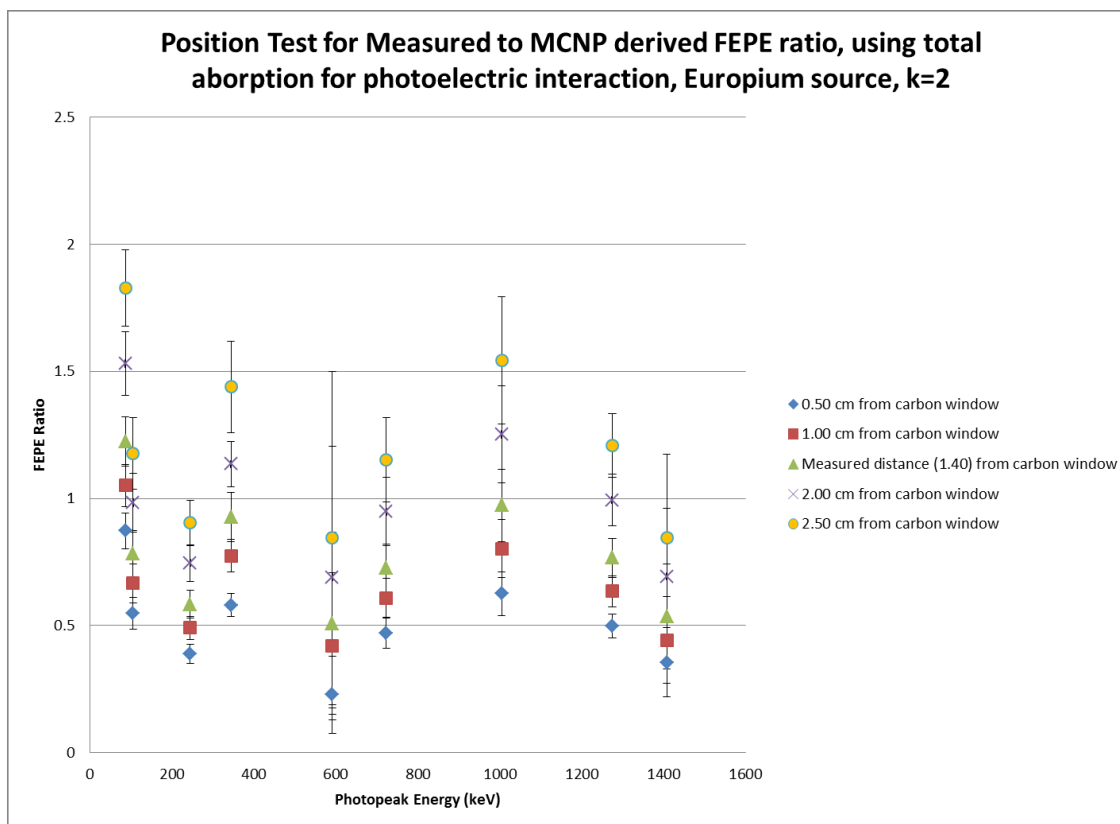


Figure 5.13. FEPE ratio as a function of simulated active sample position only, actual position is ~ 1.40 cm above, between Position 2 and Position 3

As can be seen (Figure 5.13), the model is sensitive to the position of the Europium sample, as FEPE values have large uncertainties often overlapping with the values/ uncertainties of the values for the other positions. The model correctly anticipates the declining net count values (and increasing uncertainty) as the simulated sample is moved farther away from the Ge mass. Due to this sensitivity any error in the actual measurement of the sample's count rate can cause a spread of FEPE ratio values. FEPE ratio spread improves when closer to detector. If all other parameters in the detector were correct (Ge front dead layer, negligence of end-cap internal structures) the model produces net peak area values that are within a factor of ~ 2 if the measured distance of 1.40 cm is considered the minimum value of the 1.40-2.50 cm range for optimal sample to window distances. Also shown in Figure 5.14 is the specific behavior of the 105.30 keV photopeaks simulated Prospect derived net cps vs source to carbon window distance.

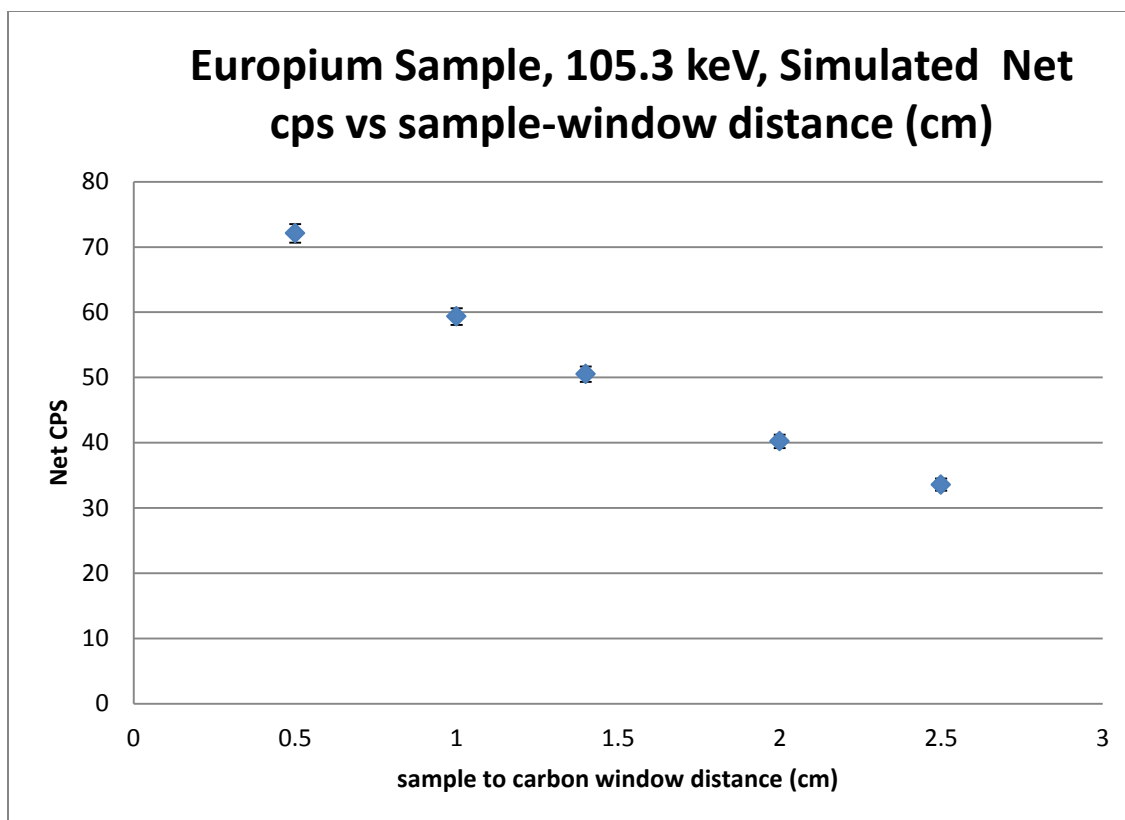


Figure 5.14. Position tests for simulated 105.3 keV photopeak from Europium inventory

Despite the relatively large area of the Ge detector to the active diameter of the europium sample, 14 times greater, the net cps decreases by approximately 50% between the positions extremes that were tested. Overall the net cps declined by a factor of 2 between the 2 tested distance extremes. For the mixed source, a similar position test was completed, the results of which is shown in Table 5.33 and Figure 5.15. It is expected that mixed source will behave in a similar manner when the source distance is changed, the multiplier used is the median, as was done for the europium position test case. Germanium dead layer thickness was kept at the given value, and all other non-source distance parameters were kept constant at their given or measured values. A specific photopeak of the mixed test case was examined, its net count rate taken at the modeled source-carbon window distances that were investigated in this section. The 5 photopeaks that were examined showed similar spread behavior compared with the photon/electron

tests. This is again attributed to the low amount of uncertainty in the simulated Prospect derived net count rate for the mixed case photopeaks. Also the 122.1 keV peak was again predicted to suffer a higher relative uncertainty than its peers, agreeing with the physical measurements.

Table 5.33. Mixed simulation FEPE, as a function of carbon window to sample distance

Pos1 (0.50)	uncertainty % k=2	Given Centroid (keV)	MCN P Centroid (keV)	% Error	MCN P Net Count rate	Uncertainty % Prospect)	FEPE (%)	Uncertainty % k=2	Measured FEPE to MCN P FEPE Ratio	Ratio Uncertainty % (k=2)
	3.500 0	59.50 00	59.56 80	0.114 3	598.8 265	0.311 4	29.91 85	3.555 0	0.546 0	5.163 9
	4.700 0	88.00 00	88.04 90	0.055 7	101.5 215	0.993 2	29.76 90	5.102 5	0.445 7	8.225 8
	4.100 0	122.1 000	121.9 530	0.120 4	10.44 27	6.342 4	25.47 46	13.33 09	0.431 6	40.21 51
	4.000 0	661.7 000	661.2 250	0.071 8	85.34 97	0.913 7	4.818 3	4.397 6	0.471 5	7.292 7
	4.000 0	1173. 2000	1172. 4380	0.065 0	63.61 02	1.048 0	2.913 0	4.515 9	0.418 7	6.951 5
Pos2 (1.00)	uncertainty % k=2	Given Centroid (keV)	MCN P Centroid (keV)	% Error	MCN P Net Count rate	Uncertainty % Prospect)	FEPE (%)	Uncertainty % k=2	Measured FEPE to MCN P FEPE Ratio	Ratio Uncertainty % (k=2)
	3.500 0	59.50 00	59.57 20	0.121 0	497.0 731	0.336 4	24.83 47	3.564 1	0.657 8	5.170 2
	4.700 0	88.00 00	88.05 50	0.062 5	83.91 44	1.087 6	24.60 61	5.178 9	0.539 2	8.273 4
	4.100 0	122.1 000	121.9 660	0.109 7	8.158 2	7.498 6	19.90 17	15.54 75	0.552 4	41.00 32
	4.000 0	661.7 000	661.2 240	0.071 9	67.12 16	1.167 5	3.789 3	4.631 6	0.599 6	7.436 1

Table 5.33. Mixed simulation FEPE, as a function of carbon window to sample distance, (cont.)

	4.000 0	1173. 2000	1172. 4420	0.064 6	49.85 54	1.183 7	2.283 1	4.648 1	0.534 3	7.038 1
Pos3 (2.00)	uncer tainty % k=2	Give n Centr oid (keV)	MCN P Centr oid (keV)	% Error	MCN P Net Coun t rate	Unce rtaint y % Prosp ect)	FEPE (%)	Unce rtaint y % k=2	Meas ured FEPE to MCN P FEPE Ratio	Ratio Unce rtaint y % (k=2)
	3.500 0	59.50 00	59.57 50	0.126 1	343.4 952	0.398 4	17.16 16	3.589 6	0.951 9	5.187 8
	4.700 0	88.00 00	88.05 20	0.059 1	57.75 94	1.308 5	16.93 67	5.379 5	0.783 4	8.400 4
	4.100 0	122.1 000	121.9 770	0.100 7	5.771 1	9.064 0	14.07 84	18.58 59	0.781 0	42.24 90
	4.000 0	661.7 000	661.2 270	0.071 5	43.90 24	2.506 2	2.478 5	6.412 7	0.916 7	8.658 4
	4.000 0	1173. 2000	1172. 4480	0.064 1	32.48 22	1.464 0	1.487 5	4.957 1	0.820 0	7.245 9
Pos4 (2.50)	uncer tainty % k=2	Give n Centr oid (keV)	MCN P Centr oid (keV)	% Error	MCN P Net Coun t rate	Unce rtaint y % Prosp ect)	FEPE (%)	Unce rtaint y % k=2	Meas ured FEPE to MCN P FEPE Ratio	Ratio Unce rtaint y % (k=2)
	3.500 0	59.50 00	59.57 50	0.126 1	287.6 034	0.434 4	14.36 92	3.606 2	1.136 8	5.199 3
	4.700 0	88.00 00	88.04 90	0.055 7	48.49 23	1.425 3	14.21 93	5.496 9	0.933 1	8.476 0
	4.100 0	122.1 000	121.9 760	0.101 6	4.709 8	10.44 05	11.48 93	21.27 97	0.956 9	43.50 13
	4.000 0	661.7 000	661.2 310	0.070 9	36.39 14	1.504 1	2.054 4	5.005 0	1.105 9	7.674 2
	4.000 0	1173. 2000	1172. 4510	0.063 8	26.86 39	1.608 3	1.230 2	5.132 9	0.991 5	7.367 3

Figure 5.15 shows the effect of changing position upon the FEPE ratio for the mixed case, similar behavior as was seen for the europium test case is observed, spread for mixed case continues to be better than when compared to europium's.

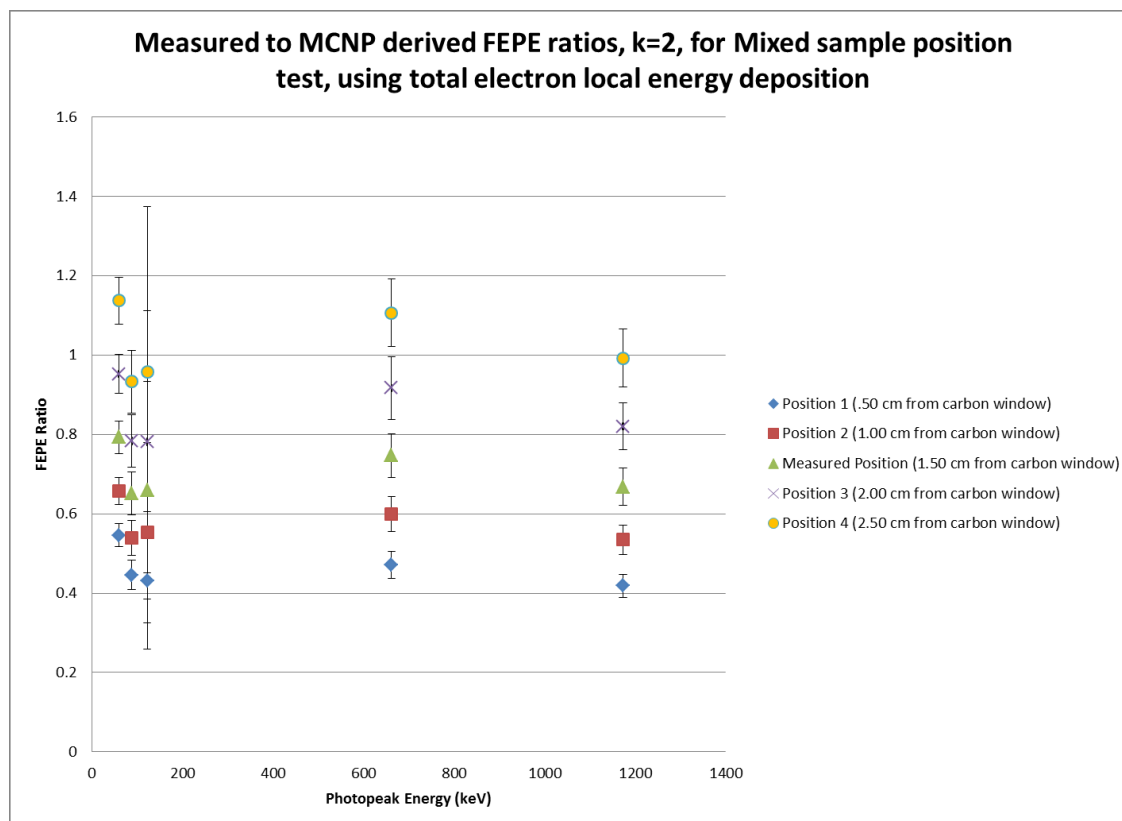


Figure 5.15. Mixed FEPE ratio, as a function of simulated active sample distance only, actual position is ~1.50 cm above carbon window, between simulated Position 1 and Position 2

As can be seen above (Figure 5.15), aside from the 121 keV photon for the mixed source, the distance range for edge of the embedded active source disk ranged from about 2.00 to 2.50 cm from the carbon window, with FEPE ratio values with low uncertainty, which provided the closest agreement between the simulated and physical detector. While the actual nearest surface of the physical sample sat on the protective cover with the approximate distance of 1.50 cm. Since the actual source to window distance was

determined, it is observed that the model tends to overestimate the net cps values for each peak with the described physical distance measurement system, which can be useful when eliminating isotope activity cases that would not yield viable peaks under the best circumstances. Since the internal geometry was better known for the mixed source, that is an active deposition on a 5 mm diameter disk embedded in a 22.5 mm diameter cylinder, its only uncertainties in validating the detector model was its distance discrepancies from the carbon window in the sample outer surface, i.e. source cylinder does not sit perfectly straight on surfaces when on side. The mixed source had an overall lower uncertainty and spread in its FEPE ratio values, as compared with the Europium source, and the simulation uncorrected the net peak area as well, which improved as closer to window simulated counts was performed. As done with the Europium source, a photopeaks net cps behavior with the source to window distance was investigated and shown in Figure 5.16.

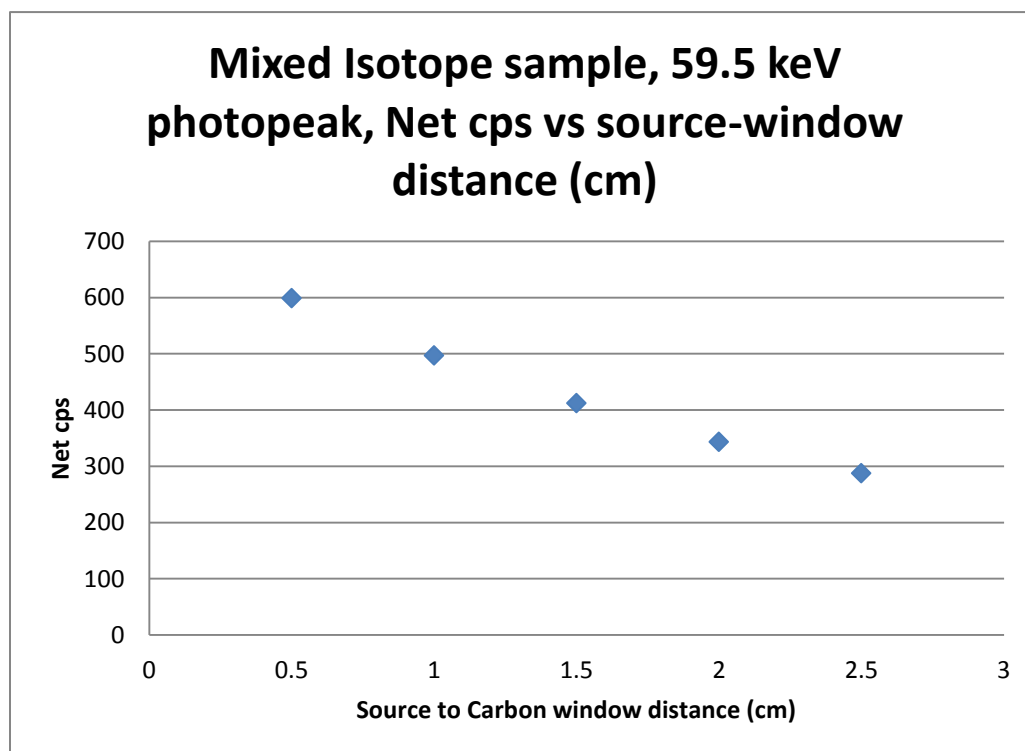


Figure 5.16. 59.5 keV source-window distance net cps test, error bars included but are not visible at utilized dimensions

Similar net cps behavior is observed when comparing the Mixed and Europium samples and their unique geometry setups, for when the position of the source relative to the window is changed.

The next parameter that was examined was the front Germanium inactive layer. This value was taken directly from the Canberra provided schematic, but it is a typical value, and based upon other work with detector models, the actual dead layer may be 2-3 orders of magnitude thicker (Diago, 2005). Regardless, the model that will examine Am241/Am242/Am242m activities will not be modified beyond what was given via the schematic. For the Europium source the results are given in Table 5.34 and Figure 5.17.

Table 5.34. Simulated Europium Ge dead layer thickness tests, using local deposition and measured source to window distance

Ge dead layer 1 (cm)	Given Centroid (keV)	MCN P Centroid (keV)	% Error	MCN P Net Count rate	Uncertainty % Prospect)	FEPE (%)	Uncertainty % k=2	Measured FEPE to MCN P FEPE Ratio	Ratio Uncertainty % (k=2)
0.0003	86.5000	86.4610	0.0451	96.1437	1.1979	22.1947	5.5444	1.2257	8.0288
	105.3000	105.1210	0.1700	50.5871	2.3178	16.9738	6.8182	0.7813	11.4645
	244.7000	245.6140	0.3735	58.9406	1.5780	18.8739	5.9127	0.5842	9.5421
	344.3000	344.1100	0.0552	78.3756	10.1676	7.1883	20.9408	0.9272	21.6910
	591.7000	591.3210	0.0641	4.7796	14.0761	3.4226	28.5928	0.5086	70.4307
	723.3000	722.6970	0.0834	18.8417	3.1514	3.3285	8.0452	0.7254	13.2182
	1004.8000	1003.5820	0.1212	18.8702	4.2322	3.7140	9.8309	0.9719	14.5485
	1274.5000	1273.4670	0.0811	19.3727	1.9994	1.9713	6.4024	0.7666	9.8986
	1408.0000	1406.9760	0.0727	15.5828	1.8752	1.8015	6.2502	0.5355	38.4692

Table 5.34. Simulated Europium Ge dead layer thickness tests, using local deposition and measured source to window distance, (cont.)

Ge dead layer 2	Given Centroid (keV)	MCN P Centroid (keV)	% Error	MCN P Net Count rate	Uncertainty % Prospect	FEPE (%)	Uncertainty % k=2	Measured FEPE to MCN P FEPE Ratio	Ratio Uncertainty % (k=2)
0.0030	86.5000	86.4580	0.0486	94.7487	1.2113	21.8726	5.5560	1.2437	8.0368
	105.3000	105.1250	0.1662	50.0112	2.3575	16.7806	6.8724	0.7903	11.4968
	244.7000	245.6130	0.3731	58.8418	1.5808	18.8423	5.9157	0.5852	9.5439
	344.3000	344.1080	0.0558	78.2563	4.3966	7.1773	10.1154	0.9286	11.5889
	591.7000	591.3240	0.0635	4.7771	13.6924	3.4208	27.8376	0.5089	70.1275
	723.3000	722.6980	0.0832	18.8362	3.1459	3.3276	8.0366	0.7256	13.2129
	1004.8000	1003.5830	0.1211	18.8933	4.2504	3.7185	9.8622	0.9707	14.5697
	1274.5000	1273.4660	0.0811	19.3317	2.0021	1.9671	6.4058	0.7682	9.9008
	1408.0000	1406.9730	0.0729	15.5684	1.8765	1.7998	6.2518	0.5360	38.4695
Ge dead layer 3	Given Centroid (keV)	MCN P Centroid (keV)	% Error	MCN P Net Count rate	Uncertainty % Prospect	FEPE (%)	Uncertainty % k=2	Measured FEPE to MCN P FEPE Ratio	Ratio Uncertainty % (k=2)
0.0300	86.5000	86.4380	0.0717	82.5050	1.3479	19.0462	5.6804	1.4283	8.1233
	105.3000	105.1120	0.1785	45.7968	2.5701	15.3665	7.1709	0.8630	11.6777
	244.7000	245.6130	0.3731	57.4250	1.6220	18.3886	5.9602	0.5996	9.5715
	344.3000	343.9860	0.0912	80.6762	1.1049	7.3993	5.4665	0.9008	7.8653
	591.7000	591.3260	0.0632	4.7243	14.4648	3.3830	29.3584	0.5146	70.7450

Table 5.34. Simulated Europium Ge dead layer thickness tests, using local deposition and measured source to window distance, (cont.)

	723.3 000	722.6 980	0.083 2	18.58 14	3.191 8	3.282 5	8.108 7	0.735 5	13.25 69
	1004. 8000	1003. 5780	0.121 6	18.71 23	4.274 1	3.682 9	9.903 1	0.980 1	14.59 74
	1274. 5000	1273. 4700	0.080 8	19.17 64	2.018 3	1.951 3	6.426 0	0.774 4	9.913 9
	1408. 0000	1406. 9700	0.073 2	15.43 60	1.886 5	1.784 5	6.263 8	0.540 6	38.47 14

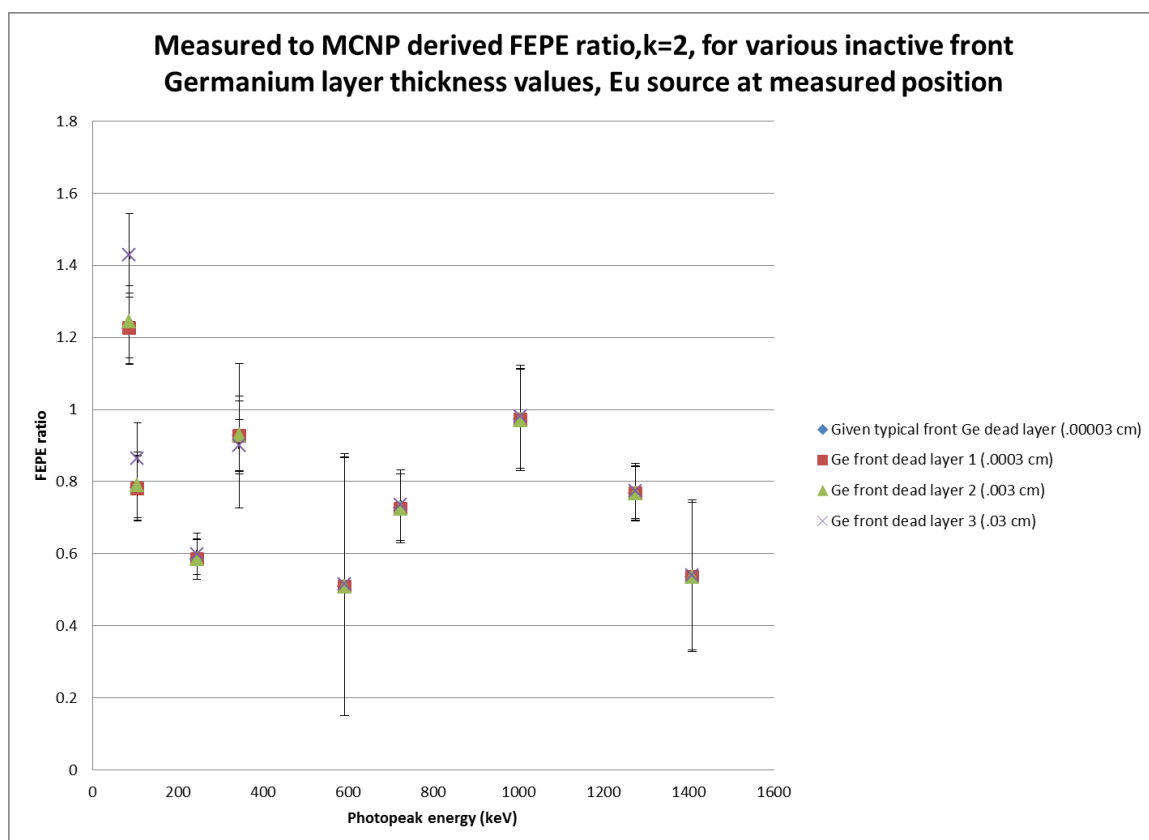


Figure 5.17. Full energy peak efficiency (FEPE) ratios as the front inactive Ge layer is increased

As expected, the inactive germanium thickness layer only affected the lower energies (less than 86 keV) in terms of the full energy peak efficiency ratio values.

Increasing the thickness value caused the low energy peak areas to decrease, which causes an increase in the FEPE ratio. A similar analysis was done for the mixed source and shown in Table 5.35 and Figure 5.18. It is primarily expected to impact the 59.5 and 88.0 keV peak to a greater degree than the other higher energy photopeaks.

Table 5.35. Simulated Mixed front inactive Ge layer tests on FEPE ratio effect

Front GE dead layer 1	uncertainty % k=2	Given Centroid (keV)	MCN P Centroid (keV)	% Error	MCN P Net Count rate	Uncertainty % Prospect	FEPE (%)	Uncertainty % k=2	Measured FEPE to MCN P FEPE Ratio	Ratio Uncertainty % (k=2)
0.0003	3.5000	59.5000	59.5740	0.1244	410.8944	0.3664	20.5290	3.5759	0.7957	5.1783
	4.7000	88.0000	88.0570	0.0648	69.4053	1.1949	20.3516	5.2727	0.6519	8.3324
	4.1000	122.1000	121.9270	0.1417	6.8241	8.2622	16.6472	17.0255	0.6605	41.5861
	4.0000	661.7000	661.2260	0.0716	53.8966	1.1442	3.0427	4.6083	0.7467	7.4216
	4.0000	1173.2000	1172.4420	0.0646	39.8749	1.3217	1.8260	4.7946	0.6680	7.1357
Front GE dead layer 2	uncertainty % k=2	Given Centroid (keV)	MCN P Centroid (keV)	% Error	MCN P Net Count rate	Uncertainty % Prospect	FEPE (%)	Uncertainty % k=2	Measured FEPE to MCN P FEPE Ratio	Ratio Uncertainty % (k=2)
0.0030	3.5000	59.5000	59.5710	0.1193	396.6349	0.3742	19.8166	3.5791	0.8243	5.1806
	4.7000	88.0000	88.0530	0.0602	68.5686	1.2066	20.1063	5.2833	0.6599	8.3391
	4.1000	122.1000	121.9280	0.1409	6.7927	8.2972	16.5705	17.0934	0.6635	41.6140
	4.0000	661.7000	661.2260	0.0716	53.8093	1.1501	3.0377	4.6142	0.7479	7.4253
	4.0000	1173.2000	1172.4420	0.0646	39.8223	1.3235	1.8236	4.7965	0.6689	7.1370

Table 5.35. Simulated Mixed front inactive Ge layer tests on FEPE ratio effect, (cont.)

Front Ge dead layer 3	uncertainty % k=2	Given Centroid (keV)	MCNP Centroid (keV)	% Error	MCNP Net Count rate	Uncertainty % Prospect	FEPE (%)	Uncertainty % k=2	Measured FEPE to MCNP FEPE Ratio	Ratio Uncertainty % (k=2)
0.0300	3.5000	59.5000	59.5470	0.0790	277.7447	0.4636	13.8766	3.6207	1.1772	5.2094
	4.7000	88.0000	88.0440	0.0500	58.0365	1.4086	17.0179	5.4796	0.7796	8.4648
	4.1000	122.1000	121.9370	0.1335	6.4256	8.7842	15.6750	18.0404	0.7014	42.0119
	4.0000	661.7000	661.2240	0.0719	53.1864	1.1620	3.0026	4.6262	0.7567	7.4327
	4.0000	1173.2000	1172.4430	0.0645	39.4993	1.3306	1.8088	4.8044	0.6743	7.1423

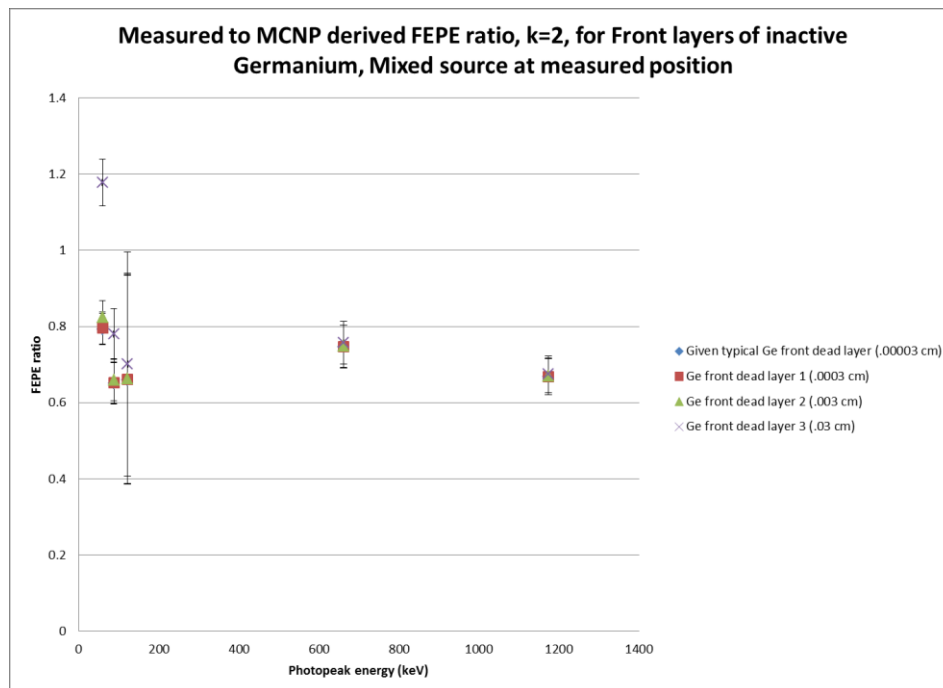


Figure 5.18. Simulated Mixed dead layer test results, all other parameters held at measured/given values

The effect of dead layer of germanium thickness on the FEPE ratio for the mixed source was similar when compared to the europium source, as only the lower energies were affected. The 59.50 and 88.00 keV FEPE ratio showed signs for possible improvement when the dead layer thickness was increased. FEPE uncertainty for the 122.10 keV, .0003 cm thickness appears anomalous when compared to other dead layer values, this is partially attributed to the Prospect automated peak search definitions that were kept constant for both the MCNP and Measured count spectrums, as setting the region of interest manually or changing the continuum initial guess would result in a net peak uncertainty closer in magnitude to uncertainties of other .0003 cm 122.10 keV photopeaks. This analysis only used Prospect output data with the given automated peak settings.

For the Europium disk source, at the measured source distance, the impact on the original FEPE ratio when changing the simulated active radius (which was unknown) was analyzed. As with the position and Ge dead layer tests, all other parameters were set to their given/determined values. Test results are shown in Table 5.36 and Figure 5.19. Europium radius was tested for its impact on the FEPE ratio values, as it was unknown.

Table 5.36. Simulated Eu FEPE analysis, as a function of active radius

Radius 1	Given Centroid (keV)	MCNP Centroid (keV)	% Error	MCNP Net Count rate	Uncertainty % Prospect	FEPE (%)	Uncertainty % k=2	Measured FEPE to MCNP FEPE Ratio	Ratio Uncertainty % (k=2)
0.0500	86.5000	86.4600	0.0462	96.3904	1.1948	22.2516	5.5417	1.2225	8.0269
	105.3000	105.1230	0.1681	50.6768	2.3170	17.0039	6.8171	0.7799	11.4639
	244.7000	245.6130	0.3731	59.0229	1.5765	18.9003	5.9111	0.5834	9.5411
	344.3000	344.0920	0.0604	82.3891	1.0838	7.5564	5.4496	0.8820	7.8536

Table 5.36. Simulated Eu FEPE analysis, as a function of active radius, (cont.)

	591.7 000	591.3 170	0.064 7	4.733 0	16.07 89	3.389 2	32.54 42	0.513 6	72.12 53
	723.3 000	722.6 990	0.083 1	18.70 58	3.229 8	3.304 5	8.168 6	0.730 6	13.29 37
	1004. 8000	1003. 5510	0.124 3	18.92 46	4.233 8	3.724 7	9.833 6	0.969 1	14.55 03
	1274. 5000	1273. 4720	0.080 7	19.36 90	1.986 4	1.970 9	6.386 1	0.766 7	9.888 1
	1408. 0000	1406. 9570	0.074 1	15.58 48	1.872 7	1.801 7	6.247 2	0.535 5	38.46 87
Radiu s 2	Given Centr oid (keV)	MCN P Centr oid (keV)	% Error	MCN P Net Count rate	Uncer tainty % Prosp ect)	FEPE (%)	Uncer tainty % k=2	Measu red FEPE to MCN P FEPE Ratio	Ratio Uncer tainty % (k=2)
1.500 0	86.50 00	86.45 90	0.047 4	92.21 47	1.227 3	21.28 77	5.570 0	1.277 9	8.046 5
	105.3 000	105.1 220	0.169 0	48.64 88	2.371 6	16.32 34	6.891 8	0.812 4	11.50 84
	244.7 000	245.6 140	0.373 5	56.25 87	1.622 4	18.01 51	5.960 6	0.612 1	9.571 8
	344.3 000	344.1 080	0.055 8	74.99 77	2.611 0	6.878 5	7.229 7	0.969 0	9.178 7
	591.7 000	591.3 120	0.065 6	4.497 5	18.61 94	3.220 6	37.57 29	0.540 5	74.52 96
	723.3 000	722.6 920	0.084 1	18.07 97	3.225 1	3.193 9	8.161 3	0.755 9	13.28 92
	1004. 8000	1003. 5730	0.122 1	18.13 79	4.386 1	3.569 9	10.09 70	1.011 1	14.72 96
	1274. 5000	1273. 4580	0.081 8	18.60 16	2.039 4	1.892 8	6.452 6	0.798 4	9.931 2
	1408. 0000	1406. 9510	0.074 5	14.89 17	1.937 9	1.721 6	6.326 3	0.560 4	38.48 16
Radiu s 3	Given Centr oid (keV)	MCN P Centr oid (keV)	% Error	MCN P Net Count rate	Uncer tainty % Prosp ect)	FEPE (%)	Uncer tainty % k=2	Measu red FEPE to MCN P FEPE Ratio	Ratio Uncer tainty % (k=2)

Table 5.36. Simulated Eu FEPE analysis, as a function of active radius, (cont.)

2.500 0	86.50 00	86.46 20	0.043 9	84.57 38	1.288 5	19.52 38	5.625 0	1.393 3	8.084 7
	105.3 000	105.1 180	0.172 8	44.71 55	2.490 4	15.00 37	7.057 5	0.883 9	11.60 84
	244.7 000	245.6 070	0.370 7	51.75 42	1.695 9	16.57 27	6.041 9	0.665 3	9.622 6
	344.3 000	344.1 030	0.057 2	69.29 74	2.282 0	6.355 7	6.769 7	1.048 7	8.821 0
	591.7 000	591.3 590	0.057 6	4.132 3	15.40 85	2.959 1	31.21 99	0.588 3	71.53 75
	723.3 000	722.7 070	0.082 0	16.32 76	20.64 56	2.884 4	41.59 29	0.837 1	42.89 48
	1004. 8000	1003. 6030	0.119 1	16.66 76	4.610 8	3.280 5	10.48 98	1.100 3	15.00 16
	1274. 5000	1273. 4680	0.081 0	17.17 73	2.118 0	1.747 9	6.553 2	0.864 6	9.996 8
	1408. 0000	1406. 9370	0.075 5	13.83 68	2.030 4	1.599 6	6.441 3	0.603 1	38.50 07

The effect that a changing radius for the unknown Europium disk source (Figure 5.19):

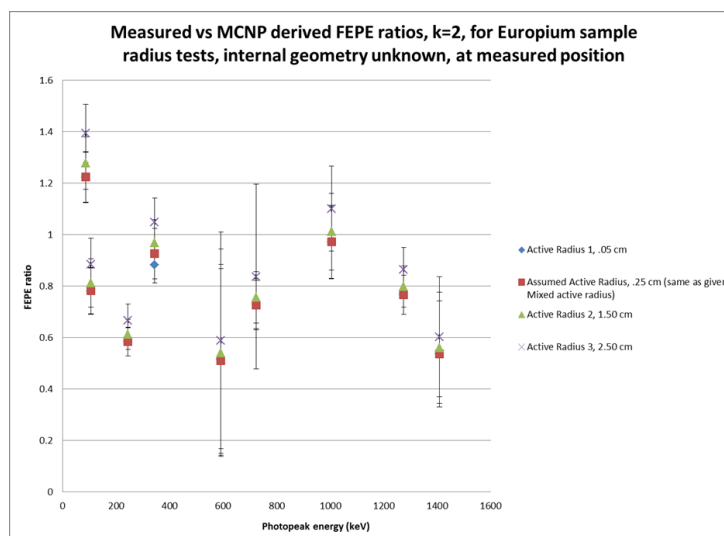


Figure 5.19. The Eu FEPE ratio, as a function of simulated active radius, all non-radius parameters fixed to measured/given, 1.40 cm source-window distance

Table 5.37. Eu simulated FEPE analysis, as a function of the multiplier, (cont.)

	86.50 00	86.46 00	0.046 2	91.44 14	1.229 7	21.10 92	5.572 2	1.288 7	8.048 0
	105.3 000	105.1 210	0.170 0	47.99 41	2.395 1	16.10 38	6.924 3	0.823 5	11.52 79
	244.7 000	245.6 120	0.372 7	56.00 70	1.618 7	17.93 45	5.956 6	0.614 8	9.569 3
	344.3 000	344.1 100	0.055 2	74.49 68	5.757 8	6.832 5	12.55 42	0.975 5	13.76 91
	591.7 000	591.3 320	0.062 2	4.540 4	14.38 91	3.251 3	29.20 93	0.535 4	70.68 32
	723.3 000	722.6 970	0.083 4	17.85 58	3.249 5	3.154 4	8.199 9	0.765 4	13.31 29
	1004. 8000	1003. 5710	0.122 3	17.92 89	4.367 3	3.528 7	10.06 45	1.022 9	14.70 74
	1274. 5000	1273. 4630	0.081 4	18.40 97	2.049 7	1.873 3	6.465 6	0.806 7	9.939 7
	1408. 0000	1406. 9580	0.074 0	14.79 86	1.928 4	1.710 8	6.314 6	0.563 9	38.47 97
High, type 1	Given Centr oid (keV)	MCN P Centr oid (keV)	% Error	MCN P Net Count rate	Uncer tainty % Prosp ect)	FEPE (%)	Uncer tainty % k=2	Meas ured FEPE to MCN P FEPE Ratio	Ratio Uncer tainty % (k=2)
	86.50 00	86.46 00	0.046 2	101.0 880	1.169 0	23.33 61	5.519 6	1.165 7	8.011 7
	105.3 000	105.1 220	0.169 0	53.04 97	2.277 7	17.80 01	6.764 0	0.745 0	11.43 23
	244.7 000	245.6 130	0.373 1	61.89 54	1.540 2	19.82 01	5.872 7	0.556 3	9.517 3
	344.3 000	344.0 930	0.060 1	86.37 65	1.058 8	7.922 1	5.429 9	0.841 3	7.839 9
	591.7 000	591.3 190	0.064 4	5.001 4	13.99 17	3.581 4	28.42 65	0.486 1	70.36 34
	723.3 000	722.6 990	0.083 1	19.76 61	3.086 6	3.491 8	7.944 1	0.691 4	13.15 69
	1004. 8000	1003. 5670	0.122 7	19.85 94	4.144 3	3.908 7	9.679 9	0.923 5	14.44 69
	1274. 5000	1273. 4690	0.080 9	20.33 56	1.939 3	2.069 2	6.328 0	0.730 3	9.850 7
	1408. 0000	1406. 9600	0.073 9	16.33 98	1.819 9	1.889 0	6.184 5	0.510 7	38.45 86

Table 5.37. Eu simulated FEPE analysis, as a function of the multiplier, (cont.)

Mid, type 1	Given Centroid (keV)	MCN P Centroid (keV)	% Error	MCN P Net Count rate	Uncertainty % Prospect)	FEPE (%)	Uncertainty % k=2	Measured FEPE to MCN P FEPE Ratio	Ratio Uncertainty % (k=2)
	86.5000	86.4600	0.0462	96.2829	1.1977	22.2268	5.5442	1.2239	8.0286
	105.3000	105.1200	0.1709	50.5065	2.3340	16.9468	6.8404	0.7825	11.4777
	244.7000	245.6120	0.3727	58.9583	1.5775	18.8796	5.9122	0.5840	9.5417
	344.3000	344.1080	0.0558	78.3996	3.6973	7.1905	8.9263	0.9269	10.5669
	591.7000	591.3270	0.0630	4.7733	14.0386	3.4181	28.5189	0.5093	70.4007
	723.3000	722.6990	0.0831	18.8282	3.1581	3.3261	8.0557	0.7259	13.2246
	1004.8000	1003.5630	0.1231	18.8598	4.2289	3.7119	9.8252	0.9724	14.5447
	1274.5000	1273.4620	0.0814	19.3733	1.9995	1.9713	6.4025	0.7666	9.8987
	1408.0000	1406.9570	0.0741	15.5828	1.8752	1.8015	6.2502	0.5355	38.4692

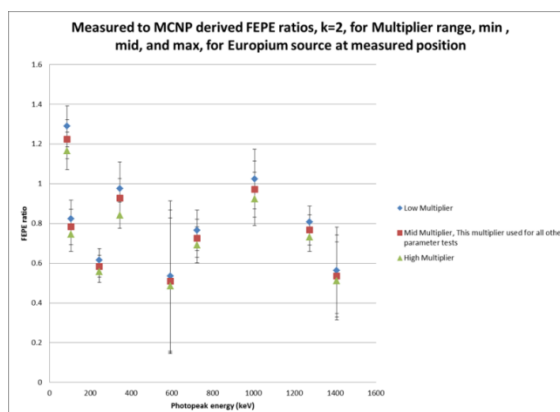


Figure 5.20. The FEPE ratio as a function of spectrum multiplier

The uncertainty caused by the multiplier causes the final FEPE ratio values to vary little within their combined uncertainty ranges. The photopeaks of 591.7 and 1408 keV displayed relatively large Prospect derived area uncertainties. This uncertainty predicted by the model matches the Europium uncertainties for the 591.7 and 1408 keV peak. For the Am241/Am242/Am242m analysis, the multiplier taken from the samples total photon rate and the expected detector live time will consider the uncertainty in the activities, which for MCNP derived quantities will be taken as the relative error in the Am241 radiative capture rate, for Am242/Am242m production. And will be ignored in the WG and RG plutonium cases, as composition is taken as the typical values for weapons/reactor grade plutonium. Uncertainty caused by the physical data (photon intensity, half-life) is ignored.

Similar analysis was performed for the Mixed Isotope source and is shown in Table 5.38 and Figure 5.21. The middle multiplier is the median of the multiplier without its maximum and minimum value taken to $k=2$. The multiplier is the source strength of the mixed source multiplied by the live time of the detector, applied to the F8 tally.

Table 5.38. Mixed FEPE analysis, as a function of multiplier

LOW	uncertainty % k=2	Given Centroid (keV)	MCNP Centroid (keV)	% Error	MCNP Net Count rate	Uncertainty % Prospect	FEP E (%)	Uncertainty % k=2	Measured FEP E to MCNP FEP E Ratio	Ratio Uncertainty % (k=2)
	3.5000	59.5000	59.5730	0.1227	397.8671	0.3720	19.8782	3.5782	0.8218	5.1799
	4.7000	88.0000	88.0510	0.0580	66.1673	1.2258	19.4021	5.3010	0.6838	8.3503
	4.1000	122.1000	121.8870	0.1744	6.5664	8.4826	16.0184	17.4537	0.6864	41.7633
	4.0000	661.7000	661.2250	0.0718	51.7389	1.1723	2.9208	4.6365	0.7778	7.4392
	4.0000	1173.2000	1172.4370	0.0650	38.3242	0.0000	1.7550	4.0000	0.6950	6.6280

Table 5.38. Mixed FEPE analysis, as a function of multiplier, (cont.)

HIGH	uncertainty % k=2	Given Centroid (keV)	MC NP Centroid (keV)	% Error	MC NP Net Count rate	Uncertainty % Prospect	FEP E (%)	Uncertainty % k=2	Measured FEP E to MC NP FEP E Ratio	Ratio Uncertainty % (k=2)
	3.5000	59.5000	59.5740	0.1244	426.8812	0.3596	21.3278	3.5731	0.7659	5.1764
	4.7000	88.0000	88.0510	0.0580	72.7732	1.1655	21.3391	5.2463	0.6218	8.3157
	4.1000	122.1000	121.9910	0.0893	6.8855	9.5043	16.7970	19.4458	0.6546	42.6342
	4.0000	661.7000	661.2260	0.0716	56.0297	1.1241	3.1631	4.5885	0.7183	7.4093
	4.0000	1173.2000	1172.4340	0.0653	41.5057	1.2936	1.9007	4.7637	0.6417	7.1150
MID	uncertainty % k=2	Given Centroid (keV)	MC NP Centroid (keV)	% Error	MC NP Net Count rate	Uncertainty % Prospect	FEP E (%)	Uncertainty % k=2	Measured FEP E to MC NP FEP E Ratio	Ratio Uncertainty % (k=2)
	3.5000	59.5000	59.5740	0.1244	412.4082	0.3659	20.6047	3.5757	0.7928	5.1782
	4.7000	88.0000	88.0550	0.0625	69.5011	1.1939	20.3797	5.2718	0.6510	8.3318
	4.1000	122.1000	121.9260	0.1425	6.8307	8.2634	16.6633	17.0278	0.6598	41.5871
	4.0000	661.7000	661.2240	0.0719	53.9017	1.1445	3.0429	4.6086	0.7466	7.4218
	4.0000	1173.2000	1172.4350	0.0652	39.8759	1.3220	1.8261	4.7949	0.6680	7.1359

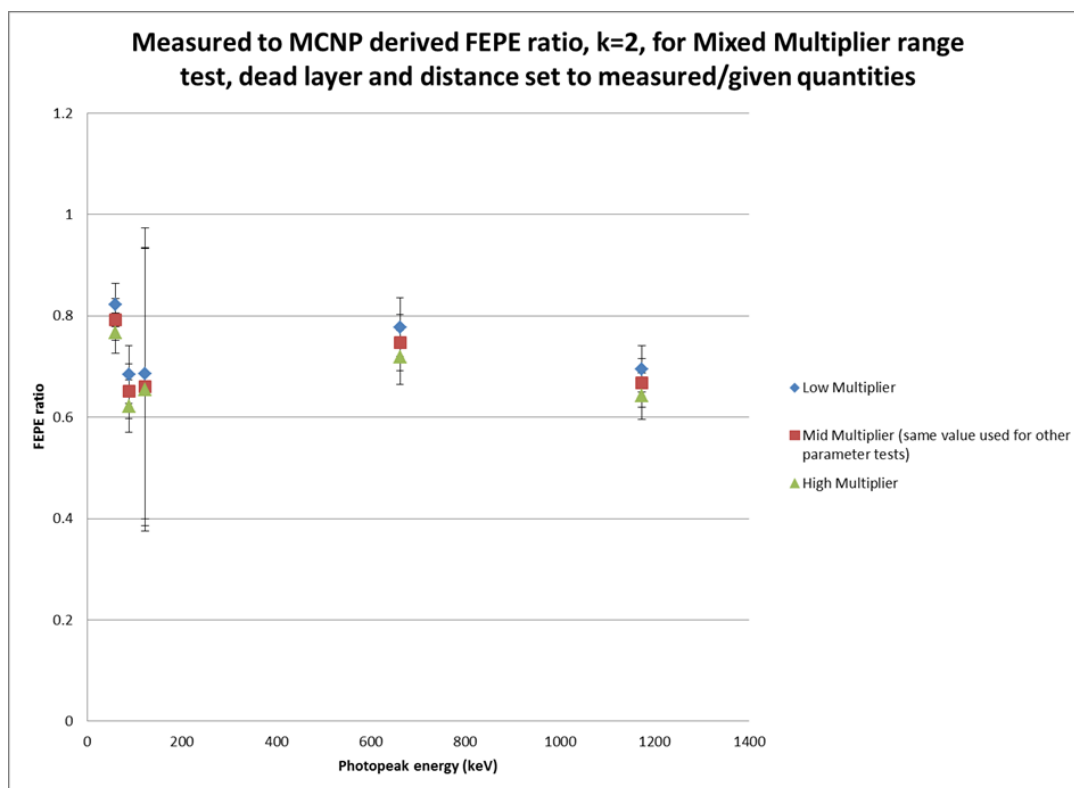


Figure 5.21. Mixed FEPE ratio as a function of multiplier

The uncertainty for 122.1 keV peak was large for some unknown reason, but relative magnitude of that uncertainty in relation to the other peaks agreed with the physical measurements for that 122.1 keV photopeak. The automated as well as manually fitted regions of interests presented similar uncertainties of magnitude when multiple MCNP runs were done using the F8 tally.

As with the Europium standard, the BEGe detector model is not very sensitive to changes in the multiplier that are used for the peak analysis software for the mixed standard, with the given activity uncertainties. Not shown is that the model greatly over predicts for energies less than 40 keV when compared to the measured spectrum. This is expected since the Ge dead layers were taken as typical values from the Canberra provided diagram and not modified. Parameters such as the dead layers were not tuned for a specific case since the internal geometry and position of the standards were not precisely known. It is assumed that the MCNP normalized spectrums, the F8 tally energy

bins, which are multiplied by the derived multiplier for each of the standard sources, mimics the actual count in each of the MCA's energy dependent channel, which is supported by the low error between the simulated peak centroids and MCNP predicted centroids. MCNP relative error for each of the major peaks that were given were less than $<.05$. MCNP parameters that were used for the analysis for both case validations and the upcoming study results are shown in Table 5.39. The source to cover distance, radius, dead layer and multiplier analysis statistical check results have been omitted from this report.

Table 5.39. BEGe model MCNP parameters for BEGe 3825 model for the validation and experiment simulation runs

nps	120,000,000
Mode	(P,E) and (P, for both validation and experiment)

Overall the MSTR model in the 101W configuration produced reasonable agreement with Kulage's 3 group neutron flux values, especially in the thermal group which has an outsized role in the potential analysis of Am241 behavior in the MSTR (Table 5.11). At 200 kW, the power of interest of in this study, the model underestimated the physical flux values when compared with Kulage's work. The BEGe 3825 model produced results that after analysis by spreadsheet and Prospect were an overestimate of the actual absolute full energy peak efficiencies for the Europium and Mixed standard. Mixed FEPE ratios were more consistent in value when compared with Eu FEPE ratios; this is attributed to low number of peaks and cleaner mixed spectrum where there were only 5 viable peaks, concurrent with the lower uncertainty in the count estimation. The general overestimation was largely expected due to such factors as the end-cap protective cover being omitted from the model, and the simplified non-germanium material geometry inside of the end-cap itself, and the lack of the coupled electron photon

transport through the Germanium and other model materials (electron transport in lead shield material not tracked during Type 3 tests). Also the dead layer of Ge, which was taken for its typical values from Canberra provided schematics, was too thin, as peaks below are at 40 keV were grossly uncorrected when compared to the overestimation of the higher energy peaks. This dead layer thinness would have a similar but decreasing effect for the higher energy photons as well. The tendency of the BEGe 3825 model to overestimate does provide a benefit when eliminating cases when considering the applications brought on through analysis of the production terms of Am241, Am242, and Am242m that would not provide a viable photopeak to measure with the Prospect software for that specific BEGe 3825. To account for this general overestimation that was observed in both the Europium and Mixed sample tests, which is assumed to carry over for any gamma/x-ray source that uses a similar level of precision in its position and geometry measurements, such as a foil, the F8 tally results for both the standard tests and Am241/Am242/Am242m foil tests were divided by a factor of 2, to provide an corrected (underestimated) spectrum, which is provided along with the natural uncorrected (overestimated) target spectrum brought on by the unmodified BEGe 3825 detector model. For the unmodified Europium and Mixed cases, the MCNP-Measured spectrum count difference with local photon deposition is shown in Figure 5.22.

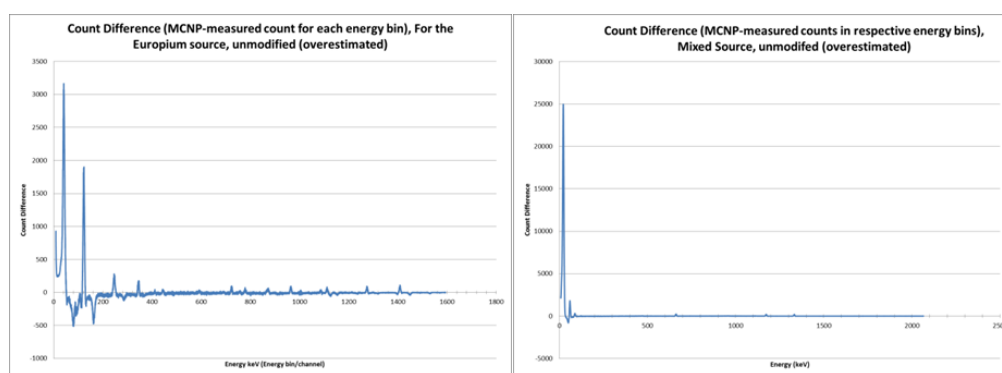


Figure 5.22. Unmodified spectrum difference between MCNP F8 derived and measured spectrum, for Europium source, underestimation occurred below 200 keV in non-examined non-validated peaks that were not a part of the given gamma/x-ray loading, BEGe model corrected (underestimated) background consistently, but uncorrected (overestimated) all photopeaks that were attributed to given source isotopes

When F8 tally result was divided by a factor of 2, based upon the above behavior of the FEPE ratio values for the Europium and Mixed case, the spectrum count difference between the MCNP and Measured inverts (effect of lack of Ge dead layer is observed for low energies, less than 40 keV) as shown in Figure 5.23.

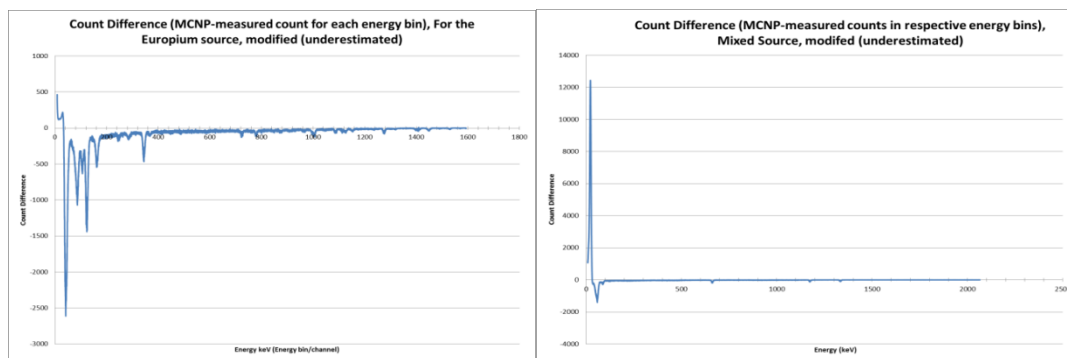


Figure 5.23. Corrected (underestimated) count difference for Mixed and Europium count spectrums

When applying the scaling factor to the Full Energy Peak efficiency values for the chosen validated peaks, the modified model is shown to provide a consistent underestimation when utilizing the F8 tally to predict peak viability via Prospect analysis and for target activity for photons greater than 40 keV. A similar scaling factor was applicable for both validation systems, this suggests that the error which causes the peak count overestimation is shared for any source-detector system in which its position, general geometry, and the use of the given detector is measured or obtained. The scaling factor also takes into account any errors brought out by the use of the Gaussian Energy broadening modification used for the tally, since its parameters were taken from FWHM calibration equation that defined the FWHM behavior when the Energy and FWHM calibration was performed upon the physical BEGe 3825 detector (confirmed calibration, but not personally performed). Results of the correction are given in Table 5.40. This will provide an underestimation, for the validation, and if same measurement system used, for any future simulations and physical comparisons.

Table 5.40. Corrected (underestimated) Europium Sample Simulation Tests, all parameters measured/given

Corrected (underestimated) Eu peak analysis, Type 1 photon/electron	Given Centroid (keV)	MCN P Centroid (keV)	% Error	MCN P Net Count rate	Uncertainty % Prospect	FEPE (%)	Uncertainty % k=2	Measured FEPE to MCN P FEPE Ratio	Ratio Uncertainty % (k=2)
	86.50 00	86.45 90	0.047 4	48.11 10	1.696 2	11.10 64	6.042 2	2.449 3	8.380 3
	105.3 000	105.1 220	0.169 0	25.25 62	3.299 7	8.474 4	8.279 6	1.564 8	12.38 95
	244.7 000	245.6 130	0.373 1	29.49 97	2.227 5	9.446 4	6.696 7	1.167 3	10.04 67
	344.3 000	344.1 080	0.055 8	39.22 32	3.210 7	3.597 4	8.138 4	1.852 8	9.910 3
	591.7 000	591.4 640	0.039 9	2.120 2	28.55 10	1.518 3	57.32 05	1.146 6	86.18 92

Table 5.40. Corrected (underestimated) Europium Sample Simulation Tests, all parameters measured/given, (cont.)

	723.3 000	722.6 800	0.085 7	9.553 3	4.848 3	1.687 7	10.90 99	1.430 6	15.13 34
	1004. 8000	1003. 5830	0.121 1	9.308 6	6.094 1	1.832 1	13.17 40	1.970 2	16.98 72
	1274. 5000	1273. 4510	0.082 3	9.614 6	3.002 5	0.978 3	7.814 1	1.544 6	10.86 52
	1408. 0000	1406. 8820	0.079 4	7.730 9	3.048 2	0.893 8	7.884 5	1.079 4	38.76 83

The same correction factor of 2 was applied to the mixed F8 tally results as given by Table 5.41. FEPE ratio values are given in Figure 5.24. This correction factor, for both the europium and mixed case assumes that the same measurement system is utilized for any potential experiments utilizing this MCNP model of the BEGe 3825. The system consisted of a standard SI ruler, and knowledge of internal geometry, and if that was lacking, as was for the europium case, visual estimations, based upon the assumption of a sealed source, and that the active material is physically covered by some material such as plastic. For future reference, the term corrected will be used to indicate that the scaling factor of 2 had been utilized and the model is expected to provide an underestimation of the counting spectrum, if the same measurement system had been used to describe or build the physical system in conjunction with the modeled universe of the source and detector system. The scaling factor will not impact the spread of the mixed and europium FEPE ratio values from their respective FEPE average value, as that is attributed to the uncertainty in their net count rate measurements as derived by Prospect, which is dependent upon the live time of the detector and the source strength of the standard sources, of which the mixed, having a higher source strength, required less live counting

time, compared to that of the europium case, which suffered from the 10 minute live time.

Table 5.41. Corrected (underestimated) Mixed sample simulation tests, all parameters measured/given

Corrected (underestimated) Mixed Peak Analysis	Uncertainty % k=2	Given Centroid (keV)	MCN P Centroid (keV)	% Error	MCN P Net Count rate	Uncertainty % Prospect)	FEPE (%)	Uncertainty % k=2	Measured FEPE to MCN P FEPE Ratio	Ratio Uncertainty % (k=2)
	3.5000	59.5000	59.5740	0.1244	206.2064	0.5170	10.3025	3.6496	1.5856	5.2295
	4.7000	88.0000	88.0550	0.0625	34.7614	1.6859	10.1930	5.7844	1.3017	8.6652
	4.1000	122.1000	121.9250	0.1433	3.2806	13.0488	8.0030	26.4177	1.3738	46.2324
	4.0000	661.7000	661.2250	0.0718	26.9555	1.6091	1.5217	5.1339	1.4930	7.7590
	4.0000	1173.2000	1172.3110	0.0758	20.1782	1.9832	0.9240	5.6332	1.3200	7.7241

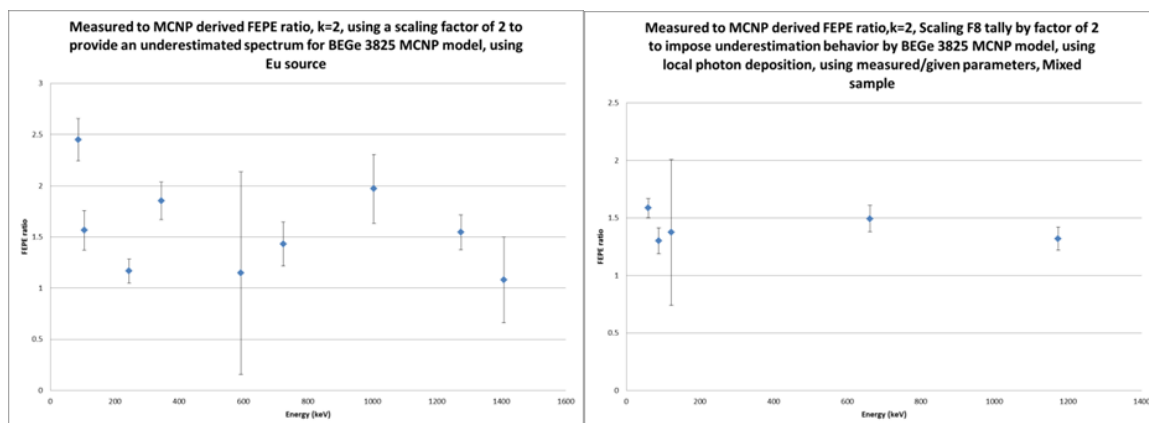


Figure 5.24. Corrected FEPE ratio for Europium and Mixed test case

The scaling factor can account for the specific discrepancies between model and physical system encountered when using the described measurement system. This scaling factor is only good for correcting flaws that affect all photopeaks uniformly, it is not meant to correct for the uncertainties in the dead layer thickness. Scaling factor considers improvement in certainty when overestimation occurs to secondary to primary purpose to provide an underestimation to establish a viability window of counts.

6. SIMULATION RESULTS

The overall goal of this study is to examine two specific applications of Am241 and to study the feasibility of performing this analysis at the MSTR with the primary aid of the specified shielded BEGe 3825 that is available in the department. Those applications being the detection and study of energy integrated production rates of Am242/Am242m from Am241 in the neutron energy environment of the MSTR and the usefulness in using the BEGe 3825 to interrogate irradiated Am241 samples and to determine the production ratio value after a short irradiation period, while the other being the use of Am241 to back extrapolate the age of initially pure Weapons/Reactor grade plutonium stockpiles through Am241 activity measurements in the specified BEGe 3825 located at the MSTR using a small mass of a typical sample that could be utilized with that detector.

In order to examine the Am241 behavior with the BEGe 3825 in the reactor for a given Plutonium stockpile, it is assumed that the activities used in the model represent a smaller fraction removed from the uniform master source. This sampling could be during any stage of the fuel reprocessing. Since the goal was to examine Am241 to date Plutonium isotopes since it was separated from the fuel material where it was generated, and it is assumed that the initially the sample was free of any Am241, the BEGe 3825 could be utilized to make activity estimates with known time estimates between them. The purpose of this test is to look at the viability of measuring a given Am241 buildup in a validated BEGe Model, which is then used to evaluate potential spectrums and count rate uncertainties for a given Plutonium sample that has undergone a given decay time of 1, 5, or 19 years. The time span between two 1 hour measurements was 0.5, 1, 1.5 and 2 years. The selections of these times are to give the best possible measurement condition, as a short measurement time could be utilized with the Pu241 still in a significant quantity. The samples were assumed to be deposited onto a 5x5x.0005 cm Al27 foil geometry (foil not activated, and played no role in photon distribution for the BEGe model, but was utilized to fulfill source containment requirement, sample self-shielding was ignored, which is consistent with BEGe model validation tests as executed in the above sections). The simulated detector used a multiplier that indicated a live time of 1 hour of live measurement, since the half-lives of the actinides of interest were greatly

beyond that measurement times. Taking the ratio of the simulated Prospect derived net count rates, and knowing the time span, the Newton-Raphson method was utilized to solve for the unknown sample age. Due to uncertainty in the net count rates, a time estimate range existed for each time case. The simulated samples assumed that a small mass fraction was taken from a larger Plutonium stockpile that had existed as a uniform mass and its composition was not disturbed during its unknown decay life. Equal masses were taken for both weapons and reactor grade plutonium types; exact mass was chosen to ensure sample activity mirrored that of radioactive standards used in BEGe 3825 model validation so that dead time could be ignored by the assumption that the system could maintain a viable live time, as shown in Table 6.1.

Table 6.1. Expected equal simulated sample mass of weapons/reactor grade plutonium, initially pure, it is assumed that the plutonium exists in some form such as plutonium dioxide

Simulated mass/atom#/activity	Weapons Grade	Reactor Grade
Mass of Sample (g)	5.00E-07	5.00E-07
Mass of Pu238 (g)	2.50E-10	5.00E-09
Mass of Pu239 (g)	4.72E-07	2.95E-07
Mass of Pu240 (g)	2.50E-08	1.20E-07
Mass of Pu241 (g)	3.00E-09	5.50E-08
Mass of Pu242 (g)	2.50E-10	2.50E-08
Atom # of Pu238	6.32E+11	1.26E+13
Atom # of Pu239	1.19E+15	7.43E+14
Atom # of Pu240	6.27E+13	3.01E+14
Atom # of Pu241	7.49E+12	1.37E+14
Atom # of Pu242	6.22E+11	6.22E+13

Table 6.1. Expected equal simulated sample mass of weapons/reactor grade plutonium, initially pure, it is assumed that the plutonium exists in some form such as plutonium dioxide, (cont.)

Activity of Pu238 (Bq)	1.58E+02	3.17E+03
Activity of Pu239 (Bq)	1.08E+03	6.77E+02
Activity of Pu240 (Bq)	2.10E+02	1.01E+03
Activity of Pu241 (Bq)	1.15E+04	2.11E+05
Activity of Pu242 (Bq)	3.66E-02	3.66E+00
Activity Total (Bq)	1.30E+04	2.16E+05

For the uncorrected (unmodified BEGe 3825 model) weapons grade plutonium sample photon inventory, the resulting simulated net count rates and subsequently, the age of the plutonium sample (considered unknown for this analysis) is given. Uncertainty was taken by applying the combined uncertainty in the ratio of net count rates and applying the minimum and maximum (to 1 standard deviation) as the new ratio values for the Newton-Raphson method to solve for the unknown Plutonium age. The analysis with the unmodified Plutonium spectrum data is given in Table 6.2. As the weapon grade plutonium has less Pu241 and Am241 per gram of plutonium compared to reactor grade, the generic 1 hour count of the specific sample mass of weapon grade plutonium is expected to cause some amount of error in the sample age estimation. As the decay time advances, the ratio change per time lessens, as Am241's 432 year half-life takes dominance. For sample ages on the order of decades, precision in the count rate ratio will be required, as Table 6.2 will show for the 19 year case, when a 6 month interval between 1 hour measurements yields a non-desirable estimate range for the sample. Improvement is shown when the span is increased to 1, 1.5 and then 2 years between measurements.

For the corrected weapons grade plutonium sample results, a similar procedure was followed and shown in Table 6.3. The corrected implies that the BEGe 3825 model uses the same measurement system to model the plutonium sample source and that there would thus be an underestimation that would still exist. Using a different measurement system would invalidate the overestimation and underestimation efforts to establish a counting window.

For both the corrected and uncorrected weapons grade plutonium sample, the uncertainty provided by the general output of 1 hour of sample counting proved too high (especially for the longer aged samples, 19 years), and its impact on the time estimate is evident for the .5 year span between the 1 hour measurements. In order to show that the uncertainty in the count rate ratio is expected to decrease if a factor other than the measurement span was increased, a special case involving increasing the count time for the sample from 1 hour to 10 days for the Weapons grade, corrected case, as this case showed the highest impact of the uncertainty upon the age estimate range as seen in Table 6.4. Increasing the count time to 10 days risks introducing error, as the change in the Am241 activity over the course of the measurement period should be less than the change that occurs over the measurement span, as such increasing the time count would be a possible reason to view the longer time spans such as 1.5 and 2 years with more validity than the .5 and 1 year, but this was not explored further, rather the goal was to show that decreasing the uncertainty in the count ratio improved the age estimate drastically.

The same procedure with 1 hour measurement time was then accomplished for an equal mass sample of initially pure plutonium isotopes of the reactor grade type. Table 6.5 gives the uncorrected (expected overestimated) reactor grade composition case Prospect analysis. As the amount of Am241 is inherently greater for a given amount of time in reactor grade plutonium, the uncertainty in the Am241 59.50 keV photopeak can be considered minimal at relatively low counting times such as 1 hour, the value used as the arbitrary simulated counting time. When a sample of plutonium's composition is unknown except for its general origin, a stockpile of purified plutonium, a count on the order of days can be utilized with the examined time spans to make a reliable estimate of the sample age, maximum sample age is dependent upon the time span utilized.

The corrected (expected underestimated) Reactor grade case is given in Table 6.6. Similar results are observed for both the underestimated and overestimated reactor grade plutonium samples. By comparing the behavior of the reactor and weapons grade simulated BEGe 3825 response, it is shown that uncertainty and thus the sample age estimate can be improved by either increasing the mass of the sample (more Pu241/Am241) or increasing the count time to the order of days, instead of hours. For both underestimated and overestimated reactor grade samples, similar signs of the sensitivity of the age estimate to the ratio when the age is in the order of decades were observed. Expanding the analysis to cover age cases of 30 to 70 years would be expected to further highlight the importance of keeping count rate ratio uncertainty low, either through increasing the overall sample mass taken from the stockpile, or increasing the count time of the sample, keeping in mind the time span between the increased count time to ensure activity errors are kept low, which was accounted for when the count time was increased from 1 hour to 10 days, and a 6 month span was utilized, the activity change in 10 days being almost small to the activity change in the 6 months that were chosen. Improvement further is observed when time span is increased to 1, 1.5 or 2 years.

Table 6.2. Weapons grade, uncorrected simulated BEGe 3825 response

Decay time (years)	MC NP Centroid (keV)	Known Centroid (keV)	Centroid % error	Am 241 59.50 keV sim. Net cps	Net CPS uncertainty	Net CPS uncertainty %	Ratio of Net CPS measurements	Ratio uncertainty %	T1	T2 (time between 1 hour measurements)	Ratio min, 1 standard deviation	Ratio max, 1 standard deviation	T_age (min K, 1 std dev)	T_age (max k)	T_age (max k, 1 std dev)	True stockpile age range (years), 1 σ uncertainty effect on net cps ratio
1.000	59.588	59.500	0.148	1.451	0.050	3.446			True age 1 year							
1.500	59.582	59.500	0.138	2.171	0.054	2.487	0.668	4.250	0.000	0.500	0.640	0.697	0.859	0.971	1.103	0.859<T_age<1.103
2.000	59.559	59.500	0.099	2.922	0.056	1.916	0.497	3.943	0.000	1.000	0.477	0.516	0.870	0.940	1.014	0.870<T_age<1.014
2.500	59.563	59.500	0.106	3.602	0.061	1.694	0.403	3.840	0.000	1.500	0.387	0.418	0.893	0.952	1.013	0.893<T_age<1.013
3.000	59.565	59.500	0.109	4.271	0.065	1.522	0.340	3.767	0.000	2.000	0.327	0.353	0.903	0.956	1.010	0.903<T_age<1.010
5.000	59.567	59.500	0.113	6.775	0.079	1.166			True age 5 year							
5.500	59.568	59.500	0.114	7.356	0.082	1.115	0.921	1.613	0.000	0.500	0.906	0.936	4.273	5.055	6.146	4.273<T_age<6.149
6.000	59.567	59.500	0.113	7.929	0.084	1.059	0.854	1.575	0.000	1.000	0.841	0.868	4.585	5.030	5.552	4.585<T_age<5.552

Table 6.2. Weapons grade, uncorrected simulated BEGe 3825 response, (cont.)

6.5 00	59.5 68	59.5 00	0.11 4	8.4 87	0.087	1.025	0.798	1.553	0.0 00	1.500	0.78 6	0.81 1	4.6 99	5.0 23	5.3 84	4.699<T_ag e<5.383
7.0 00	59.5 67	59.5 00	0.11 3	9.0 30	0.089	0.986	0.750	1.527	0.0 00	2.000	0.73 9	0.76 2	4.7 61	5.0 22	5.3 04	4.761<T_ag e<5.304
19. 000	59.5 71	59.5 00	0.11 9	18. 640	0.125	0.671			True age 19 year							
19. 500	59.5 71	59.5 00	0.11 9	18. 931	0.126	0.666	0.985	0.945	0.0 00	0.500	0.97 5	0.99 4	13. 543	18. 764	31. 362	13.542<T_a ge<31.36
20. 000	59.5 71	59.5 00	0.11 9	19. 203	0.126	0.656	0.971	0.938	0.0 00	1.000	0.96 2	0.98 0	15. 826	19. 004	23. 831	15.826<T_a ge<23.831
20. 500	59.5 71	59.5 00	0.11 9	19. 476	0.127	0.652	0.957	0.935	0.0 00	1.50 0	0.94 8	0.96 6	16. 680	18. 969	21. 983	16.680<T_a ge<21.983
21. 000	59.5 70	59.5 00	0.11 8	19. 736	0.128	0.649	0.944	0.933	0.0 00	2.000	0.93 6	0.95 3	17. 196	19. 015	21. 252	17.196<T_a ge<21.251

Table 6.3. Weapons grade, corrected simulated BEGe 3825 response

WG																
True Time	MC NP Centroid (keV)	Known Centroid (keV)	Centroid % error	Am 241 59.50 keV sim Net cps	Net CPS uncertainty	Net CPS uncertainty %	Ratio of Net CPS measurements	Ratio uncertainty %	T1	T2 (time between 1 hour measurements)	Ratio min, 1 standard deviation	Ratio max, 1 standard deviation	T_age (min K, 1 std dev)	T_age (mean k)	T_age (max k, 1std dev)	True stockpile age range (years), 1 σ uncertainty effect on net cps ratio
1.000	59.568	59.500	0.114	0.719	0.042	5.841			True age 1 year							
1.500	59.560	59.500	0.101	1.093	0.046	4.209	0.658	7.200	0.000	0.500	0.610	0.705	0.759	0.927	1.147	0.759<T_age<1.147
2.000	59.574	59.500	0.124	1.407	0.048	3.412	0.511	6.765	0.000	1.000	0.476	0.546	0.868	0.994	1.138	0.868<T_age<1.138
2.500	59.582	59.500	0.138	1.754	0.050	2.851	0.410	6.500	0.000	1.500	0.383	0.437	0.878	0.979	1.089	0.878<T_age<1.089
3.000	59.579	59.500	0.133	2.085	0.049	2.350	0.345	6.296	0.000	2.000	0.323	0.367	0.888	0.977	1.072	0.888<T_age<1.071
5.000	59.562	59.500	0.104	3.381	0.055	1.627			True age 5 year							
5.500	59.566	59.500	0.111	3.674	0.058	1.579	0.920	2.267	0.000	0.500	0.899	0.941	3.986	5.009	6.641	3.985<T_age<6.640

Table 6.3. Weapons grade, corrected simulated BEGe 3825 response, (cont.)

6.0 00	59.5 62	59.5 00	0.10 4	3.9 58	0.059	1.491	0.854	2.206	0. 00 0	1.000	0.83 5	0.87 3	4.4 18	5.0 21	5.7 77	4.418<T_ag e<5.777
6.5 00	59.5 65	59.5 00	0.10 9	4.2 38	0.061	1.439	0.798	2.172	0. 00 0	1.500	0.78 0	0.81 5	4.5 67	5.0 10	5.5 22	4.567<T_ag e<5.522
7.0 00	59.5 63	59.5 00	0.10 6	4.5 12	0.063	1.396	0.749	2.144	0. 00 0	2.000	0.73 3	0.76 5	4.6 42	5.0 00	5.3 99	4.642<T_ag e<5.399
19. 00 0	59.5 69	59.5 00	0.11 6	9.3 14	0.088	0.945			True age 19 year							
19. 50 0	59.5 68	59.5 00	0.11 4	9.4 63	0.089	0.941	0.984	1.333	0. 00 0	0.500	0.97 1	0.99 7	12. 03 7	18. 47 6	43. 65 4	12.037<T_a ge<43.654
20. 00 0	59.5 69	59.5 00	0.11 6	9.5 95	0.089	0.928	0.971	1.324	0. 00 0	1.000	0.95 8	0.98 4	14. 81 4	19. 01 7	26. 70 1	14.814<T_a ge<26.701
20. 50 0	59.5 69	59.5 00	0.11 6	9.7 32	0.090	0.925	0.957	1.322	0. 00 0	1.500	0.94 4	0.97 0	15. 87 9	18. 96 1	23. 52 5	15.879<T_a ge<23.525
21. 00 0	59.5 69	59.5 00	0.11 6	9.8 63	0.090	0.913	0.944	1.314	0. 00 0	2.000	0.93 2	0.95 7	16. 52 5	18. 98 5	22. 28 1	16.525<T_a ge<22.281

Table 6.4. Weapons grade, corrected, 10 day measurement time, 19 year decay time tests

WG	Simulated Live Count time changed from	1 hour to 10 days														live count time changed from 1 hour to 10 days
True Time	MC NP Centroid (keV)	Known Centroid (keV)	Centroid % error	Am 241 59.50 keV sim Net cps	Net CPS uncertainty*	Net CPS uncertainty %	Ratio of Net CPS measurements	Ratio uncertainty %	T1	T2 (time between 1 hour measurements)	Ratio min, 1 standard deviation	Ratio max, 1 standard deviation	T_age (min K, 1 std dev)	T_age (mean k)	T_age (max k, 1std dev)	True stockpile age range (years), 1 σ uncertainty effect on net cps ratio
19.000	59.572	59.500	0.121	9.323	0.006	0.064			True age 19 year		0.000	0.000				True age=19 years

Table 6.4. Weapons grade, corrected, 10 day measurement time, 19 year decay time tests, (cont.)

19.500	59.571	59.500	0.119	9.467	0.006	0.063	0.985	0.090	0.000	0.500	0.984	0.986	18.210	18.891	19.628	18.210<T _{age} <19.627
20.000	59.571	59.500	0.119	9.605	0.006	0.062	0.971	0.090	0.000	1.000	0.970	0.972	18.629	18.986	19.358	18.628<T _{age} <19.358
20.500	59.571	59.500	0.119	9.741	0.006	0.062	0.957	0.089	0.000	1.500	0.956	0.958	18.728	18.972	19.223	18.728<T _{age} <19.223
21.000	59.571	59.500	0.119	9.871	0.006	0.061	0.944	0.089	0.000	2.000	0.944	0.945	18.830	19.019	19.211	18.830<T _{age} <19.211

Table 6.5. Reactor grade, uncorrected

RG																
True Time	MC NP Centroid (keV)	Known Centroid (keV)	Centroid % error	Am 241 59.50 keV sim. Net cps	Net CPS uncertainty	Net CPS uncertainty %	Ratio of Net CPS measurements	Ratio uncertainty %	T1	T2 (time between 1 hour measurements)	Ratio min, 1 standard deviation	Ratio max, 1 standard deviation	T _{age} (min K, 1 std dev)	T _{age} (mean k)	T _{age} (max k, 1st d dev)	True stockpile age range (years), 1 σ uncertainty effect on net cps ratio
1.000	59.599	59.500	0.166	27.136	0.153	0.564			True age 1 year							
1.500	59.589	59.500	0.150	40.251	0.182	0.452	0.674	0.723	0.000	0.500	0.669	0.679	0.975	0.996	1.018	0.975<T _{age} <1.018

Table 6.5. Reactor grade, uncorrected, (cont.)

2.0 00	59.5 84	59.5 00	0.14 1	53. 046	0.208	0.392	0.512	0.687	0. 00 0	1.000	0.50 8	0.51 5	0.9 83	0.9 96	1.0 10	0.982<T_a ge<1.009
2.5 00	59.5 81	59.5 00	0.13 6	65. 527	0.231	0.353	0.414	0.665	0. 00 0	1.500	0.41 1	0.41 7	0.9 85	0.9 96	1.0 07	0.985<T_a ge<1.007
3.0 00	59.5 80	59.5 00	0.13 4	77. 707	0.251	0.323	0.349	0.650	0. 00 0	2.000	0.34 7	0.35 1	0.9 86	0.9 96	1.0 05	0.986<T_a ge<1.005
5.0 00	59.5 77	59.5 00	0.12 9	123 .34 9	0.314	0.255			True age 5 year							
5.5 00	59.5 77	59.5 00	0.12 9	134 .07 1	0.327	0.244	0.920	0.353	0. 00 0	0.500	0.91 7	0.92 3	4.8 07	4.9 95	5.1 97	4.807<T_a ge<5.197
6.0 00	59.5 77	59.5 00	0.12 9	144 .52 0	0.339	0.235	0.854	0.346	0. 00 0	1.000	0.85 1	0.85 6	4.8 94	4.9 96	5.1 02	4.894<T_a ge<5.102
6.5 00	59.5 76	59.5 00	0.12 8	154 .71 6	0.351	0.227	0.797	0.341	0. 00 0	1.500	0.79 5	0.80 0	4.9 22	4.9 95	5.0 70	4.922<T_a ge<5.070
7.0 00	59.5 76	59.5 00	0.12 8	164 .62 2	0.361	0.219	0.749	0.336	0. 00 0	2.000	0.74 7	0.75 2	4.9 40	4.9 99	5.0 58	4.940<T_a ge<5.058
19. 00 0	59.5 74	59.5 00	0.12 4	340 .47 2	0.517	0.152			True age 19 year							
19. 50 0	59.5 74	59.5 00	0.12 4	345 .68 6	0.521	0.151	0.985	0.214	0. 00 0	0.500	0.98 3	0.98 7	17. 44 2	18. 99 3	20. 86 3	17.442<T_a ge<20.862

Table 6.5. Reactor grade, uncorrected, (cont.)

20.000	59.574	59.500	0.124	350.751	0.525	0.150	0.971	0.213	0.000	1.000	0.969	0.973	18.178	19.009	19.921	18.178<T_age<19.921
20.500	59.574	59.500	0.124	355.698	0.529	0.149	0.957	0.213	0.000	1.500	0.955	0.959	18.428	19.003	19.615	18.428<T_age<19.615
21.000	59.574	59.500	0.124	360.527	0.532	0.148	0.944	0.212	0.000	2.000	0.942	0.946	18.550	18.994	19.458	18.549<T_age<19.458

Table 6.6. Reactor grade corrected

RG																
True Time	MC NP Centroid (keV)	Known Centroid (keV)	Centroid % error	Am 241 59.50 keV sim. Net cps	Net CPS uncertainty	Net CPS uncertainty %	Ratio of Net CPS measurements	Ratio uncertainty %	T1	T2 (time between 1 hour measurements)	Ratio min, 1 standard deviation	Ratio max, 1 standard deviation	T_age (min K, 1 std dev)	T_age (mean k)	T_age (max k, 1std dev)	True stockpile age range (years), 1 σ uncertainty effect on net cps ratio
1.000	59.601	59.500	0.170	13.571	0.108	0.796				True age 1 year						

Table 6.6. Reactor grade corrected, (cont.)

1.5 00	59.5 90	59.5 00	0.15 1	20. 127	0.129	0.641	0.674	1.022	0. 00 0	0.500	0.66 7	0.68 1	0.9 67	0.9 97	1.0 28	0.967<T_a ge<1.028
2.0 00	59.5 85	59.5 00	0.14 3	26. 532	0.147	0.554	0.511	0.970	0. 00 0	1.000	0.50 7	0.51 6	0.9 77	0.9 96	1.0 15	0.977<T_a ge<1.015
2.5 00	59.5 81	59.5 00	0.13 6	32. 765	0.163	0.497	0.414	0.939	0. 00 0	1.500	0.41 0	0.41 8	0.9 81	0.9 96	1.0 12	0.981<T_a ge<1.012
3.0 00	59.5 80	59.5 00	0.13 4	38. 856	0.177	0.456	0.349	0.917	0. 00 0	2.000	0.34 6	0.35 2	0.9 82	0.9 96	1.0 10	0.982<T_a ge<1.001
5.0 00	59.5 77	59.5 00	0.12 9	61. 679	0.222	0.360			True age 5 year							
5.5 00	59.5 77	59.5 00	0.12 9	67. 039	0.231	0.345	0.920	0.498	0. 00 0	0.500	0.91 5	0.92 5	4.7 34	4.9 96	5.2 86	4.734<T_a ge<5.286
6.0 00	59.5 77	59.5 00	0.12 9	72. 262	0.240	0.332	0.854	0.490	0. 00 0	1.000	0.84 9	0.85 8	4.8 54	4.9 98	5.1 49	4.853<T_a ge<5.149
6.5 00	59.5 77	59.5 00	0.12 9	77. 364	0.248	0.321	0.797	0.482	0. 00 0	1.500	0.79 3	0.80 1	4.8 92	4.9 95	5.1 02	4.892<T_a ge<5.102
7.0 00	59.5 76	59.5 00	0.12 8	82. 311	0.256	0.311	0.749	0.476	0. 00 0	2.000	0.74 6	0.75 3	4.9 17	5.0 00	5.0 85	4.917<T_a ge<5.084

Table 6.6. Reactor grade corrected, (cont.)

19. 00 0	59.5 74	59.5 00	0.12 4	170 .23 8	0.366	0.215			True age 19 year							
19. 50 0	59.5 74	59.5 00	0.12 4	172 .84 9	0.368	0.213	0.985	0.303	0. 00 0	0.500	0.98 2	0.98 8	16. 85 9	18. 97 5	21. 73 2	16.859<T_ age<21.732
20. 00 0	59.5 74	59.5 00	0.12 4	175 .37 8	0.371	0.212	0.971	0.302	0. 00 0	1.000	0.96 8	0.97 4	17. 85 4	19. 00 8	20. 32 4	17.854<T_ age<20.324
20. 50 0	59.5 74	59.5 00	0.12 4	177 .84 9	0.374	0.210	0.957	0.301	0. 00 0	1.500	0.95 4	0.96 0	18. 20 3	19. 00 6	19. 88 4	18.203<T_ age<19.884
21. 00 0	59.5 74	59.5 00	0.12 4	180 .26 6	0.376	0.209	0.944	0.300	0. 00 0	2.000	0.94 2	0.94 7	18. 37 1	18. 99 3	19. 65 7	18.371<T_ age<19.657

As obvious from the results, 1 hour measurement are sufficient for RG fuel interrogation but longer measurement times are needed for WG fuel to ascertain the age with confidence. As both the uncorrected and corrected results show, it is extremely likely that the BEGe 3825 located in the MSTR is capable of determining the age of weapons/reactor grade plutonium stockpile samples of active masses at or greater than $5.00\text{E-}07$ g. Figure of merits of the above analysis are not included in this study. As this study only examined about 1 to 19 years, it is expected that a higher count time than 1 hour or larger sample would be necessary to decrease net cps ratio uncertainty to ensure a precise time estimate range when measuring a 20-70 year old samples, as was shown for the corrected WG 19 year case when the sensitivity in the net count rate ratio becomes greater. As stated above in the procedure section, convergence in the newton method was only observed when the production rate of Am241 exceeded or equaled that of its decay rate.

The next goal of this study was to determine which irradiation times and initial activities of Am241 led to viable photopeaks of Am242 and Am242m that could be physically measured in the BEGe 3825 (No physical measurements of Am242/Am242m were performed in this study) using two cases of initial Am241 activity, each with three irradiation time sub-cases. These initial Am241 activities were irradiated at the full power that the MSTR can provide (200 kW), for times of 1 min, 30 min and 8 hours followed by a 2 hour decay for each time case to allow the expected major photon contributor Al-28 to decay away. Since the model isotope activity is kept steady state, and thus the photon energy and probability distribution is kept constant, in order to accurately model the impact of the short half-lives of the fission products and Am242 short detector live times of 20 minutes were used for the determination of the tally multiplier, which will overestimate the photon contribution from the shortest lived fission products regardless (constant activity during measurement). For the best scenario, since the shortest half-life being analyzed is 16 hours, a simulated measurement time of 20 minutes was taken to avoid a large error in the Am242 activity estimates, as one would do for a physical sample of Am242. Simulated dead time was not considered for the simulated measurement times as the decay time of 2 hours for each irradiation case is expected to cause total sample activity to lessen greatly and allow the sample to be within Prospect

tolerances where the use of a live time is feasible. The continued build-up of actinides isotopes due to decay after the irradiation and the 2 hour decay where build-up was kept track of is ignored, and the activities that are given by MCNPX after the 2 hour decay is assumed to remain constant throughout the measurement live-time, which is selected to produce low error results with Am242 16 hour half-life. This consideration was not made for Am241 in the above WG/RG Plutonium, Am241 buildup, as the half-life of Am241 is ~3 times greater than Am242m, whose error response to a certain simulated live time is given in Figure 6.2 compared to Am242 in Figure 6.1.

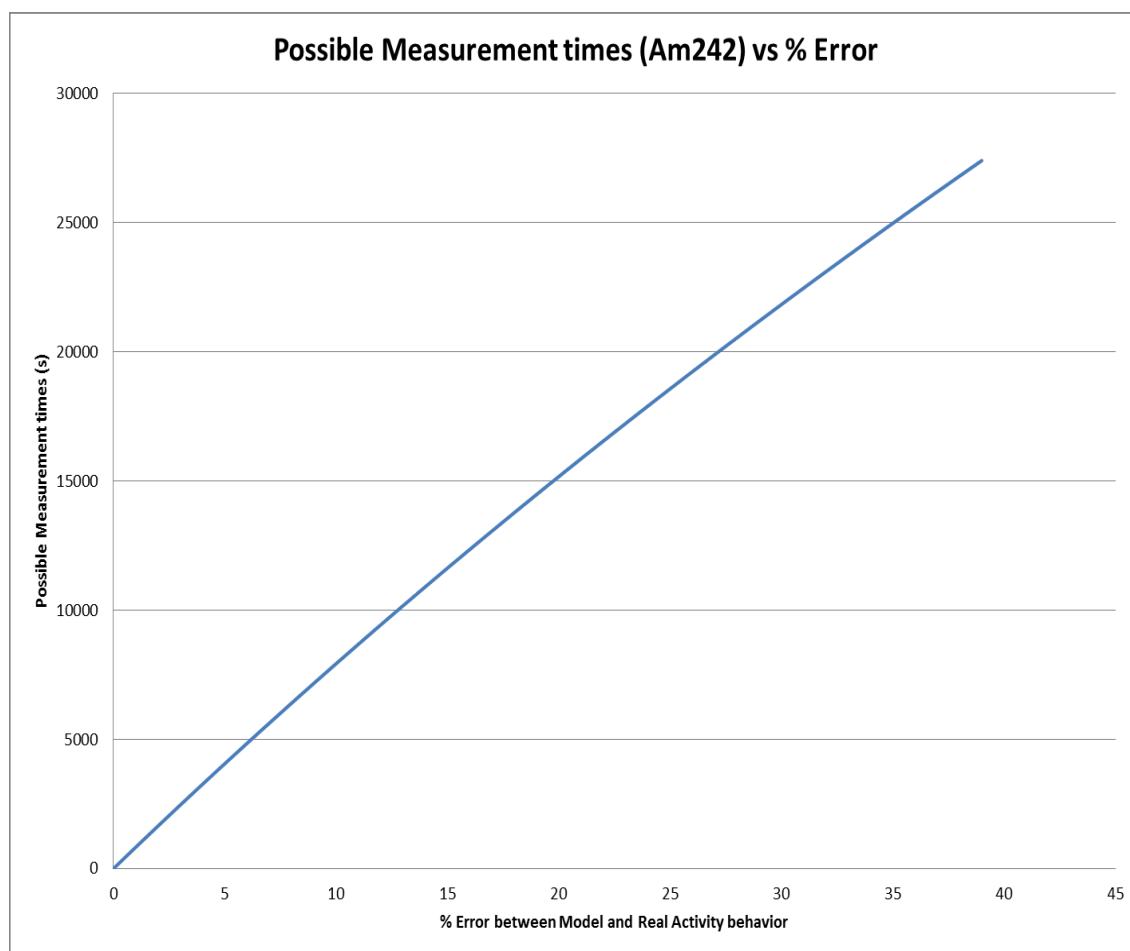


Figure 6.1. Gives a suitable multiplier for an accepted error of Am242, based off of suitably short live measurement time for short lived Am242, ~16 hours

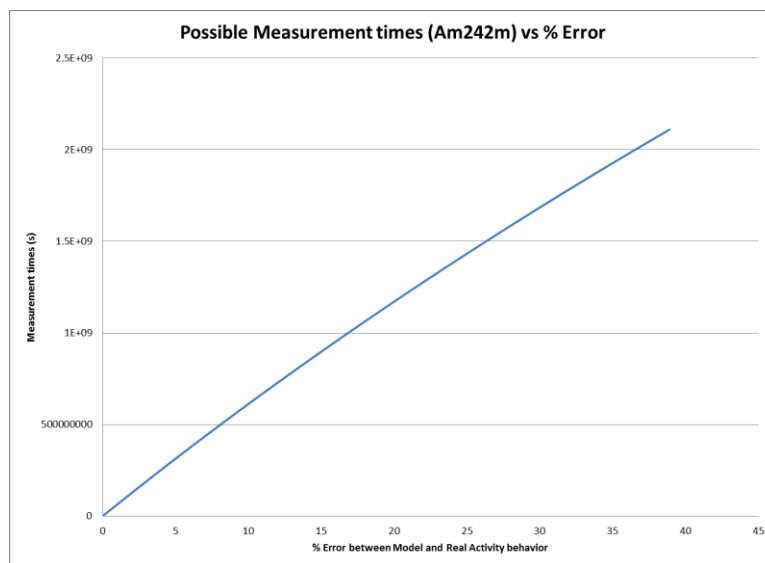


Figure 6.2. Gives a suitable multiplier for an accepted error of Am242m, to be used in conjunction with the above, longer half-life allows for larger live measurement time where Am242m activity can be considered constant

This relatively short simulated burn time will keep the activity net build-up behavior linear in nature and allow for the reaction rate ratio from the base material Am241 to be measured. It is assumed that the discrepancy between the live and dead time in all scenarios are minimal, which is not necessarily true for higher inventory activities. The goal was to determine at which initial activity of a sample of pure Am241 deposited onto an Aluminum foil backing, the shortest burn time/decay time/live measurement time that could produce measurable peaks (Table 2.4, Table 2.5) at 200 kW within the validated BEGe 3825 model within 10% error for the Prospect derived uncertainty for the Am242m and Am242 peaks of interest. The activity limit for this study was capped at 1 μCi , while the initial activity of .05 μCi was investigated since it is an exempt quantity of Am241 from the campus regulations. Activity values are given in Table 6.7. The activity of the Am241 sample is only expected to impact the resulting magnitude of the simulated Am242/Am242m photopeaks, in the BEGe 3825 model. Relations such as Am241 photon rates to Am242/Am242m photon rates for certain irradiation times between the 2 initial activities of Am241 are expected remain equal. Magnitudes of saturation activity (not examined in this study) would vary as well between the test cases.

Table 6.7. Initial activities and irradiation time cases to allow for irradiation times to be investigated in determining the feasibility of using the BEGe 3825 to determine Am242/Am242m production rates in MSTR

Case #	Initial Am241 Activity (μCi) and irradiation time (min)
1	.05 μCi
1, S1 (irradiation time)	1 min
1, S2 (irradiation time)	30 min
1, S3 (irradiation time)	480 min
2	1 μCi
2, S1 (irradiation time)	1 min
2, S2 (irradiation time)	30 min
2, S3 (irradiation time)	480 min

For each case, the sample of Am241 with .05 μCi was irradiated in increasing time duration at 1 minute, 30 minutes, and hour at 200 kW s, each followed by a 2 hours of decay/cooling off time. The uncertainty of using the multiplier on the normalized F8 tallies will be ignored, since this analysis is only to determine a general time scale at which viable peaks of Am242 and Am242m can observed and measured for a upper end realistic irradiation time of 8 hours. Since the use of the unmodified multiplier is expected to produce an uncorrected (overestimation) target peak area, an Prospect analysis that will be an corrected (underestimation) will be provided as well for each case by dividing the F8 tally results by a factor of 2, as was done for the WG/RG analysis (taken from observations of Mixed and Europium Standard tests). Viability of peaks is defined by the inclusion of Gross area for a peak, as well as peak area uncertainty less than 100%. For Case 1 and 2, all Prospect analysis was done at the specified initial continuum estimate, .2 FWHM, peaks that have their gross area determined but still

display greater than a 100% peak uncertainty will still be listed in the corrected, uncorrected analysis below, but are still counted as a non-viable peak with the specific Prospect analysis settings.

For case 1, the modified F8 tally subjected to the entire gamma/x-ray distribution from all fission products, actinides and activation products produced and still existing within a $1\text{E-}60$ atomic fraction limit when compared to the base Al27 in the foil after 2 hours of decay. The tally produced a spectrum (after corrected) that when analyzed by Canberra's Prospect software gave net count rates for the peaks of interest, which for this case is only from Am242, as none of Am242m peaks were viable. Am242 peaks were from x-ray emissions in the 102 keV and 118 keV regions. All uncertainties regarding the photon emission rate were taken from the MCNP derived relative error for the corrected radiative capture rates of Am241 in the burn time duration. The uncertainty obtained from multiplying the normalized MCNP F8 tally spectrum by the total photon count will be ignored for these estimations based upon the observations of the multiplier effect on the FEPE ratios of Eu and Mixed standard source validations, where the resulting ratio values were all within their combined uncertainty ranges. Due to the closeness of many of Am242 photon emissions in the energy regions of interest, and the desire to maintain fidelity with the actual detector FWHM calibration equation parameters, the resulting peaks are the summation of photon rates around them. 2 hours of decay time after a 1 min, 30 min, and 8 hour burn, for the Am242 peaks measured by Prospect from the total isotope inventory in the $.05\mu\text{Ci}$ initial activity of the simulated sample of Am241, 20 minute live count time of measurement. Photon rate uncertainty is taken from the MCNP derived relative error in the Am241 radiative capture rates for each of the burn-up runs. MCNP tally errors were ignored since for each energy bin in a given peak of interest the relative MCNP error fraction was less than .02 and at that point, counts were then considered to mimic actual photon counts where Prospect counting error statistics could be applied and would be considered alone. MCNP uncertainty and Prospect uncertainty were considered uncorrelated and are combined when comparing the Prospect derived count rate and the MCNP photon/s. This is done for Case 1 and Case 2, for both uncorrected and corrected models. For case 1 the Am242m to Am242 Energy integrated production ratio is given in the Am242 peak analysis Tables 6.8 and 6.9 (both values are

the same, but included for completeness), due to no viable peaks of Am242m being detected by Prospect, the Production Ratio calculation utilized the MCNPX derived activity values for each burn time directly, with the 1 minute burn of particular value as it was the shortest analyzed in this study. Since the Am242m peaks were not viable for the conditions used in this study, The efficacy of the BEGe model's ability to determine the Am242m to Am242 production ratio directly could not be examined, and is given below (Table 6.8 and 6.9) as an expected value (same for both corrected and uncorrected spectrums).

Table 6.8. Case 1 Am242 simulated peaks of interest, no viable Am242m peaks, 200 kW, used same Prospect peak search settings as with Mixed and Europium source validation, continuum=.2 FWHM, uncorrected F8 tally/Prospect results (unmodified model)

CA SE 1 S1	Given Photon Rate uncertainty (%)	Weighted Centroid (keV)	MCNP Centroid (keV)	% Error	Given Photon/s rate	MCNP Net Count rate	Uncertainty (Prospect)	Uncertainty % Prospect)	FE PE (%)	Uncertainty %	Energy Integrated Am242m /Am242 Production Ratio
	3.6	102.616 (Am242)	102.212	0.394	2.221	0.376	0.134	35.566	16.909	35.748	0.110
	3.6	118.247 (Am242)	NA	NA	0.605	0.000	0.000	NA	0.000	NA	
CA SE 1 S2	Given Photon Rate uncertainty (%)	Weighted Centroid (keV)	MCNP Centroid (keV)	% Error	Given Photon/s rate	MCNP Net Count rate	Uncertainty (Prospect)	Uncertainty % Prospect)	FE PE (%)	Uncertainty %	Energy Integrated Am242m /Am242 Production Ratio

Table 6.8. Case 1 Am242 simulated peaks of interest, no viable Am242m peaks, 200 kW, used same Prospect peak search settings as with Mixed and Europium source validation, continuum=.2 FWHM, uncorrected F8 tally/Prospect results (unmodified model), (cont.)

	3.43	102.616 (Am 242)	102.252	0.355	62.247	11.764	0.236	2.002	18.898	3.972	0.109
	3.43	118.247 (Am 242)	118.536	0.244	16.947	2.431	3.781	155.534	14.346	155.572	
CASE 1 S3	Given Photon Rate uncertainty (%)	Weighted Centroid (keV)	MC NP Centroid (keV)	% Error	Given Photon/s rate	MC NP Net Count rate	Uncertainty (Prospect)	Uncertainty % Prospect)	FE PE (%)	Uncertainty %	Energy Integrated Am242m /Am242 Production Ratio
	4	102.616 (Am 242)	102.235	0.371	846.049	157.360	0.595	0.378	18.599	4.018	0.128
	4	118.247 (Am 242)	118.622	0.317	230.342	32.700	0.307	0.939*	14.196	4.109	

*no gross area was obtained by Prospect for these 118.247 keV peaks

For the corrected case 1, in which the F8 tallies were divided by 2 due to observations from the Mixed and Europium validation tests, the resultant Am242 Prospect Analysis for the 102 and 118 peaks revealed agreement with the above overestimation case. Uncertainty for Energy Integrated Production ratio is omitted, as uncertainty is taken as the error in the radiative capture rate of Am241 as provided by MCNPX which is used as the uncertainty in the combined photon rate for Am242's peak analysis.

Table 6.9. Case 1 Prospect analysis for Am242 102 and 118 peaks, using a corrected MCNP derived tally spectrum (modified BEGe 3825 model)

Case	Given Photon Rate uncertainty (%)	Weighted Centroid (keV)	MC NP Centroid (keV)	% Error	Given Photon/s rate	MC NP Net Count rate	Uncertainty (Prospect)	Uncertainty % Prospect	FE PE (%)	Uncertainty %	Energy Integrated Am242m /Am242 Production Ratio
S1	3.600	102.616 (Am 242)	102.326	0.283	2.221	0.186	0.087	46.871	8.379	47.009	0.110
	3.600	118.247 (Am 242)	NA	NA	0.605	0.000	0.000	NA	0.000	NA	
S2	3.430	102.616 (Am 242)	102.293	0.315	62.247	6.287	0.159	2.535	10.101	4.265	0.109
	3.430	118.247 (Am 242)	118.468	0.187	16.947	1.124	0.933	82.999	6.630	83.070	
S3	4.000	102.616 (Am 242)	102.234	0.372	846.049	78.674	0.419	0.532	9.299	4.035	Energy Integrated Am242m /Am242 Production Ratio at irradiation time

Table 6.9. Case 1 Prospect analysis for Am242 102 and 118 peaks, using a corrected MCNP derived tally spectrum (modified BEGe 3825 model), (cont.)

	4.000	118.247 (Am 242)	118.616	0.312	230.342	16.364	0.216	1.323*	7.104	4.213	0.128
--	-------	---------------------	---------	-------	---------	--------	-------	--------	-------	-------	-------

*no gross area was obtained by Prospect for these 118.247 keV peaks

Unlike the Am241 buildup in plutonium stockpiles, in which its dominant 59.50 keV peak was very well defined, and thus relatively easy (no observed peak analysis anomalies) for Prospect to analyze, Am242 and its two dominant summed peaks of 102 and 118 existed in close proximity. This is assumed to have caused the lesser 118 keV peak to suffer and cause the automated peak analysis to fail in determining peak gross area. To show that the Am242 102 peak is more reliable than its 118 keV peak, the Prospect analysis continuum estimate was adjusted from its minimum of .01 FWHM to 2 FWHM (keV) in for each of the time cases for this initial Am241 activity, testing for the viability of both peaks and to determine which photopeak will offer a well-defined enough counts that can be auto analyzed by Prospect. A peak that has zero gross area or an uncertainty exceeding 100% will be considered suspect and not reliable (viable), regardless of the existence of its net peak area. Based on Table 6.10 and 6.11, the main peak that is of relevance is the 102.616 keV peak. No viable peaks (86 keV) of Am242m were detected via BEGe model and subsequent Prospect analysis, regardless of peak sensitivity settings. Tables 6.12 and 6.13 give the Am241 interference fraction in the target energy regions. It is noted that the 102 peak was favored over the 118 keV peak when the automated peak analysis feature was utilized, manual setting of the peaks were on some instances could avoid the anomalies that were observed. For the ability to reproduce measurements consistently, the automate measurements were utilized, as otherwise, manual peak analysis suffered from variable peak locating which had a significant impact on the final Prospect results. The behavior of the 102 and 118 keV peaks when examined for under the described analysis parameters will indicate which photopeak is the more stable and thus reliable value to quantify the presence of Am242.

Table 6.10. Case 1 Am242 peaks differed in reliability when analyzed by Prospect; changing the continuum setting in increments of .2 FWHM for 11 runs showcased the well-defined Am242 peak of 102.616 keV, while the 118.247 suffered from its close proximity to said 102.616 keV peak (uncorrected case) (unmodified model)

	S1 viability fraction (out of 11 runs)	S2 viability fraction (out of 11 runs)	S3 viability fraction (out of 11 runs)
102.616	10/11	11/11	11/11
118.247	0/11	0/11	0/11

Table 6.11. Case 1 Peak analysis by Prospect, testing effect of continuum setting from .01 to 2 FWHM, for the assumed corrected spectrum tally (modified model)

	S1 viability fraction (out of 11 runs)	S2 viability fraction (out of 11 runs)	S3 viability fraction (out of 11 runs)
102.616	10/11	11/11	11/11
118.247	0/11	1/11	0/11

Table 6.12 gives the contamination Am241 gamma rays for Am242's 102 and 118 composite x-ray peaks. As expected, during the 1 minute irradiations, Am241 in these energy regions remain the dominant source, and a substantial fraction of Am242's respective photon rates for the 102 and 118 keV photopeaks. At later irradiation times, Am241's competing photopeaks became minimal in comparison. Although at larger time scales of irradiation the Am241 interference becomes negligible, if the goal is to determine the production rate ratio of Am242m to Am242 the irradiation times should be on the order of hours at most. If the goal is to reach saturation activity of Am242/Am242m, then irradiation time is no longer an upper constraint.

Table 6.12. Comparison between the photon rates of Am242 and the pre-existing Am241 photon rates for Case 1 in the energy regions of interest

Energy (keV)	S1, Photon Rate (Am242)	S2, Photon Rate (Am242)	S3, Photon Rate (Am242)	Energy (keV)	S1, Photon Rate (Am241)	S2, Photon Rate (Am241)	S3, Photon Rate (Am241)
99.979	0.859	24.074	327.206	97.498	0.020	0.020	0.020
104.279	1.362	38.173	518.844	98.970	0.375	0.375	0.375
116.802	0.158	4.427	60.166	101.574	0.033	0.033	0.033
117.372	0.310	8.684	118.030	102.980	0.361	0.361	0.361
118.372	0.006	0.162	2.205	113.834	0.004	0.004	0.004
118.573	0.007	0.183	2.482	114.778	0.008	0.008	0.008
120.979	0.040	1.115	15.157	115.341	0.000	0.000	0.000
121.244	0.081	2.273	30.896	115.532	0.000	0.000	0.000
121.507	0.002	0.049	0.660	117.880	0.001	0.001	0.001
121.550	0.002	0.055	0.746	118.120	0.002	0.002	0.002
X	X	X	X	118.380	0.000	0.000	0.000
X	X	X	X	118.430	0.000	0.000	0.000
X	X	X	X	120.360	0.000	0.000	0.000
X	X	X	X	123.050	0.018	0.018	0.018
X	X	X	X	125.300	0.075	0.075	0.075

Table 6.13. Comparison of Am241 and Am242 photon rates for the peaks of interest used to measure Am242 for Case 1

Rate Sum	S1		S2		S3	
	99-105	113-124	99-105	113-124	99-105	113-124
Energy Region (keV)						
Am242 Rate	2.221142	0.604718	62.24656	16.946971	846.0494	230.34168

Table 6.13. Comparison of Am241 and Am242 photon rates for the peaks of interest used to measure Am242 for Case 1, (cont.)

Am241 Combine d Rate	0.789856	0.1093334	0.789856	0.1093334	0.789856	0.1093334
A241 Rate sum Percenta ge of Am242 Rate sum (%)	35.560806 11	18.080063 77	1.2689151 01	0.6451500 98	0.0933581 42	0.0474657 47

All other peaks in these energy regions of interest were negligible but are considered in the analysis, but not shown above. Photon rates were summed into 2 macro peaks due to observations of the models response with the compact energy lines when using the same GEB parameters introduced during the validation phase. Uncertainties regarding the Am242 photon rates in the above tables were omitted, as they are assumed to be equal to the MCNP derived uncertainty in the activation rate value of Am241. At the low end of the time scales investigated, the target peaks of interest are contaminated by the ever present Am241 gamma/x-ray emissions. At higher irradiation times interference from Am241 became negligible as compared to Am242 99-104 and 113-124 keV peaks and hence can be ignored. No peaks of Am242m were detected with the Prospect software with the count spectrum obtained from the MCNP model of the BEGe 3825 of interest in the full spectrum for each Am241 activity case and its irradiation time's subcases of S1, S2, and S3. For both the corrected and uncorrected F8 tally analysis by Prospect, the 118.247 combined Am242 peak was not shown to be viable by Prospect for either a 1 minute or a 480 minute burn, and suffered conflicting results as the

peak continuum estimate was incremented by .2 FWHM. As too high of a continuum estimate resulted in non-accurate curve fitting, only at 30 minutes at for the corrected results did a single initial continuum trial result in analysis that did not give a null gross peak area or an peak uncertainty exceeding 100%. The uncorrected Peak analysis for the 1 minute, 30 minute, and the 480 minute times were repeatedly and completely unviable for the 118 keV peak of Am242, regardless of initial continuum estimate. Similar behavior was seen for the corrected 118 and 102 peaks, in which the 118 peak suffered in its Prospect analysis. The results of case 1 reveal that the 102.616 is the better choice to measure the activity of Am242 at an irradiation time of greater than 30 minutes.

For Case 2, the Am242m to Am242 Energy integrated production ratio is included in the Am242 peak analysis Tables 6.14 and 6.15, due to no viable peaks of Am242m being detected by Prospect, Production Ratio utilized MCNPX derived activity values for each burn time, with the 1 minute burn of particular value as it was the shortest analyzed in this study. This must be held in consideration of the contamination of the photopeaks of Am242 and Am242m with similar energy photopeaks of Am241. As the magnitude of the amount of Am241 is not expected change to any great degree over the examined simulated irradiation times, buildup of the shorter lived Am242 is required to exceed the 102 and 118 combined photon rates emitted by the ever present Am241. To account for this, knowledge of the Am241's (a calibrated measured source/irradiation foil) activity at the time of a short irradiation (assumed to not change) could allow the count rate of these photopeaks to be known if detector efficiency is also known. These interfering count rates could be removed from the total Prospect derived count rates to determine the true rates from Am242/Am242m alone. The other choice is to irradiate until the photon rates from Am242 and Am242m exceed that of Am241. As no viable peaks of Am242m were found via the simulation, the analysis of the study primarily focuses upon the detection of Am242 through its 102 and 118 keV photopeaks. Given its 16 hour half-life, minimal buildup is required before its photon rate in the 102 and 118 keV energy regions exceed that of Am241. Irradiation time must be kept short in order to ensure the mentioned simplifications in the buildup differential equation remain true, and that the behavior is primarily linear from a given point in time when the amount of Am242 is non-existent.

Table 6.14. Case 2 Am242 peaks, no viable peaks of Am242m were detected, net cps and uncertainty values were obtained using Prospect peak setting 'continuum' value of .2 FWHM, similar to Mixed and Europium comparison tests. uncorrected Prospect analysis (unmodified BEGe 3825 model)

CASE 2 S1	Given Photon Rate uncertainty (%)	Weighted Centroid (keV)	MC NP Centroid (keV)	% Error	Given Photon/s rate	MC NP Net Count rate	Uncertainty (Prospect)	Uncertainty % Prospect)	FE PE (%)	Uncertainty %	Energy Integrated Am242 m/Am242 Production Ratio at irradiation time
	3.600	102.616 (Am242)	101.802	0.793	44.437	12.087	0.202	1.672	27.201	3.969	0.110
	3.600	118.247 (Am242)	118.752	0.427	12.098	1.605	0.917	57.141	13.265	57.255	
CASE 2 S2	Given Photon Rate uncertainty (%)	Weighted Centroid (keV)	MC NP Centroid (keV)	% Error	Given Photon/s rate	MC NP Net Count rate	Uncertainty (Prospect)	Uncertainty % Prospect)	FE PE (%)	Uncertainty %	Energy Integrated Am242 m/Am242 Production Ratio
	3.540	102.616 (Am242)	102.297	0.311	1253.329	245.910	0.940	0.382	19.621	3.561	0.109
	3.540	118.247 (Am242)	118.648	0.339	341.226	48.669	0.374	0.767*	14.263	3.622	

Table 6.14. Case 2 Am242 peaks, no viable peaks of Am242m were detected, net cps and uncertainty values were obtained using Prospect peak setting 'continuum' value of .2 FWHM, similar to Mixed and Europium comparison tests. uncorrected Prospect analysis (unmodified BEGe 3825 model), (cont.)

CASE	Given Photon Rate uncertainty (%)	Weighted Centroid (keV)	MCNP Centroid (keV)	% Error	Given Photon/s rate	MCNP Net Count rate	Uncertainty (Prospect)	Uncertainty % Prospect)	FEPE (%)	Uncertainty %	Energy Integrated Am242m/Am242 Production Ratio derived at irradiation time
S3	4.520	102.616 (Am242)	102.234	0.372	18596.990	3454.247	2.786	0.081	18.574	4.521	0.124
	4.520	118.247 (Am242)	118.582	0.283	5063.134	720.820	1.414	0.196*	14.237	4.524	

*no gross area was obtained by Prospect for these 118.247 keV peaks

The underestimation of the Am242 peak analysis through Prospect was obtained similar to Case 1, with the same scaling factor of 2 that was used to provide a corrected spectrum count for the Mixed and Europium standard tests. As with Case 1, the Energy integrated Am242m to Am242 production rate was taken for the specified irradiation location, due to the short irradiation time assumption, the 1 minute and 30 minute values are more valid than the 8 hour production ratio. Also similar to Case 1, due to the lack of a viable Am242m peak to analyze, the production ratios were taken directly from the activities determined by MCNPX for the given irradiation time. Production ratios for Am242m to Am242 were taken from the amount of respective atoms of Am242m and Am242 and divided by the irradiation time. In short irradiation times, scale of hours, this is valid, as the amount of Am241 initially in the sample, and thus the production rate far exceeds the rate Am242 and Am242m that could be destroyed by further activation or from decay.

Table 6.15. Case 2 corrected simulated BEGe 3825 response for Am242 102 and 118 keV peak analyses (modified BEGe 3825 model)

CASE 2 S1	Given Photon Rate uncertainty (%)	Weighted Centroid (keV)	MC NP Centroid (keV)	% Error	Given Photon/s rate	MC NP Net Count rate	Uncertainty (Prospect)	Uncertainty % Prospect)	FE PE (%)	Uncertainty %	Energy Integrated Am242m /Am242 Production Ratio derived at irradiation time
	3.600	102.616 (Am242)	101.810	0.785	44.437	6.104	0.140	2.294	13.736	4.269	0.110
	3.600	118.247 (Am242)	118.546	0.253	12.098	0.697	0.374	53.670	5.763	53.790	
CASE 2 S2	Given Photon Rate uncertainty (%)	Weighted Centroid (keV)	MC NP Centroid (keV)	% Error	Given Photon/s rate	MC NP Net Count rate	Uncertainty (Prospect)	Uncertainty % Prospect)	FE PE (%)	Uncertainty %	Energy Integrated Am242m /Am242 Production Ratio derived at irradiation time
	3.540	102.616 (Am242)	102.201	0.404	1253.329	117.286	0.518	0.441	9.358	3.567	0.109
	3.540	118.247 (Am242)	118.645	0.337	341.226	24.338	0.264	1.083*	7.133	3.702	0.109

Table 6.15. Case 2 corrected simulated BEGe 3825 response for Am242 102 and 118 keV peak analyses (modified BEGe 3825 model), (cont.)

CASE 2 S3	Given Photon Rate uncertainty (%)	Weighted Centroid (keV)	MC NP Centroid (keV)	% Error	Given Photon/s rate	MC NP Net Count rate	Uncertainty (Prospect)	Uncertainty % Prospect)	FE PE (%)	Uncertainty %	Energy Integrated Am242m /Am242 Production Ratio derived at irradiation time
	4.520	102.616 (Am242)	102.234	0.372	18596.990	1727.136	1.970	0.114	9.287	4.521	0.124
	4.520	118.247 (Am242)	118.581	0.282	5063.134	360.418	1.000	0.277*	7.118	4.529	

*no gross area was obtained by Prospect for these 118.247 keV peaks

To show that the 102 peak is more reliable than the 118 keV peak, for case 2 as it was shown for case 1, the Prospect analysis continuum estimate was again adjusted from its minimum of .01 FWHM to 2 FWHM in for each of the time cases for this the Am241 activity of 1 μ Ci, testing for the viability of both peaks and to determine which photopeak would offer a sufficiently well-defined peak that can be auto analyzed by Prospect repeatedly and not suffer contradiction with slight adjustments in the settings. A peak that has zero gross area will be considered suspect and not reliable, regardless of the existence of its net peak area. Tables 6.16 and 6.17 give the viability of Am242's 102 and 118 keV photopeaks when analyzed by the Prospect software. Similar to case 1, Am242's 102 keV peak was superior to its 118 keV peak. In order to minimize counting time, the 102 keV peak should alone be utilized to quantify Am242, with the 118 keV peak being used to provide a general indicator that Am242 exists. Also similar to Case 1, no peaks of Am242m, such as its gamma, 86 keV, could be found. Based upon these simulations it is

not deemed feasible that Am242m could be measured or identified with the BEGe 3825 that exists on campus in the reactor bay.

Table 6.16. Outcome of Prospect peak analysis when the setting ‘continuum estimate’ is increased by .2 FWHM for 11 runs for Case 2, uncorrected (unmodified model F8 tally)

	S1 viability fraction (out of 11 runs)	S2 viability fraction (out of 11 runs)	S3 viability fraction (out of 11 runs)
102.616	11/11	11/11	11/11
118.247	2/11	0/11	0/11

Table 6.17. Outcome of Prospect peak analysis when the setting 'continuum estimate' is increased by .2 FWHM for 11 runs for Case 2, corrected (modified model F8 tally)

	S1 viability fraction (out of 11 runs)	S2 viability fraction (out of 11 runs)	S3 viability fraction (out of 11 runs)
102.616	11/11	11/11	11/11
118.247	3/11	0/11	0/11

For the uncorrected Case 2 (unmodified model) and the corrected Case 2 (modified model), Prospect analysis of the 102 and 118 peaks from Am242 predicted the general viability of the 102 peak over the 118 peak, regardless of irradiation time. Since the 118.247 keV photopeak from Am242 is close to the dominant 102.616 keV photopeak also from Am242, it is observed that for an irradiation of 1, 30 and 480 minutes at 200 kW, the automated Prospect peak finder software predicts that both the corrected and uncorrected peak (118.247) to be non-viable via Prospect (0 gross peak

Table 6.18. Compiles photon rate of Am242 to Am241 for Case 2 burn data in the energy regions of interest, (cont.)

99.979	17.186	484.719	7192.29 9	97.498	0.405	0.405	0.405
104.279	27.251	768.610	11404.6 9	98.970	7.509	7.509	7.509
116.802	3.160	89.130	1322.51 6	101.574	0.669	0.669	0.669
117.372	6.199	174.849	2594.42 0	102.980	7.214	7.214	7.213
118.372	0.116	3.266	48.457	113.834	0.080	0.080	0.080
118.573	0.130	3.677	54.552	114.778	0.157	0.157	0.157
120.979	0.796	22.454	333.173	115.341	0.003	0.003	0.003
121.244	1.623	45.769	679.121	115.532	0.003	0.003	0.003
121.507	0.035	0.977	14.504	117.880	0.020	0.020	0.020
121.550	0.039	1.105	16.390	118.120	0.041	0.041	0.041
X	X	X	X	118.380	0.001	0.001	0.001
X	X	X	X	118.430	0.001	0.001	0.001
X	X	X	X	120.360	0.002	0.002	0.002
X	X	X	X	123.050	0.370	0.370	0.370
X	X	X	X	125.300	1.509	1.509	1.509

Table 6.19 gives the combined contamination rates of Am241 in Am242's two dominant photopeaks for the case 2 initial Am241 activity. As expected, its fraction of the Am242 photon rate is very similar to case 1, as the magnitudes of the photon rates are the only change between the two activity cases. Based upon these results, irradiations greater than 30 minutes are recommended to avoid contamination of Am242 with

Am241. Irradiation times on the scale of days should be avoided to ensure that the production term of Am242/Am242m outpaces the destruction terms (decay and absorption) as it builds up in the sample during neutron interaction.

Table 6.19. Compares photon rates in energy ranges 99-105 and 113-124 for photopeaks of Am241 to generated photon rates of Am242 at the given burn times for Case 2, to show that small times Am241 contaminates the energy regions of interest for Am242

Rate Sum	S1		S2		S3	
	99-105	113-124	99-105	113-124	99-105	113-124
Am242	44.43684	12.098176	1253.3287	341.2257	18596.989	5063.13347
Am241	15.797114	2.186669	15.797114	2.186669	15.795534	2.186451
A241 Rate sum Percentage of Am242 Rate sum (%)	35.54958903	18.07436923	1.260412691	0.640827757	0.084935975	0.043183752

No viable peaks from Am242m (86 keV) were detected or reliably attributed for any of the times with a 200 kW burn, indicating that Spectroscopy is not a feasible tool to determine Am242m activities in an irradiated sample of Am241, regardless of Prospect peak sensitivity settings, which had no effect upon the Am241/Am242m dominated spectrum. Since no viable peaks for Am242m, an 86 keV peak was of interest, its photon rate analysis and comparison will be omitted for both Case 1 and Case 2.

As with Case 1, the time frame chosen for irradiation, up to 8 hours, is expected to allow for a linear Am242 and Am242m activity buildup to occur, regardless of the inability to measure the Am242m photon emission via the BEGe model, and thus the physical detector, knowledge of the neutron energy group makeup would allow an estimation of the Am242m to Am242 Production ratio. Using this ratio, an estimate of the Am242m activity could be made once the Am242 was counted, and its activity derived to its value at the end of its irradiation period. The $\sim .10$ Energy integrated Am242m/Am242 production ratio was expected, as the Am241 to Am242 branch fraction dominates at $\sim 90\%$ at thermal values, which describes a dominant fraction of the MSTR neutron energy groups. All Weapons/Reactor grade plutonium Am241 buildup and Am242/Am242m that utilized the BEGe 3825 model via the F8 tally had their tally check bin pass the 10 statistical checks. The FOM and runtime for each F8 tally has been omitted.

7. CONCLUSIONS/LIMITATIONS

The primary goal of the project was to investigate feasibility of using Americium isotope's buildup to ascertain the age of Pu in MOX fuel for special material accounting and control. The first phase of the project focused on detectability of the low energy 59.35 keV gamma peak emitted directly by Am241. Since no Am241 source was available at the time of this study a mixed source and an Eu source was used to collect expected data at the from the actual physical source and compare it to a detailed MCNP model for the BEGe3825 detector based on manufacturer's (Canberra) description of the detector assembly. The purpose of this effort was to validate our MCNP model for the BEGe3825 detector. Subsequent analyses were based on the validated MCNP model only. Photon/Electron interaction models were investigated for BEGe 3825 simulation. In the final analysis, electron behavior in Ge crystal mass made little to no tangible contribution in Full Energy Peak Efficiency (FEPE) ratio with test sources but the runtime could be decreased from ~340 minutes to ~20 minutes by ignoring electron transport model. Therefore, this simplification was used for the entire analysis.

Source to Window distance tests revealed that the model results were most sensitive to this parameter for deviation from FEPE ratio unity, also impacted FEPE spread from average as well. Uncertainties in the net count rate, simulated and measured are expected to cause deviation from FEPE ratio average for each test case. At a positions closer to Ge mass, count rate and thus uncertainty is expected to improve, which was seen as decreasing the spread for the mixed and europium test cases when taken to extremely close values. Due to comparison with the physical measurements done at the 10 minute live time, the improvement in the spread for the europium case was noticeable when testing impact of source positions on deviation from unity (as seen in charts and error bar ranges).

The assumption was made that initially pure Pu239 (without any Americium buildup) was produced and stored for a period of time before reusing the material for the production of MOX fuel. All the analysis is targeted towards monitoring and control during reprocessing before irradiation of the MOX in the reactor. The source of Plutonium tested for the analysis was the weapon grade and the reactor grade as described by (Travers, 1999). The purpose of this validation of the age is to confirm the

declared age of the material by the source/supplier. Feasibility of detection at MSTR with all other peaks from the fission and capture products after operating at 200 kW was also examined.

To account for the general FEPE ratio discrepancy from unity (assumed to be caused by geometrical errors, ignoring potential spread contribution), a corrected spectrum was attained by scaling the F8 tally by a factor of 2 to generate a forced underestimated count spectrum. It is assumed that this higher and lower count window will be maintained for future physical samples measured with the same level of precision as was done for the validation phase (source-window distance). The average FEPE ratio value (ignoring individual uncertainty) for mixed photopeaks was 1.415 ± 1084 , and for the corrected Europium Source the corrected average FEPE ratio value for all peaks was 1.578 ± 4236 , at $k=2$.

Investigation into Plutonium age estimation utilized a forward Euler scheme involving 12 actinides, all of the specified plutonium isotopes and their respective decay products, with some secondary decay products. Further expansion of secondary and tertiary decay products was deemed not necessary due to primary decay products having half-lives around $10E5$ to $10E7$ years. Short lived secondary isotopes such as Pa233 (27 days) and Th231 (1 day) were forced into a secular equilibrium with their respective parent resulting in a highly negligible activity (and photon rates) compared to Pu241 and Am241.

For the analysis of Am241 in typical weapons grade and reactor grade plutonium, the BEGe model produced viable tally results when examining the Am241 peak of 59.50 keV, in a initially pure minimum mass test case of $5E-7$ g of RG and WG plutonium on a 5X5 cm foil. For the time estimate range, as determined by the Newton-Raphson method, uncertainty in the net count rate for the 59.50 keV peak is the primary cause of the quality of the precision in the age estimate range.

For the decay time cases of 1, 5, and 19 years, each with a respective 0.5, 1, 1.5 and 2 year time between the 1 hour measurement periods, the corrected WG suffered a net cps ratio uncertainty of (max, min) (7.2%, 1.314%), while a slight improvement was observed for the uncorrected WG time cases (max, min) (4.250%, 0.933%) due to the uncorrected spectrum providing an overestimation. The BEGe 3825 model that exists on

campus is expected to give high precision sample age estimates up to 19 years, it is expected that if uncertainty in the count is managed, the upper age limit can be increased indefinitely, along with the correct time span in the measurement.

The Newton-Raphson method can converge for the unknown age value when the net cps ratio is less than or equal to 1, the sample's Am241 production rate must exceed its destruction rate relative to a given measurement interval (dependent upon isotopes half-lives, ratio less than 1) and it can also converge if the ratio exceeds 1 (for the examined time spans) if the time span is great enough. Eventually as the ratio increases for the examined time spans the method diverges to infinity and does not yield a viable/correct solution, depending upon the magnitude of the time span utilized. If the time span between measurements is too small for a given net count ratio, then the maximum available age estimate for the sample age will also be small. Time spans on the order of decades to centuries allows the method to converge if given a ratio greatly exceeding 1. It is assumed that due to the limitation of the spacing of the test ratios, (not Prospect related count ratios) and the behavior of larger time spans on the order of years, that fraction of a year time spans can converge beyond the ratio=1 value by some minuscule amount as well, but this matter was not explored in this study. Using the time spans examined in this study, gives a range of ages $< \sim 70$ years if ratio is kept less than or equal to 1, but can proceed to ~ 300 years (order of centuries) in the case of the 2 year (on the order of years) time span given the test ratio step sizes (very sensitive to ratio). It is noted that these age estimate range values are obtained by using the time spans described in this study, i.e., less than 2 but greater than .5 year measurement spans. Different time spans, larger or smaller will cause different behavior, and the study makes no claim to the validity of one span over the other beyond those examined (.5, 1, 1.5 and 2) for the age test values. Too small of a time span limits the age estimate upper value. This study only examines the .5, 1, 1.5 and 2 year spans for a sample up 19 years, with a general age value of 72 years when the ratio=1 (arbitrary milestone, actual age value when ratio equals 1 depends on time span). For ratio values greater than 1, the upper age limit continues, increasing for increasing time spans. Maximum ratio that could be used by procedure used in study before divergence was ~ 1.003 at about 300 years for a sample age for the 2 year span between measurements scenario and given the spacing in test ratio values as described in

Appendix A for the Newton-Raphson scheme, noted sensitivity to ratio values means that any upper age limit for a time span before the sample diverges should be seen as a general approximate value, a true age estimate would use count data and the general knowledge that the sample plutonium was most likely generated at some time after 1940.

As expected, due to increased amounts of Am241 for a given decay time, the reactor grade uncorrected and corrected maximum and minimum net cps ratio uncertainties are (0.723%, 0.212%) and (1.022%, 0.300%), respectively.

The age estimate range could also be improved by increasing the counting time (increased from 1 hour to 10 days), this was applied to the WG, 19 years decay, which was the most affected case that this study examined. When the simulated counting time was increased, the corrected WG 19 year decay case, improved its net cps ratio uncertainty (considering all spans within the 19 year case) to (max,min) (0.090%,0.089%) and thus it's time estimate range precision, for the 0.5 year span, (most affected case) to $18.2 < T < 19.63$, compared to previously $12.04 < T < 43.65$. This increase in precision due to increasing the counting time is expected for all other decay times and time spans.

For the purpose of investigating possible irradiation times for a given initial Am241 activity, the expected 5x5x.0005 cm foil was simulated to be about 1 cm above the end-cap carbon window, based on the desire to not contaminate the protective detector surface when doing a future physical experiment, and is expected to provide the test case to determine viable irradiation times and initial Am241 activities. For both the exempt (.05 μ Ci) and non-exempt (1 μ Ci) case of initial Am241, the BEGe 3825 model examined the resultant simulated isotope complete photon (gamma/x-ray) loading obtained from the irradiation simulation performed with the MSTR model through MCNPX. No viable peaks from Am242m were determined or attributed to Am242m, there were two peaks from Am242, the summed 102.616 and 118.247 keV peaks that were present and whose photon rates were several orders of magnitude greater than non Am241 peaks of similar energies. A potential method to counteract the inability to directly measure Am242m would be to use the fact that around 99.541% of Am242m undergoes the isomeric transition to Am242, allowing the sample to decay (for the immediately generated amount of Am242 to die off, secular equilibrium of Am242

resulting from the decay of the invisible Am^{242m} (to gamma spectroscopy) would allow knowledge of the Am^{242m} activity to be known, if the Am²⁴² created from the Am^{242m} decay builds up to such a measurable degree. Immediate measurement of the Am²⁴²'s 102 keV photopeak (Am²⁴² activity) and later measurement of Am²⁴² once secular equilibrium has been obtained, would allow the production ratio of Am^{242m}/Am²⁴² to be known for short irradiation times and if the decay time of the activated sample is not too long relative to Am^{242m}'s half-life.

Corrected BEGe 3825 model results with Prospect derived Am²⁴² 102.616 net cps uncertainty values of 46.871%, 2.535% and .5323% for the 1, 30, and 480 minute irradiation at 200 kW in the source holder tube, with the exempt quantity of Am²⁴¹. Am²⁴² 118.247 peak proved to be unreliable in nearly all setting tests. Am^{242m} photon peaks could not be detected with the BEGe 3825 model. For the non-exempt 1 μ Ci of Am²⁴¹, the corrected model results gave a Prospect derived net cps uncertainty of 2.294%, 0.4415% and 0.1140% for the 1,30,480 minute irradiation at 200 kW in the source holder tube, centered, z midplane. 1 minute irradiations, suffered from Am²⁴¹ contamination in the 102 and 118 energy regions, at ~35% of Am²⁴² respective photon rate for both Am²⁴¹ activity cases. At 30 minutes and then at 8 hours, this fraction became negligible, ~0.085% (8 hours).

APPENDIX A
SIMULATION CODES AND SCHEMES

General form of the MCNP code used to approximate the MSTR used in this study, multiple variations and additions were used for specific purposes:

PROJECT MSTR_APPROXIMATE

C

1 1 -3.871703458 1 -2 5 -6 9 -10 8 u=1 vol=25.88063 imp:n=1 \$fuel meat U3Si2-Al fuel plate

2 2 -2.7 3 -1 5 -6 9 -10 8 u=1 imp:n=1 \$fuel cladding no overlap on edges Al 6061

3 2 -2.7 2 -4 5 -6 9 -10 8 u=1 imp:n=1 \$fuel cladding other side .038cm thick

264 2 -2.7 201 -3 5 -6 9 -10 8 u=1 vol=32.559 imp:n=1

C 4 4 -1.0 4 -12 5 -6 9 -10 8 u=1 vol=25.88063 imp:n=1 \$water gap .315

4 like 1 but trcl (0 .445 0) u=1 vol=25.88063 imp:n=1 \$fp2 fuel meat

5 like 2 but trcl (0 .445 0) u=1 imp:n=1 \$fp2 bottom cladding

6 like 3 but trcl (0 .445 0) u=1 imp:n=1 \$fp2 top cladd

C 8 like 4 but trcl (0 .445 0) imp:n=1 \$fp2 water gap

7 like 1 but trcl (0 .89 0) u=1 vol=25.88063 imp:n=1 \$fp3 fuel meat

8 like 2 but trcl (0 .89 0) u=1 imp:n=1 \$fp3 bottom cladd

9 like 3 but trcl (0 .89 0) u=1 imp:n=1 \$fp3 top cladd

C 12 like 4 but trcl (0 .89 0) imp:n=1 \$fp3 water gap

10 like 1 but trcl (0 1.335 0) u=1 vol=25.88063 imp:n=1 \$fp4 fuel meat

11 like 2 but trcl (0 1.335 0) u=1 imp:n=1 \$fp4 bottom cladd

12 like 3 but trcl (0 1.335 0) u=1 imp:n=1 \$fp4 top cladd

C 16 like 4 but trcl (0 1.335 0) imp:n=1 \$fp4 water gap

13 like 1 but trcl (0 1.78 0) u=1 vol=25.88063 imp:n=1 \$fp5 fuel meat

14 like 2 but trcl (0 1.78 0) u=1 imp:n=1 \$fp5 bottom cladd

15 like 3 but trcl (0 1.78 0) u=1 imp:n=1 \$fp5 top cladd

C 20 like 4 but trcl (0 1.78 0) imp:n=1 \$fp5 water gap

16 like 1 but trcl (0 2.225 0) u=1 vol=25.88063 imp:n=1 \$fp6 fuel meat

17 like 2 but trcl (0 2.225 0) u=1 imp:n=1 \$fp6 bottom cladd

18 like 3 but trcl (0 2.225 0) u=1 imp:n=1 \$fp6 top cladd

C

19 like 1 but trcl (0 2.67 0) u=1 vol=25.88063 imp:n=1 \$fp7 fuel meat

20 like 2 but trcl (0 2.67 0) u=1 imp:n=1 \$fp7 bottom cladd

21 like 3 but trcl (0 2.67 0) u=1 imp:n=1 \$fp7 top cladd

C

22 like 1 but trcl (0 3.115 0) u=1 vol=25.88063 imp:n=1 \$fp8 fuel meat

23 like 2 but trcl (0 3.115 0) u=1 imp:n=1 \$fp8 bottom cladd

24 like 3 but trcl (0 3.115 0) u=1 imp:n=1 \$fp8 top cladd

C

25 like 1 but trcl (0 3.56 0) u=1 vol=25.88063 imp:n=1 \$fp9 fuel meat

26 like 2 but trcl (0 3.56 0) u=1 imp:n=1 \$fp9 bottom cladd

27 like 3 but trcl (0 3.56 0) u=1 imp:n=1 \$fp9 top cladd

C

28 like 1 but trcl (0 4.005 0) u=1 vol=25.88063 imp:n=1 \$fp10 fuel meat

29 like 2 but trcl (0 4.005 0) u=1 imp:n=1 \$fp10 bottom cladd

30 like 3 but trcl (0 4.005 0) u=1 imp:n=1 \$fp10 top cladd

C

31 like 1 but trcl (0 4.45 0) u=1 vol=25.88063 imp:n=1 \$fp11 fuel meat

32 like 2 but trcl (0 4.45 0) u=1 imp:n=1 \$fp11 bottom cladd

33 like 3 but trcl (0 4.45 0) u=1 imp:n=1 \$fp11 top cladd

C

34 like 1 but trcl (0 4.895 0) u=1 vol=25.88063 imp:n=1 \$fp12 fuel meat

35 like 2 but trcl (0 4.895 0) u=1 imp:n=1 \$fp12 bottom cladd

36 like 3 but trcl (0 4.895 0) u=1 imp:n=1 \$fp12 top cladd

C

37 like 1 but trcl (0 5.34 0) u=1 vol=25.88063 imp:n=1 \$fp13 fuel meat

38 like 2 but trcl (0 5.34 0) u=1 imp:n=1 \$fp13 bottom cladd

39 like 3 but trcl (0 5.34 0) u=1 imp:n=1 \$fp13 top cladd

C

40 like 1 but trcl (0 5.785 0) u=1 vol=25.88063 imp:n=1 \$fp14 fuel meat

41 like 2 but trcl (0 5.785 0) u=1 imp:n=1 \$fp14 bottom cladd

42 like 3 but trcl (0 5.785 0) u=1 imp:n=1 \$fp14 top cladd

C

43 like 1 but trcl (0 6.23 0) u=1 vol=25.88063 imp:n=1 \$fp15 fuel meat

44 like 2 but trcl (0 6.23 0) u=1 imp:n=1 \$fp15 bottom cladd

45 like 3 but trcl (0 6.23 0) u=1 imp:n=1 \$fp15 top cladd

C

46 like 1 but trcl (0 6.675 0) u=1 vol=25.88063 imp:n=1 \$fp16 fuel meat

47 like 2 but trcl (0 6.675 0) u=1 imp:n=1 \$fp16 bottom cladd

48 like 3 but trcl (0 6.675 0) u=1 imp:n=1 \$fp16 top cladd

C

49 like 1 but trcl (0 7.12 0) u=1 vol=25.88063 imp:n=1 \$fp17 fuel meat

50 like 2 but trcl (0 7.12 0) u=1 imp:n=1 \$fp17 bottom cladd

51 like 3 but trcl (0 7.12 0) u=1 imp:n=1 \$fp17 top cladd

C

52 like 1 but trcl (0 7.565 0) u=1 vol=25.88063 imp:n=1 \$fp18 fuel meat

53 like 2 but trcl (0 7.565 0) u=1 imp:n=1 \$fp18 bottom cladd

54 like 3 but trcl (0 7.565 0) u=1 imp:n=1 \$fp18 top cladd

C

55 2 -2.7 -5 52 8 -11 9 -10 u=1 vol=176.1557 imp:n=1 \$left alum side plate

56 2 -2.7 6 -51 8 -11 9 -10 u=1 vol=176.1557 imp:n=1 \$right alum side plate

57 4 -1 #1 #2 #3 #4 #5 #6 #7 #8 #9 #10 #11 #12 & \$fills in .315 cm gaps between plates
with water, as well as any geometry flaws

#13 #14 #15 #16 #17 #18 #19 #20 #21 #22 #23 &

#24 #25 #26 #27 #28 #29 #30 #31 #32 #33 #34 &

#35 #36 #37 #38 #39 #40 #41 #42 #43 #44 #45 &

#46 #47 #48 #49 #50 #51 #52 #53 #54 #55 #56 &

#264 52 -51 9 -10 8 -14 u=1 imp:n=1

58 4 -1 -52:51:-9:10:-8:14 u=1 imp:n=1 \$infinite cell of water, to fill a universe

C control rod universe need to change cell numbers-----

59 1 -3.871703458 1 -2 5 -6 9 -10 8 u=2 vol=25.88063 imp:n=1 \$fuel meat U3Si2-Al

60 2 -2.7 3 -1 5 -6 9 -10 8 u=2 imp:n=1 \$fuel cladding no overlap on edges Al 6061

61 2 -2.7 2 -4 5 -6 9 -10 8 u=2 imp:n=1 \$fuel cladding other side .038cm thick

265 2 -2.7 201 -3 5 -6 9 -10 8 u=2 imp:n=1

62 like 59 but trcl (0 .445 0) u=2 vol=25.88063 imp:n=1 \$fp2 fuel meat

63 like 60 but trcl (0 .445 0) u=2 imp:n=1 \$fp2 bottom cladding

64 like 61 but trcl (0 .445 0) u=2 imp:n=1 \$fp2 top cladd

65 like 59 but trcl (0 .89 0) u=2 vol=25.88063 imp:n=1 \$fp3 fuel meat

66 like 60 but trcl (0 .89 0) u=2 imp:n=1 \$fp3 bottom cladd

67 like 61 but trcl (0 .89 0) u=2 imp:n=1 \$fp3 top cladd

68 like 59 but trcl (0 1.335 0) u=2 vol=25.88063 imp:n=1 \$fp4 fuel meat

69 like 60 but trcl (0 1.335 0) u=2 imp:n=1 \$fp4 bottom cladd

70 like 61 but trcl (0 1.335 0) u=2 imp:n=1 \$fp4 top cladd

71 like 59 but trcl (0 1.78 0) u=2 vol=25.88063 imp:n=1 \$fp5 fuel meat

72 like 60 but trcl (0 1.78 0) u=2 imp:n=1 \$fp5 bottom cladd

73 like 61 but trcl (0 1.78 0) u=2 imp:n=1 \$fp5 top cladd

74 4 -1 41 -42 -49 25 63 -159:-33 63 -159 u=2 vol=31.96578 imp:n=1 \$a groove \$63 cr removed, 9 cr inserted

75 4 -1 43 -44 -49 25 63 -159:-34 63 -159 u=2 vol=31.96578 imp:n=1 \$b groove

76 4 -1 43 -44 50 -24 63 -159:-35 63 -159 u=2 vol=31.96578 imp:n=1 \$c groove

77 4 -1 41 -42 50 -24 63 -159:-36 63 -159 u=2 vol=31.96578 imp:n=1 \$d groove

78 4 -1 46 -45 50 -24 63 -159:-37 63 -159 u=2 vol=31.96578 imp:n=1 \$e groove

79 4 -1 48 -47 50 -24 63 -159:-38 63 -159 u=2 vol=31.96578 imp:n=1 \$f groove

80 4 -1 48 -47 25 -49 63 -159:-39 63 -159 u=2 vol=31.96578 imp:n=1 \$g groove

81 4 -1 46 -45 25 -49 63 -159:-40 63 -159 u=2 vol=31.96578 imp:n=1 \$h groove

82 2 -2.7 (-16 17 21 -23 9 -159):(18 -19 21 -23 9 -159) & \$guide tube cell

:(-22 23 18 -16 9 -159):(20 -21 -16 18 9 -159) &

u=2 vol=316.6029729 imp:n=1

83 like 59 but trcl (0 5.785 0) u=2 vol=25.88063 imp:n=1 \$fp14 fuel meat

84 like 60 but trcl (0 5.785 0) u=2 imp:n=1 \$fp14 bottom cladd

85 like 61 but trcl (0 5.785 0) u=2 imp:n=1 \$fp14 top cladd

C

86 like 59 but trcl (0 6.23 0) u=2 vol=25.88063 imp:n=1 \$fp15 fuel meat

87 like 60 but trcl (0 6.23 0) u=2 imp:n=1 \$fp15 bottom cladd

88 like 61 but trcl (0 6.23 0) u=2 imp:n=1 \$fp15 top cladd

C

89 like 59 but trcl (0 6.675 0) u=2 vol=25.88063 imp:n=1 \$fp16 fuel meat

90 like 60 but trcl (0 6.675 0) u=2 imp:n=1 \$fp16 bottom cladd

91 like 61 but trcl (0 6.675 0) u=2 imp:n=1 \$fp16 top cladd

C

92 like 59 but trcl (0 7.12 0) u=2 vol=25.88063 imp:n=1 \$fp17 fuel meat

93 like 60 but trcl (0 7.12 0) u=2 imp:n=1 \$fp17 bottom cladd

94 like 61 but trcl (0 7.12 0) u=2 imp:n=1 \$fp17 top cladd

C

95 like 59 but trcl (0 7.565 0) u=2 vol=25.88063 imp:n=1 \$fp18 fuel meat

96 like 60 but trcl (0 7.565 0) u=2 imp:n=1 \$fp18 bottom cladd

97 like 61 but trcl (0 7.565 0) u=2 imp:n=1 \$fp18 top cladd

98 3 -8.68 (-26 -24 25 63 -159:26 27 -24 25 63 & \$control rod-----

-159 -31 32:-27 -24 25 63 -159) &

(#74 #75 #76 #77 #78 #79 #80 #81) u=2 imp:n=1

99 2 -2.7 -5 52 8 -11 9 -10 u=2 vol=176.1557 imp:n=1 \$left alum side plate

100 2 -2.7 6 -51 8 -11 9 -10 u=2 vol=176.1557 imp:n=1 \$right alum side plate

101 4 -1 #59 #60 #61 #62 #63 #64 #65 #66 #67 &

#68 #69 #70 #71 #72 #73 #74 #75 #76 #77 #78 #79 #80 #81 &

#82 #83 #84 #85 #86 &

#87 #88 #89 #90 &

#91 #92 #93 #94 #95 #96 #97 #98 #99 #100 &

#265 52 -51 9 -200 8 -14 u=2 imp:n=1

102 4 -1 -52:51:-9:200:-8:14 u=2 imp:n=1

C Regulating rod universe need to change cell numbers-----

103 1 -3.871703458 1 -2 5 -6 9 -10 8 u=8 vol=25.88063 imp:n=1 \$fuel meat U3Si2-Al

104 2 -2.7 3 -1 5 -6 9 -10 8 u=8 imp:n=1 \$fuel cladding no overlap on edges Al 6061

105 2 -2.7 2 -4 5 -6 9 -10 8 u=8 imp:n=1 \$fuel cladding other side .038cm thick

266 2 -2.7 201 -3 5 -6 9 -10 8 u=8 vol=32.559 imp:n=1

106 like 103 but trcl (0 .445 0) u=8 vol=25.88063 imp:n=1 \$fp2 fuel meat

107 like 104 but trcl (0 .445 0) u=8 imp:n=1 \$fp2 bottom cladding

108 like 105 but trcl (0 .445 0) u=8 imp:n=1 \$fp2 top cladd

109 like 103 but trcl (0 .89 0) u=8 vol=25.88063 imp:n=1 \$fp3 fuel meat

110 like 104 but trcl (0 .89 0) u=8 imp:n=1 \$fp3 bottom cladd

111 like 105 but trcl (0 .89 0) u=8 imp:n=1 \$fp3 top cladd

112 like 103 but trcl (0 1.335 0) u=8 vol=25.88063 imp:n=1 \$fp4 fuel meat

113 like 104 but trcl (0 1.335 0) u=8 imp:n=1 \$fp4 bottom cladd

114 like 105 but trcl (0 1.335 0) u=8 imp:n=1 \$fp4 top cladd

115 like 103 but trcl (0 1.78 0) u=8 vol=25.88063 imp:n=1 \$fp5 fuel meat

116 like 104 but trcl (0 1.78 0) u=8 imp:n=1 \$fp5 bottom cladd

117 like 105 but trcl (0 1.78 0) u=8 imp:n=1 \$fp5 top cladd

118 2 -2.7 (-16 17 21 -23 9 -159):(18 -19 21 -23 9 -159) & \$guide tube cell

:(-22 23 18 -16 9 -159):(20 -21 -16 18 9 -159) &

u=8 vol=316.6029729 imp:n=1

119 5 -8.68 (129 -159 71 -70 74 -75):(129 -159 70 77 -76) &

:(129 -159 71 -70 72 -73):(129 -159 -71 79 -78) u=8 vol=138.9598 imp:n=1 \$reg rod,
hollow oval like construct

120 like 103 but trcl (0 5.785 0) u=8 vol=25.88063 imp:n=1 \$fp14 fuel meat

121 like 104 but trcl (0 5.785 0) u=8 imp:n=1 \$fp14 bottom cladd

122 like 105 but trcl (0 5.785 0) u=8 imp:n=1 \$fp14 top cladd

C

123 like 103 but trcl (0 6.23 0) u=8 vol=25.88063 imp:n=1 \$fp15 fuel meat

124 like 104 but trcl (0 6.23 0) u=8 imp:n=1 \$fp15 bottom cladd

125 like 105 but trcl (0 6.23 0) u=8 imp:n=1 \$fp15 top cladd

C

126 like 103 but trcl (0 6.675 0) u=8 vol=25.88063 imp:n=1 \$fp16 fuel meat

127 like 104 but trcl (0 6.675 0) u=8 imp:n=1 \$fp16 bottom cladd

128 like 105 but trcl (0 6.675 0) u=8 imp:n=1 \$fp16 top cladd

C

129 like 103 but trcl (0 7.12 0) u=8 vol=25.88063 imp:n=1 \$fp17 fuel meat

130 like 104 but trcl (0 7.12 0) u=8 imp:n=1 \$fp17 bottom cladd

131 like 105 but trcl (0 7.12 0) u=8 imp:n=1 \$fp17 top cladd

C

132 like 103 but trcl (0 7.565 0) u=8 vol=25.88063 imp:n=1 \$fp18 fuel meat

133 like 104 but trcl (0 7.565 0) u=8 imp:n=1 \$fp18 bottom cladd

134 like 105 but trcl (0 7.565 0) u=8 imp:n=1 \$fp18 top cladd

135 2 -2.7 -5 52 8 -11 9 -10 u=8 vol=176.1557 imp:n=1 \$left alum side plate

136 2 -2.7 6 -51 8 -11 9 -10 u=8 vol=176.1557 imp:n=1 \$right alum side plate

137 4 -1 #103 #104 #105 #106 #107 #108 #109 #110 #111 &

#112 #113 #114 #115 #116 #117 #118 #119 #120 #121 #122 #123 #124 #125 &

#126 #127 #128 #129 #130 &

#131 #132 #133 #134 &

#135 #136 #266 &

52 -51 9 -200 8 -14 u=8 imp:n=1 \$to fill any non-material gaps with water

138 4 -1 -52:51:-9:200:-8:14 u=8 imp:n=1

C end of reg rod universe designation

C building the bare rabbit tube with sample

139 5 -8.68 81 -80 9 -10 u=11 vol=.01 imp:n=1 \$ bare rabit tube cylinder1

140 5 -8.68 -82 83 9 -10 u=11 vol=.001 imp:n=1 \$pressure tube for bare rabbit tube

141 36 -11.68 119 -120 -123 u=11 imp:n=1 \$beta sample actual

142 2 -2.7 -120 121 -124 #141 u=11 imp:n=1 \$beta sample cylinder A

143 2 -2.7 122 -121 -125 u=11 imp:n=1 \$beta sample cylinder B

144 6 -.001251 -81 9 -10 #141 #142 #143 u=11 imp:n=1 \$Nitrogen transport medium

145 6 -.001251 -83 9 -10 u=11 imp:n=1 \$Nitrogen transport medium

146 4 -1 #139 #140 #141 #142 #143 #144 #145 u=11 imp:n=1 \$everything not in tubes is water

C building the cadmium lined rabbit tube with sample

147 5 -8.68 81 -80 9 -10 u=12 vol=.01 imp:n=1 \$ bare rabbit tube cylinder1

148 36 -11.68 119 -120 -123 u=12 imp:n=1 \$beta sample actual

149 5 -8.68 -82 83 9 -10 u=12 vol=.001 imp:n=1 \$pressure tube for bare rabbit tube

150 6 -.001251 -83 9 -10 u=12 imp:n=1 \$Nitrogen transport medium

151 7 -8.65 -84 80 9 -10 u=12 imp:n=1 \$cadmium layer for cylinder 1

152 7 -8.65 -85 82 9 -10 u=12 imp:n=1 \$cadmium layer for pressure tube

153 2 -2.7 -120 121 -124 #148 u=12 imp:n=1 \$beta sample cylinder A

154 2 -2.7 122 -121 -125 u=12 imp:n=1 \$beta sample cylinder B

155 6 -.001251 -81 9 -10 #148 #153 #154 u=12 imp:n=1 \$Nitrogen transport medium

156 4 -1 #147 #148 #149 #150 #151 #152 #153 #154 #155 u=12 imp:n=1 \$ everything
not in tubes is water

C compilation of universes

157 4 -1 52 -51 9 -159 8 -14 u=3 imp:n=1 \$water universe

158 4 -1 -52:51:-9:159:-8:14 u=3 imp:n=1 \$water universe

159 4 -1 -61 9 -159 u=5 imp:n=1 \$target material

160 4 -1 61:-9:159 u=5 imp:n=1 \$targets infinite water medium

C building the aluminum void tube filled with air and target material (soon)

161 2 -2.7 (86 -62 89 -87):(-62 87 -88):(-62 9 -89) u=6 vol=365.1787 &

imp:n=1 \$void tube filled with air, needed for 'void' sample irradiation

162 9 -12 -90 89 -87 u=6 vol=0.0169646 imp:n=1 \$T-1

163 10 -12 -91 89 -87 u=6 vol=0.0169646 imp:n=1 \$T-2
164 11 -12 -92 89 -87 u=6 vol=0.0169646 imp:n=1 \$T-3
165 12 -12 -93 89 -87 u=6 vol=0.0169646 imp:n=1 \$T-4
166 13 -12 -94 89 -87 u=6 vol=0.0169646 imp:n=1 \$T-5
167 14 -12 -95 89 -87 u=6 vol=0.0169646 imp:n=1 \$T-6
168 15 -12 -96 89 -87 u=6 vol=0.0169646 imp:n=1 \$T-7
169 16 -12 -97 89 -87 u=6 vol=0.0169646 imp:n=1 \$T-8
170 17 -10.3115 -98 89 -87 u=6 vol=0.0169646 imp:n=1 \$T-9
171 18 -12 -99 89 -87 u=6 vol=0.0169646 imp:n=1 \$T-10
172 19 -12 -100 89 -87 u=6 vol=0.0169646 imp:n=1 \$T-11
173 20 -12 -101 89 -87 u=6 vol=0.0169646 imp:n=1 \$T-12
174 21 -12 -102 89 -87 u=6 vol=0.0169646 imp:n=1 \$T-13
175 22 -10.31659 -103 89 -87 u=6 vol=0.0169646 imp:n=1 \$T-14
176 23 -12 -104 89 -87 u=6 vol=0.0169646 imp:n=1 \$T-15
177 24 -12 -105 89 -87 u=6 vol=0.0169646 imp:n=1 \$T-16
178 25 -12 -106 89 -87 u=6 vol=0.0169646 imp:n=1 \$T-17
179 26 -12 -107 89 -87 u=6 vol=0.0169646 imp:n=1 \$T-18
180 27 -10.3215 -108 89 -87 u=6 vol=0.0169646 imp:n=1 \$T-19
181 28 -12 -109 89 -87 u=6 vol=0.0169646 imp:n=1 \$T-20
182 29 -1.358 -110 89 -87 u=6 vol=0.0169646 imp:n=1 \$T-21
183 30 -12 -111 89 -87 u=6 vol=0.0169646 imp:n=1 \$T-22

184 31 -12 -112 89 -87 u=6 vol=0.0169646 imp:n=1 \$T-23

185 32 -12 -113 89 -87 u=6 vol=0.0169646 imp:n=1 \$T-24

186 33 -12 -114 89 -87 u=6 vol=0.0169646 imp:n=1 \$T-25

187 34 -12 -115 89 -87 u=6 vol=0.0169646 imp:n=1 \$T-26

188 35 -12 -116 89 -87 u=6 vol=0.0169646 imp:n=1 \$T-27

189 8 -.001225 #162 #163 #164 #165 #166 &

#167 #168 #169 #170 #171 #172 #173 #174 #175 &

#176 #177 #178 #179 #180 #181 #182 &

#183 #184 #185 #186 #187 #188 -86 89 -87 u=6 imp:n=1 \$ inside of void tube

190 4 -1 62:88:-9 u=6 imp:n=1 \$all space outside of tube is water

C building the aluminum void tube filled with water and target material (soon)

191 2 -2.7 (86 -62 89 -87):(-62 87 -88):(-62 9 -89) u=15 vol=365.1787 imp:n=1 \$void
tube filled water, needed for 'no void' sample irradiation

192 9 -12 -90 89 -87 u=15 vol=0.0169646 imp:n=1 \$T-1

193 10 -12 -91 89 -87 u=15 vol=0.0169646 imp:n=1 \$T-2

194 11 -12 -92 89 -87 u=15 vol=0.0169646 imp:n=1 \$T-3

195 12 -12 -93 89 -87 u=15 vol=0.0169646 imp:n=1 \$T-4

196 13 -12 -94 89 -87 u=15 vol=0.0169646 imp:n=1 \$T-5

197 14 -12 -95 89 -87 u=15 vol=0.0169646 imp:n=1 \$T-6

198 15 -12 -96 89 -87 u=15 vol=0.0169646 imp:n=1 \$T-7

199 16 -12 -97 89 -87 u=15 vol=0.0169646 imp:n=1 \$T-8

200 17 -10.3115 -98 89 -87 u=15 vol=0.0169646 imp:n=1 \$T-9
201 18 -12 -99 89 -87 u=15 vol=0.0169646 imp:n=1 \$T-10
202 19 -12 -100 89 -87 u=15 vol=0.0169646 imp:n=1 \$T-11
203 20 -12 -101 89 -87 u=15 vol=0.0169646 imp:n=1 \$T-12
204 21 -12 -102 89 -87 u=15 vol=0.0169646 imp:n=1 \$T-13
205 22 -10.31659 -103 89 -87 u=15 vol=0.0169646 imp:n=1 \$T-14
206 23 -12 -104 89 -87 u=15 vol=0.0169646 imp:n=1 \$T-15
207 24 -12 -105 89 -87 u=15 vol=0.0169646 imp:n=1 \$T-16
208 25 -12 -106 89 -87 u=15 vol=0.0169646 imp:n=1 \$T-17
209 26 -12 -107 89 -87 u=15 vol=0.0169646 imp:n=1 \$T-18
210 27 -10.3215 -108 89 -87 u=15 vol=0.0169646 imp:n=1 \$T-19
211 28 -12 -109 89 -87 u=15 vol=0.0169646 imp:n=1 \$T-20
212 29 -1.358 -110 89 -87 u=15 vol=0.0169646 imp:n=1 \$T-21
213 30 -12 -111 89 -87 u=15 vol=0.0169646 imp:n=1 \$T-22
214 31 -12 -112 89 -87 u=15 vol=0.0169646 imp:n=1 \$T-23
215 32 -12 -113 89 -87 u=15 vol=0.0169646 imp:n=1 \$T-24
216 33 -12 -114 89 -87 u=15 vol=0.0169646 imp:n=1 \$T-25
217 34 -12 -115 89 -87 u=15 vol=0.0169646 imp:n=1 \$T-26
218 35 -12 -116 89 -87 u=15 vol=0.0169646 imp:n=1 \$T-27
219 4 -1 #191 #192 #193 #194 #195 &

#196 #197 #198 #199 #200 #201 #202 &

#203 #204 #205 #206 #207 #208 #209 &

#210 #211 #212 #213 #214 #215 #216 &

#217 #218 -86 89 -87 u=15 imp:n=1 \$ inside of void tube

220 4 -1 62:88:-9 u=15 imp:n=1 \$all space outside of tube is water

C

221 4 -1 -62 9 -10 u=5 imp:n=1 \$target water cylinder, optimized same volume as void cylinder

222 4 -1 62:-9:10 u=5 imp:n=1

C building the bare rabbit tube, with no sample

223 5 -8.68 81 -80 9 -10 u=44 imp:n=1 \$ bare rabbit tube cylinder1

224 5 -8.68 -82 83 9 -10 u=44 imp:n=1 \$pressure tube for bare rabbit tube

225 6 -.001251 -81 127 -126 u=44 imp:n=1 \$target cylinder for flux determination, sample will sit inside

226 6 -.001251 -81 9 -10 #225 u=44 imp:n=1 \$Nitrogen transport medium

227 6 -.001251 -83 9 -10 u=44 imp:n=1 \$Nitrogen transport medium

228 4 -1 #223 #224 #225 #226 #227 u=44 imp:n=1 \$everything not in tubes is water

C building the cd rabbit tube, with no sample

229 5 -8.68 81 -80 9 -10 u=45 imp:n=1 \$ bare rabbit tube cylinder1

230 6 -.001251 -81 127 -126 u=45 imp:n=1 \$target cylinder for flux determination, sample will sit inside

231 6 -.001251 -81 9 -10 #230 u=45 imp:n=1 \$Nitrogen transport medium

232 5 -8.68 -82 83 9 -10 u=45 imp:n=1 \$pressure tube for bare rabbit tube

233 6 -.001251 -83 9 -10 u=45 imp:n=1 \$Nitrogen transport medium

234 7 -8.65 -84 80 9 -10 u=45 imp:n=1 \$cadmium layer for cylinder 1

235 7 -8.65 -85 82 9 -10 u=45 imp:n=1 \$cadmium layer for pressure tube

236 4 -1 #229 #230 #231 #232 #233 #234 #235 u=45 vol=5872 imp:n=1 \$ everything not
in tubes is water

C building the test water universe with test cylinder

237 5 -8.68 203 -202 u=77 imp:n=1 \$hollow source tube

267 4 -1 204 -205 206 -207 208 -209 u=77 vol=.0125 imp:n=1 \$test geometry for
Benchmark test

238 4 -1 52 -51 9 -159 8 -14 #237 #267 u=77 imp:n=1 \$water universe

239 4 -1 -52:51:-9:159:-8:14 u=77 imp:n=1 \$water universe

C

C

240 0 -53 54 -56 55 u=4 lat=1 fill= 0:8 0:5 0:0 & \$grid filled with universes

3 3 3 3 3 3 3 3 3 &

3 3 3 3 77 3 3 3 3 &

3 3 1 1 1 8 3 3 3 &

3 1 1 2 1 1 1 3 3 &

3 1 1 2 1 2 1 3 3 &

3 1 44 1 3 1 45 3 3 imp:n=1

241 0 54 -59 55 -60 57 -200 fill=4 imp:n=1 \$window

242 2 -2.7 135 -136 137 -57 imp:n=1 \$(3,5) lower hollow cylinder

C See excel for easy rescaling

302 like 242 but trcl (-16.91 0 0) imp:n=1

303 like 242 but trcl (-8.455 0 0) imp:n=1

305 like 242 but trcl (8.455 0 0) imp:n=1

310 like 242 but trcl (-25.365 8.215 0) imp:n=1

311 like 242 but trcl (-16.91 8.215 0) imp:n=1

312 like 242 but trcl (-8.455 8.215 0) imp:n=1

313 like 242 but trcl (0 8.215 0) imp:n=1

314 like 242 but trcl (8.455 8.215 0) imp:n=1

315 like 242 but trcl (16.91 8.215 0) imp:n=1

319 like 242 but trcl (-25.365 16.43 0) imp:n=1

320 like 242 but trcl (-16.91 16.43 0) imp:n=1

321 like 242 but trcl (-8.455 16.43 0) imp:n=1

322 like 242 but trcl (0 16.43 0) imp:n=1

323 like 242 but trcl (8.455 16.43 0) imp:n=1

324 like 242 but trcl (16.91 16.43 0) imp:n=1

328 like 242 but trcl (-25.365 24.645 0) imp:n=1

330 like 242 but trcl (-8.455 24.645 0) imp:n=1

332 like 242 but trcl (8.455 24.645 0) imp:n=1

C

261 38 -2.71 134 -161 -59 55 -60 54 136 141 142 &

143 144 145 146 147 148 149 150 151 152 153 154 &
 155 156 157 158 162 163 164 165 166 167 168 169 &
 170 171 172 173 174 175 176 177 178 179 180 181 &
 182 183 184 185 186 187 188 189 190 191 192 193 &
 194 195 196 imp:n=1 \$lower Al-6061 grid plate approximation, to crush the wings
 262 4 -1 64 -65 66 -67 68 -69 #241 #242 #302 &
 #303 #305 #310 #311 #312 #313 #314 &
 #315 #319 #320 #321 #322 #323 #324 &
 #328 #330 #332 #261 imp:n=1 \$outside
 263 0 -64:65:-66:67:-68:69 imp:n=0 \$super outside

C surface cards

1 rcc 0 -13.45 0 0 0 62.5348 14.008 \$fuel meat lower cylinder, fuel meat plate width
 .054cm same curvature
 2 rcc 0 -13.45 0 0 0 62.5348 14.062 \$fuel meat upper cylinder
 3 rcc 0 -13.45 0 0 0 62.5348 13.97 \$full fuel plate inner cylinder, total fuel plate width
 .13cm same 13.97 radius of curvature
 4 rcc 0 -13.45 0 0 0 62.5348 14.1 \$full fuel plate outer cylinder
 5 px -3.7846 \$bounding wall for fuel cell
 6 px 3.7846 \$bounding wall for fuel cell
 7 py .445 \$bounding wall for fuel cell
 8 py 0 \$bounding wall for fuel cell

9 pz 0 \$bounding wall for fuel cell

10 pz 62.5348 \$bounding wall for fuel cell

11 py 8.215 \$bounding wall for full fuel assembly, 18 fully enriched plates

12 rcc 0 -13.45 0 0 0 62.5348 14.415 \$.315 water gap

13 rcc 0 0 0 0 0 100 15

14 py 8.215 \$quite generous

15 rcc 0 -11.225 0 0 0 62.5348 13.97

51 px 4.1275 \$right alum side plate

52 px -4.1275 \$left alum side plate

C Control rod specific surfaces \$-----

16 px 3.27914 \$right outer vertical guide tube wall

17 px 2.99974 \$right vertical inner guide tube wall

18 px -3.27914 \$left outer vertical guide tube wall

19 px -2.99974 \$left inner vertical guide tube wall

20 py 2.57715 \$ 2.83715 bottom outer horizontal guide tube wall

21 py 2.85655 \$ 3.11655 bottom inner horizontal guide tube wall

22 py 5.63785 \$ 5.89785 top outer horizontal guide tube wall

23 py 5.35845 \$ 5.61845 top inner horizontal guide tube wall

24 py 5.196525 \$top y boundary for control rod

25 py 3.018475 \$bottom y boundary for control rod

26 c/z -1.734185 4.1075 1.08839 \$left major arc

27 c/z 1.734185 4.1075 1.08839 \$right major arc
28 px 1.984375 \$right end of straight plane before major arc
29 px -1.984375 \$left end of straight plane before major arc
30 px 0
31 px 1.8
32 px -1.8
33 c/z .555625 3.5741 .3175 \$a
34 c/z 1.666875 3.5741 .3175 \$b
35 c/z 1.666875 4.6409 .3175 \$c
36 c/z .555625 4.6409 .3175 \$d
37 c/z -.555625 4.6409 .3175 \$e
38 c/z -1.666875 4.6409 .3175 \$f
39 c/z -1.666875 3.5741 .3175 \$g
40 c/z -.555625 3.5741 .3175 \$h
41 px .238125
42 px .873125
43 px 1.349375
44 px 1.984375
45 px -.238125
46 px -.873125
47 px -1.349375

48 px -1.984375

49 py 3.5741

50 py 4.6409

53 px 4.2275 \$right assembly bound, water bound

54 px -4.2275 \$left assembly bound, water bound

55 py 0 \$modify this for water bound between fuel assemblies

56 py 8.215 \$^

57 pz 0 \$lower z bound for core space

58 pz 62.5348

59 px 71.8675

60 py 49.29

61 c/z 0 4.1075 1

62 c/z 0 4.1075 4 \$void tube geometry, corrected for assembly rescaling

63 pz 52.3748 \$controls the insertion of control rod materials into core

64 px -87.98

65 px 186.02

66 py -457.71

67 py 121.29

68 pz -50

69 pz 800

70 px 1.745 \$right reg rod rectangle bound

- 71 px -1.745 \$left reg rod rectangle bound
- 72 py 2.9925 \$ outer bottom reg rod rectangle bound
- 73 py 3.1575 \$ inner bottom reg rod rectangle bound
- 74 py 5.0575 \$ inner top reg rod rectangle bound
- 75 py 5.2225 \$ outer top reg rod rectangle bound
- 76 c/z 1.745 4.1075 1.115 \$outer right reg rod half circle curve
- 77 c/z 1.745 4.1075 .95 \$inner right reg rod half circle curve
- 78 c/z -1.745 4.1075 1.115 \$outer left reg rod half circle curve
- 79 c/z -1.745 4.1075 .95 \$inner left reg rod half circle curve
- 80 c/z 0 2.472 2.4 \$ SS bare rabbit tube outer cylinder estimated
- 81 c/z 0 2.472 2.3 \$SS bare rabbit tube inner cylinder estimated
- 82 c/z 0 6.444 1.3 \$SS bare 2 rabbit tube outer cylinder estimated
- 83 c/z 0 6.444 1.2 \$SS bare 2 rabbit tube inner cylinder estimated
- 84 c/z 0 2.472 2.41 \$ outer cylinder for the cadmium layer
- 85 c/z 0 6.444 1.31 \$ outer cylinder for the cadmium layer on pressure tube
- 86 c/z 0 4.1075 3.8 \$ inner cylinder for void tube
- 87 pz 55 \$upper inner z limit for void tube, upper limit for target material
- 88 pz 56 \$upper outer z limit for void tube
- 89 pz 1 \$lower inner z limit for void tube, lower limit for target material
- 90 c/z -.83782125 1.2575 .01 \$T-1
- 91 c/z .837821249 1.2575 .01 \$T-2

92 c/z -1.64544827 2.2075 .01 \$T-3
93 c/z 0 2.2075 .01 \$T-4
94 c/z 1.645448267 2.2075 .01 \$T-5
95 c/z -2.45288945 3.1575 .01 \$T-6
96 c/z -1.22644473 3.1575 .01 \$T-7
97 c/z 0 3.1575 .01 \$T-8
98 c/z 1.226444726 3.1575 .01 \$T-9
99 c/z 2.452889453 3.1575 .01 \$T-10
100 c/z -2.85 4.1075 .01 \$T-11
101 c/z -1.9 4.1075 .01 \$T-12
102 c/z -.95 4.1075 .01 \$T-13
103 c/z 0 4.1075 .01 \$T-14
104 c/z .95 4.1075 .01 \$T-15
105 c/z 1.9 4.1075 .01 \$T-16
106 c/z 2.85 4.1075 .01 \$T-17
107 c/z -2.45288945 5.0575 .01 \$T-18
108 c/z -1.22644473 5.0575 .01 \$T-19
109 c/z 0 5.0575 .01 \$T-20
110 c/z 1.226444726 5.0575 .01 \$T-21
111 c/z 2.452889453 5.0575 .01 \$T-22
112 c/z -1.64544827 6.0075 .01 \$T-23

113 c/z 0 6.0075 .01 \$T-24

114 c/z 1.645448267 6.0075 .01 \$T-25

115 c/z -.83782125 6.9575 .01 \$T-26

116 c/z .837821249 6.9575 .01 \$T-27

117 px 1

118 px 2

119 pz 10

120 pz 18 \$not true

121 pz 9.715000811

122 pz 9.650000811

123 c/z 0 2.472 .1

124 c/z 0 2.472 .25

125 c/z 0 2.472 .3

126 pz 14

127 pz 6

128 pz 60.96 \$replacement for surface 10 for control and reg rod material constructions

129 pz 38.28796 \$controls the reg rod tube height in MSTR

130 pz 20 \$for the test vial

131 pz 25 \$ for the test vial

132 c/z 0 2.472 1 \$for the test vial

133 pz 75 \$top bound for top al-6061 slab

160 c/z 52.53 30.2525 3.63

161 pz -5 \$to replace 57 for grid plate approximation

134 pz -17.7 \$bottom bound for grid plate, al-6061 slab

135 c/z 33.82 20.5375 2.65938 \$grid position 3,5 lower inner cylinder

137 pz -17.78 \$lower z bound for cylinder 3,5 hollow

138 c/z 33.82 20.5375 3.63 \$ top outer cylinder (3,5)

139 c/z 33.82 20.5375 3.30 \$top inner cylinder (3,5)

140 pz 67.9323 \$upper bound for top cylinder paired with pz 58

159 pz 113.3348 \$top bound for control rod material outside of core box

C beginning of cylinders to create holes in grid plate see excel

162 c/z 0 4.1075 3.01625

163 c/z 8.455 4.1075 3.01625

164 c/z 16.91 4.1075 3.01625

165 c/z 25.365 4.1075 3.01625

166 c/z 33.82 4.1075 3.01625

167 c/z 42.275 4.1075 3.01625

168 c/z 50.73 4.1075 3.01625

169 c/z 59.185 4.1075 3.01625

170 c/z 67.64 4.1075 3.01625

171 c/z 0 12.3225 3.01625

172 c/z 8.455 12.3225 3.01625

173 c/z 16.91 12.3225 3.01625
174 c/z 25.365 12.3225 3.01625
175 c/z 33.82 12.3225 3.01625
176 c/z 42.275 12.3225 3.01625
177 c/z 50.73 12.3225 3.01625
178 c/z 59.185 12.3225 3.01625
179 c/z 67.64 12.3225 3.01625
180 c/z 0 20.5375 3.01625
181 c/z 8.455 20.5375 3.01625
182 c/z 16.91 20.5375 3.01625
183 c/z 25.365 20.5375 3.01625
136 c/z 33.82 20.5375 3.01625
141 c/z 42.275 20.5375 3.01625
142 c/z 50.73 20.5375 3.01625
143 c/z 59.185 20.5375 3.01625
184 c/z 67.64 20.5375 3.01625
185 c/z 0 28.7525 3.01625
186 c/z 8.455 28.7525 3.01625
187 c/z 16.91 28.7525 3.01625
144 c/z 25.365 28.7525 3.01625
145 c/z 33.82 28.7525 3.01625

146 c/z 42.275 28.7525 3.01625

147 c/z 50.73 28.7525 3.01625

148 c/z 59.185 28.7525 3.01625

149 c/z 67.64 28.7525 3.01625

188 c/z 0 36.9675 3.01625

189 c/z 8.455 36.9675 3.01625

190 c/z 16.91 36.9675 3.01625

150 c/z 25.365 36.9675 3.01625

151 c/z 33.82 36.9675 3.01625

152 c/z 42.275 36.9675 3.01625

153 c/z 50.73 36.9675 3.01625

154 c/z 59.185 36.9675 3.01625

155 c/z 67.64 36.9675 3.01625

191 c/z 0 45.1825 3.01625

192 c/z 8.455 45.1825 3.01625

193 c/z 16.91 45.1825 3.01625

195 c/z 25.365 45.1825 3.01625

156 c/z 33.82 45.1825 3.01625

196 c/z 42.275 45.1825 3.01625

157 c/z 50.73 45.1825 3.01625

194 c/z 59.185 45.1825 3.01625

158 c/z 67.64 45.1825 3.01625

C

200 pz 113.3348 \$ use to control the core box height,to replace 159

201 rcc 0 -13.45 0 0 0 62.5348 13.9

202 rcc 0 4.1075 0 0 0 113.3348 4 \$outer SS for source holder tube

203 rcc 0 4.1075 0 0 0 113.3348 3.5 \$inner SS for source holder tube

204 pz 28.7674

205 pz 33.7674

206 px -2.5

207 px 2.5

208 py 4.10725

209 py 4.10775 \$end of similar with MSTR_FIN_120W_F2_V3.txt surfaces

210 py 8.21

211 py 8.2105

212 py .0045

213 py .005

214 py 4.10719

215 px -4.1205

216 px -4.12

217 px 4.1225

218 px 4.123

219 py 1.6075

220 py 6.6075

221 px -.00025

222 px .00025

223 py 4.10775 \$copies 209

C Data

mode n

kcode 10000 1.0 50 250

ksrc 5 45 30 &

8 45 30 &

8 49 30 &

11 45 30 &

8 42 30 &

25 42 30 &

24 45 30 &

22 45 30 &

28 45 30 &

25 48 30 &

42 45 30 &

42 42 30 &

39 45 30 &

42 48 30 &

45 45 30 &

8 37 30 &

8 34 30 &

5 37 30 &

8 41 30 &

11 37 30 &

17 37 30 &

17 34 30 &

14 37 30 &

17 40 30 &

20 37 30 &

34 37 30 &

34 34 30 &

31 37 30 &

34 41 30 &

37 37 30 &

50 37 30 &

51 34 30 &

48 37 30 &

50 40 30 &

54 37 30 &

8 29 30 &

8 26 30 &

5 29 30 &

8 32 30 &

11 29 30 &

17 29 30 &

17 26 30 &

14 29 30 &

17 32 30 &

20 29 30 &

34 29 30 &

24 26 30 &

31 29 30 &

33 32 30 &

37 29 30 &

42 29 30 &

42 26 30 &

39 29 30 &

42 32 30 &

45 29 30 &

51 29 30 &

51 26 30 &

48 29 30 &

51 32 30 &

54 29 30 &

17 21 30 &

17 17 30 &

14 21 30 &

17 24 30 &

20 21 30 &

25 21 30 &

25 17 30 &

22 20 30 &

25 24 30 &

28 21 30 &

34 21 30 &

34 17 30 &

31 21 30 &

34 24 30 &

36 21 30 &

42 24 30 &

42 17 30 &

25 32 30 &

25 25 30 &

25 40 30 &

25 34 30 &

42 40 30 &

42 34 30

f54:n 267

e54 .000000625 .1 20

FMESH24:n geom=xyz origin= -4.2275 0 0 imesh=71.8675 &

iints=1 jmesh=49.29 jint=1 kmesh=62.5348 kints=1 &

Emesh .000000625 .1 20

m1 92235.66c -0.125008306 92238.66c -0.5000332 14028.66c -0.045282453 &

14029.66c -0.002374764 14030.66c -0.00163065 13027.66c -0.325670603 \$ U3Si2-Al
fuel meat

m2 13027.66c -.96 12000.66c -.012 14000.21c -.008 &

26000.42c -.007 29000.50c -.004 30000.40c -.0025 &

22000.42c -.0015 25055.42c -.0015 24000.42c -.0035 \$al 6061 wall tubes and cladd

m3 24000.42c -.18 28000.42c -.08 6000.66c -.0008 &

25055.42c -.02 14000.21c -.01 15031.72c -.00045 &

16000.66c -.0003 5010.66c -.002764093 &

5011.66c -.012237294 26000.42c -.69345 \$control rod material 1.5% boron

m4 1001.66c 66.6590 1002.66c .0077 8016.66c 33.3206 8017.66c .0127 \$water

m5 24000.42c -.18 28000.42c -.08 6000.66c -.0008 &

25055.42c -.02 14000.21c -.01 15031.72c -.00045 &

16000.66c -.0003 26000.42c -.708451387 \$reg rod material, no boron ss304, also bare
rabbit tube

m6 7014.70c .99636 7015.70c .00364 \$nitrogen gas medium

m7 48000.51c 1 \$cadmium for the layer around the bare rabbit tube

m8 8016.62c -.23209 7014.70c -.755107 &

18000.42c -.0128 36078.70c -9.76353E-9 &

36080.70c -6.43733E-8 &

36082.70c -3.40174E-7 36083.70c -3.41361E-7 &

36084.70c -1.71232E-6 36086.70c -5.32084E-7 \$air for the void tube

m9 95243.69c -1

m10 95243.69c -1

m11 95243.69c -1

m12 95243.69c -1

m13 95243.69c -1

m14 95243.69c -1

m15 95243.69c -1

m16 95243.69c -1

m17 95241.69c -1 \$pure Am241 target for non-actinide and actinide production analysis

m18 95243.69c -1

m19 95243.69c -1

m20 95243.69c -1

m21 95243.69c -1

m22 95242.70c -1 \$pure Am242m target for non-actinide and actinide production analysis

m23 95243.69c -1

m24 95243.69c -1

m25 95243.69c -1

m26 95243.69c -1

m27 95243.69c -1 \$pure Am243 target for non-actinide and actinide production analysis

m28 95243.69c -1

m29 8016.62c -1 \$pure (O16)2

m30 95243.69c -1

m31 95243.69c -1

m32 95243.69c -1

m33 95243.69c -1

m34 95243.69c -1

m35 95243.69c -1

m36 95241.69c -1

m37 29000.50c -1

m38 13027.66c 99.9469 29063.60c .0367 29065.70c .0164 \$Grid Plate

m39 13027.66c 97.8233 14028.66c .6140 14029.66c .0312 &

14030.66c .0206 6000.66c 1.0536 26054.66c .0133 26056.66c .2093 &

26057.66c .0048 26058.66c .0006 24050.66c .0049 24052.66c .0939 &

24053.66c .0106 24054.66c .0026 29063.66c .0811 29065.66c .0362 \$fuel upper handle

m40 79197.70c 0.999999951 95241.70c 4.93993E-08 95642.70c 1E-36

Then the code used for the BEGe model (Photon distributions have been omitted for brevity):

PROJECT BEGE 3825

C cell cards

1 1 -7.92 2 -1 imp:p=1 \$outer SS layer
 2 2 -11.34 3 -2 imp:p=1 \$lead layers
 3 3 -8.96 5 -4 imp:p=1 \$copper layer 5 -4
 4 4 -6.99 4 -3 imp:p=1 \$tin layer 4 -3
 5 6 -2.67 7 -6 imp:p=1 \$ Al detector end cap
 6 3 -8.96 9 -8 imp:p=1 \$ Cu detector holder
 7 7 -5.33 -10 imp:p=1 \$Ge detector
 13 7 -5.33 -13 imp:p=1 \$dead top Ge layer
 15 7 -5.33 -15 10 imp:p=1 \$ dead radial Ge layer
 16 7 -5.33 -16 imp:p=1 \$dead bottom Ge layer
 8 8 -1.42 -11 imp:p=1 \$carbon epoxy window
 9 0 -7 #5 #6 #7 #8 #13 #15 #16 imp:p=1 \$vacuum interior #13
 C 10 9 -2 -12 imp:p=1 \$Am241 sample cell
 C 17 9 -2 -17 #10 imp:p=1 \$blocking material
 11 5 -.001225 -5 6 #8 imp:p=1 \$ air inside
 12 0 1 imp:p=0

C surface cards

1 rcc 0 0 0 0 0 63.5 25.4 \$outer SS
2 rcc 0 0 .95 0 0 61.6 24.45 \$inner SS, outer Pb
3 rcc 0 0 12.48 0 0 41.12 14.21 \$inner Pb, outer Cu
4 rcc 0 0 12.64 0 0 40.8 14.05 \$inner Cu, outer Sn
5 rcc 0 0 12.74 0 0 40.6 13.95 \$inner Sn, fills air interior
6 rcc 0 0 12.74 0 0 18 4.45 \$outer Al layer
7 rcc 0 0 13.24 0 0 17.5 4.3 \$inner Al layer
8 rcc 0 0 26.29 0 0 3.9 3.7 \$outer Cu holder layer
9 rcc 0 0 27.29 0 0 2.9 3.55 \$inner Cu holder layer
10 rcc 0 0 27.64 0 0 2.5 3.5 \$Ge cylinder
11 rcc 0 0 30.74 0 0 .06 4.45 \$carbon epoxy layer
C 12 rcc 0 -.15 32.1 0 .3 0 1.025 \$Mixed sample, sits on window
13 rcc 0 0 30.14 0 0 0.00003 3.5 \$Ge dead layer old .0005
14 rcc 0 0 33 0 0 .563 1.025 \$blocking layer
15 rcc 0 0 27.64 0 0 2.5 3.55 \$radial Ge dead layer
16 rcc 0 0 27.59 0 0 .05 3.5 \$bottom Ge dead layer
C 17 rcc 0 -2.69 32.1 0 5.08 0 1.025 \$vial material, not active

C Data

mode p

```

phys:p 100 1 0 0 0

sdef erg=d1 par=2 pos= 0 0 32.2 axs 0 1 0 rad=d2 ext=0

Si2 0 .25

SP2 -21 1

Si1 L 0

Sp1 D 0

f8:p 7

e8 0 .00005 .0005 10i .008162 &

0.00836194890737533 16382i 3.0252549495697

FT8 GEB .007508 2.73758E-05 0

C FT8 GEB .007339 .0009172 .0002192

C FT8 GEB .007508 8.657E-07 0

f18:p 7

e18 0 .00005 .0005 100i .008361949 16383i 3.02525495

C m1 32070.70c .2038 32072.70c .2731 32073.70c .0776 &

C 32074.70c .3672 32076.70c .0783

C m2 95241.70c 1

C m3 82000.50c 1

nps 100000000

m1 24000.04p -.18 28000.04p -.08 6000.04p -.0008 &

25000.04p -.02 14000.04p -.01 15000.04p -.00045 &

```

```

16000.04p -.0003 26000.04p -.708451387

m2 82000.04p 1

m3 29000.04p 1

m4 50000.04p 1

m5 8000.04p -.23209 7000.04p -.755107 &

18000.04p -.0128 36000.04p -9.76353E-9 &

36000.04p -2.9903123E-06

m6 13000.04p 1

m7 32000.04p 1

m8 6000.04p -.834 8000.04p -.093 1000.04p -.073

m9 6000.04p .5 1000.04p .5

C m9 95000.04p 0.976028304 58000.04p 3.29684E-07 &

C 50000.04p 1.15446E-07 55000.04p 0.023971161 &

C 39000.04p 9.02947E-08

m10 6000.04p 1

```

The Matlab code for the typical LEU fuel, and power/time, Pu241 and Am241 buildup behavior (not covered by MCNP simulation), a variation was used to determine the buildup of Am241 from typical reactor and weapons grade plutonium of their respective compositions:

```
function[]= Net_Burn()
```

```
for h=1:l
```

```
act_abs=[6.8366E-22; 5.18042E-24; 4.54002E-22; 2.68336E-24; 3.65834E-23;  
1.91667E-23; 4.76463E-22; 6.52734E-23; 1.19688E-22; 1.75826E-22;  
2.06488E-21; 6.80944E-23; 7.12136E-24; 2.13925E-22; 1.52876E-22;  
7.08122E-24; 4.30572E-22; 1.01854E-21; 2.85899E-22; 1.37523E-21;  
1.85108E-23; 3.06508E-22; 5.91336E-22; 2.42714E-21; 6.86605E-21;  
7.52926E-23];  
  
act_rad=[9.86828E-23; 5.13332E-24; 4.523E-22; 2.68334E-24; 2.23325E-23;  
1.91657E-23; 4.76047E-22; 8.76659E-24; 3.10951E-24; 1.75806E-22;  
2.85384E-22; 6.76631E-23; 7.12103E-24; 7.50417E-24; 4.85815E-23;  
6.92801E-24; 4.12806E-22; 2.70701E-22; 2.85839E-22; 3.63011E-22;  
1.8509E-23; 8.74137E-23; 5.88159E-22; 3.29191E-22; 1.26698E-21;  
7.50967E-23];  
  
act_con=[3.12292E-17; 9.38475E-16; 1.18852E-06; 4.91924E-18; 0.000492642;  
1.36554E-05; 0.002310491; 0.00018663; 0.001600063; 1.02514E-14;  
3.78958E-06; 3.40515E-06; 0.000831112; 0.005251115; 0.002100446;  
0.006244569; 2.50445E-10; 9.10993E-13; 3.34767E-12; 1.53702E-09;  
5.88058E-14; 3.88501E-05; 5.07722E-11; 1.20188E-05; 1.55773E-10;  
2.98019E-12];  
  
ti=0;  
  
tf=24*3600*h*365*1;  
  
dt=100;  
  
time_step(1,1)=0;  
  
t_total=(tf-ti)/dt;  
  
therm_flux=3.1165*10^13;
```

```

N_act=zeros(26,t_total+1);

N_act(1,1)=5.13*10^27;

N_act(4,1)=2.48*10^29;

for i=1:t_total

    time_step(i+1,1)=dt*(i);

    %U235

    N_act(1,i+1)=(dt*((-act_con(1,1)*N_act(1,i))-
(N_act(1,i)*act_abs(1,1)*therm_flux)+(act_con(18,1)*N_act(18,i))))+N_act(1,i);

    %U236

    N_act(2,i+1)=(dt*((-act_con(2,1)*N_act(2,i))-
(N_act(2,i)*act_abs(2,1)*therm_flux)+(act_rad(1,1)*N_act(1,i)*therm_flux)+(act_con(1
9,1)*N_act(19,i))))+N_act(2,i);

    %U237

    N_act(3,i+1)=(dt*((-act_con(3,1)*N_act(3,i))-
(N_act(3,i)*act_abs(3,1)*therm_flux)+(N_act(2,i)*act_rad(2,1)*therm_flux)+(0.0000245*
act_con(20,1)*N_act(20,i))))+N_act(3,i);

    %U238

    N_act(4,i+1)=(dt*((-act_con(4,1)*N_act(4,i))-
(N_act(4,i)*act_abs(4,1)*therm_flux)+(N_act(3,i)*act_rad(3,1)*therm_flux)+(act_con(2
1,1)*N_act(21,i))))+(N_act(4,i));

    %U239

    N_act(5,i+1)=(dt*((-act_con(5,1)*N_act(5,i))-
(N_act(5,i)*act_abs(5,1)*therm_flux)+(N_act(4,i)*act_rad(4,1)*therm_flux)))+N_act(5,i
);

```

%U240

$$N_act(6,i+1)=(dt*((-act_con(6,1)*N_act(6,i))- \\ (N_act(6,i)*act_abs(6,1)*therm_flux)+(N_act(5,i)*act_rad(5,1)*therm_flux)))+N_act(6,i \\);$$

%U241

$$N_act(7,i+1)=(dt*((-act_con(7,1)*N_act(7,i))- \\ (N_act(7,i)*act_abs(7,1)*therm_flux)+(N_act(6,i)*act_rad(6,1)*therm_flux)))+N_act(7,i \\);$$

%Np240

$$N_act(8,i+1)=(dt*((-act_con(8,1)*N_act(8,i))- \\ (N_act(8,i)*act_abs(8,1)*therm_flux)+(.6744834*N_act(12,i)*act_rad(12,1)*therm_flux) \\ +(.0012*act_con(9,1)*N_act(9,i))))+N_act(8,i);$$

%Np240m

$$N_act(9,i+1)=(dt*((-act_con(9,1)*N_act(9,i))- \\ (N_act(9,i)*act_abs(9,1)*therm_flux)+(.3255166*N_act(12,i)*act_rad(12,1)*therm_flux) \\ +(act_con(6,1)*N_act(6,i))))+N_act(9,i);$$

%Np237

$$N_act(10,i+1)=(dt*((-act_con(10,1)*N_act(10,i))- \\ (N_act(10,i)*act_abs(10,1)*therm_flux)+(act_con(3,1)*N_act(3,i))+(act_con(23,1)*N_ac \\ t(23,i))))+N_act(10,i);$$

%Np238

$$N_act(11,i+1)=(dt*((-act_con(11,1)*N_act(11,i))- \\ (N_act(11,i)*act_abs(11,1)*therm_flux)+(N_act(10,i)*act_rad(10,1)*therm_flux)+(.0045 \\ 9*act_con(25,1)*N_act(25,i))))+N_act(11,i);$$

%Np239

```

N_act(12,i+1)=(dt*((-act_con(12,1)*N_act(12,i))-
(N_act(12,i)*act_abs(12,1)*therm_flux)+(N_act(11,i)*act_rad(11,1)*therm_flux)+(act_c
on(5,1)*N_act(5,i))+(act_con(26,1)*N_act(26,i))))+N_act(12,i);

```

```
%Np241
```

```

N_act(13,i+1)=(dt*((-act_con(13,1)*N_act(13,i))-
(N_act(13,i)*act_abs(13,1)*therm_flux)+(N_act(8,i)*act_rad(8,1)*therm_flux)+(N_act(9
,i)*act_rad(9,1)*therm_flux)+(act_con(7,1)*N_act(7,i))))+N_act(13,i);

```

```
%Np242
```

```

N_act(14,i+1)=(dt*((-act_con(14,1)*N_act(14,i))-
(N_act(14,i)*act_abs(14,1)*therm_flux)+(.8977549*N_act(13,i)*act_rad(13,1)*therm_fl
ux)))+N_act(14,i);

```

```
%Np242m
```

```

N_act(15,i+1)=(dt*((-act_con(15,1)*N_act(15,i))-
(N_act(15,i)*act_abs(15,1)*therm_flux)+(.1022444*N_act(13,i)*act_rad(13,1)*therm_fl
ux)))+N_act(15,i);

```

```
%Np243
```

```

N_act(16,i+1)=(dt*((-act_con(16,1)*N_act(16,i))-
(N_act(16,i)*act_abs(16,1)*therm_flux)+(N_act(14,i)*act_rad(14,1)*therm_flux)+(N_ac
t(15,i)*act_rad(15,1)*therm_flux)))+N_act(16,i);

```

```
%Pu238
```

```

N_act(17,i+1)=(dt*((-act_con(17,1)*N_act(17,i))-
(N_act(17,i)*act_abs(17,1)*therm_flux)+(N_act(11,i)*act_con(11,1))))+N_act(17,i);

```

```
%Pu239
```

$$N_{act}(18,i+1)=(dt*((-act_con(18,1)*N_{act}(18,i))-$$

$$(N_{act}(18,i)*act_abs(18,1)*therm_flux)+(act_con(12,1)*N_{act}(12,i))+(N_{act}(17,i)*act_rad(17,1)*therm_flux)))+N_{act}(18,i);$$

%Pu240

$$N_{act}(19,i+1)=(dt*((-act_con(19,1)*N_{act}(19,i))-$$

$$(N_{act}(19,i)*act_abs(19,1)*therm_flux)+(N_{act}(18,i)*act_rad(18,1)*therm_flux)+(N_{act}(8,i)*act_con(8,1))+(.9988*N_{act}(9,i)*act_con(9,1)))))+N_{act}(19,i);$$

%Pu241

$$N_{act}(20,i+1)=(dt*((-act_con(20,1)*N_{act}(20,i))-$$

$$(N_{act}(20,i)*act_abs(20,1)*therm_flux)+(N_{act}(19,i)*act_rad(19,1)*therm_flux)+(N_{act}(13,i)*act_con(13,1)))))+N_{act}(20,i);$$

%Pu242

$$N_{act}(21,i+1)=(dt*((-act_con(21,1)*N_{act}(21,i))-$$

$$(N_{act}(21,i)*act_abs(21,1)*therm_flux)+(act_con(14,1)*N_{act}(14,i))+(act_con(15,1)*N_{act}(15,i))+(.173*act_con(24,1)*N_{act}(24,i))+(N_{act}(20,i)*act_rad(20,1)*therm_flux)))+N_{act}(21,i);$$

%Pu243

$$N_{act}(22,i+1)=(dt*((-act_con(22,1)*N_{act}(22,i))-$$

$$(N_{act}(22,i)*act_abs(22,1)*therm_flux)-(act_con(16,1)*N_{act}(16,i))+(N_{act}(21,i)*act_rad(21,1)*therm_flux)))+N_{act}(22,i);$$

%Am241

$$N_{act}(23,i+1)=(dt*((-act_con(23,1)*N_{act}(23,i))-$$

$$(N_{act}(23,i)*act_abs(23,1)*therm_flux)+(N_{act}(20,i)*act_con(20,1)*.999976)))+N_{act}(23,i);$$

%Am242


```

N_act(24,i+1)=(dt*((-act_con(24,1)*N_act(24,i))-
(N_act(24,i)*act_abs(24,1)*therm_flux)+(0.8664053*N_act(23,i)*act_rad(23,1)*therm_flux)+(0.99541*N_act(25,i)*act_con(25,1))))+N_act(24,i);

```

```

%Am242m

```

```

N_act(25,i+1)=(dt*((-act_con(25,1)*N_act(25,i))-
(N_act(25,i)*act_abs(25,1)*therm_flux)+(0.1335947*N_act(23,i)*act_rad(23,1)*therm_flux)))+(N_act(25,i));

```

```

%Am243

```

```

N_act(26,i+1)=(dt*((-act_con(26,1)*N_act(26,i))-
(N_act(26,i)*act_abs(26,1)*therm_flux)+(N_act(24,i)*act_rad(24,1)*therm_flux)+(N_act(25,i)*act_rad(25,1)*therm_flux)+(act_con(22,1)*N_act(22,i))))+N_act(26,i);

```

```

end

```

```

figure;

```

```

loglog(time_step,N_act(1,:));

```

```

hold on;

```

```

loglog(time_step,N_act(23,:));

```

```

hold on;

```

```

loglog(time_step,N_act(26,:));

```

```

hold on;

```

```

loglog(time_step,N_act(24,:));

```

```

hold on;

```

```

loglog(time_step,N_act(25,:));

```

```

hold on;

```

```

loglog(time_step,N_act(20,:));

%hold on;

%loglog(time_step,N_act(22,:));

title(['Burn-up, Net production, iteration ',num2str(h),]);

xlabel('time (s)');

ylabel('atom count');

legend('U235','Am241','Am243','Am242','Am242m','Pu241','Location','northwest');

disp(N_act(23,t_total+1));

disp(N_act(26,t_total+1));

ti2=0;

tf2=24*3600*h*365*5;

dt=100;

time_step2(1,1)=0;

t_total2=(tf2-ti2)/dt;

therm_flux=0;%reactor shut down, decay allowed without further neutron activation
production

N_act_V2=zeros(26,t_total2+1);

N_act_V2(:,1)=N_act(:,t_total+1);

%N_act(4,1)=3*10^26;

for i=1:t_total2

```

time_step2(i+1,1)=dt*(i);

%U235

N_act_V2(1,i+1)=(dt*((-act_con(1,1)*N_act_V2(1,i)-
(N_act_V2(1,i)*act_abs(1,1)*therm_flux)+(act_con(18,1)*N_act_V2(18,i))))+N_act_V2
(1,i);

%U236

N_act_V2(2,i+1)=(dt*((-act_con(2,1)*N_act_V2(2,i)-
(N_act_V2(2,i)*act_abs(2,1)*therm_flux)+(act_rad(1,1)*N_act_V2(1,i)*therm_flux)+(ac
t_con(19,1)*N_act_V2(19,i))))+N_act_V2(2,i);

%U237

N_act_V2(3,i+1)=(dt*((-act_con(3,1)*N_act_V2(3,i)-
(N_act_V2(3,i)*act_abs(3,1)*therm_flux)+(N_act_V2(2,i)*act_rad(2,1)*therm_flux)+(0
000245*act_con(20,1)*N_act_V2(20,i))))+N_act_V2(3,i);

%U238

N_act_V2(4,i+1)=(dt*((-act_con(4,1)*N_act_V2(4,i)-
(N_act_V2(4,i)*act_abs(4,1)*therm_flux)+(N_act_V2(3,i)*act_rad(3,1)*therm_flux)+(ac
t_con(21,1)*N_act_V2(21,i))))+(N_act_V2(4,i));

%U239

N_act_V2(5,i+1)=(dt*((-act_con(5,1)*N_act_V2(5,i)-
(N_act_V2(5,i)*act_abs(5,1)*therm_flux)+(N_act_V2(4,i)*act_rad(4,1)*therm_flux)))+
N_act_V2(5,i);

%U240

N_act_V2(6,i+1)=(dt*((-act_con(6,1)*N_act_V2(6,i)-
(N_act_V2(6,i)*act_abs(6,1)*therm_flux)+(N_act_V2(5,i)*act_rad(5,1)*therm_flux)))+
N_act_V2(6,i);

%U241

$$N_act_V2(7,i+1)=(dt*((-act_con(7,1)*N_act_V2(7,i))- \\ (N_act_V2(7,i)*act_abs(7,1)*therm_flux)+(N_act_V2(6,i)*act_rad(6,1)*therm_flux)))+ \\ N_act_V2(7,i);$$

%Np240

$$N_act_V2(8,i+1)=(dt*((-act_con(8,1)*N_act_V2(8,i))- \\ (N_act_V2(8,i)*act_abs(8,1)*therm_flux)+(0.6744834*N_act_V2(12,i)*act_rad(12,1)*the \\ rm_flux)+(0.0012*act_con(9,1)*N_act_V2(9,i))))+N_act_V2(8,i);$$

%Np240m

$$N_act_V2(9,i+1)=(dt*((-act_con(9,1)*N_act_V2(9,i))- \\ (N_act_V2(9,i)*act_abs(9,1)*therm_flux)+(0.3255166*N_act_V2(12,i)*act_rad(12,1)*the \\ rm_flux)+(act_con(6,1)*N_act_V2(6,i))))+N_act_V2(9,i);$$

%Np237

$$N_act_V2(10,i+1)=(dt*((-act_con(10,1)*N_act_V2(10,i))- \\ (N_act_V2(10,i)*act_abs(10,1)*therm_flux)+(act_con(3,1)*N_act_V2(3,i)+(act_con(23, \\ 1)*N_act_V2(23,i))))+N_act_V2(10,i);$$

%Np238

$$N_act_V2(11,i+1)=(dt*((-act_con(11,1)*N_act_V2(11,i))- \\ (N_act_V2(11,i)*act_abs(11,1)*therm_flux)+(N_act_V2(10,i)*act_rad(10,1)*therm_flux \\)+(0.00459*act_con(25,1)*N_act_V2(25,i))))+N_act_V2(11,i);$$

%Np239

$$N_act_V2(12,i+1)=(dt*((-act_con(12,1)*N_act_V2(12,i))- \\ (N_act_V2(12,i)*act_abs(12,1)*therm_flux)+(N_act_V2(11,i)*act_rad(11,1)*therm_flux \\)+(act_con(5,1)*N_act_V2(5,i)+(act_con(26,1)*N_act_V2(26,i))))+N_act_V2(12,i);$$

%Np241

```

N_act_V2(13,i+1)=(dt*((-act_con(13,1)*N_act_V2(13,i))-
(N_act_V2(13,i)*act_abs(13,1)*therm_flux)+(N_act_V2(8,i)*act_rad(8,1)*therm_flux)+
(N_act_V2(9,i)*act_rad(9,1)*therm_flux)+(act_con(7,1)*N_act_V2(7,i))))+N_act_V2(1
3,i);

```

```
%Np242
```

```

N_act_V2(14,i+1)=(dt*((-act_con(14,1)*N_act_V2(14,i))-
(N_act_V2(14,i)*act_abs(14,1)*therm_flux)+(0.8977549*N_act_V2(13,i)*act_rad(13,1)*t
herm_flux)))+N_act_V2(14,i);

```

```
%Np242m
```

```

N_act_V2(15,i+1)=(dt*((-act_con(15,1)*N_act_V2(15,i))-
(N_act_V2(15,i)*act_abs(15,1)*therm_flux)+(0.1022444*N_act_V2(13,i)*act_rad(13,1)*t
herm_flux)))+N_act_V2(15,i);

```

```
%Np243
```

```

N_act_V2(16,i+1)=(dt*((-act_con(16,1)*N_act_V2(16,i))-
(N_act_V2(16,i)*act_abs(16,1)*therm_flux)+(N_act_V2(14,i)*act_rad(14,1)*therm_flux
)+(N_act_V2(15,i)*act_rad(15,1)*therm_flux)))+N_act_V2(16,i);

```

```
%Pu238
```

```

N_act_V2(17,i+1)=(dt*((-act_con(17,1)*N_act_V2(17,i))-
(N_act_V2(17,i)*act_abs(17,1)*therm_flux)+(N_act_V2(11,i)*act_con(11,1))))+N_act_
V2(17,i);

```

```
%Pu239
```

```

N_act_V2(18,i+1)=(dt*((-act_con(18,1)*N_act_V2(18,i))-
(N_act_V2(18,i)*act_abs(18,1)*therm_flux)+(act_con(12,1)*N_act_V2(12,i)))+(N_act_V
2(17,i)*act_rad(17,1)*therm_flux)))+N_act_V2(18,i);

```

```
%Pu240
```

```

N_act_V2(19,i+1)=(dt*((-act_con(19,1)*N_act_V2(19,i))-
(N_act_V2(19,i)*act_abs(19,1)*therm_flux)+(N_act_V2(18,i)*act_rad(18,1)*therm_flux
)+(N_act_V2(8,i)*act_con(8,1))+(.9988*N_act_V2(9,i)*act_con(9,1))))+N_act_V2(19,i)
;

```

```
%Pu241
```

```

N_act_V2(20,i+1)=(dt*((-act_con(20,1)*N_act_V2(20,i))-
(N_act_V2(20,i)*act_abs(20,1)*therm_flux)+(N_act_V2(19,i)*act_rad(19,1)*therm_flux
)+(N_act_V2(13,i)*act_con(13,1))))+N_act_V2(20,i);

```

```
%Pu242
```

```

N_act_V2(21,i+1)=(dt*((-act_con(21,1)*N_act_V2(21,i))-
(N_act_V2(21,i)*act_abs(21,1)*therm_flux)+(act_con(14,1)*N_act_V2(14,i))+(act_con(
15,1)*N_act_V2(15,i))+(.173*act_con(24,1)*N_act_V2(24,i))+(N_act_V2(20,i)*act_rad
(20,1)*therm_flux)))+N_act_V2(21,i);

```

```
%Pu243
```

```

N_act_V2(22,i+1)=(dt*((-act_con(22,1)*N_act_V2(22,i))-
(N_act_V2(22,i)*act_abs(22,1)*therm_flux)-
(act_con(16,1)*N_act_V2(16,i))+(N_act_V2(21,i)*act_rad(21,1)*therm_flux)))+N_act_
V2(22,i);

```

```
%Am241
```

```

N_act_V2(23,i+1)=(dt*((-act_con(23,1)*N_act_V2(23,i))-
(N_act_V2(23,i)*act_abs(23,1)*therm_flux)+(N_act_V2(20,i)*act_con(20,1)*.999976)))
+N_act_V2(23,i);

```

```
%Am242
```

```

N_act_V2(24,i+1)=(dt*((-act_con(24,1)*N_act_V2(24,i))-
(N_act_V2(24,i)*act_abs(24,1)*therm_flux)+(.8664053*N_act_V2(23,i)*act_rad(23,1)*t
herm_flux)+(N_act_V2(25,i)*act_con(25,1))))+N_act_V2(24,i);

```

```

%Am242m

N_act_V2(25,i+1)=(dt*((-act_con(25,1)*N_act_V2(25,i))-
(N_act_V2(25,i)*act_abs(25,1)*therm_flux)+(.1335947*N_act_V2(23,i)*act_rad(23,1)*t
herm_flux)))+(N_act_V2(25,i));

%Am243

N_act_V2(26,i+1)=(dt*((-act_con(26,1)*N_act_V2(26,i))-
(N_act_V2(26,i)*act_abs(26,1)*therm_flux)+(N_act_V2(24,i)*act_rad(24,1)*therm_flux
)+(N_act_V2(25,i)*act_rad(25,1)*therm_flux)+(act_con(22,1)*N_act_V2(22,i))))+N_act
_V2(26,i);

end

figure;

loglog(time_step2,N_act_V2(1,:));

hold on;

loglog(time_step2,N_act_V2(23,:));

hold on;

loglog(time_step2,N_act_V2(26,:));

hold on;

loglog(time_step2,N_act_V2(24,:));

hold on;

loglog(time_step2,N_act_V2(25,:));

hold on;

loglog(time_step2,N_act_V2(20,:));

%hold on;

```

```

%loglog(time_step2,N_act_V2(22,:));

title(['Decay only, Net production,iteration ',num2str(h),]);

xlabel('time (s)');

ylabel('atom');

legend('U235','Am241','Am243','Am242','Am242m','Pu241','Location','northwest');

end

end

```

Newton-Raphson method in Matlab utilized to solve for the ‘unknown’ age of the plutonium sample (when Am241 was non-existent).

```

function [] = PU_RG_UNCORRECTED_12_CASE

%Eric Feissle

format long;

%for g=1:10

% n=1;

% x=zeros();

%initial guesses for the newton/Raphson method

%K_vector=[0.639951625286253; 0.719654337797267; 0.790468978122802;
            0.824160000556767; 0.618319473742697; 0.906159300839712;
            0.913466522490492; 0.920479980643814; 0.926501688333058;
            0.478666990838003; 0.975325365427586; 0.976621703843034;
            0.976861774124237; 0.977750277583439];

%K_vector=[0.696759567712365; 0.76631417691868; 0.831963004109291;
            0.862564419953653; 0.642492334375384; 0.935874413135274;

```


0.942000749548857; 0.948024791360428; 0.953232530936045;
0.49021712933367; 0.993931409174918; 0.995049389215342;
0.995103721870834; 0.995901931577486];

K_1=[0.669297099705177;0.674169585848799;0.679042071992421];

K_2=[0.508042796000403;0.511556007993063;0.515069219985722];

K_3=[0.411365631322586;0.41411937064111;0.416873109959633];

K_4=[0.346940061579728;0.349209208951575;0.351478356323421];

K_5=[0.916783918081804;0.920027448143148;0.923270978204493];

K_6=[0.850553684525083;0.853508164959867;0.856462645394651];

K_7=[0.794542248495533;0.797260787507433;0.799979326519333];

K_8=[0.746768706994242;0.749286243636938;0.751803780279634];

K_9=[0.98280975997935;0.98491694775027;0.987024135521191];

K_10=[0.968624622971181;0.970694310208667;0.972763997446152];

K_11=[0.955159543053654;0.957194024144077;0.9592285052345];

K_12=[0.942373516824221;0.944373098270032;0.946372679715843];

for yy=1:12

%-----

```
if yy==1 %1 year, .5 yr measurement span

K_vector=K_1;

T1_vector=[0;0;0];
T2_vector=[.5;.5;.5];

end

if yy==2 %1 year, 1 yr measurement

K_vector=K_2;

T1_vector=[0;0;0];

T2_vector=[1;1;1];

end

if yy==3 %1 year, 1.5 yr measurement span

K_vector=K_3;
```

```
T1_vector=[0;0;0];  
T2_vector=[1.5;1.5;1.5];  
  
end  
  
if yy==4 %1 year, 2 yr measurement span  
    K_vector=K_4;  
    T1_vector=[0;0;0];  
T2_vector=[2;2;2];  
end  
  
if yy==5 % 5 year, .5 yr measurement span  
    K_vector=K_5;  
    T1_vector=[0;0;0];  
    T2_vector=[.5;.5;.5];  
  
end  
  
if yy==6 % 5 year, 1 yr measurement span  
    K_vector=K_6;  
    T1_vector=[0;0;0];  
    T2_vector=[1;1;1];  
  
end
```

```
if yy==7 % 5 year, 1.5 yr measurement span
```

```
    K_vector=K_7;
```

```
    T1_vector=[0;0;0];
```

```
    T2_vector=[1.5;1.5;1.5];
```

```
end
```

```
if yy==8 % 5 year, 2 yr measurement span
```

```
    K_vector=K_8;
```

```
    T1_vector=[0;0;0];
```

```
    T2_vector=[2;2;2];
```

```
end
```

```
if yy==9 % 19 year, .5 measurement span
```

```
    K_vector=K_9;
```

```
    T1_vector=[0;0;0];
```

```
    T2_vector=[.5;.5;.5];
```

```
end
```

```
if yy==10 % 19 year, 1 measurement span
```

```
    K_vector=K_10;
```

```
    T1_vector=[0;0;0];
```

```
    T2_vector=[1;1;1];
```

```
end
```

```
if yy==11 % 19 year, 1.5 measurement span
```

```
    K_vector=K_11;
```

```
    T1_vector=[0;0;0];
```

```
    T2_vector=[1.5;1.5;1.5];
```

```
end
```

```
if yy==12 %19 year, 2 measurement span
```

```
    K_vector=K_12;
```

```
    T1_vector=[0;0;0];
```

```
    T2_vector=[2;2;2];
```

```
end
```

```
%-----
```

```
for g=1:length(K_vector)
```

```
    x(1)=0;
```

```
    n=1;
```

```
    x=zeros();
```

```
    x(2)=x(1)-
```

```
    fun9(x(1),K_vector(g,1),T1_vector(g,1),T2_vector(g,1))/fun10(x(1),T1_vector(g,1),T2_v  
ector(g,1));
```

```

err1=.000000000000001;

err2=.000000000000001;

err3=.000000000000001;

M=20;

while abs(x(n+1)-x(n))>=err1 && n<=M-1

    n=n+1;

    x(n+1)=x(n)-
(fun9(x(n),K_vector(g,1),T1_vector(g,1),T2_vector(g,1))/fun10(x(n),T1_vector(g,1),T2_
vector(g,1)));

    if      abs(fun9(x(n+1),K_vector(g,1),T1_vector(g,1),T2_vector(g,1)))<err2      ||
abs(fun10(x(n+1),T1_vector(g,1),T2_vector(g,1)))<err3

        %disp('what');

        %break;

    end

end

constep=1:n+1;

estimated_age(g,1)=x(n+1);

```

```
H=[constep',x'];

%disp('count step      x');

%disp(H);

%disp('-----');

clear x;

clear constep;

%end

% if g==1

%  disp('min K value, 1 std dev');

% end

% if g==2

%  disp('mean K value, 1 std dev');

% end

% if g==3

%  disp('max K value, 1 std dev');

% end

end

if yy==1

disp('true age is 1 year, 0.5 year measurement span');

end

if yy==2
```

```
    disp('true age is 1 year, 1 year measurement span');  
end  
  
if yy==3  
    disp('true age is 1 year, 1.5 year measurement span');  
end  
  
if yy==4  
    disp('true age is 1 year, 2 year measurement span');  
end  
  
if yy==5  
    disp('true age is 5 years, 0.5 year measurement span');  
end  
  
if yy==6  
    disp('true age is 5 years, 1 year measurement span');  
end  
  
if yy==7  
    disp('true age is 5 years, 1.5 year measurement span');  
end  
  
if yy==8  
    disp('true age is 5 years, 2 year measurement span');  
end  
  
if yy==9
```



```
    disp('true age is 19 years, 0.5 year measurement span');  
end  
  
if yy==10  
    disp('true age is 19 years, 1.0 year measurement span');  
end  
  
if yy==11  
    disp('true age is 19 years, 1.5 year measurement span');  
end  
  
if yy==12  
    disp('true age is 19 years, 2.0 year measurement span');  
end  
  
disp(estimated_age);  
  
clear estimated_age;  
  
end  
  
end  
  
function [ff9]= fun9(x,K,t1,t2)  
  
%input function=0  
  
%ff9=atan(x);  
  
%ff9=3*x-1;  
  
%K=.629906;
```

```

%K=.970673;

%K=0.352573453;

lam_Am241=0.00160225; %yrs^-1

lam_Pu241=0.048504699; %yrs^-1

%t1=0;

%t2=15;

A=exp(-lam_Pu241*(t1+x));

B=exp(-lam_Am241*(t1+x));

C=exp(-lam_Pu241*(t2+x));

D=exp(-lam_Am241*(t2+x));

ff9=((A-B)/(C-D))-K;

end

function [ff10]= fun10(x,t1,t2)

%input the derivative of the fun9 function

%ff10=1/(1+x^2);

%ff10=3;

%t1=0;

%t2=15;

lam_Am241=0.00160225; %yrs^-1

lam_Pu241=0.048504699; %yrs^-1

A=lam_Am241*exp(-lam_Am241*(t1+x))-lam_Pu241*exp(-lam_Pu241*(t1+x));

```

$$F=\exp(-\text{lam_Pu241}*(t2+x))-\exp(-\text{lam_Am241}*(t2+x));$$

$$B=\exp(-\text{lam_Pu241}*(t1+x))-\exp(-\text{lam_Am241}*(t1+x));$$

$$C=\text{lam_Am241}*\exp(-\text{lam_Am241}*(t2+x))-\text{lam_Pu241}*\exp(-\text{lam_Pu241}*(t2+x));$$

$$D=\exp(-\text{lam_Pu241}*(t2+x))-\exp(-\text{lam_Am241}*(t2+x));$$

$$\text{ff10}=(A/F)-((B*C)/(D^2));$$

end

APPENDIX B
SOURCE CERTIFICATES AND CORE CONFIGURATION

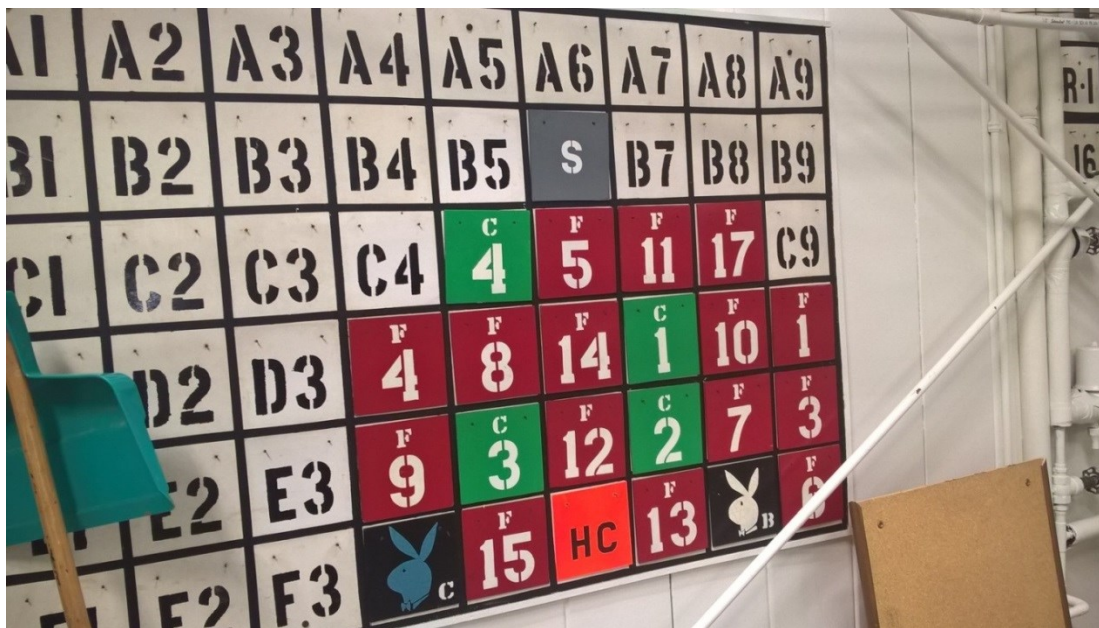
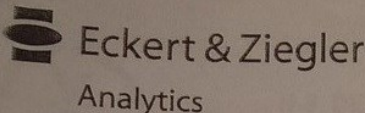


Figure B.1. the MSTR configuration as of 10-18-2016

 Eckert & Ziegler
Analytics

1380 Seaboard Industrial Blvd.
Atlanta, Georgia 30318
Tel 404-352-8677
Fax 404-352-2837
www.analytinc.com

CERTIFICATE OF CALIBRATION
Standard Radionuclide Source

91818
~20.5 mm Diameter x 3 mm Thick Button Centered in Poly Vial

Customer: Missouri S&T University of Science & Technology
P.O. No.: JOHNSON 17AUG12, Item 1
Reference Date: 01-Oct-2012 12:00 PM EST **Grams of Master Source:** 0.017109


This standard radionuclide source was prepared using aliquots measured gravimetrically from master radionuclide solutions. Additional radionuclides were added gravimetrically from solutions calibrated by gamma-ray spectrometry, ionization chamber, or liquid scintillation counting. Calibration and purity were checked using a germanium gamma spectrometer system. At the time of calibration no interfering gamma-ray emitting impurities were detected. The gamma-ray emission rates for the most intense gamma-ray lines are given. Eckert & Ziegler Analytics (EZA) maintains traceability to the National Institute of Standards and Technology through a Measurements Assurance Program as described in USNRC Regulatory Guide 4.15, Revision 2, July 2007, and compliance with ANSI N42.22-1995, "Traceability of Radioactive Sources to NIST." EZA is accredited by the Health Physics Society (HPS) for the production of NIST-traceable sources, and this source was produced in accordance with the HPS accreditation requirements. Customers may report any concerns with the accreditation program to the HPS Secretariat, 1313 Dolley Madison Blvd., Ste. 402, McLean, VA 22101.

Nuclide	Gamma-Ray Energy (keV)	Half-Life, Days	Master Source* $\mu\text{ps}/\text{gram}$	This Source μps	Uncertainty*, %			Calibration Method*
					u_A	u_B	U	
Am-241	59.5	1.580E+05	—	2.014E+03	0.1	1.7	3.5	4 π LS
Cd-109	88.0	4.626E+02	1.664E+05	2.846E+03	0.5	2.3	4.7	HPGe
Co-57	122.1	2.718E+02	8.865E+04	1.517E+03	0.4	2.0	4.1	HPGe
Ce-139	165.9	1.376E+02	1.256E+05	2.148E+03	0.4	1.9	3.9	HPGe
Hg-203	279.2	4.661E+01	2.683E+05	4.591E+03	0.3	1.9	3.8	HPGe
Sn-113	391.7	1.151E+02	1.723E+05	2.948E+03	0.4	1.9	3.9	HPGe
Cs-137	661.7	1.098E+04	1.132E+05	1.937E+03	0.7	1.9	4.0	HPGe
Y-88	898.0	1.066E+02	4.173E+05	7.140E+03	0.5	1.9	3.9	HPGe
Co-60	1173.2	1.925E+03	2.126E+05	3.636E+03	0.6	1.9	4.0	HPGe
Co-60	1332.5	1.925E+03	2.126E+05	3.637E+03	0.7	1.9	4.0	HPGe
Y-88	1836.1	1.066E+02	4.418E+05	7.559E+03	0.7	1.9	4.0	HPGe

* Master Source refers to Analytics' 8-isotope mixture which is calibrated quarterly.

Calibration Methods: 4 π LS - 4 pi Liquid Scintillation Counting, HPGe - High Purity Germanium Gamma-Ray Spectrometer, IC - Ionization Chamber. **Uncertainty:** U - Relative expanded uncertainty, k = 2. See NIST Technical Note 1297, "Guidelines for Evaluating and Expressing the Uncertainty of NIST Measurement Results."

(Certificate continued on reverse side)



MGS Certificate Rev 4, 22 August 2012 Page 1 of 2

Corporate Office Laboratory

Figure B.2. Mixed Isotope Source

COPY

Certificate of Calibration

MULTI-GAMMA RAY STANDARD

MGS-1

Serial Number: 1119 Type: 2" disk
Calibration Date: 27-Jun-02 Julian Day: (245) 2453
Total Activity: 28 400 Bq 0.768 μCi

This source has been calibrated with a HPGe detector for which the efficiency has been established with IAEA or NIST traceable standards. The gamma lines listed were measured to determine the stated activity as a weighted average with an uncertainty estimated at 5%.

Peak No.	Energy (keV)	Eu-152 13.6 y Photons/s	Eu-154 8.59 y Photons/s	Eu-155 4.76 y Photons/s
1	40.1 (SmKa)	4 910		
2	60.0			122
3	86.5			3 440
4	105.3			2 400
5	121.8 - doublet	2 410		
	123.1		3 560	
6	244.7	635		
7	344.3	2 250		
8	591.7		406	
9	723.3		1 740	
10	873.2		1 070	
11	1004.8		1 550	
12	1274.5		3 040	
13	1408.0	1 760		
14	1596.5		163	

* calculated

Activity (Becquerels)	8 470	8 820	11 100
Activity (Microcuries)	0.229	0.238	0.300
Half-Life (Days)	4.96E+03	3.14E+03	1.74E+03
Decay Constant (Days ⁻¹)	1.40E-04	2.21E-04	3.98E-04

Certified by: Carmen Jones Date: 6-27-02

CANBERRA INDUSTRIES, INC.
107 Union Valley Road
Oak Ridge, Tennessee 37830, USA
Telephone (865) 220-6333
Fax (865) 483-0406

Figure B.3. Europium Source

REFERENCES

- Ackleh, A. S., Allen, E. J., Hearfott, R. B., & Seshaiyer, P. (n.d.). *Classical and Modern Numerical Analysis*. CRC Press.
- Bell, S. (1999). *A Beginner's Guide to Uncertainty of Measurement*. National Physical Laboratory.
- Benetti, P., Cesana, A., Cinotti, L., Raselli, G., & Terrani, M. (2006). *Americium 242m and its potential use in space applications*. IOP Publishing Ltd.
- Canberra. (2012). *ProSpect Gamma Spectroscopy Software*.
- Canberra. (n.d.). *Germanium Detectors*.
- Canberra Industries. (2013). *Model 747 and 747E Lead Shield*. Canberra Industries.
- Castrup, H. (2004). *Estimating and Combining Uncertainties*. ITEA.
- Chadwick, M. B., Herman, M., Oblozinsky, P., & et al. (2011). ENDF/B-VII.1 nuclear data for science and technology: Cross sections, covariances, fission product yields and decay data. *Nuclear Data Sheets*, 2887-2996.
- Chadwick, M. B., Oblozinsky, P., Herman, M., & al, a. (2006). "ENDF/B-VII.0: Next Generation Evaluated Nuclear Data Library for Nuclear Science and Technology". *Nuclear Data Sheets*, vol. 107, 2931-3060.
- Diago, J. R. (2005). *Simulation of detector Calibration using MCNP*. CHERNE.
- Duderstadt, & Hamilton. (1976). *Nuclear Reactor Analysis*. Hoboken: Wiley.
- El-Khatib, A. M., Mona, M. G., Mohamed, S. B., Sherif, S. N., & Ekram, E.-M. A. (2013). *Computation of the Full Energy Peak Efficiency of an HPGE Detector Using a New Compact Simulation Analytical Approach for Spherical Sources*. *Journal of Engineering Science and Technology*.
- Fantinova, K., & Fojtik, P. (2014). *Monte Carlo simulation of the BEGe detector response function for in vivo measurements of Am241 in the skull*. *Radiation Physics and Chemistry*.
- Kulage, Z., Castano, C. H., Usman, S., & Mueller, G. (2013). *Characterization of the neutron flux energy spectrum at the Missouri University of Science and Technology Research Reactor (MSTR)*. *Nuclear Engineering and Design*.
- Lamarsh, J. R., & Baratta, A. J. (2001). *Introduction to Nuclear Engineering*. Prentice Hall.
- LNHB. (n.d.). *Laboratoire National Henri Becquerel*.

- Luca, A. (2010). *Determination of the characteristic limits (decision threshold, detection limit and limits of the confidence interval) for measurements of ionizing radiation -- Fundamentals and application*. ISO.
- Nardo, L. D. (n.d.). *On the Propagation of Statistical Errors*. BNL.
- NIST. (n.d.). *Critical Values of the Student's t Distribution*. Retrieved from NIST.
- NIST. (n.d.). *Expanded Uncertainty and Coverage factor*. Retrieved from The NIST Reference on Constants, Units, and Uncertainty.
- NRC. (n.d.). *Part 30-Rules of General Applicability To Domestic Licensing of Byproduct Material*. Retrieved from U.S. NRC.
- OECD-NEA. (2013, September). *Janis 4.0*.
- Richardson, B., Castano, C., King, J., Alajo, A., & Usman, S. (2012). *Modeling and Validation of approach to criticality and axial flux profile experiments at the Missouri S&T Reactor (MSTR)*. Nuclear Engineering and Design.
- Travers, W. D. (1999). *Mixed-Oxide Fuel Use in Commercial Light Water Reactors*. Washington D.C: NRC.
- Tsoufanidis, N. (2013). *The Nuclear Fuel Cycle*. LaGrange Park: American Nuclear Society.
- Tsoufanidis, N., & Landsberger, S. (2011). *Measurement and Detection of Radiation*. CRC Press.
- X-5 Monte Carlo Team. (2003). *MCNP-A General Monte Carlo N-Particle Transport Code, Version 5*. Los Alamos National Laboratory.
- X-5 Monte Carlo Team. (2003). *MCNP-A General Monte Carlo N-Particle Transport Code, Version 5, Volume II: User's Guide*. Los Alamos National Laboratory.

VITA

In May of 2015 Eric Feissle received his B.S in Nuclear Engineering at the Missouri University of Science and Technology. He then received his Master's degree in Nuclear Engineering from the Missouri University of Science and Technology in May 2017.